UNIVERSITÀ
DEGLI STUDI
FIRENZE

DOTTORATO DI RICERCA IN
Area del Farmaco e Trattamenti Innovativi

CICLO XXXII

COORDINATORE: Prof.ssa Elisabetta Teodori

Hybrid Pharmacophores as Carbonic Anhydrase Inhibitors

Settore Scientifico Disciplinare CHIM/08

Dottoranda
Dott.ssa Silvia Bua

Tutore Scientifico
Prof. Claudiu T. Supuran

Tutore Teorico
Prof.ssa Silvia Selleri

Coordinatore
Prof.ssa Elisabetta Teodori

Anni 2016/2019

Abstract

Carbonic anhydrases (CAs, EC 4.2.1.1) are ubiquitous metalloenzymes encoded in most organisms of the tree of life and classified in eight evolutionarily unrelated families: α-, β-, γ-, δ-, ζ-, η-, θ- and ι-CAs. The CAs catalyse a simple, but physiologically crucial reaction for all living beings, that is the reversible hydration of carbon dioxide to bicarbonate and proton. The CAs are involved in respiration, pH and CO_2 homeostasis, transport of CO_2/HCO_3^- and a multitude of biosynthetic reactions in many organisms. Fifteen α-class CA isoforms were identified in human, which are further implicated in electrolytes secretion in many tissues/organs, metabolic reactions such as gluconeogenesis, lipogenesis, ureagenesis, bone resorption, calcification, and carcinogenesis. As a result, a multitude of human physio/pathological processes which show abnormal expression or activity of specific human CAs could be target of pharmacological intervention based on CA modulation.

In addition, a number of α-, β-, γ- and η-CAs was identified in many bacteria, fungi and protozoa that are human pathogens. In this context, CAs were shown to be crucial for the virulence, growth or acclimatization of the parasites in the hosts with their inhibition, that produces growth impairment and defects in the pathogen, being a promising strategy for chemotherapy.

The research activity included in this Ph.D. thesis fits in the context of the spreading interest of the scientific community on CAs as drug targets for the treatment of a multitude of disorders. Thus, a set of projects involving drug-design, synthesis and biological evaluation of new CAs modulators, among which most based on the multi-target approach, were the focus of the three-years Ph.D. cycle.

In recent years, the choice of multi-potent hybrid agents is spreading worldwide and overcoming the co-administration of multiple drugs because of improved pharmacokinetics, better patient compliance, reduced drug-drug interactions as well as a synergistic effect in the treatment of the pathology. Thus, in the present Ph.D. thesis I exploited the validated efficacy of CA inhibition in the treatment of many disorders for designing several multi-target strategies including CAIs against cancer, inflammation, glaucoma and infections. My activity included both design, synthesis and *in vitro* kinetic evaluation by a Stopped-flow assay of the new CAI derivatives.

As first and second projects of the Ph.D. period, two series of multi-target nonsteroidal anti-inflammatory drug (NSAID) - CAI derivatives for the management of rheumatoid arthritis were reported, which differ for the type of linker, amide or ester, connecting the active portions. A coumarin scaffold was chosen as CAI to induce a selective inhibition of CA IX and XII, that are overexpressed in inflamed tissues. In spite of a different plasma stability, and thus predicted pharmacokinetics, a subset of multi-potent derivatives from both series showed more efficient pain-relieving action than clinically used NSAIDs in a rat model of rheumatoid arthritis. Of note, the derivatives were shown *in vitro* and *in silico* to produce cyclooxygenase 1/2 inhibition even as integral hybrids.

In contrast, for pharmacologically hitting glaucoma, CAIs of the sulfonamide type were assembled with portions able to block the $\beta_{1/2}$-adrenergic receptors that, as hCA II, IV and XII, are involved in the pathogenesis of the ocular disorder. Multi-potent derivatives identified within the series were evaluated in a rabbit model of glaucoma and showed to possess more effective internal ocular pressure lowering properties as eye drops than the leads, clinically used dorzolamide and timolol, and even the combination of them which is a globally marketed antiglaucoma medication.

Both sulfonamide and coumarin scaffolds were incorporated as CA IX and XII inhibitors in nitric oxide (*NO*)-donor derivatives based on a benzofuroxan scaffold, that was shown to induce a potent cytotoxic action against several types of cancer cells as well as an antimetastatic activity. Further, benzofuroxans were recently shown to possess activity against *Trypanosoma cruzi*, *Mycobacterium Tuberculosis* and *Leishmania*, which was assumed to be enhanced by inhibiting the α- and β-CAs encoded in these pathogens. To date, the outcomes of this study are limited to design, synthesis and *in vitro* kinetic assessment.

As it was recently found that two of the world's most marketed sweeteners, saccharin (**SAC**) and acesulfame K (**ACE**), selectively inhibit the tumor-associated CAs IX and XII over ubiquitous CAs, we planned a drug design strategy that considered **SAC** and **ACE** as leads and produced a new CAI chemotype, namely the 2H-benzo[e][1,2,4]thiadiazin-3(4H)-one 1,1-dioxide (**BTD**). Many synthesized derivatives showed enhanced potency and in some cases selectivity, when compared to the leads against the target CA IX and XII over off-target isoforms. A subset of compounds displayed effective cytotoxic action against A549, PC-3 and HCT-116 cell lines and anticancer effects on apoptotic markers.

During my Ph.D. period, I performed a multitude of kinetic studies with inhibitors and activators of several isoforms of CA belonging to the classes α, β, γ, δ, ζ, η and θ. These studies allowed to draw up the inhibition or activation profiles of hundreds of derivatives from collaborators of us. Additionally, I performed the *ex novo* complete kinetic characterization of the CA isoforms identified in the protozoan human parasite *Entamoeba histolytica* and in the coral *Stylophora pistillata*.

TABLE OF CONTENTS

List of Abbreviations and Acronyms

α-CA	α-Carbonic Anhydrase
β-CA	β-Carbonic Anhydrase
γ-CA	γ-Carbonic Anhydrase
β-ADRs	β-Adrenergic Receptors
AAZ	Acetazolamide
ACE	Acesulfame K
ACG	Angle-closure Glaucoma
AE2	Anion Exchangers
AG	Anchoring Group
AS	Ankylosing Spondylitis
BBr_3	Boron Tribromide
BRZ	Brinzolamide
BTD	2H-benzo[e][1,2,4]thiadiazin-3(4H)-one 1,1-dioxide
BZA	Benzolamide
CA	Carbonic Anhydrase
CAI	Carbonic Anhydrase Inhibitor
CAAs	Carbonic Anhydrase Activators
Can2	*Cryptococcus neoformans* Carbonic Anhydrase
CARPs	CA-Related Proteins
CFA	Complete Freund's Adjuvant
CLX	Celecoxib
CMC	Carboxymethylcellulose
CNS	Central Nervous System
COX	Cyclooxygenase
CSI	Chlorosulfonyl Isocyanate
DCP	Dichlorophenamide
DCM	Dichloromethane
DMF	Dimetilformammide
DMAP	4-Dimethylaminopyridine
DMARD	Disease-modifying Antirheumatic Drugs
DTCs	Dithiocarbamates
DZA	Dorzolamide
EDCI	1-Ethyl-3-(3-dimethylaminopropyl)carbodiimide
EhiCA	*Entamoeba histolytica*
EZA	Ethoxzolamide
hpαCA	*H. pylori* α-Carbonic Anhydrase
hpβCA	*H. pylori* β-Carbonic Anhydrase
hCA	Human Carbonic Anhydrase
hCOX	Human CycloOxygenase
HCT	Hydrochlorothiazide
HPLC	High Performance Liquid Chromatography
HRMS	High-Resolution Mass Spectrometry
ia	intra-articular
IC_{50}	Half Maximal Inhibitory Concentration
IND	Indisulam
IOP	Intraocular Pressure
JIA	Juvenile Idiopathic Arthritis
K_A	Activation Constant
K_I	Inhibition Constant
LC-MS/MS	Tandem Mass Spectrometry Mode
LdcCA	*Leishmania chagasi* Carbonic Anhydrase
MgCA	*Malassezia globosa* Carbonic Anhydrase
MCT4	Monocarboxylate Transporters
MD	Molecular Dynamics
MS	Mass Spectrometry
MZA	Methazolamide
NBCe1	Sodium-bicarbonate Transporters
NHE1	Sodium-proton Exchangers
NHS	*N*-hydroxysuccinamide
NSAID	Nonsteroidal Anti-Inflammatory Drug
NO	Nitric Oxide
OAG	Open-angle Glaucoma
PBS	Phosphate Buffer Solution
PDB	Protein Data Bank
PgE_2	Prostaglandin E_2
pK_i	Inhibition Binding Constants
RA	Rheumatoid Arthritis
RMSD	Root-mean-square Deviation
RNS	Reactive Nitrogen Species
ROS	Reactive Oxygen Species
SA	Sulfanilamide
SAC	Saccharin
SAR	Structure-Activity Relationship
SG	Sticky Group
SGC	Saccharin-Glucose Conjugate
SI	*Selectivity Index*
SLP	Sulpiride
SLT	Sulthiame
SpiCA	*Stylophora pistillata* Carbonic Anhydrase
TcCA	*Trypanosoma cruzi* Carbonic Anhydrase
TFA	Trifluoroacetic Acid
TPM	Topiramate
VchCA	*Vibrio cholerae* Carbonic Anhydrase
VLX	Valdecoxib
ZBG	Zinc Binding Group
ZNS	Zonisamide

Part I

Introduction

Chapter 1. Classification, Biochemistry and Structure of Carbonic Anhydrases

Carbonic anhydrases (CAs, EC 4.2.1.1) are ubiquitous metalloenzymes spread in most organisms of the tree of life and classified in eight evolutionarily unrelated families: α-, β-, γ-, δ-, ζ-, η-, θ- and ι-CAs.[1-12] CAs were primarily identified in red blood cells of bovine, and successively shown to exist in all mammalian tissues, as well as in plants, algae and bacteria.[13] The ubiquity of CAs is owed to the catalysis of a simple, but physiologically crucial reaction for living beings,[1] that is the reversible hydration of carbon dioxide to bicarbonate and proton (Equation 1).

$$\mathbf{CO_2 + H_2O \leftrightharpoons HCO_3^- + H^+} \quad \text{(Eq.1)}$$

In fact, as the carbon dioxide hydration occurs slowly at the pH values typically marking most tissues and organisms (turnover number - k_{cat} - of 10^{-1} s^{-1}), enzymes able to catalyse it evolved for handling the great loads of CO_2 produced by most organisms, making its substrates easily available for physiologic processes and tuning acid-base equilibria.[1-3] As a result, CAs are present in organisms of all life kingdoms (Bacteria, Archaea, Eukarya). The CAs are among the fastest enzymes known effectively speeding up the rate of the overall reaction up to 10^6 s^{-1}.[14]

Respiration, pH and CO_2 homeostasis, transport of CO_2/HCO_3^- and a multitude of biosynthetic reactions are physiologic processes in which CAs play crucial roles in many organisms.[1-4] Additionally, in mammals, CAs are involved in electrolytes secretion in many tissues/organs, metabolic reactions such as gluconeogenesis, lipogenesis, ureagenesis, bone resorption, calcification, and tumorigenicity.[15-24] In algae, cyanobacteria and plants, these enzymes promote the photosynthesis,[6-9] whereas in diatoms CAs play a pivotal role in CO_2 fixation and in the SiO_2 cycle.[11] In pathogen microorganisms, such as bacteria, fungi and protozoa, CAs were shown to be crucial for the virulence, growth or acclimatization of the parasites in the hosts.[12]

1.1 Carbonic Anhydrases

As stated above, the CAs are classified in eight evolutionarily unrelated families: α-, β-, γ-, δ-, ζ-, η-, θ- and ι-CAs.[1-12]

The α-CAs are present in vertebrates, protozoa, algae, corals, bacteria and green plants.[1,12] The β-CAs have been identified in bacteria, fungi, Archaea, algae and chloroplasts of both mono- and dicotyledons.[12,25,26] The γ-CAs are encoded in Archaea, bacteria and plants.[9] The δ-CAs were found in marine phytoplankton, such as haptophytes, dinoflagellates, diatoms and chlorophyte prasinophytes,[8] whereas ζ-CAs seem to be present only in marine diatoms.[4] A unique η-CA has been identified to date in the protozoa *Plasmodium falciparum*.[7] Recently, θ-CAs were detected in the marine diatom *Phaeodactylum tricornutum*[11] and the first iota-CA was identified in the marine diatom *Thalassiosira pseudonana.*[5]

A collection of kinetic and X-ray crystallographic data enabled a detailed comprehension of the structure–function relationship in the CAs superfamily.[2,14,27] These metalloenzymes are catalytically effective when a metal ion is bound within the active site cavity. The catalytic system commonly include a metal(II) ion in a tetrahedral geometry, three coordinated amino acid residues, and a water molecule/hydroxide ion completing the coordination sphere. Zn(II) is the metal ion spread in all CA genetic families, but it can be exchanged with Cd(II) in ζ-CAs[4] and Fe(II) is presumably present in γ-CAs in anaerobic conditions.[8] A Co(II) ion can replace the zinc ion in several α-CAs not giving a significant loss of the catalytic efficiency.[8]

1.2 Catalytic Mechanism of Carbonic Anhydrases

$$E\text{-}M^{2+}\text{–}\,OH^- + CO_2 \rightleftharpoons E\text{-}M^{2+}\text{–}\,HCO_3^- \overset{H_2O}{\rightleftharpoons} E\text{-}M^{2+}\text{–}H_2O + HCO_3^- \quad \text{(Eq. 2)}$$

$$E\text{-}M^{2+}\text{–}\,H_2O + B \rightleftharpoons E\text{-}M^{2+}\text{–}\,OH^- + BH^+ \quad \text{(Eq. 3)}$$

In all CA classes the catalytic mechanism occurs in two steps (Eq. 2 and 3). The metal hydroxide species of the enzyme ($E\text{-}M^{2+}\text{-}OH^-$) is that catalytically active. In the first step of reaction this species acts as strong nucleophile (at neutral pH) against the CO_2 molecule bound in a hydrophobic pocket nearby, with consequent formation of HCO_3^-. Therefore, the bicarbonate ion is displaced by a second water molecule and released

outwards (Eq. 2). When a water molecule is bound to the zinc ion, the enzyme is in its acidic, catalytically inactive form. In the second and rate-determining step, the catalytically active metal hydroxide species is regenerated by a proton transfer reaction from the metal bound water to an exogenous proton acceptor or to an active site residue, represented by B in Equation 3.[1-3] The overall catalytic mechanism is shown in Figure 1A. In the catalytically very active isozymes, (such as human isoforms II, IV, VI, VII, IX, XII, XIII and XIV), the proton transfer process is assisted by a histidine residue placed at the entrance of the active site (His64 known as "proton shuttle residue"), or by a cluster of histidines (Figure 1B), which protrudes from the rim of the active site to the surface of the enzyme, thus assuring efficient proton-transfer pathways.[2] The absence of His64 in other CAs markedly decreases their catalytic efficiency.

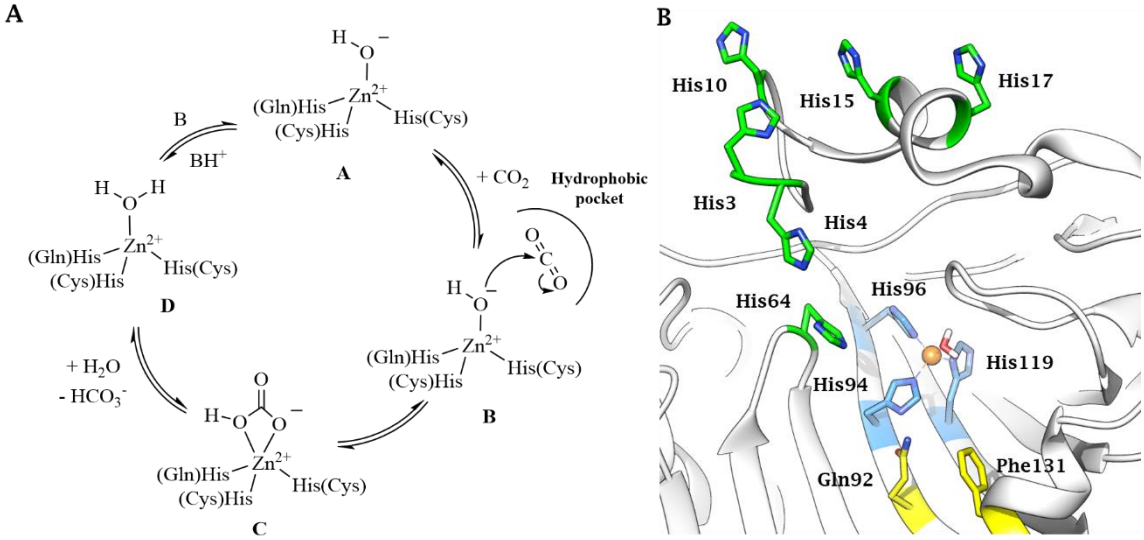

Figure 1. (A) Schematic representation of the CA catalytic mechanism; (B) His64, known as "proton shuttle residue" and cluster of His residues which ensure an efficient proton-transfer pathway (shown in hCA II, PDB 3KKX).

A catalytic turn-over reaching k_{cat}/K_M values over 10^8 M^{-1} x s^{-1} in some α- and ζ-CAs places CAs among the most efficient natural catalysts.[28] This efficient catalysis is also due to a peculiar architecture common among all CA families that differentiates the active site in two very different environments: one is made of hydrophobic residues and the other is lined by hydrophilic amino acids.[14,28] Indeed, a possible explanation assigns to the hydrophobic part the role of entrapping the CO_2 molecule and identifies in the hydrophilic one the escape outwards of the polar species produced by the CO_2 hydration

reaction.[2] The latter process was demonstrated at least for the protons, which are aided by a network of water molecules and His residues to reach the outside of the cavity.[3]

1.3 Characteristics of the Major Families of Carbonic Anhydrases

Here following, the structural characteristics of the main classes of CAs, that are α, β and γ, are discussed. A specific section is dedicated human CAs and their distribution in the human body. The research activity carried out in the present Ph.D. thesis focused CA isoforms belonging to α and β classes as drugs target.

1.3.1 α-Carbonic Anhydrases

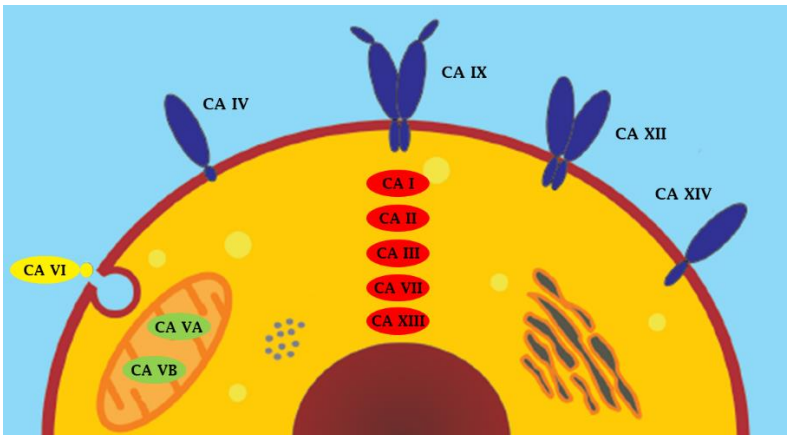

Figure 2. Schematic illustration of domain composition and subcellular localization of catalytically active human α-CAs.

α-CAs are spread in vertebrates, protozoa, algae, corals, bacteria and green plants. A wealth of studies allowed to identify sixteen different isozymes in mammals, and several other isozymes in non-mammalian vertebrates.[1,2] Undeniably, the most important α-CAs subset is represented by the fifteen isoforms identified to date in human.[1-3,17] These isoenzymes differ by molecular features (Table 1), oligomeric arrangement, cellular localization, distribution in organs and tissues, expression levels, kinetic properties and response to different classes of inhibitors.[1-3] Twelve are catalytically active isoforms (I, II, III, IV, VA, VB, VI, VII, IX, XII, XIII, XIV), whereas the remaining three (VIII, X, XI), called CA-related proteins (CARPs), have no activity as they lack one or more histidine residues coordinating the zinc ion in the active site.[1-3]

Table 1. Organ/Tissue Distribution, Subcellular Localization, CO_2 Hydrase Activity and Diseases in which each isoform is involved.

	Organ/tissue distribution	**Subcellular localization**	**k_{cat}/K_M ($M^{-1}s^{-1}$)**	**Diseases in which the isoform is involved**
CA I	Erythrocytes, gastrointestinal tract,	Cytosol	5.0×10^7	Retinal/cerebral edema
CA II	Erythrocytes, eye, gastrointestinal tract, bone osteoclasts, kidney, lung, testis, brain	Cytosol	1.5×10^8	Glaucoma, edema, epilepsy, altitude sickness, cancer
CA III	Skeletal muscle, adipocytes	Cytosol	2.5×10^5	Oxidative stress
CA IV	Kidney, lung, pancreas, brain capillaries, colon, heart muscle, eye	Membrane-bound	5.1×10^7	Glaucoma, retinis pigmentosa, stroke
CA VA	Liver, brain	Mitochondria	2.9×10^7	Obesity, diabetic cerebrovascular disease
CA VB	Heart and skeletal muscle, pancreas, kidney, spinal cord, gastrointestinal tract	Mitochondria	9.8×10^7	Obesity
CA VI	Salivary and mammary glands	Secreted	4.9×10^7	Cariogenesis
CA VII	CNS	Cytosol	8.3×10^7	Epilepsy, neuropathic pain
CA IX	Tumors, gastrointestinal mucosa	Transmembrane	5.4×10^7	Cancer
CA XII	Renal, intestinal, reproductive epithelia, eye, tumors	Transmembrane	3.5×10^7	Cancer, glaucoma
CA XIII	Kidney, brain, lung, gut, reproductive tract	Cytosol	1.1×10^7	Sterility
CA XIV	Kidney, brain, liver, skeletal muscle	Transmembrane	3.9×10^7	Epilepsy, rethinopathies

Human CAs can be grouped into four different subsets depending on their subcellular localization (Figure 2). CA I, II, III, VII, VIII, X, XI, XIIII are cytosolic proteins, CA VA and VB are present in the mitochondrial matrix, CA VI is a secreted enzyme, CA IV is a glycosylphosphatidylinositol (GPI)-anchored protein and CA IX, XII and XIV are trans-membrane isoforms.[13] These enzymes are widely distributed in many tissues and organs where they are involved in a wealth of essential physiological processes. Thus, their

dysregulated expression and/or abnormal activity can result in severe pathological conditions (Table 1).

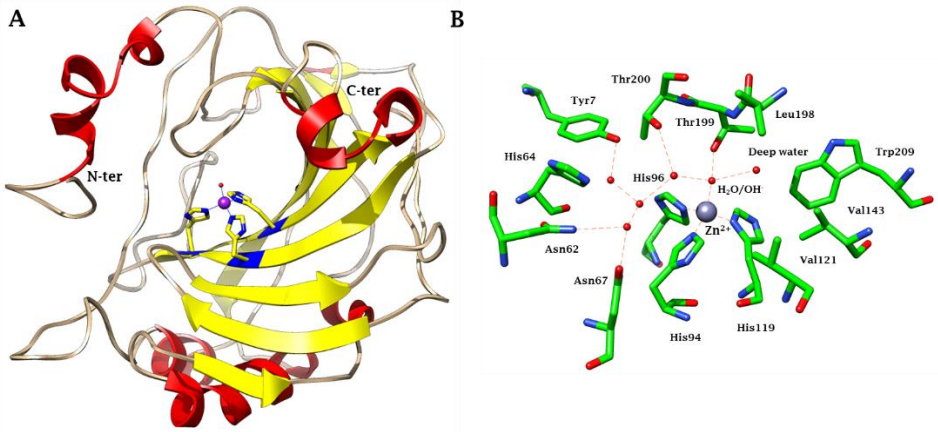

Figure 3. (A) Ribbon diagram of hCA II structure (PDB code 1CA2), which has been chosen as representative CA isoform. The active site Zn^{2+} coordination is also shown. Helix and β-strand regions are coloured in red and yellow, respectively. (B) View of CA II active site. The Zn^{2+} is tetrahedrally coordinated by the three catalytic histidines and a water molecule/hydroxide ion, which is engaged in a well-defined network of hydrogen bonds. Water molecules are indicated as red circles.

The 3D structures of all human isoforms except CA VB was determined which show that these enzymes hold common structural features independently on their subcellular localization. In fact, in agreement with the high sequence identity among hCA isoforms, structural studies have demonstrated that all these enzymes share the same fold characterized by a central ten-stranded β-sheet, surrounded by α- and 3_{10}- helices and additional β-strands (Figure 3A). The active site is located in a large conical cavity, about 15 Å deep, at the base of which the zinc ion is accommodated, coordinated by three conserved histidine residues (His94, His96 and His119) and the solvent molecule/hydroxide ion. The Zn^{2+}-bound water molecule/hydroxide ion is involved in a network of hydrogen bonds which enhance its nucleophilicity (Figure 3B). In particular, it establishes a hydrogen bond with the hydroxyl moiety of the conserved Thr199 residue and with two water molecules, located on two opposite sides: the first one, also called the "deep water", is located in a hydrophobic cavity delimited by conserved residues in position 121, 143, 198, and 209, while the second one is in a hydrophilic environment toward the entrance of the active site (Figure 4A).

As generally stated in paragraph 1.2, these two peculiar active site environments are supposed be responsible of the rapid catalytic cycle of CO_2 to bicarbonate; in fact, the

hydrophobic region is necessary to sequester the CO_2 substrate and orient the carbon atom for nucleophilic attack by the zinc-bound hydroxide (Figure 4B), while the hydrophilic region creates a well-ordered hydrogen-bonded solvent network, which is necessary to allow the proton transfer reaction from the zinc-bound water molecule to the bulk solvent (Figure 4C).[13,28]

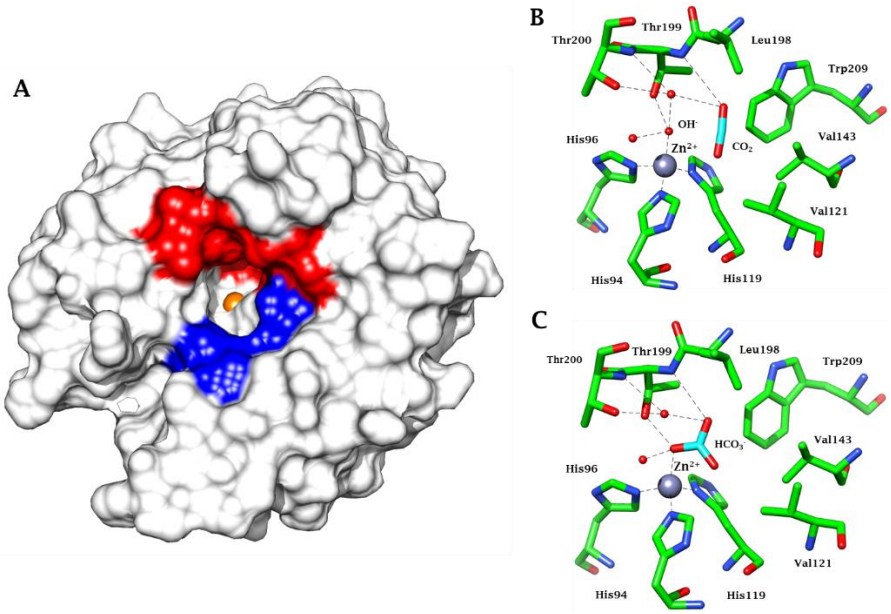

Figure 4. (A) Solvent accessible surface of CA II. Residues delimiting the hydrophobic half of the active site cleft are shown in red (Ile91, Phe131, Val121, Val135, Leu141, Val143, Leu198, Pro202, Leu204Val207 and Trp209), while residues delimiting the hydrophilic one is shown in blue (Asn62, His64, Asn67 and Gln92). Active site of CA II showing: (B) the position of CO_2 molecule (PDB code 2VVA), and (C) the binding of the bicarbonate ion (PDB code 2VVB). The Zn^{2+} coordination and polar interactions are also reported.

A detailed comparison between all hCA isoforms reveals that the main sequence and structural differences between these enzymes are observed in the region 127-136 (Figure 3A), which thus has to be considered a ‘‘hot spot’’ in the structure-based drug design of selective hCA inhibitors.[28] The 12 catalytically active isoforms show also important differences in the quaternary structure; indeed, whereas CAs I-IV, VA, VB, VII, XIII and XIV are monomers, CAs VI, IX and XII are dimers. Interestingly, the dimeric interface is different in each one of these hCA dimers. One of the most important achievements of CA structural studies is the obtainment of 3D models of the full-length CA IX and CA XII. Indeed, in both cases other domains are present beyond the CA catalytic one (Figure 5).[29,30] These models represent an important starting point for the rational drug design of

specific inhibitors with potential applications as diagnostic and therapeutic tools in tumour treatment.

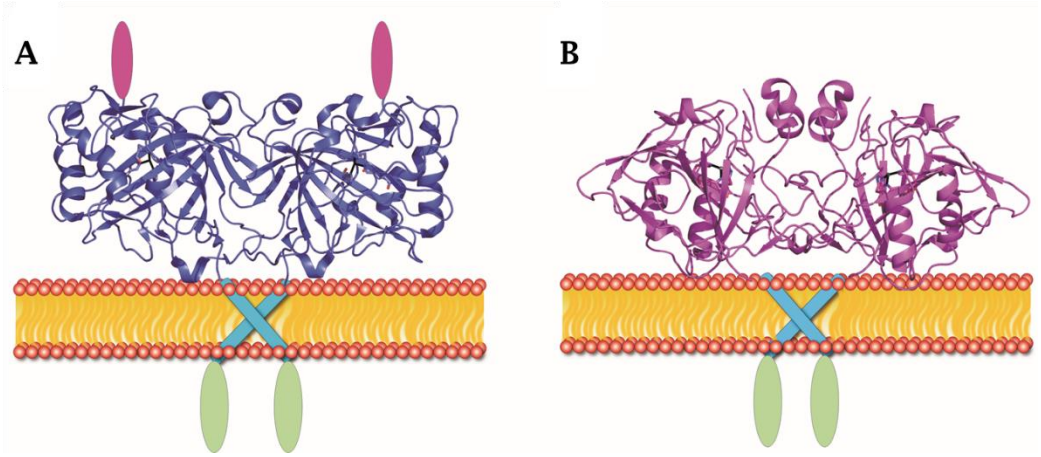

Figure 5. Proposed models of full-length CA IX (A) and CA XII (B) on the cell membrane. Both CA IX and CA XII contain an extracellular CA domain, a transmembrane region (cyan) and an intracellular tail (green). Additionally, CA IX contains a proteoglycan-like (PG) domain (magenta) at the N-terminus.

Differently, the bacterial α-CAs, such as those identified in *Sulfurihydrogenibium yellowstonense*, *Sulfurihydrogenibium azorense* and *Neisseriagonorrhoeae*, are dimers formed by two identical active monomers.[12]

Additionally, α-CAs possess a certain catalytic versatility that enables the fulfilment of several other hydrolytic processes presumably involving non-physiological substrates. These reactions include the hydration of cyanate to carbamic acid (Equation 4), or of cyanamide to urea (Equation 5), the aldehyde hydration to gem-diols (Equation 6), the hydrolysis of carboxylic, sulfonic and phosphate esters (Equations 7-9).[2]

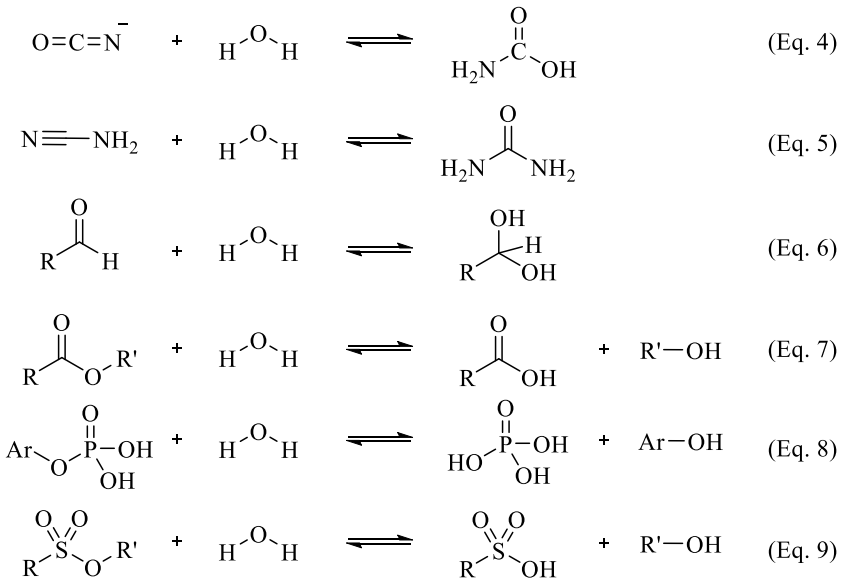

1.3.2 β-Carbonic Anhydrases

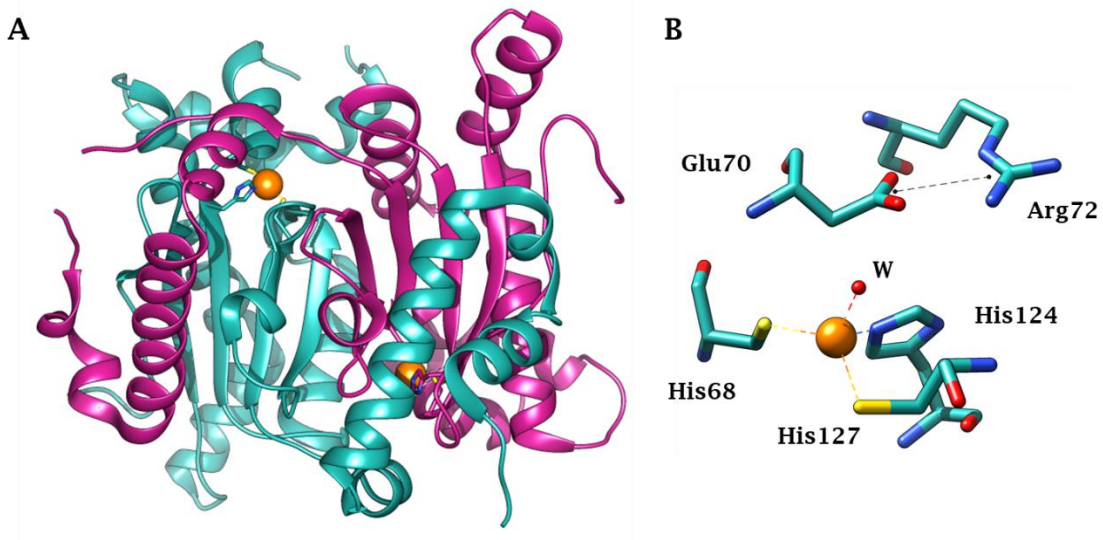

Figure 6. (A) Overall structure of the β-CA from fungi *Cryptococcus Neoformans* (Can2) dimer. One monomer is colored magenta, while the other one is colored sea green. The Zn^{2+} ions are shown as orange spheres. (B) Active site of Can2. Coordination of the active-site Zn(II) by Cys68, His124, Cys127, and a water molecule is shown by colored dashed lines, and Asp70-Arg72 salt bridge is colored black.

The β-class CAs are broadly distributed and identified in plants, yeast, bacteria, archaea, fungi, and invertebrates.[10] Conversely from α-class isozymes, β-CAs are oligomers formed by two or more identical subunits, generally dimers, tetramers and octamers (Figure 6A). The monomers consist primarily of α-helices that surround a 2-1-3-4 ordered β-sheet and show α/β fold unique to these enzymes. The monomer has a molecular weight of 25-30 kDa and the active form of the enzyme requires two subunits to reconstitute the catalytic site.[13,31] The active site exists at the dimer interface and contains hydrophobic and hydrophilic areas similarly to hCAs. The residues of the catalytic triade are highly conserved among β-CA isoforms: the Zn(II) ion is coordinated by two Cys residues, a residue of His and the carboxyl group of a residue of Asp or alternatively a water molecule/hydroxide ion (Figure 6B and Figure 7). The β-CA from fungi *Cryptococcus Neoformans* (Can2) was taken as representative).[10,31]

At a pH of 7.5 or lower, the β-CA active site, formed by residues belonging to two different subunits, is “locked, since the carboxyl group of an aspartic acid coordinates the zinc ion, thus completing the coordination sphere (Figure 7A). For pH values higher than 8.3, the enzyme active site was instead found in its open and active form, due to the salt

bridge that the aspartate residue forms with an arginine residue conserved in all the β-CA.[10,13,21] A molecule of water/hydroxide ion completes the tetrahedral geometry coordination pattern of the metal ion (Figure 7B). The catalytic mechanism of β-CAs with the active site in the "open" form is rather similar to α-class enzymes.

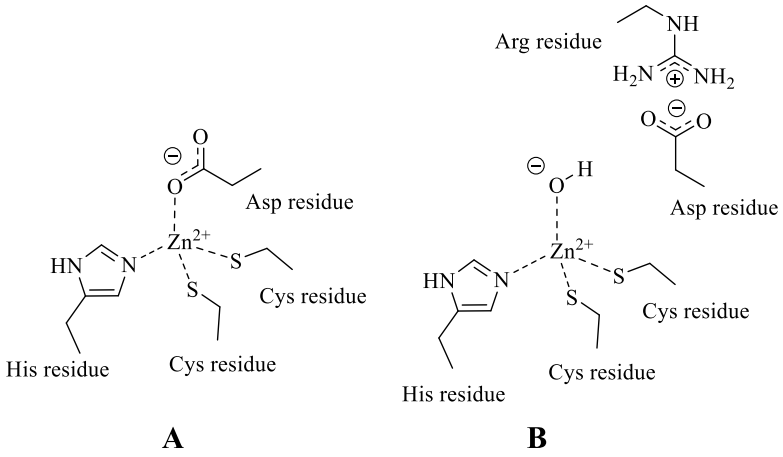

Figure 7. Inactive (A) and active (B) forms of β-CAs active sites.

1.3.3 γ-Carbonic Anhydrases

Up to now γ-Class CAs have been identified in archaea, bacteria and plants.[9] Cam, the carbonic anhydrase from the methanoarcheon *Methanosarcina thermophila*, is the prototype of the γ-class.[32] The crystal structure of Cam showed that one monomer consists of seven complete turns of a left-handed parallel β-helix topped by a short α-helix, followed by a second C-terminal α-helix which is positioned antiparallel to the axis of the β-helix (Figure 8A).[32] Each face of the beta-helix is comprised of parallel beta-strands, containing two or three residues each, and is connected to the subsequent face by a 120° turn, so that the cross section of the β-helix resembles an equilateral triangle. Each turn of the β-helix contains two type II β-turns positioned between strands 1 and 2 and between strands 2 and 3 and is completed by a loop, connecting strand 3 with strand 1 of the next turn. The interior of the helix is dominated by hydrophobic interactions between aliphatic side chains of residues originating from equivalent positions in adjacent turns of the helix. The active enzyme is a homotrimer resulting from the packing of three left handed β-helices with the axis all parallel (Figure 8B and 8C). Three residues, Arg59, Asp61 and Asp76, are important amino acids for *trimer* formation. Arg59 forms a salt

bridge with Asp61 of the same monomer and Asp76 of another monomer. These three residues are almost entirely conserved in all proteins sharing homology with Cam.

The active site is localized at the interfaces between two subunits. In the active site a Zn(II) ion is coordinated by His81 and His122, which extend from equivalent positions of adjacent turn of one monomer, and by His117 located in a neighbouring monomer (Figure 8C). Two water molecules complete the zinc coordination sphere forming a distorted trigonal bipyramidal geometry. The two water molecules are within hydrogen bond distance of the side chain of Gln75 and Glu62.[13,32]

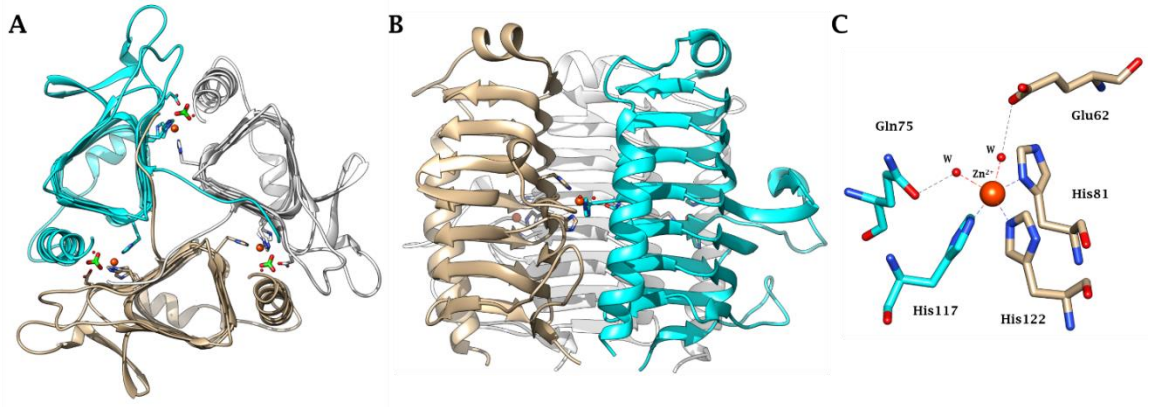

Figure 8. Ribbon representation of the Cam trimer. (A) Top view of the enzyme / HCO_3^- complex (PDB 1QRL). (B) Side view (PDB 1QRG). The overall fold is a left-handed β-helix, consisting of three untwisted, parallel β-sheets connected by left-handed crossovers. (C) Metal coordination within the active site which consists in a distorted trigonal bipyramidal geometry. Residues belonging to different subunits are depicted using different colours.

Chapter 2. Carbonic Anhydrases as drug targets

2.1 Human Carbonic Anhydrases

Human CAs have been the first isoforms to have been studied as drug-targets from both the inhibition and activation standpoints.[1] Human CA inhibitors (CAIs) have written a long pharmacological history in many fields due to the involvement of CAs in a variety of important physio/pathological processes such as respiration, pH regulation, calcification, gluconeogenesis, lipogenesis or tumorigenesis.[15-24] In contrast, CA activators have been much less studied to date.[13,33] Nonetheless, as a subset of CAs is abundant in the brain and was shown to be activatable by drug-like compounds, the possibility to design agents that enhance cognition have been recently emerging, with potential therapeutic applications in aging and neurodegenerative diseases as well as tissue engineering.[1-4,13]

CAIs of the sulfonamide/sulfamate type have been long used as diuretics, systemic anti-convulsivants, topically acting anti-glaucoma agents or for the treatment of altitude sickness.[1,15-24,34] More recently CAIs have shown promising results as anti-obesity, anti-inflammatory, anti-neuropathic pain and anti-tumor agents/diagnostic tools.[13-24]

CAIs of the first-generation show an isoform promiscuous inhibitory activity, which leads to serious side effects for all pathologies in which they are used.[3] Hence, in the last decades some innovative strategies were adopted to produce isoform-selective sulfonamide-like derivatives as well as new classes of isoform-specific CAIs were produced which showed alternative mechanisms of action. Understanding the factors governing selective inhibition of the single isoforms is clearly of pivotal importance and represents the breakthrough step to yield potential drugs which avoid the serious side effects due to promiscuous inhibition in the treatment of all pathologies in which CAIs will be employed.[3] In fact, the great potential of hCAs as drug targets resides in the wide multitude of diseases that can be targeted by selectively modulating the different isoforms.[34-58]

CA I is abundantly expressed in red blood cells and colon, but is still considered an "orphan target" as it remains an "obscure object" for medicinal chemists.[13,35] Further difficulties have been encountered in developing CA I selective inhibitors.[1] However,

several pieces of evidence have demonstrated that CA I is involved in some types of anemia and chronic acidosis, diabetic macular edema and the proliferative diabetic retinopathy.[13,28]

The deregulation of the activity of the most physiologically relevant CA II has important pathological consequences in one or more tissues, such as glaucoma, edema, epilepsy, and is also involved in other pathologies such as acute mountain sickness[22] and, apparently, atherosclerosis[21] and osteoporosis.[28] CA II is also a target for imaging in various pathological conditions, in organs where the enzyme is present, such as the brain and cerebrospinal fluid or the gastrointestinal tract.[13]

Inhibition of CA III has not been determined to be advantageous for treating several diseases.[13] On the contrary, several natural and non-natural amino acid and aromatic/heterocyclic activators of CA III have been discovered, which might increase the defense mechanism against reactive oxygen species (ROS) in hepatocytes especially in the case of hepatotumorogenesis or infection by hepatitis B or C virus or might be beneficial therapeutics aimed to treat obesity.[28,37] However, because CA III has recently been proposed to be associated with acute myeloid leukemia and the progression of liver carcinoma, CA III specific inhibitors may have potential against in tumor proliferation and invasiveness in myeloid and liver tissue.[50]

CA IV was proven to be a promising drug target in the treatment of glaucoma, inflammation, retinis pigmentosa, some types of brain cancers and stroke.[35-38]

The involvement of CA VA and VB in *de novo* lipogenesis and the clear indications that the antiepileptic drugs topiramate and zonisamide (also potent inhibitors of the mitochondrial CAs) elicit significant weight loss in obese patients suffering with epilepsy led pharmaceutical companies to show interest in hCA V enzymes as novel drug targets for the treatment of obesity.[40] Activators of CA V (probably CA VB) might have clinical potential in diabetes, due to the implication of CA V in glucose-mediated insulin secretion from pancreatic β-cells.[28] CAVA has been also recently proposed as a specific target for prevention of diabetic cerebrovascular pathology.[13]

It could be speculated that the caries-inducing effect of CA VI is a result of enzymatic activity, and thus the inhibition of CA VI could reduce carcinogenesis. A CA inhibitor might be added to oral hygiene products, such as toothpaste, mouthwash, tooth varnish, and chewing gum, to reduce the risk for the formation of enamel caries lesions.[43,44]

CA VII might represent a safe drug-target in the treatment of febrile seizure or eventually other epileptiform diseases as it is involved these pathologies and almost uniquely expressed in the central nervous system (CNS).[28,45] As the treatment with acetazolamide in combination with midazolam synergistically reduces neuropathic allodynia after spinal nerve damage,[47] CA VII together with CA II may represent a new drug target for managing neuropathic pain. Considering the importance of pH and ion homeostasis in reproductive organs to ensure a normal fertilization, the use of CA XIII inhibitors could be used for the development of anti-contraceptive agents.[55]

Data are available on the involvement of CA XIV in some retinopathies and epileptogenesis, which make CA XIV inhibitors useful agents for the management of such diseases.[57]

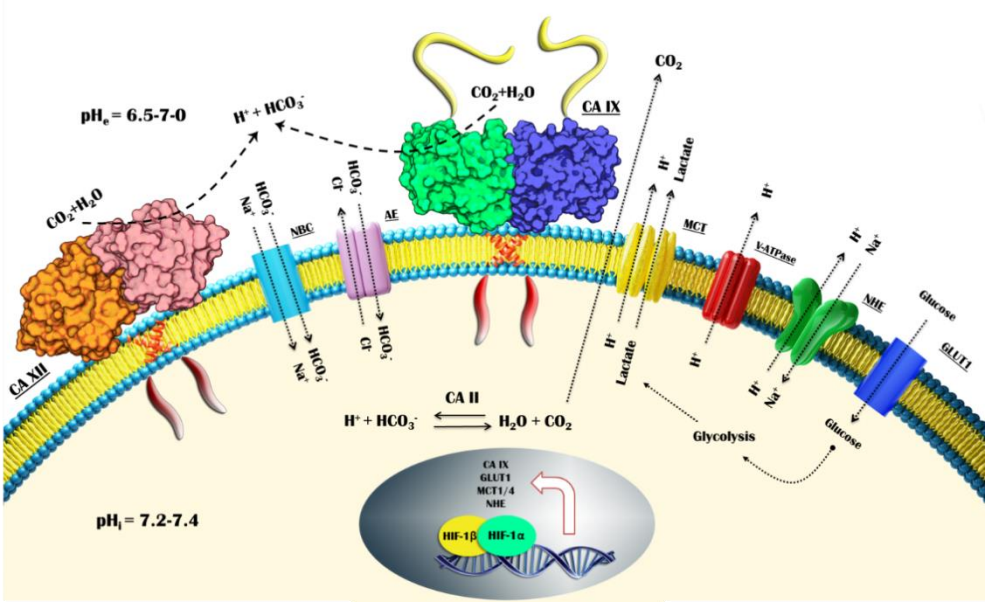

Figure 9. pH modulation machinery in hypoxic tumor cells. HIF-1 upregulates the expression of glucose transporters (GLUT1), glycolytic enzymes and proteins involved in pH regulation: monocarboxylate transporter (MCT), V-type H^+ATP (V-ATPase), Na^+/H^+ exchanger (NHE), bicarbonate co-transport (NBC), anion exchanger (AE), carbonic anhydrase IX (CA IX) and XII (CA XII).

The tumor (and inflammation) associated CA IX and XII deserve a specific section as main focus of the Ph.D. thesis. These CAs were consistently validated as drug-targets and markers of disease progression in many solid tumors.[23,48,49] Overexpression of tumor-associated CAs is part of tumor cells adaptive responses to hypoxic conditions.[48] In fact, the inadequate delivery of oxygen to tumor cells (hypoxia) does induce a shift to the glycolytic metabolism. The high glycolytic rate of tumor cells leads to an increased

production of acid metabolites, including lactate, carbon dioxide and protons that creates an intracellular acidosis (pH_i) incompatible with the basic cellular functions. To survive and reduce intracellular acidification, cells activate complex molecular mechanisms involving ion exchangers, pumps, transporters and carbonic anhydrases, which maintain a slightly alkaline pH_i acidifying the extracellular environment (pH_e) (Figure 9).[23]

CA IX was even more studied in this context being almost uniquely overexpressed in hypoxic tumors by major pathway of HIF-1 transcription factor and serving as prognostic/predictive factor for hypoxic, aggressive, and malignant tumors.[29,49] Nonetheless, both CA IX and XII were shown to be involved in chemoresistance, tumor cell migration, invasion and maintenance of cancer cell stemness.[13,23]

In addition, CA IX and XII were lately identified to be overexpressed in inflamed tissues, being likely implicated in the acidification marking these tissues.[39]

Furthermore, CA XII is also a validated target for the treatment of glaucoma.[34]

The 3D structures are available for all human isoforms except CA VB and are of significant importance for structure-based drug design campaigns for yielding disease-targeting CA selective modulators.[59-68]

2.2 Carbonic Anhydrases from pathogens

CAs are also emerging as innovative targets for the development of anti-infective agents with novel mechanisms of actions to overcome cross resistance shown against various existing anti-microbial drugs. A *plethora* of α-, β-, γ-CAs were cloned and characterized in many bacterial, fungal and protozoan pathogens and were shown to be promising anti-infective targets, though to date no CAI as anti-microbial agent is available for clinical use. CAs are essential in the pathogens life cycle and their inhibition can lead to growth impairment and defects.[15,69] One of the best studied bacterial α-CA is the one from the gastric pathogen provoking ulcer and gastric cancer, *Helicobacter pylori*.[70-72] In fact, the genome of *H. pylori* encodes two CAs with different subcellular localization: a periplasmic α-class CA (hpαCA) and a cytoplasmic β-class CA (hpβCA).[70-72] These two enzymes were shown to be catalytically efficient, exhibiting an almost identical activity as the human isoform hCA I in the CO_2 hydration reaction, and are highly inhibited by many clinically used sulfonamides/sulfamates.[72] Since the efficacy of *H. pylori*

eradication therapies currently employed has been decreasing due to drug resistance and side effects of the commonly used drugs, the dual inhibition of α- and/or β-CAs of *H. pylori* could be applied as an alternative therapy against the infection or for the prevention of gastroduodenal diseases provoked by this widespread pathogen.[71,72]

Vibrio cholerae is a Gram-negative bacterium, causative agent of cholera, that colonizes the upper small intestine where sodium bicarbonate, an inducer of virulence gene expression, is present at a high concentration. *V. cholera* utilizes the CA system to accumulate bicarbonate into its cells, thus suggesting a pivotal role of this metalloenzymes in the microbial virulence.[73] *V. cholera* encodes CAs of three distinct classes, which are called VchCAα, VchCAβ and VchCAγ. These enzymes are efficient catalysts for CO_2 hydration.[73,74]

CAs are also abundantly spread in fungi and yeasts.[21,75-80] *Saccharomyces cerevisiae*,[79] *Candida albicans*[75,76] and *Candida glabrata*[76,77] have only one β-CA, whereas multiple copies of β-CA- and α-CA-encoding genes were reported in other fungi.[78] A recent work demonstrated that these CAs play an important role in the CO_2-sensing of the fungal pathogens and in the regulation of sexual development.[77] Finally, another yeast, which has been investigated in detail for the presence of CAs is *Malassezia globosa*, which induced the production dandruff.[80] As the above-mentioned fungi/yeasts, it contains only one β-CA, denominated MgCA. Few protozoan parasites have been investigated for the presence and druggability of CAs. The malaria-provoking *Plasmodium falciparum* encodes the unique example of η-CA identified to date.[7,78-83] An α-CA has also been cloned and characterized in the unicellular protozoan *Trypanosoma cruzi*, the causative agent of Chagas disease.[74-85] The enzyme (TcCA) has a very high catalytic activity for the CO_2 hydration reaction, being similar kinetically to the human isoform hCA II.

In addition, another β-CA from the unicellular parasitic protozoan *Leishmania donovani chagasi* (LdcCA), which causes visceral leishmaniasis was identified, cloned, and characterized.[86]

2.3 Main Categories of Carbonic Anhydrase Inhibitors

The mechanisms through which CAs are inhibited or activated have been studied for decades and are well-understood processes. However, new discoveries in the field

continuously emerge.[3,87-127] Four inhibition mechanisms have been kinetically and structurally validated, while a significant subset of CA inhibitors lacks mechanistic characterization yet. A superimposition of compounds binding to the representative CA II by four distinct inhibition mechanisms is depicted in Figure 10 and a classification is reported below:

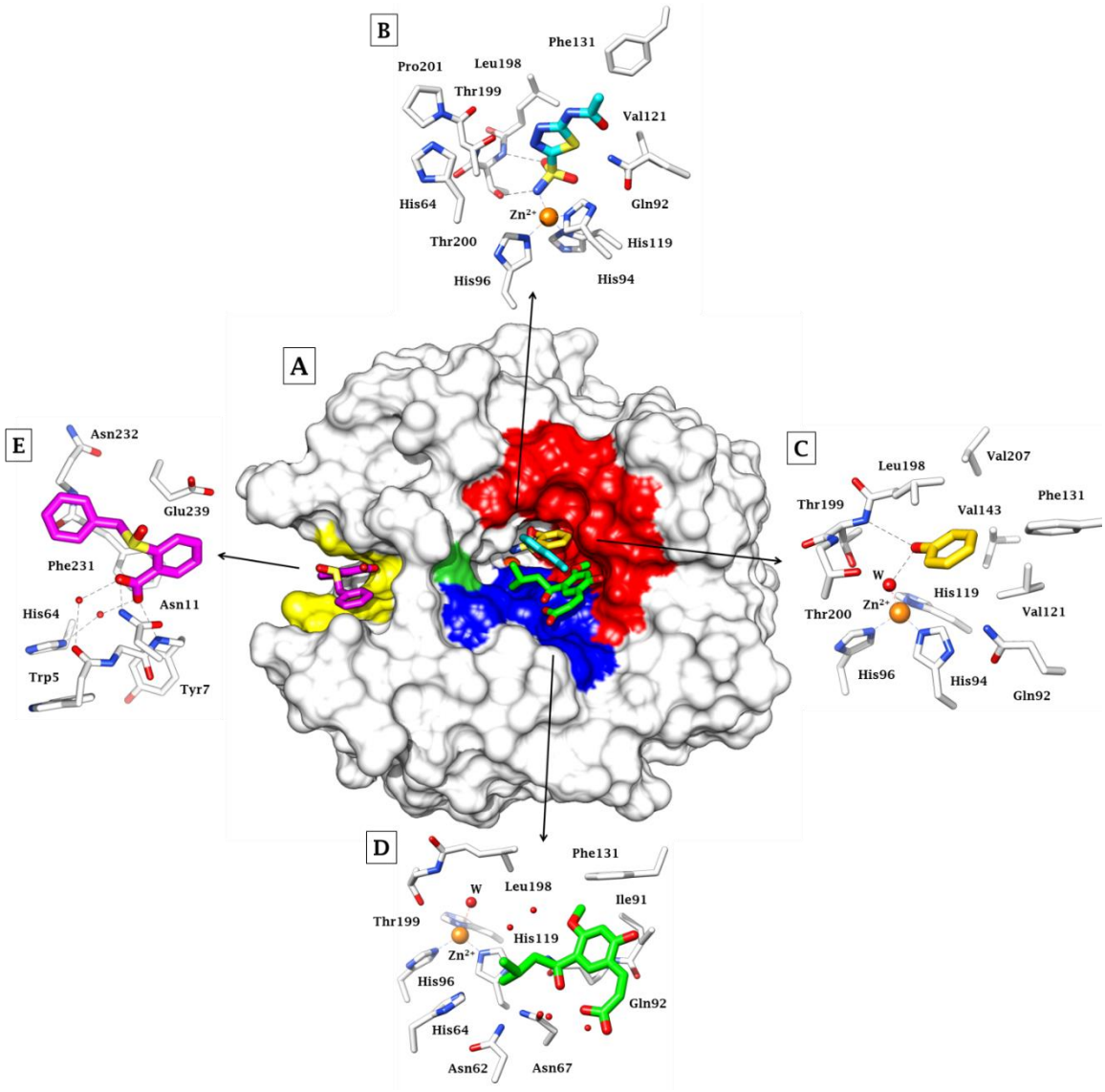

Figure 10. (A) hCA II active site with three superimposed inhibitors: acetazolamide (blue); phenol (yellow), hydrolyzed natural product coumarin (green). The hydrophobic half of the active site is colored in red, the hydrophilic one in blue. His64, the proton shuttle residue is in green (surface representation) (PDB files codes: 3HS4, 3F8E, 4QY3). The hydrophobic adjacent pocket where inhibitors bind outside the active site is shown in yellow with a benzoic acid derivative represented in magenta. The detailed interactions for the binding of the four inhibitors, with their different inhibition mechanisms are shown in (B) for acetazolamide, (C) for phenol, (D) for the 2-hydroxy-cinammic acid derivative and (E) for the benzoic acid derivative.

- the zinc-binders, among which inorganic anions, sulfonamides and their bioisosters (sulfamates, sulfamides, etc), dithiocarbamates (and bioisosters), hydroxamates, carboxylic acids, phosphates, benzoxaboroles (Figure 10B).[91-111]
- compounds that anchor to the zinc-bound water molecule/hydroxide ion, such as phenols, polyamines, sulfocoumarins, thioxocoumarins (Figure 10C).[112-119]
- compounds that occlude the entrance of the active site, namely coumarins and their bioisosters (Figure 10D).[120-127]
- compounds binding out of the active site (this inhibition mechanism has been shown for 2-(benzylsulfonyl)-benzoic acid – Figure 10E).[128]

Compounds such as secondary/tertiary sulfonamides, N-substituted saccharin, imatinib and nilotinib inhibit specific CA by unknown mechanism of action.[129,130]

The three main subsets of CAIs are discussed below.

2.3.1 Zinc binders

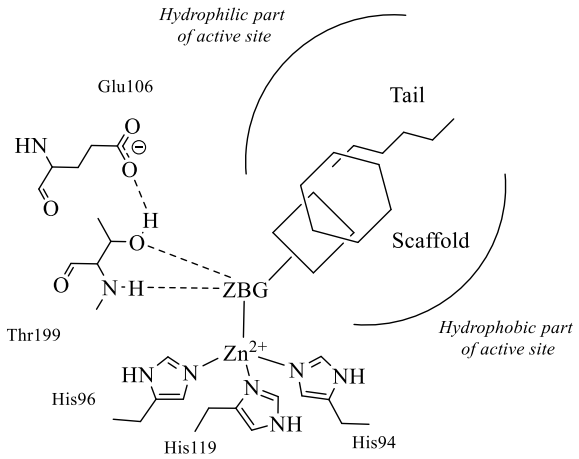

Figure 11. Schematic illustration of the key interactions between a zinc-binder and a representative human CA active site.

Compounds containing a zinc binding group (ZBG) directly coordinate the metal ion with a tetrahedral or trigonal bipyramidal geometry, displacing the zinc-bound nucleophile (water molecule or hydroxide ion; Figure 11).[1-3,81] In addition, the ZBG interacts with various residues nearby the metal ion, mainly by hydrogen bonds (such as with Thr199, a conserved residue in all α-CAs), whereas the scaffold of the inhibitor participates in several other interactions with the hydrophilic and/or hydrophobic areas of the active site. The sulfonamide group ($R\text{-}SO_2NH_2$) is the most important and widely used zinc binding

function for designing CAIs,[87-91] with at least 20 such compounds in clinical use for decades or clinical development in the last period (Figure 12).[87-93]

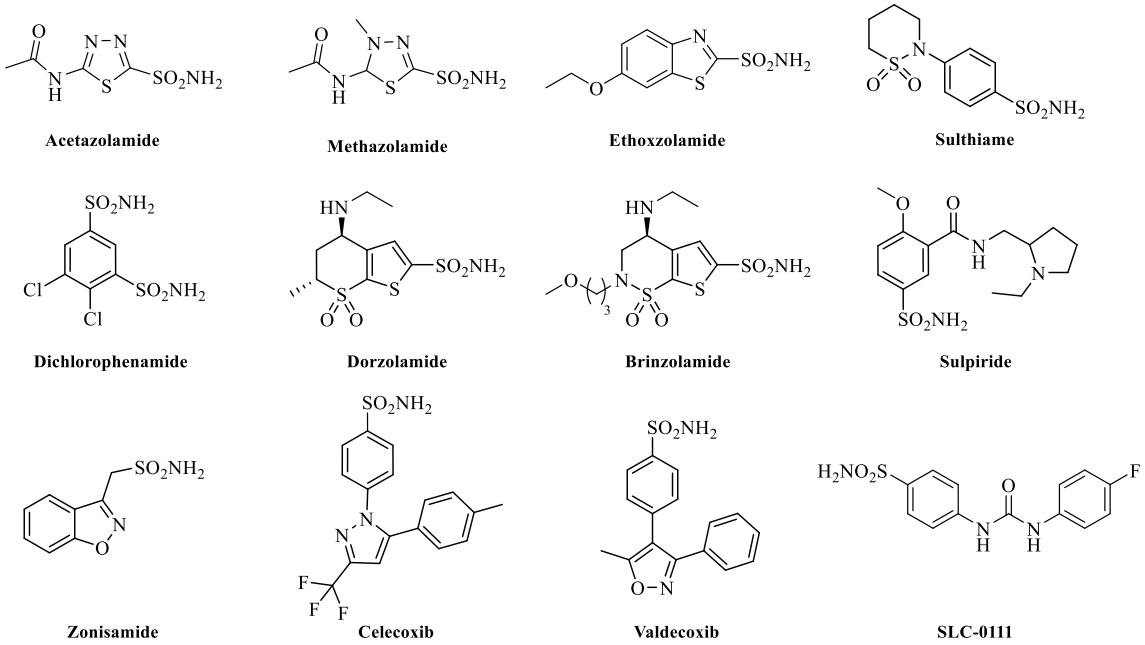

Figure 12. Examples of clinically used or studied sulfonamides.

A wealth of X-ray crystallographic evidences showed the binding mode of the zinc-binder type CAIs, to which sulfonamides and their bioisosters sulfamates and sulfamides belong. The latter binds in deprotonated form to the Zn(II) ion from the enzyme active site, replacing the zinc-bound water molecule and retaining the tetrahedral coordination geometry (Figure 13).[1,2,90,91,93]

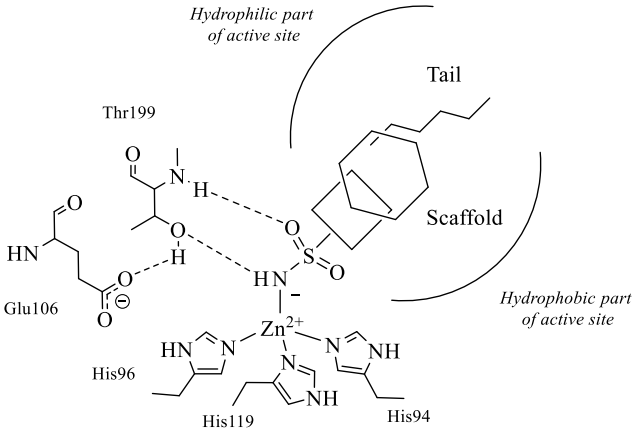

Figure 13. Schematic illustration of the key interactions between a primary sulfonamide and the hCA II active site as determined by X-ray crystallography.

It is commonly accepted that the sulfonamide group is the ideal ZBG for the CAs as it combines a negative charge of the deprotonated nitrogen with the positively charged zinc ion and, on the other hand, the presence of one proton on the coordinated nitrogen atom satisfies the hydrogen bond acceptor character of Thr199 OG1 atom.[1-3,27]

The first- and second-generation sulfonamide CAIs and their sulfamate/sulfamide analogs act as non-selective and rather efficient inhibitors of all CA isoforms. The consequence of this inhibition profile is the multitude of undesired side effects due to inhibition of isoforms not involved in the targeted pathology. This was and it is in fact the main drawback of the first- and second-generation CAIs, although they are still in clinical use.[1-3] As most differences among hCAs active site occur at the entrance of the cavity, compounds which would interact with that part may lead to isoform-selective inhibitors. The idea to attach "tails" to the scaffolds of the sulfonamide inhibitors thus emerged in 1999,[91-93] and indeed led to a certain degree of isoform selectivity already with the initial derivatives for which it has been proposed. Originally conceived for the design of water soluble, antiglaucoma sulfonamides,[96-98] the tail approach was subsequently extended for the design of a multitude of CAIs possessing a variety of desired physico-chemical properties, among which membrane impermeability,[98] enhanced liposolubility,[97] and more importantly, isoform-selective inhibitory profiles.[3] In fact, nowadays it is the most used synthetic approach for designing CAIs belonging to a variety of classes. The main outcome to date of the application of the tail approach is an ureidobenzenesulfonamide **SLC-0111** (Figure 12), selective inhibitor of CAs IX and XII over CAs I and II, which successfully completed Phase I clinical trials for the treatment of advanced, metastatic hypoxic tumors over-expressing hCA IX, and is currently in Phase Ib/II clinical trials in a multi-center, open-label study of oral in combination with gemcitabine (administered *i.v.*) in subjects affected by metastatic pancreatic ductal adenocarcinoma.[99,100]

Beyond sulfonamides, in the last period a multitude of new ZBG for CAs have been identified, among which carboxylates,[105,106] hydroxamates,[107,108] phosphonates[109] and lately crucial advances have been made in this field with mono- and dithiocarbammates,[101-103] xanthates,[103] thioxanthates,[103] boroles,[110] phosphonamidates[109] and selenols[111] identified as novel zinc-binders. X-ray crystallographic evidence was achieved for dithiocarbamates (Figure 14A) and their derivatives,[101] hydroxamates,[107] some carboxylates,[105] one phosphonate,[109] and some boroles (Figure 14B).[110] It should be

stressed that a certain versatility was observed in the binding mode of some such ZBGs, with hydroxamates and boroles coordinating the metal ion in monodentate or bidentate manners.[91]

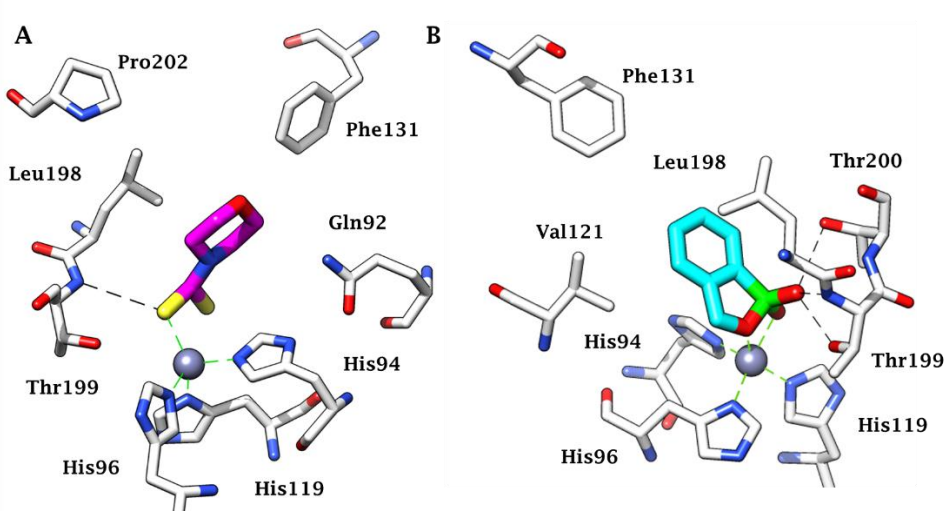

Figure 14. Active site view of the hCA II adduct with (A) a DTC (PDB 3P5A) and (B) benzoxaborole (PDB 5JQT).

2.3.2 Anchorage to the metal-bound water/hydroxide ion

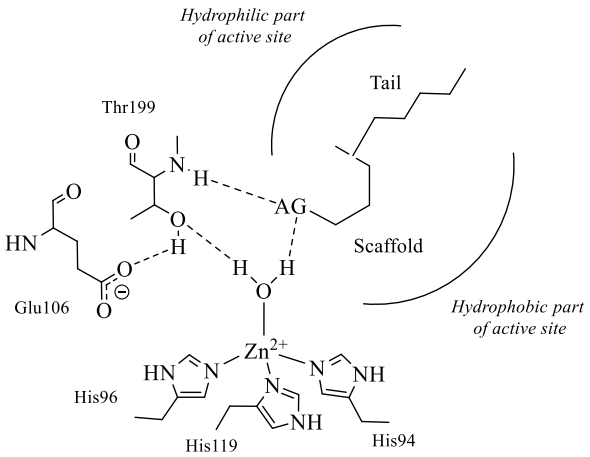

Figure 15. Compounds which anchor to the Zn(II)-coordinated water molecule/hydroxide ion. The anchoring group (**AG**) is of the phenol, amino, carboxylic acid, ester (COOR), sulfonate type.

Phenols, polyamines (*e.g.* spermine and spermidine), some carboxylates, sulfocoumarins (after having been hydrolysed by the sulfatase activity of α-CAs to the corresponding hydroxyphenyl-ω-ethenylsulfonic acid), and thioxocoumarins have been chronologically shown to anchor to the zinc-bound water molecule/hydroxide ion by means of X-ray

crystallography (Figure 15).[112-119,131] The anchoring is granted by a H-bond between the zinc-ligand and a precise anchoring group (AG) in the inhibitor of the OH, NH_2, COOH, $COOCH_3$ and SO_3H type. As in the case of zinc-binders, the ligand/target adduct is stabilized by further interactions the inhibitor scaffold establishes with amino acid residues from the active site.

The phenol is anchored to the Zn-bound hydroxide ion (preponderant species at the pH at which the experiments were done) by a hydrogen bond between the donor zinc bound hydroxide ion and the ligand OH.[112] In addition, a second hydrogen bond involves the gate-keeping residue Thr199, whose backbone NH group participates in a second hydrogen bond with the phenol (Figure 16A). Spermine binds in a rather similar manner as phenol, although with a slightly different network of hydrogen bonding (Figure 16A).[114] Thus, one of the primary amine moieties of the inhibitor, probably as ammonium salt, anchors by means of a hydrogen bond to the zinc-coordinated water molecule/hydroxide ion, and also makes a second hydrogen bond with the side chain OH group of Thr199. The other terminal primary amine of spermine participates in hydrogen bonding with Thr200 and Pro201 (Figure 16B). The sulfonic acid from the hydrolized sulfocoumarin derivative was found to anchor to the Zn-bound hydroxide ion, thus making this CA inhibition mechanism much more general than initially considered when phenols were discovered as inhibitors (Figure 16C).[118]

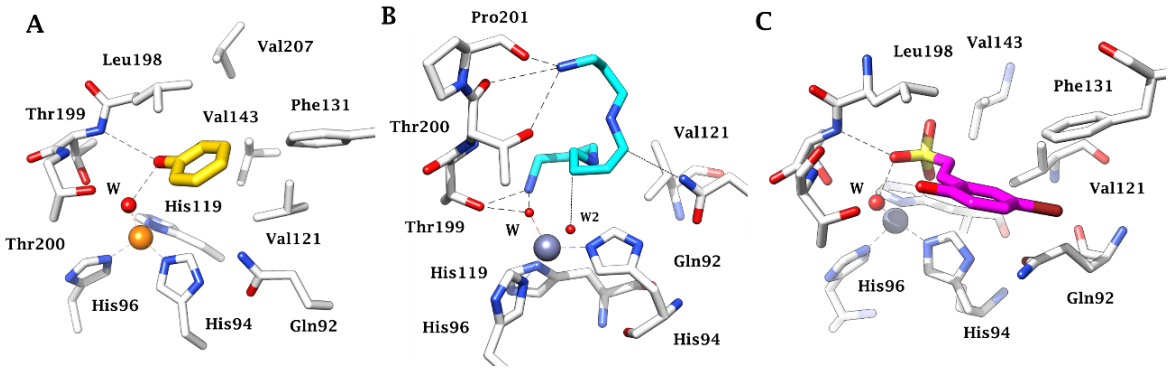

Figure 16. Active site view of the hCA II adduct with (A) phenol, (B) spermine (PDB 3KWA) and (C) hydroxyphenyl-ω-ethenylsulfonic acid deriving from sulfocoumarin hydrolysis (PDB 4BCW).

2.3.3 Occlusion of the active site entrance

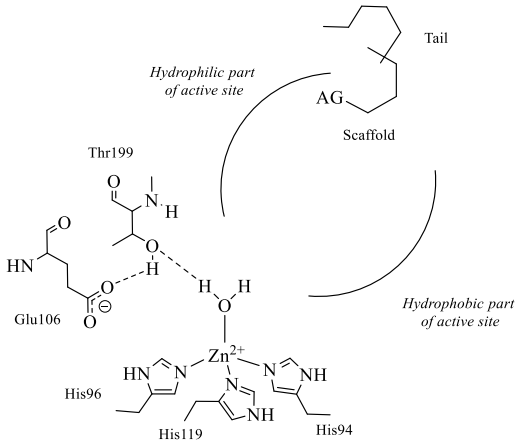

Figure 17. Schematic representation of compounds occluding the entrance to the active site. **AG** represents an anchoring group, of the phenol, carboxylic acid or amide type for sticking at the entrance of the active site cavity whereas the tail, when present, interacts with residues at the outer edge of the cleft.

The third main CA inhibition mechanism consists in the active site entrance occlusion (Figure 17). These inhibitors bind further away from the metal ion compared to the zinc binders in compounds anchoring to the zinc coordinated water molecule.[3,81] The occlusion of the entrance of the binding site cavity as inhibition mechanism has been evidenced for the first time for coumarins,[120] but thereafter other compounds such as the antiepileptic drug lacosamide,[121] 5- and 6-membered lactones and thiolactones or quinolinones[123-125] were observed to possess significant CA inhibitory properties probably sharing a common mechanism of action (Figure 18).

X-ray crystallography studies primarily conducted on the coumarin derivatives isolated from the Australian plant *Leionema ellipticum* showed that coumarins (as the sulfocoumarins) acts as prodrug - at least- in human CAs and are hydrolysed to the active species 2-hydroxycinnamic acids by the CA esterase activity (Figure 18).[120] In fact, unexpectedly the electron density data for the hCA II adduct with coumarins revealed that the actual inhibitory species is the coumarin hydrolysed form that, depending on how bulky the moieties attached on the scaffold are, might bind as *cis* isomers (Figure 19A) or as *trans*-isomers (Figure 19B). Indeed, for not bulky substitution pattern on the coumarin scaffold the trans isomer was observed in the CA active site, whereas for bulkier such groups the isomerization did not occur.

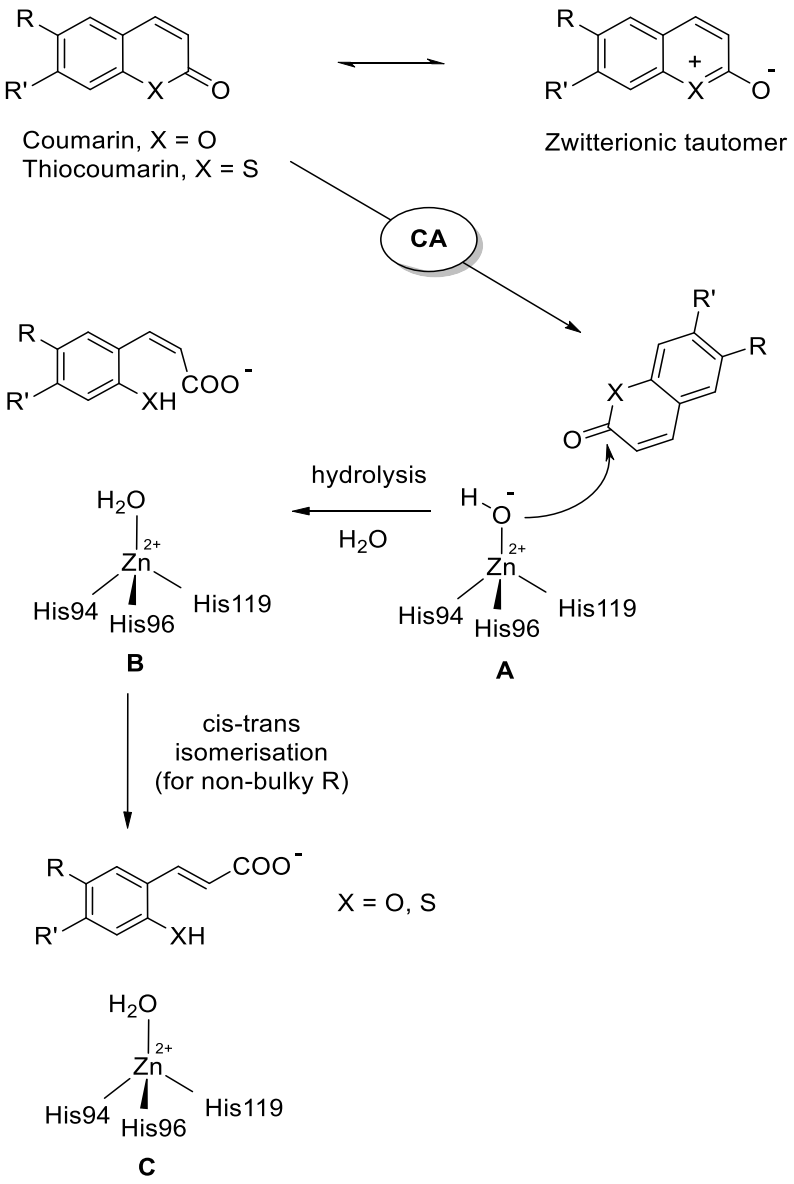

Figure 18. Proposed inhibition mechanism of CAs by coumarins/thiocoumarins, leading to *cis*- or *trans*-2-hydroxy/mercapto-cinnamic acids. A) Hydrolysis of the lactone ring. B) Movement of the hydrolysis product (as *cis* stereoisomer) towards the entrance of the active site cavity. C. *Cis-trans* isomerisation of the hydrolysis product.[121]

The most notable aspect of this inhibition mechanism is the fact that the inhibitors bind in an active site region where most significant differences in the amino acid compositions among hCAs occur.[1-3] This produces important consequences in the inhibition profiles exhibited by such a class of derivatives which showed a unique isoform-selective action. In fact, wide series of diversely substituted coumarin/thiocoumarin derivatives were investigated which reported significantly selective inhibition against isoforms such as CA IX, XII, XIII and XIV over the ubiquitous CA I and II.[120-127]

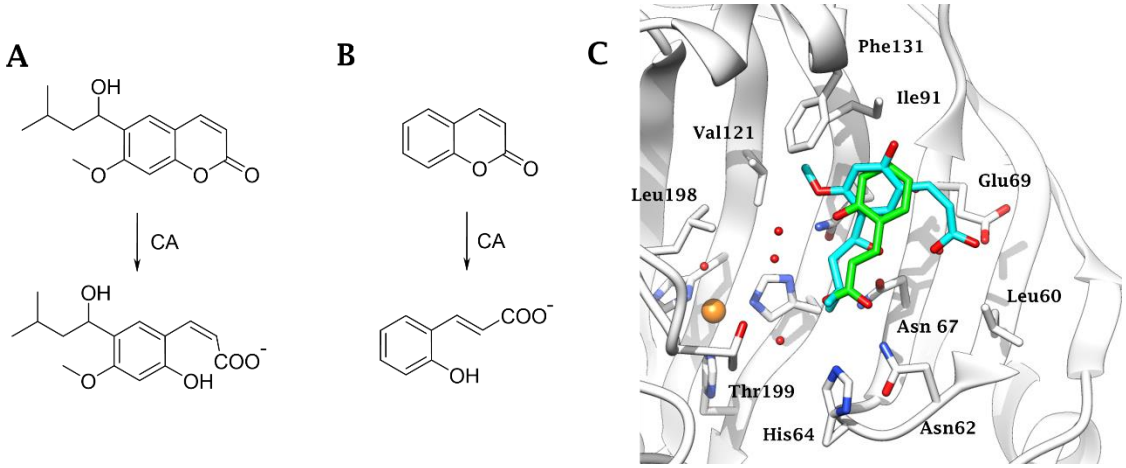

Figure 19. CA-mediated hydrolysis of (A) the coumarin extracted from *Leionema ellipticum* and (B) coumarin. (C) Active site view of the superimposed hCA II adducts with of the coumarins hydrolysis products shown in panel A (blue, PDB 3F8E) and B (green PDB 5BNL).

2.4 Carbonic Anhydrase Activators

CA activation with biogenic amines, such as histamine, amino acids and peptides was reported in the early 40s, but it was validated only in the late 90s.[1] Using methods such as stopped-flow kinetic assays, spectroscopy and X-ray crystallography, the CA activators (CAAs) were shown take part in the catalytic cycle, as shown in equation 10 below.[33,132-134]

$$EZn^{2+}–OH_2 + A \rightleftharpoons [EZn^{2+}–OH_2 \text{ - } A] \rightleftharpoons [EZn^{2+}–HO^- \text{ - } AH^+] \rightleftharpoons EZn^{2+}–HO^- + AH^+ \quad \text{(Eq. 10)}$$

The CAA binds within the enzyme active site with formation of enzyme – activator complex, in which the activator participates to the rate-determining step of the catalytic cycle, which is the proton shuttling between the zinc coordinated water and the reaction medium. In many CA isoforms, His64 placed in the middle of the CA active site plays this role through its imidazole moiety with a pK_a in the range of 6-7.[33] In the enzyme-activator complexes, this proton transfer reaction is achieved in a more efficient manner both by His64 and the activator molecule. The activator does not influence K_M (the affinity for the substrate) but has an effect on k_{cat} of the enzyme-catalyzed reaction, leading thus to the efficient formation of the nucleophilic species of the enzyme ($EZn^{2+}–HO^-$).[13,33]

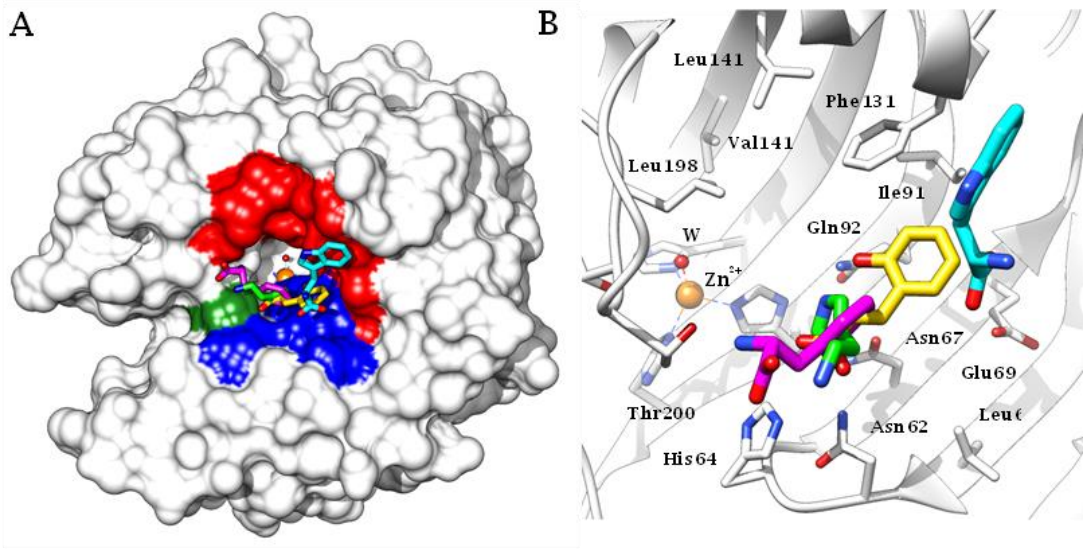

Figure 20. hCA II complexed with CAAs and the hydrolyzed coumarin (2-hydroxycinamic acid). Histamine is shown in green (PDB 1AVN) D-Phe in magenta (PDB 2EZ7) and D-Trp in cyan (PDB 3EFI). 2-Hydroxycinnamic acid (in yellow, PDB 5BNL) is also superimposed to the hCA II – activator adducts. a) Complete view of the enzyme / ligands superimposed adducts. b) Active site view of the three activators and the hydrolyzed coumarin in a slightly different orientation, compared to panel A.

To date, several X-ray crystal structures of CAAs bound to several hCA isoforms have been reported (Figure 20).[132-137] The histamine–hCA II adduct crystallography was the first published such study,[132] and successively activators of the amines and amino acid type, such as L- and D-His, L- and D-Phe, D-Trp and L-adrenaline were studied by this technique.[3,13,132-137] All these activators except D-Trp bind in the same region of the CA active site, which has been denominated the activator binding site A (Figure 20).[33] In this position, at the entrance of the active site and not far away from His64, the activator participates in favorable interactions with several amino acid residues and water molecules, supplementing the proton shuttling effects of His64.

It is supervising the activator binding site and the coumarin-binding site are in fact superimposable, as shown in Figure 20.

A series of drug design studies are also available for CAAs, mainly using histamine and histidine as lead molecules.[3,33] Some of these compounds showed increased affinity for many CA isoforms (compared to histamine), but the level of isoform selectivity achieved up to now is very poor.[3]

Part II

Chemistry and Enzyme Kinetics Projects

Chapter 3. At the Forefront of Medicinal Chemistry with Multi-Target Strategies Including Carbonic Anhydrases Inhibitors

3.1 Scope of the thesis: drug-design, synthesis and biological evaluation of molecular hybrids including CAIs for treating a multitude of diseases

In the context of pharmacologic strategies hitting multiple targets in physio-pathological processes, the choice of multi-potent agents is spreading worldwide overwhelming the co-administration of multiple drugs.[138-141] In fact, pharmacokinetic and metabolic issues deriving from multiple drugs intake are reduced by administration of a single multi-target agent, which provides an improved pharmacokinetic, better patient compliance, reduced drug-drug interactions as well as a synergistic effect in the treatment of the pathology.[138]

It is important to correctly accomplish the molecular hybridization approach between scaffolds affecting the distinct targets to avoid the loss of multi-target action. The achievement of balanced hybrids which equally affect the two systems is desirable to trigger a synergic effect at the biological level.[140]

The involvement of CAs in a multitude of diseases, mainly in an isoform-specific manner, have paved the way for decades to combination therapies such as in the case of eye drops for the treatment of glaucoma.[3] Moreover, it should be noted that even **SLC-0111**, which successfully completed Phase I clinical trials for the treatment of advanced, metastatic hypoxic tumors over-expressing CA IX, is currently in Phase Ib/II clinical trials in combination with gemcitabine (administered *i.v.*) in subjects affected by metastatic pancreatic ductal adenocarcinoma because of an intense synergic anticancer efficacy.[100]

Hence, it is now time to exploit the validated efficacy of CA inhibition in the treatment of many disorders such as cancer, inflammation, glaucoma, infections, by the extensive design of multi-target CAIs which has been limited to few studies up to now.

In the present Ph.D. thesis several multi-target strategies including CAIs have been designed with the main aim of hitting inflammation, glaucoma and cancer. My work included both design, synthesis and *in vitro* kinetic evaluation of the molecular hybrids. All projects were supervised by Dr. Alessio Nocentini (except for Project/Series A, supervised by Dr. Fabrizio Carta). In addition, I performed further enzyme kinetic studies

to characterize *ex novo* new CAs isolated for the first time by the pathogenic protozoa *Entamoeba histolytica* and from the coral *Stylophora pistillata.*

The discussion of the research done in the Ph.D. period will be discussed below according to the several undertaken projects.

3.2 Design and Synthesis of Novel Nonsteroidal Anti-Inflammatory Drug and Carbonic Anhydrase Inhibitor Hybrids for the Treatment of Rheumatoid Arthritis (Series A)

Rheumatoid arthritis (RA) is a chronic and systemic inflammatory disease caused by a faulty autoimmune response, which primary affects the lining of the joints, thus causing erosion of the cartilage, bone damage, and joints deformity at the later stages. The dimension and the impact of RA in the society are well reported within the Rochester Epidemiology Project.[142] Data showed that in the period 1995−2007, each year about 4.1% of the American population was diagnosed with RA. The incidence of the disease was strictly age dependent, being present in 0.9% among patients aged 18−34 years, 5.4% among those aged over 85 years, with the peak (8.9%) in the population aged between 65 and 74 years. Data analysis of the same period among gender showed that the incidence rates increased to 2.5% each year in women; conversely a decrease of about 0.5% was observed in men.[142] RA symptoms have high impact on the life quality of the affected patients, who are progressively unable to carry out activities in every domain of their lives such as work, social relations, and leisure.[143,144]

A number of studies have shown high hydrogen ions concentration in various inflammatory diseases, such as RA and its pediatric form defined as juvenile idiopathic arthritis (JIA).[39] Therein, local acidosis has been indicated as the valid linker between inflammation and the associated pain.[143] The pH of the synovial fluid of RA patients was testified to vary according to the intensity of the inflammatory state. In the early inflammatory phases marked by a predominance of polymorphonuclear leukocytes, the concentration of hydrogen ions is relatively low (pH around 7.4), but the progression of inflammation and change in cell type to the mononuclear phagocytic cells drove the pH to values around 6.5.[144] The low pH reduces the proliferation of lymphocytes and polymorphs, impairs chemotaxis and inhibits antibody production. The progressive acidity triggers swelling, pain, stiffness, and redness in the joints. Furthermore, the local pH imbalance can also affect the tissues around the joints, such as the tendons, ligaments, muscles causing at later stages joints deformity up to the loss of joint function.[145]

Several CA isoforms have been identified in joint ailments, including CA I which is over-expressed in the synovium of the patients with ankylosing spondylitis (AS).[38,146-148]

Transgenic mice over-expressing CA I showed aggravated joint inflammation and destruction.[10] Furthermore, antibodies to CA III and IV have been identified in rheumatoid arthritis.[11] The latter study also witnessed that the CA activity in RA was significantly higher than that of the control groups.

The first report of the potentiality of CAIs as antiarthritic drugs dates back to 1991.[12] Nolan et al. showed that sulfonamide CAIs, such as acetazolamide (AAZ), ethoxzolamide (ETZ), methazolamide (MZA), and dichlorphenamide (DCP), reduced paw edema and attenuated the deterioration of the joints of rats with adjuvant arthritis, but the authors ascribed their activity in the chronic model of inflammation to inhibition of bone resorption. As a breakthrough in the field of CA in inflammation, in 2016 Cimaz et al. demonstrated that isoforms CA IX and XII, which are usually expressed in hypoxic tumors, are also overexpressed in inflamed synovium of patients affected by JIA.[6] As stated above, over the last two decades these isoforms have been at the forefront of the research over CA inhibitors area as new targets for the treatment/imaging of hypoxic tumors. The discoveries made on anticancer selective CA IX/XII inhibitors might be applied in the treatment of inflammation with CAIs because as a common aim with antitumor strategies there is the reduction of extracellular acidity avoiding side effects deriving from inhibition of ubiquitous CAs.

State-of-the-art RA pharmacological treatments include two main classes. Disease-modifying antirheumatic drugs (DMARDs), such as methotrexate, are able to slow or stop the course of the disease improving physical function and inhibiting progression of joint damage. On the other hand, therapies that improve symptoms, such as nonsteroidal anti-inflammatory drugs (NSAIDs), that act on cyclooxygenase (COX) or pain medications are used widespread as adjunctive symptomatic therapy to reduce pain and swelling.[25,149,150] Usually a therapeutic RA protocol accounts for the combination of both drug classes along with the recommendation to conduct proper physical activities, with the intent to tackle the symptoms as well as the progression of the pathology.[145,151]

Despite recent progresses in RA treatment, there is still no effective cure. Many research efforts are constantly reported in the literature, thus offering innovative diagnostic tools, new biological targets, and a multitude of potential drug lead compounds.[152-163]

Considering the interplay between various CA isoforms and the arthritis-like diseases, we attempt here to target several of the enzymes presumably involved in this condition by

dual inhibitors incorporating both a CA-binding moiety (of the coumarin type) and a COX inhibitor of the NSAID type, the most widely used pain-relief medication to date.[149] In this first Ph.D. project, we report the design, synthesis of low molecular weight hybrid compounds containing a selective hCA IX and/or XII inhibitor head, such as the coumarin one,[120,121,125,164-166] linked through a physiologically cleavable amide linker to a commercially available, clinically used NSAID tail, of the carboxylic acid type cyclooxygenase inhibitor (indomethacin, sulindac, ketoprofen, ibuprofen, diclofenac, ketorolac, etc.). The ability of such compounds to inhibit the relevant hCAs activity as well as to reduce the pain symptoms was assessed by means of *in vitro* kinetics and *in vivo* RA model, respectively. Our scope was not to investigate cyclooxygenase inhibition role in RA with the hybrid compounds, which is well documented for decades, but to show that CA IX/XII inhibition may represent an additional anti-inflammatory mechanism, poorly investigated at this moment for the management of RA.

The drug design rational of this project is based upon the synthesis of small molecular hybrids containing a selective hCA IX (XII) inhibitor head linked through a physiologically cleavable amide linker to a carboxylic acid NSAID (COX inhibitor) tail in a 1:1 *ratio* (Figure 21).

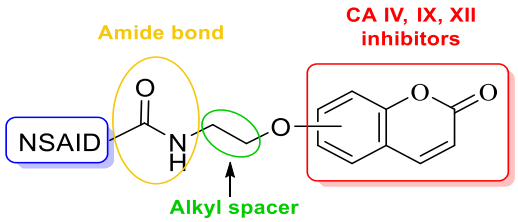

Figure 21. General Structures of amide-based hybrid compounds CAI-NSAID.

As mentioned above, we did not expect COX inhibitory activity of our compounds once the COOH moiety essential for this COX inhibition has been derivatized.[165]

Since the 6- and 7-substituted coumarins are usually reported selective inhibitors of the hCA IX/XII over the other isoforms,[126,127,167,168] we planned our hybrids on these moieties, thus ensuring they are committed with our recent findings on hCA IX and XII overexpression in synovium specimen of JIA affected patients.[39] For the scope of this work we considered a simple two-carbon linear unit spacer connecting the hCA IX (XII) inhibitor head and the NSAID terminal section. In particular, we focused on the ethanolamine fragment, which allows us (i) to insert a physiologically cleavable moiety,

such as the amide, by making use of the NSAID carboxylic function and (ii) to install the biologically compatible and not cleavable ether moiety, thus virtually ensuring a single break point on the hybrid, and (iii) all needed synthetic intermediates are easily accessible by means of efficient procedures.

As reported in Scheme 1, the 6- and 7-coumarin substituted hybrids **A19−34** respectively were obtained by coupling the commercially available NSAIDs **A1-8** by means of their *N*-hydroxysuccinamide (NHS) activated esters **A9-16**, with the *in situ* liberated amines **A17** and **A18** (Scheme 2).

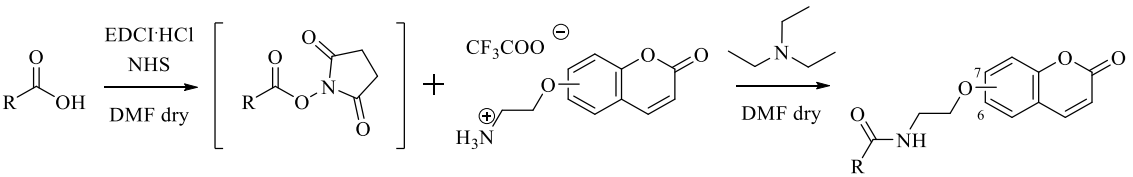

A1=Indometacin **A5**=Dichlofenac
A2=Sulindac **A6**=Flurbiprofen
A3=Ketoprofen **A7**=Naproxen
A4=Ibuprofen **A8**=Ketorolac

Scheme 1. General Synthetic Scheme of Hybrid Compounds **A19-34**.

The key intermediates **A17**, **A18** were obtained by means of Williamson's etherification of the commercially available 6-and 7-hydroxycoumarins with the Boc-protected 1-bromoethylamine **A35**, followed by deprotection with trifluoroacetic acid (TFA) (Scheme 2).

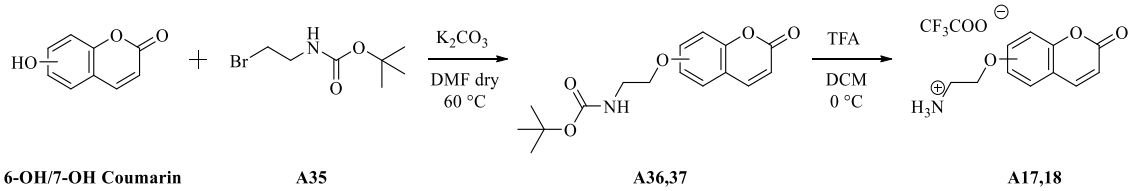

Scheme 2. Synthesis of the Key Intermediates **A17** and **A18**.

All final compounds (Figure 22) as well as their intermediates were characterized by means of ^{1}H, ^{13}C, ^{19}F NMR spectroscopy and High-Resolution Mass Spectrometry (HRMS) and were >95% pure, as determined by High Performance Liquid Chromatography (HPLC).

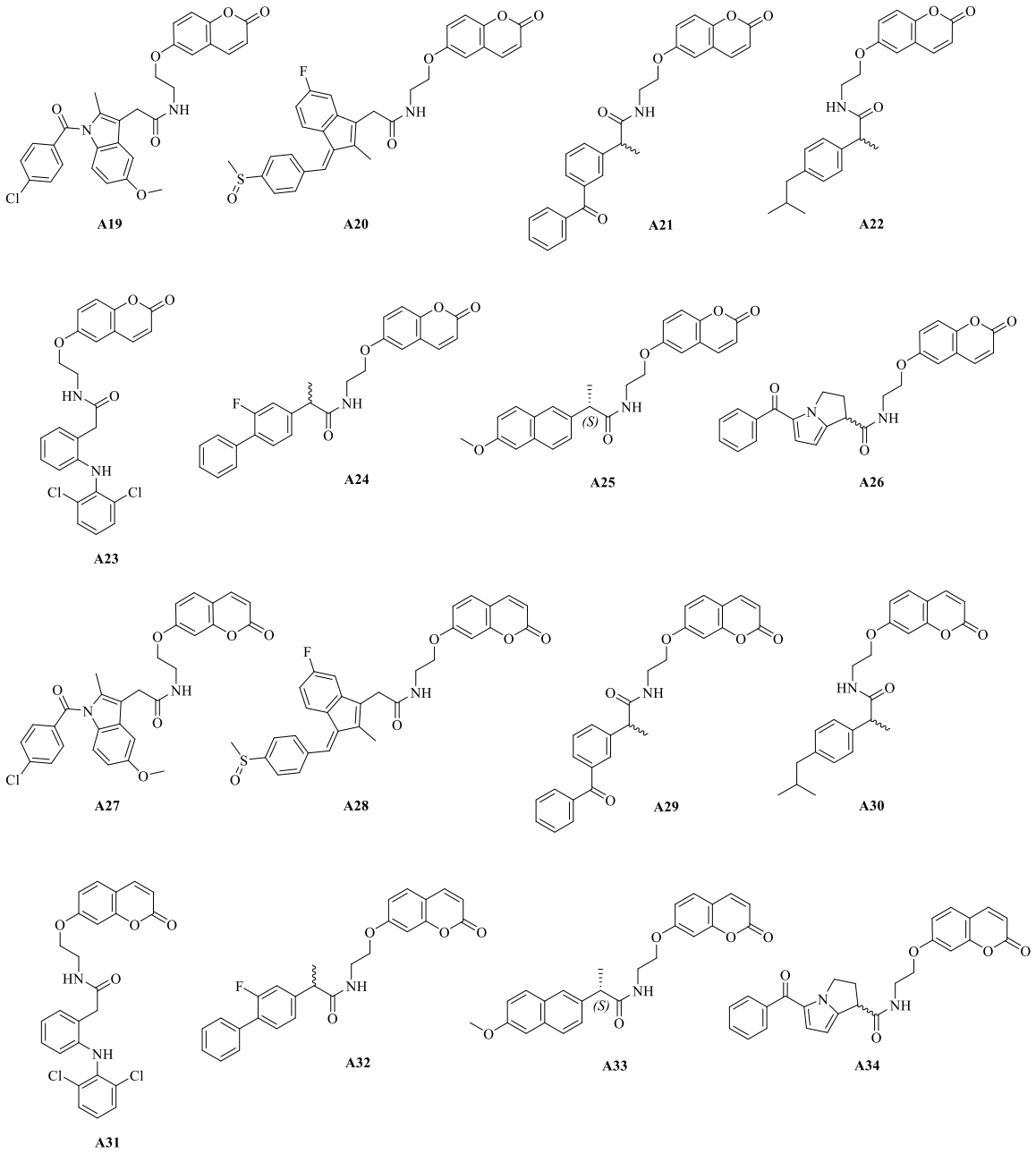

Figure 22. Structures of the compounds **A19-34**.

All synthesized compounds, **A19-34**, were tested *in vitro* for their inhibitory properties against the physiological relevant hCA isoforms (I, II, IV, VII, IX, and XII) by means of the stopped-flow carbon dioxide hydration assay,[169] and their activities were compared to the standard CAI acetazolamide (Table 2). Overall, the data reported in Table 2 clearly showed that all compounds were ineffective in inhibiting the highly abundant cytosolic hCA I and II as well as the central nervous system (CNS) expressed hCA VII (inhibition constant - K_I - > 10 μM). The only exception was represented from

the coumarin substituted at 7-position with ketoprofen (**A29**), which was a high nanomolar hCA II inhibitor (K_I = 85.4 nM).

Table 2. hCA I, II, IV, VII, IX, and XII Inhibition Data with Compounds **A19-34** by a Stopped-Flow CO_2 Hydrase Assay.[169]

		K_I^* (nM)					
Hybrid	**NSAID**	**hCA I**	**hCA II**	**hCA IV**	**hCA VII**	**hCA IX**	**hCA XII**
A19	Indometacin	>10000	>10000	2.6	>10000	31.3	59.1
A20	Sulindac	>10000	>10000	7.5	>10000	30.8	81.7
A21	Ketoprofen	>10000	>10000	4.4	>10000	54.7	>10000
A22	Ibuprofen	>10000	>10000	0.44	>10000	112.9	>10000
A23	Diclofenac	>10000	>10000	5.6	>10000	28.9	92.6
A24	Flurbiprofen	>10000	>10000	0.81	>10000	23.5	5.9
A25	Naproxen	>10000	>10000	0.79	>10000	31,8	>10000
A26	Ketorolac	>10000	>10000	0.73	>10000	106.9	>10000
A27	Indometacin	>10000	>10000	8.3	>10000	20.1	6.5
A28	Sulindac	>10000	>10000	9.0	>10000	27.9	7.7
A29	Ketoprofen	>10000	85.4	9.5	>10000	178.9	57.8
A30	Ibuprofen	>10000	>10000	9.1	>10000	258.2	39.0
A31	Diclofenac	>10000	>10000	9.1	>10000	89.7	80.8
A32	Flurbiprofen	>10000	>10000	8.8	>10000	159.4	>10000
A33	Naproxen	>10000	>10000	9.4	>10000	145.7	>10000
A34	Ketorolac	>10000	>10000	9.8	>10000	114.3	80.7
AAZ	-	250	12	74	2.5	25	5.7

*Mean values from three different assays. Errors were within ±5−10% of the reported values (data not shown).

The following structure−activity-relationships (SARs) for the remaining hCA isoforms are reported.

(i) The membrane bound hCA IV, which is of interest since it seems to be overexpressed in RA (at least antibodies against this isoform were reported in the RA patients' samples),[38] was highly inhibited by the compounds included in this study. All compounds showed K_I values in the low nanomolar range and between 0.44 and 9.8 nM, thus significantly more potent when compared to the standard CAI acetazolamide (K_I = 74.2 nM). The 6-substituted coumarins (**A19-26**) were 1.2- to 20.7-fold more potent than the 7-substituted ones (**A27-34**) in inhibiting the hCA IV isoform.

(ii) Interesting data were obtained for the tumor associated and RA overexpressed hCA IX isoform, as the 6-substituted compounds **A19**, **A20** and **A23**, **A24**, **A26** showed K_I values of 23.5 and 31.8, thus comparable to the standard CAI **AAZ** (K_I = 25.1 nM). The introduction at the 6-position of the coumarin scaffold of either ibuprofen (**A22**) or naproxen (**A25**) determined loss of the inhibitory activity (K_I values of >100 nM). Within the 7-substituted series, only the compounds **A27** and **A28** were effective inhibitors of hCA IX (K_I values of 20.1 and 27.9 nM, respectively), whereas the diclofenac counterpart (**A31**) was a high nanomolar inhibitor (K_I of 89.7 nM). All other compounds were ineffective, thus demonstrating that the substitution position at the coumarin ring resulted in potent effects on the inhibition potencies of these compounds.

(iii) The second RA relevant hCA isoform (*i.e.*, XII) was potently inhibited by the 6-coumarin substituted flurbiprofen derivative **A24** (K_I = 5.9 nM), with a potency comparable to the standard CAI AAZ (5.7 nM). The introduction at the same position of the coumarin scaffold of all the NSAIDs herein considered determined either decrease (**A19**, **A20**, **A23**) or loss (**A21**, **A22**, **A25**, **A26**) of the hCA XII inhibition potency (see data in Table 2). Swap of the NSAID moieties from the 6- to the 7-position of the coumarin ring determined a significant increase of the inhibition potency of the derivatives **A27-30** with K_I values in the low−medium nM range (Table 2). Noteworthy the indomethacin and the sulindac derivatives (**A27**, **A28**) were particularly active in inhibiting the hCA XII, with K_I values of 6.5 and 7.7 nM, respectively, thus comparable to the standard CAI AAZ (5.7 nM). Conversely, introduction of the diclofenac and naproxen moieties at the 7-position of the coumarin scaffold (**A31** and **A23**) determined a slight increase of the inhibition potencies with K_I values of 80.8 and 92.6 nM, respectively. Finally, the inhibition activities of the flurbiprofen **A32** and ketorolac **A34** derivatives were unvaried and worsened compared to their 6-substituted counterparts (Table 2).

The pain relief efficacy of compounds **A19**, **A24**, and **A27-32** and **A34** (10 mg kg^{-1} p.o.) was evaluated in a rat model of rheumatoid arthritis induced by intra-articular (ia) complete Freund's adjuvant (CFA) injection. The *in vivo* study was conducted by Dr. Lorenzo Di Cesare Mannelli and Prof. Carla Ghelardini, Neurofarba Dept., University of Florence. The effects of compounds herein reported were compared with 100 mg kg^{-1} ibuprofen, the classical NSAID administered at the active dosage usually employed in

this model.[170] The hypersensitivity to a mechanical noxious stimulus (Paw Pressure Test) is reported in Figure 23.[171,172]

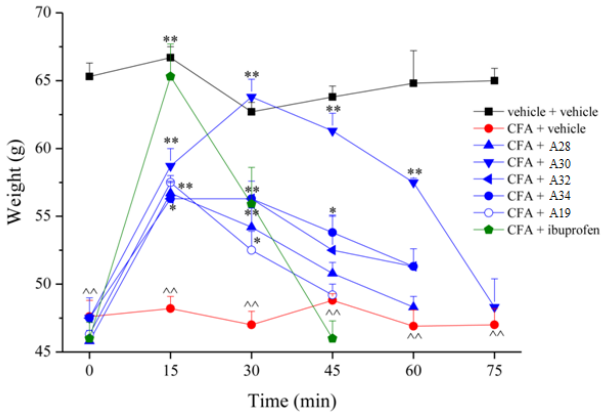

Figure 23. Acute pain-relieving effect of **A19**, **A28**, **A30**, **A32**, **A34** and ibuprofen (**A4**) in a rat model of rheumatoid arthritis induced by CFA ia injection measured through Paw Pressure Test.

Data collection at day 14 after CFA injection showed that the reference group (vehicle + vehicle; 1% CMC) had a nociceptive threshold stable over the time course of the experiments and that the pain threshold of the ipsilateral paw of the CFA + vehicle group was significantly decreased when compared to the reference (47.6 ± 1.2 g and 65.3 ± 1.0 g, respectively). A single oral administration of the 7-susbstituted coumarin ibuprofen derivative (**A30**) was able to significantly increase the weight tolerated on the ipsilateral paw at 15 min (58.7 ± 1.3 g) and with a maximum effect between 30 and 45 min (63.8 ± 1.3 g and 61.3 ± 1.3 g, respectively) after treatment. The antinociceptive effect completely disappeared at 75 min (Figure 23). Interestingly, the effect of ibuprofen per se administered at a 10-fold higher dosage peaked 15 min after administration lasting up to 30 min. The sulindac derivative **A28** increased the pain threshold of the ipsilateral paw starting 15 min after administration (56.7 ± 0.8 g), and the antihypersensitivity effect was still significant after 30- and 45-min. Compounds **A19**, **A32**, and **A34** induced a significant reduction of hypersensitivity showing comparable efficacy (about 56 g). The effect peaked at 15 min and disappeared 45 min after treatment (Figure 23). Compounds **A24**, **A27**, **A29**, and **A31** were not able to counteract the hypersensitivity induced by CFA ia injection (data not shown). Moreover, none of the compounds herein considered altered the pain threshold of the contralateral paw, thus suggesting that these molecules do not influence the normal pain sensitivity.

The compound efficacies were also evaluated by means of the incapacitance test against the spontaneous pain. We measured the hind limb weight bearing alterations caused by unilateral damage (Figure 24).

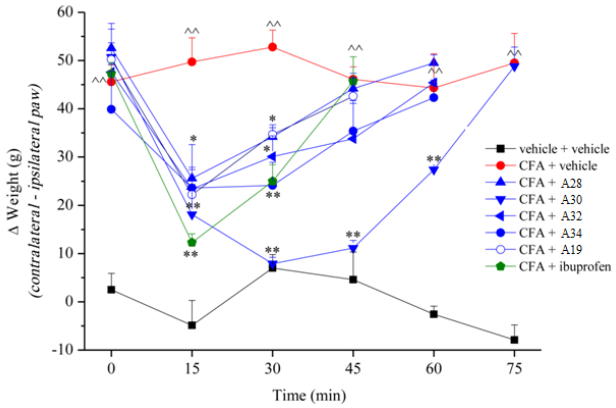

Figure 24. Acute pain-relieving effect of **A19**, **A28**, **A30**, **A32**, **A34** and ibuprofen (**A4**) in a rat model of rheumatoid arthritis induced by CFA ia injection measured through Incapacitance Test.

As above reported, the difference between the weight burdened on the contralateral and the ipsilateral paw (Δweight) was significantly increased in the CFA + vehicle treated animals compared to the control group (45.6 ± 3.5 g and 2.5 ± 3.4 g, respectively). Such results obtained after compounds acute treatments matched those recorded with the paw pressure test previously reported in Figure 23. The best performing compound was the 7-coumarin substituted ibuprofen (**A30**) at a concentration of 10 mg kg^{-1}, which was able to fully reduce the Δweight between 30 and 45 min after treatment (7.9 ± 1.3 g and 11.1 ± 1.6 g, respectively). The effect lasted up to 60 min. On the contrary compounds **A19**, **A28**, and **A32** partially reduced the postural imbalance starting from 15 min until 30 min after administration. The effect of ibuprofen (100 mg kg^{-1}) per se was comparable to that induced from these latter compounds.

In this first project, we report for the first time the design and synthesis of a series of low molecular weight NSAID−CAI hybrids as agents for the treatment of RA and related inflammatory diseases. Most compounds showed *in vitro* potency as inhibitors of the RA overexpressed hCA IV, IX, and XII, with K_I values in the low nanomolar range. The ability of the obtained compounds to affect the inflammation process was assessed by means of the paw-pressure and incapacitance tests on a CFA induced arthritis model in rats. Among the compounds considered, the 7-coumarin substituted ibuprofen derivative **A30** showed a potent antihyperalgesic effect, which was maintained for 60 min

after administration. Hybrid **A30**, which is the most relevant compound in this research, showed interesting antihyperalgesic effects, and its inhibitory activity on hCAs was limited to the isoforms IV and XII and not IX. Inhibitors of the hCA IV, IX, and XII, such as **A19**, **A28**, and **A30**, failed instead in the *in vivo* RA model. We demonstrated for the first time that NSAID−CAI hybrids are highly promising tools for the treatment of symptoms, such as pain, originating from RA and related diseases in an animal model of this disease. Furthermore, the inhibition of the RA overexpressed hCA isoforms IV, IX, and XII can significantly contribute to reduction of the joint local acidosis and thus to restore the humoral and cellular immunity processes which are hampered in such pathologies.

The experimental procedures are reported in Chapter 5 and the data and results of this research were published in Silvia Bua, et al. *J. Med. Chem.* **2017**, *60*, 1159-1170.

3.3 Bioisosteric development of multi-target NSAID - carbonic anhydrases inhibitor anti-arthritic agents: synthesis, enzyme kinetic, plasma stability and anti-inflammatory evaluation (Series B)

Basing on the multi-target approach, which is gaining raising interest among medicinal chemists worldwide, we reported a series of hybrid compounds (series A) which incorporate in a single molecule a CA-inhibiting moiety and a COX inhibitor of the NSAID type linked by amide bonds.[173,174] The latter was supposed to be hydrolyzed *in vivo* by specific amidases, releasing the two anti-inflammatory portions.

Successively, the chemical stability of the NSAID-coumarin hybrids towards spontaneous or enzymatic hydrolysis (phosphate buffer solution, human and rat plasma) was evaluated by application of tandem mass spectrometry mode (LC-MS/MS) methods to gain insights on their behavior in biological matrices and to address their optimization (Table 3).[175] This study was conducted by Prof. Gianluca Bartolucci, Neurofarba Dept., University of Florence.

Table 3. t ½ of amides samples (**A19-33**) by drug stability studies.

Amides	$t_{1/2}$ (min)	
	H-Plasma	R-Plasma
A19	>240	>240
A20	>240	>240
A21	>240	>240
A22	>240	>240
A23	>240	>240
A24	>240	>240
A25	>240	>240
A27	>240	>240
A28	>240	>240
A29	>240	>240
A30	>240	>240
A31	>240	>240
A32	>240	>240
A33	>240	>240

All compounds were stable in all the tested matrices at the used experimental conditions. Therefore, it has been reasonable to assume that these amide-linked compounds reach the target tissues unmodified. However, a successive hydrolysis in the inflamed synovium cannot be excluded as well as an anti-inflammatory action as non-cleaved multi-targeted compounds.

Hence, an additional set of hybrid compounds (Series B) containing a NSAID and a coumarin fragment was designed by bioisosteric substitution of the amide moiety to ester, which more easily undergoes cleavage by esterases and/or acidic conditions present in the target tissues (Figure 25). The main aim of the present study was the obtainment of *in vivo* more cleavable multi-target derivatives than those previously reported, to evaluate their effectiveness as CAIs and to assess their anti-inflammatory and analgesic effects *in vitro/vivo*.

Again, CAIs of the coumarin type were chosen to achieve a selective inhibition of CA IV, IX and XII over the ubiquitous CA I and II.[172,173] The adopted molecular hybridization strategy foresees also in this case a 1:1 *ratio* for the CAI and the NSAID portions which have been spaced by 2-carbon and linked by an ester bond to compare the results to those of the previously reported amide-linked derivatives.

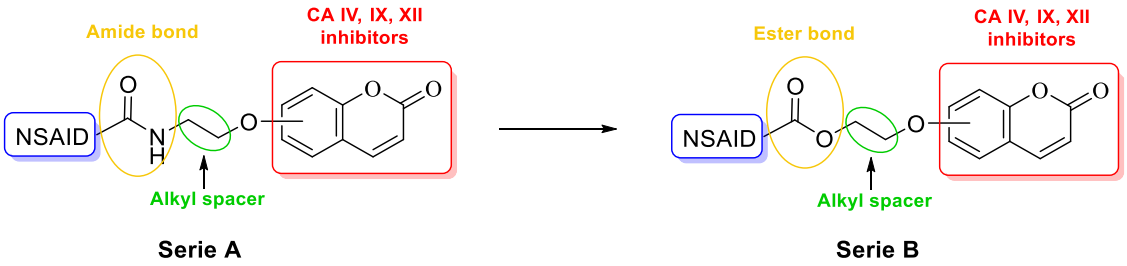

Figure 25. Bioisosteric substitution of the amide moiety (**A19-34**) to ester (**B3-16**).

The key intermediates **B1** and **B2** were obtained by nucleophilic substitution of the commercially available 6- and 7-hydroxycoumarins with the 2-chloro-ethanol (Scheme 3).

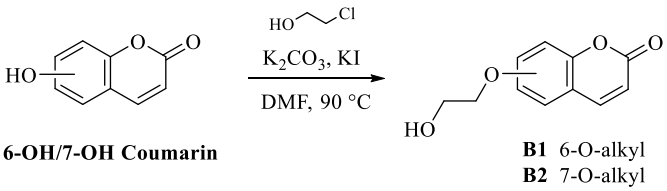

Scheme 3. Synthesis of the intermediates **B1** and **B2**.

As reported in Scheme 5, the final hybrids **B3-16** were obtained in good yields by linking intermediates **B1** and **B2** to commercially available NSAIDs **A1-7** by a coupling reaction with EDCI·HCl and catalytic DMAP in dry DMF under a N_2 atmosphere.

All final compounds (Scheme 4 and Figure 26) as well as intermediates were purified by silica gel column chromatography eluting with the appropriate mixture of EtOAc/*n*-hexane and were >95% pure, as determined by HPLC and were characterized by means of ^{1}H, ^{13}C, ^{19}F NMR spectroscopy and HRMS.

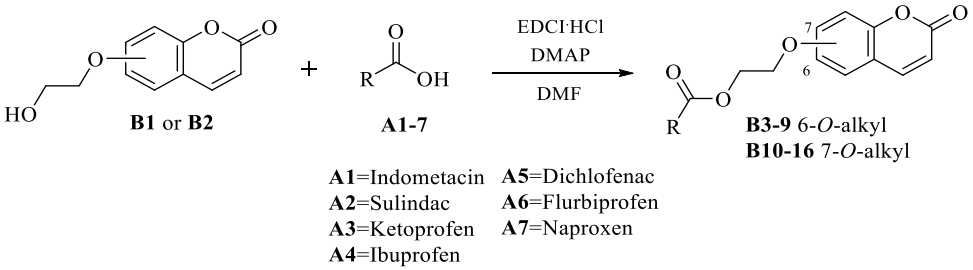

Scheme 4. General synthetic path of compounds **B3-9** and **B10-16**.

Also reported molecular hybrids (**B3-16**) were evaluated for their inhibition against the cytosolic CA I, II and VII and the membrane-bound CA IV, IX and XII by using a Stopped-flow CO_2 hydrase assay method.[169] The clinically used AAZ was used as standard drug in the kinetic assessment (Table 4). The inhibition profiles of **B3-16** were compared to those measured for the amide-based analogs previously reported (**A19-25**, **A27-33**).[173]

The following SAR can be drawn up according to the inhibition data shown in Table 4. The alcohol intermediates **B1** and **B2** showed inhibition profiles that are compliant to literature data and to the scope of the project that consists in the selective targeting of CA IV, IX and XII over ubiquitous CAs. Inhibition constants (K_Is) span in the range 6.8-8.4 nM against CA IV, 305.6-334.6 nM against CA IX, and 236.1-250.9 nM against CA XII, whereas no inhibition of CAs I, II and VII was detected below 10 μM. The switching of the alcoholic pendant from the 6- to 7- position of the coumarin scaffold had no influence on the CAs inhibition.

The inhibition profiles reported in Table 4 for the esters **B3-9** and **B10-16** depict a scenario superimposable with that previously reported for amide-based CAI/NSAID hybrids (Series A, Figure 22). Specifically, the ester-based compounds act as inefficient

inhibitors of the cytosolic isoforms CA I, II and VII with K_Is above 10 μM, showing, in contrast, great potency, and thus selectivity, against CA IV, IX and CA XII. Compounds **B3** and **B4** are the unique exceptions to this general trend, because they showed K_I of 815.8 and 746.6 nM against CA VII, respectively. In contrast, the amide analog of derivative **B12** had been the outlier of its series because of an 85.4 nM K_I unexpectedly measured against CA II.

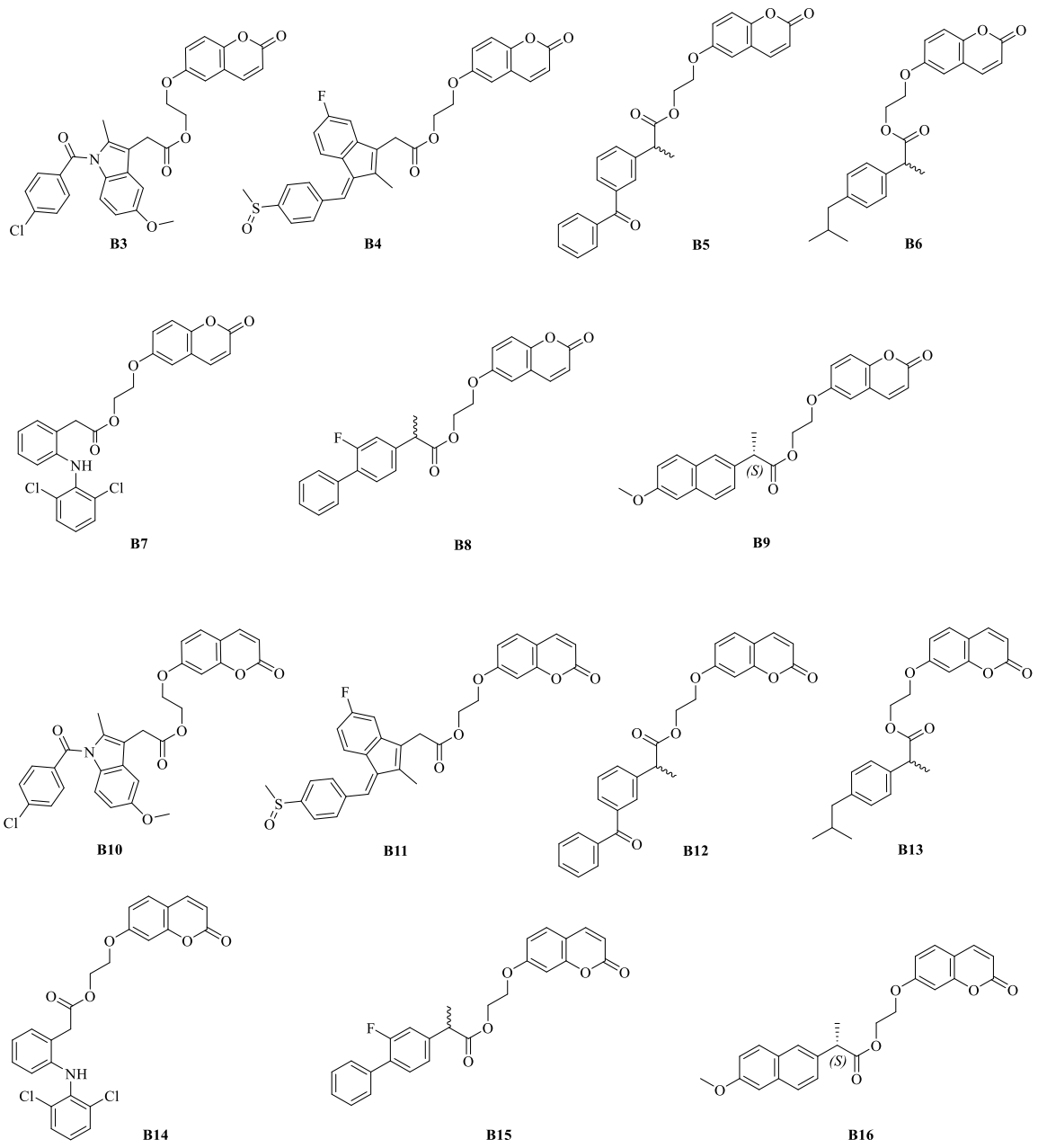

Figure 26. Structures of the compounds **B3-16**.

Table 4. Inhibition data of CA I, CA II, CA IV, CA VII, CA IX and CA XII with alcohols **B1** and **B2** hybrids **B3-16** (K_I Ester), amide-based analog compounds **A19-33** (K_I Amide)[173], and the standard inhibitor acetazolamide (AAZ) by a stopped flow CO_2 hydrase assay.[169]

		$K_{I\ Ester}$ (nM)[a] / $K_{I\ Amide}$ (nM)[b]					
Cmpd	**NSAID**	**hCA I**	**hCA II**	**hCA IV**	**hCA VII**	**hCA IX**	**hCA XII**
B1	-	>10 µM	>10 µM	6.8	>10 µM	305.6	250.9
B2	-	>10 µM	>10 µM	8.4	>10 µM	334.6	236.1
B3	Indometacin	>10 µM	>10 µM	3.7	815.8	27.7	51.5
		>10 µM	>10 µM	2.6	>10 µM	31.3	59.1
B4	Sulindac	>10 µM	>10 µM	6.5	746.6	19.3	96.5
		>10 µM	>10 µM	7.5	>10 µM	30.8	81.7
B5	Ketoprofen	>10 µM	>10 µM	2.3	>10 µM	36.9	83.1
		>10 µM	>10 µM	4.4	>10 µM	54.7	>10 µM
B6	Ibuprofen	>10 µM	>10 µM	3.6	>10 µM	25.3	459.0
		>10 µM	>10 µM	0.44	>10 µM	112.9	>10 µM
B7	Diclofenac	>10 µM	>10 µM	2.2	>10 µM	33.5	87.5
		>10 µM	>10 µM	5.6	>10 µM	28.9	92.6
B8	Flurbiprofen	>10 µM	>10 µM	7.3	>10 µM	28.0	7.7
		>10 µM	>10 µM	0.81	>10 µM	23.5	5.9
B9	Naproxen	>10 µM	>10 µM	6.8	>10 µM	4.4	827.9
		>10 µM	>10 µM	0.73	>10 µM	106.9	>10 µM
B10	Indometacin	>10 µM	>10 µM	7.1	>10 µM	42.8	68.4
		>10 µM	>10 µM	8.3	>10 µM	20.1	6.5
B11	Sulindac	>10 µM	>10 µM	17	>10 µM	33.3	6.3
		>10 µM	>10 µM	9.0	>10 µM	27.9	7.7
B12	Ketoprofen	>10 µM	>10 µM	6.7	>10 µM	35.4	55.4
		>10 µM	85.4	9.5	>10 µM	178.9	57.8
B13	Ibuprofen	>10 µM	>10 µM	6.5	>10 µM	3.9	5.3
		>10 µM	>10 µM	9.1	>10 µM	258.2	39.0
B14	Diclofenac	>10 µM	>10 µM	4.3	>10 µM	4.5	88.1
		>10 µM	>10 µM	9.3	>10 µM	89.7	80.8
B15	Flurbiprofen	>10 µM	>10 µM	7.5	>10 µM	37	>10 µM
		>10 µM	>10 µM	8.8	>10 µM	159.4	>10 µM
B16	Naproxen	>10 µM	>10 µM	6.3	>10 µM	13.3	73.7
		>10 µM	>10 µM	8.8	>10 µM	114.3	80.7
AAZ	-	250	12	74.2	2.5	25.1	5.7

a. Mean from 3 different assays by a stopped flow technique (errors in the range of ± 5-10 % of the reported values); b. Data from ref. 173.

The membrane-bound CA IV exhibits the greatest inhibition by **B3-9** and **B10-16** among the screened CAs with K_Is spanning between 2.2 and 17.0 nM. Generally, the 6-substituted coumarins (**B3-9**) produce a lightly more efficient inhibition (K_Is of 2.2-7.3 nM) than the 7-substituted ones (**B10-16**, K_Is ranging between 4.3 and 17.0 nM). The diclofenac derivative **B7** reported the best CA IV inhibitory activity with a K_I of 2.2 nM as well as its ketoprofen analog which shows a K_I of 2.3 nM. Among the 7-substituted

coumarins, the diclofenac derivative **B14** is the most potent CA IV inhibitor with a K_I of 4.3 nM. When the 6- to 7- position switching has no effect on the inhibitory activity of most couples such as **B8**/**B15** (K_Is of 7.3 and 7.5 nM) and **B9**/**B16** (K_Is of 6.8 and 6.3 nM), an almost 3-fold drop of efficacy was measured with the indomethacin couple **B4**/**B11** (K_Is of 6.5 and 17.0 nM).

It should be noted that no ester shows a subnanomolar efficacy against CA IV, in contrast to some amide-based analogs such as those of **B6**, **B8** and **B9** (K_Is of 0.44-0.81 nM).

The membrane-associated isoform CA IX is efficiently inhibited by derivatives **B3-9**, **B10-16**. K_Is of the first subset (**B3-9**) span from 4.4 nM (**B9**) to 36.9 nM (**B5**) whereas those of **B10-B16** range between 3.9 nM (**B13**) to 42.8 nM (**B10**). The best CA IX inhibitory activities were measured with compounds **B9**, **B14** and **B15** which report single-digit K_Is of 4.4, 3.9, and 4.5 nM, respectively. Interestingly, the ibuprofen (**B6**/**B13**) and diclofenac (**B7**/**B14**) derivatives couples show a 6- and 7-fold increase of efficacy upon swapping the substitution position from 6- to 7- (K_I values from 25.3 and 3.9 nM for ibuprofen and from 33.5 to 4.5 nM for diclofenac). While most other couples of positional isosters do not display significant K_I differences, uniquely for the naproxen pair **B9**/**B16** a 3-fold decrease of inhibition efficacy was reported by switching from the 6- to 7- position on the coumarin scaffold (K_I value from 4.4 to 13.3 nM).

Except for compounds **B3**, **B4**, **B5**, **B7**, **B8**, **B10** and **B11** which do not exhibit significantly different CA IX inhibition compared to the amide-based analogs, the other ester derivatives act as 4- to 66-fold more potent CA IX inhibitors than the corresponding amides. Specifically, the naproxen compound **B8** in the 6-substituted subset and the ibuprofen (**B13**) and diclofenac (**B14**) derivatives in the 7-substituted series show enhanced inhibitory profiles against CA IX upon switching the amide linker to an ester, i.e. 24, 66 and 19 times, respectively.

The other tumor-associated isoform, CA XII, is in the whole less inhibited than CA IX by esters **B3-9**, **B10-16**, though some such derivatives, that are **B8**, **B11** and **B13**, report single-digit K_I values (5.3-7.7 nM). While the half compounds exhibit CA XII inhibition in the 50-100 nM, the 6-substituted coumarins **B6** and **B9** demonstrate a weaker efficacy which occurs in the high nanomolar range (K_Is of 459.0 and 827.9 nM). Solely the flurbiprofen derivative **B15** does not inhibit CA XII up to 10 μM, in similar manner with its amide analog. In this case the 7-substituted compounds (**B10-16**) were shown to act as

better inhibitors than their isosters **B3-9**. Except for the sulindac, ketoprofen and diclofenac isosters **B3**/**B10**, **B5**/**B12** and **B7**/**B14** that show no significantly different K_Is within the couple, the other pairs of compounds report marked variations in the K_I values when swapping the substitution position from 6- to 7-, with the exception of the flurbiprofen couple **B8**/**B15** in which the 6-substituted derivative is a low nanomolar CA XII inhibitor and its isoster does not inhibit the isozyme up to 10 μM. The inhibition efficacy increases by 11 times in the naproxen couple **B9**/**B16** (K_I from 827.9 to 73.7 nM), and 15-fold inhibition enhancements were measured within the couple **B4**/**B11** (K_I from 96.5 to 6.3 nM). This enhancement increases to 86-fold with the ibuprofen derivatives **B6**/**B13** (K_I from 459.0 to 5.3 nM), and reach a maximum in the flurbiprofen couple, being **B8** a single-digit nanomolar inhibitor and **B15** inactive against CA XII.
Nine ester compounds within the two subsets show no significant variations of CA XII inhibition when compared to their amide-base analogs. In contrast, esters **B4**, **B6**, **B9**, and **B13** are more efficient (7- to above 20-fold) CA XII inhibitors than the corresponding amides, whereas solely the indometacin derivative **B10** acts a 10-fold weaker CAI against this isoform than the amide-based analog.

Drug stability studies in phosphate buffer solution (PBS) and plasma matrices were conducted for compounds **B3-9**, **B10-16** to evaluate whether the swapping of the amide linker with the more cleavable ester could endow them with a prodrug character, having in fact previously assessed the plasma stability of the corresponding amide derivatives. Both human and rat plasma were used to investigate the hydrolytic efficiency of plasma enzymes of both species against the NSAID ester derivatives and figure out the behavior of the hybrid molecules in biological matrices. The PBS media was included in the study to evaluate the spontaneous hydrolysis that can occur due to the characteristic of the solution (pH or ionic strength). This study was carried out by using liquid chromatography coupled with a mass spectrometer operating in tandem mass spectrometry mode (LC-MS/MS) that is considered the method of choice for quantitative determination of drugs and their metabolites in biological matrices, in terms of sensitivity and specificity. This study was conducted by Prof. Gianluca Bartolucci, Neurofarba Dept., University of Florence.

All the tested compounds resulted stable in PBS media, while various behaviors were noted in plasmatic matrices. It was quite unexpected to observe all esters rapid hydrolysis in rat plasma (t½ spanning between <1 to 5.5 min), and not in human media (Table 5).

Table 5. t ½ of esters **B3-16** compared to that of the corresponding amides of **series A**.

Amides	$t_{1/2}$ (min)		Esters	$t_{1/2}$ (min)	
	H-Plasma	R-Plasma		H-Plasma	R-Plasma
A19	>240	>240	**B3**	>240	2.8
A20	>240	>240	**B4**	>240	2.0
A21	>240	>240	**B5**	>240	5.5
A22	>240	>240	**B6**	>240	16.6
A23	>240	>240	**B7**	**31**	4.7
A24	>240	>240	**B8**	**12**	2.1
A25	>240	>240	**B9**	>240	3.5
A27	>240	>240	**B10**	>240	3.2
A28	>240	>240	**B11**	**32**	<1
A29	>240	>240	**B12**	**18**	<1
A30	>240	>240	**B13**	>240	1.3
A31	>240	>240	**B14**	>240	2.4
A32	>240	>240	**B15**	>240	1.1
A33	>240	>240	**B16**	>240	<1

In detail, solely the couple of derivatives of ketoprofen (**B5** and **B12**) and diclofenac (**B7** and **B14**) are hydrolyzed both in human and rat plasma. Therefore, the human plasma hydrolytic enzymes have the ability to cleave the ester bond depending on the type of NSAID present in the hybrid compound. It is worth to note that also the coumarinic part of the molecule affect the hydrolytic process. In fact, the 6-substituted coumarins **B5** and **B7** show a hydrolysis t½ which is two times (31 and 32 min respectively) that of the 7-substituted isomers **B12** and **B14** (12 and 18 min respectively). Therefore, the collected information indicate that most esters derivatives exhibited human plasma stability.

A subset of NSAID-CAI compounds was selected to assess *in vitro* their anti-inflammatory effects. The pair of amide-linked ibuprofen derivatives **A22** and **A30** of series A (Figure 22) was selected as **A30** had shown the best *in vivo* anti-inflammatory efficacy;[173] hence, the ibuprofen esters couple, undergoing hydrolysis in rat plasma, was assessed *in vitro* as well. Both esters of ketoprofen (**B5** and **B12**), that showed to undergo

rapid hydrolysis in plasma from both species, were also selected, as well as the pair of diclofenac amide derivatives (Figure 22), among which **A31** oddly had not exhibited *in vivo* anti-inflammatory action.[173] This study was conducted by Dr. Laura Lucarini and Prof. Emanuela Masini, Neurofarba Dept., University of Florence.

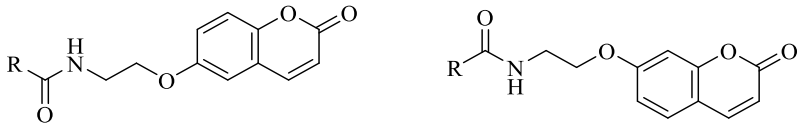

A22,23 **A30,31**

A22,30 = Ibuprofen
A23,31 = Diclofenac

Figure 27. Structures of amide derivatives assayed *in vitro* as anti-inflammatory.

Two *in vitro* tests were performed to assess the effects of the selected compounds on the arachidonic acid cascade in inflammation processes, namely platelet aggregation to evaluate the COX-1 (ubiquitous) inhibition (Figure 28) and the reduction of prostaglandin E_2 (PgE_2) production to appraise the COX-2 (over-expressed in inflammation) inhibition (Figure 29).[176,177] It should be stressed that derivatives showing COX-2 selective inhibition profiles over COX-1 might be preferred for their increased anti-inflammation activity and in order to avoid the side effects related to the ubiquitous isoform inhibition.[178]

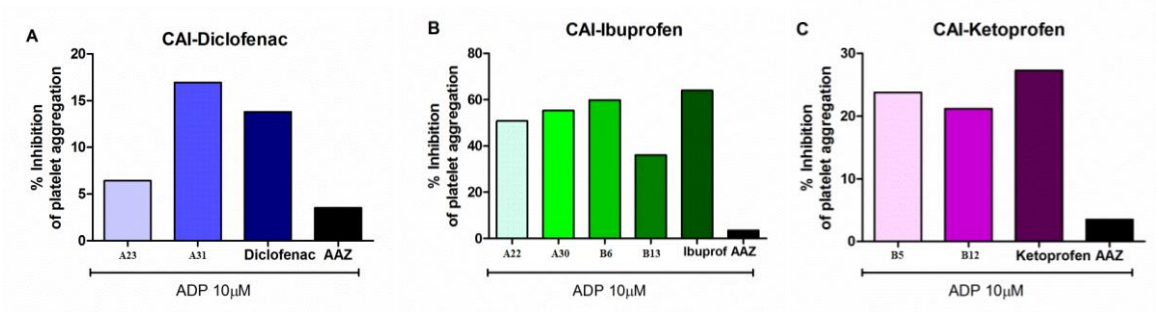

Figure 28. Inhibition of platelet aggregation with compounds **B5**, **B12**, **B6**, **B13**, **A22**, **A30**, **A23** and **A31**, standard NSAIDs and the CAI **AAZ** as comparison. Concentration of drugs 10 μM. Values represent the mean % of four independent experiments.

Among the tested standard NSAID, ibuprofen showed the best inhibition of platelet aggregation, that is more than 60%, whereas that of diclofenac and ketoprofen resulted to be by about the 15% and 25 %, respectively. All the assayed hybrids showed a lower platelet aggregation inhibition than the corresponding reference NSAID with a decrease

spanning in the range 5-30%, except the diclofenac amide derivative **A31**, that is slightly more potent that the standard. As for the inhibition exhibited by isomers within each pair, the 7-substitution on the coumarin ring produced a more pronounced inhibition effect that 6-substitution in case of amide derivatives **A22-A30** and **A23-A31.** In contrast, when an ester bond linked the two inhibitory portions, the 6-substitution of the coumarin ring turned out to be preferred, particularly as in the case of the ibuprofen pair **B6-B13** (ca. 30% inhibition variation). The CAI **AAZ** did not produce significant inhibition of platelet inhibition.

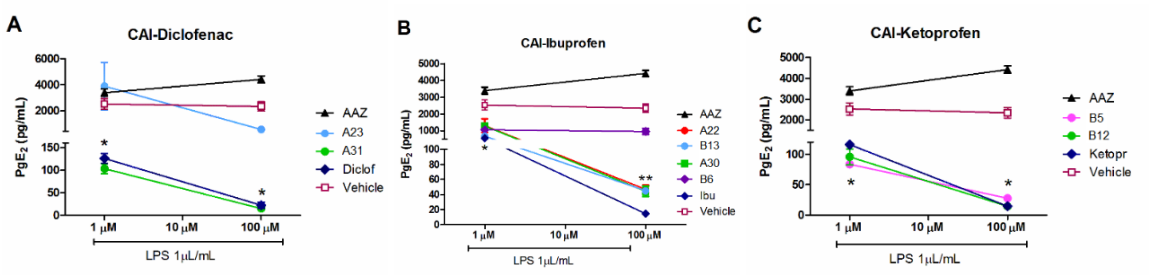

Figure 29. Inhibition of PgE_2 production induced by LPS in RAW 264.7 macrophages treated with the selected compounds, using A) diclofenac, B) ibuprofen and C) ketoprofen as standard. PgE_2 production of naive cells (not treated with LPS) is 34.50±2.78 pg/mL, while PgE_2 levels of vehicle (LPS-treated) cells is 2437±93.17 pg/mL. Values represent the mean ± SEM of eight independent experiments (*$p<0.05$ *vs* AAZ).

The evaluation of the anti-COX-2 effect of the selected compounds was made evaluating the level reduction of its enzymatic product PgE_2.[176] AAZ, the standard NSAIDs and the hybrid derivatives were assayed at the concentrations of 1µM and 100µM.

Figure 28A shows the effect of the assayed diclofenac derivatives to PgE_2 production. Diclofenac at both tested concentrations yielded a great reduction of PgE_2 levels (126.0±7.35 pg/mL at 1 µM and 22.3±4.9 pg/mL at 100 µM) when compared to the vehicle (LPS-treated) cells (2437±93.17 pg/mL). Such a potent efficacy is held by the 7-substituted amide derivative **A31** (103.0±7.65 pg/mL and 15.15±0.85 pg/mL, respectively), whereas it dropped for its isomer **A23.** In fact, the latter, 6-substituted coumarin, led to a 75% reduction at 100µM in comparison to cells treated only with vehicle (579.1±14.75 pg/mL and 2437 ±93.17 pg/mL, respectively), but did not produce any effect at 1µM concentration (3891±1296 pg/mL), resulting to be comparable with **AAZ** effect (3394±207.0 pg/mL).

Ketoprofen provoked a PgE_2 level reduction comparable to that produced by diclofenac (Figure 29C) at both screened concentrations (116.1±3.1 pg/mL at 1 µM and 14.90±3.3

pg/mL at 100 μM). The two ketoprofen ester derivatives **B5** and **B12** reported a feebly more potent effect than the reference NSAID at 100μM (27.85±2.85 pg/mL and 14.60±2.0 pg/mL, respectively), and comparable with it at 1μM (83.85±1.25 pg/mL and 95.95±12.95 pg/mL, respectively). Unlike the diclofenac amide derivatives **A23-A31**, differences in the *in vitro* effect depending on the coumarin substitution position were not observed.

Ibuprofen and its screened amide and ester derivatives resulted to be the weakest modulators of PgE_2 production here measured (Figure 29B). First, ibuprofen 1μM was reported to drop the PgE_2 production just below the 50% (554.9±49.40 pg/mL), whereas PgE_2 production dropped below 1% when the NSAID concentration was raised to 100μM (14.65±1.35 pg/mL). The *in vitro* profiles of its amide derivatives **A22** and **A30** and of the 7-substituted ester **B13** are almost superimposable with the reference ibuprofen at 1μM (**A22**, 1306±289.2 pg/mL; **A30**, 1286±56.5 pg/mL; **B13**, 677.0±26.70 pg/mL) and approximately 4-fold worse than the NSAID at 100μM (**A22**, 46.90±3.8 pg/mL; **A30**, 44.20±4.8 pg/mL; **B13**, 45.0±1.4 pg/mL). The 6-substituted ester **B6** did not report variations in the PgE_2 level reduction raising the concentration from 1μM (1052±64.60 pg/mL) to 100 μM (961.6±119.7), with PgE_2 production settling at 50%, approximately, in comparison to cells treated only with vehicle. Thus, the substitution position of the coumarin ring becomes again significant in the pair of ibuprofen ester derivatives **B6-B13**, contrariwise to what happens with the amide analogs.

According to literature data, diclofenac and ketoprofen, as well as their derivatives, inhibit COX-2 more markedly than COX-1, contrariwise to the inhibition profiles shown by ibuprofen and its derivatives.[177] On the whole, none among the tested hybrid derivatives showed a particularly enhanced COX-2 based anti-inflammatory action when compared to their reference NSAID. In contrast, one could aim to hold the reference NSAID capability to lower PgE_2 level, decreasing instead the inhibition of platelet aggregation that derives from COX-1 inhibition. The analysis of the *in vitro* results from this new standpoint shows that: (i) the diclofenac amide derivative **A23** is not a good candidate because, though exhibiting a minor COX-1 effect than diclofenac, its COX-2 based anti-inflammatory action dropped when compared to the reference compound; (ii) conversely, its 7-substituted isomer **A31** inhibit platelet aggregation more potently than diclofenac, even if inducing a great PgE_2 level reduction; (iii) among ibuprofen

derivatives, solely the ester **B13** is noteworthy, owing to a 30% less platelet aggregation inhibition than ibuprofen, notwithstanding the COX-2 related effect is almost 4-fold lower than the reference; (iv) both ketoprofen ester derivatives, particularly the 7-substituted coumarin **B12**, experience a small decrease of COX-1 related anti-inflammatory effect, when reporting a good PgE_2 level reduction profile at both assayed concentrations.

According to the expected mechanism of action, the CAI **AAZ** is inactive *in vitro* because does not directly affect COX enzymes. The CAI is expected to act as an adjuvant *in vivo* at the level of the inflamed tissue where it can reduce the acidification alleviating the symptoms.

The furnished data do not allow to work out a detailed relationship between the prodrug character of the ester compounds and the measured anti-inflammatory *in vitro* efficacy. Nevertheless, one could speculate that, as for the stable amide derivatives, also the activities measured *in vitro* for **B5**, **B6**, **B12**, and **B13** owe to the complete, not cleaved hybrids. In fact, though the platelet aggregation inhibition assay is conducted in platelet-enriched human plasma, the experimental times are too short to provide significant hydrolysis of the ketoprofen esters, whereas those of ibuprofen are stable in such a media. In the PgE_2 level assessment assays, the experiments are performed on macrophages cell cultures, thus no kind of hydrolysis is expected.

The experimental evidence of the amide compounds stability, or slow degradation of the esters in human plasma, added to the tested compounds *in vitro* anti-inflammatory action as integral hybrids, focused the matter on their mode of binding to human COX-1 and COX-2. Of note, in literature a crystal structure of a COX-1 in adduct with flurbiprofen methyl ester is reported, which testifies that the presence of a free carboxylate is not mandatory to bind the COXs active site.

The crystal structures of COX-2 from human is available in the protein data bank.[179] On the contrary, the availability in the data bank of ovine COX-1 solved complexes made it possible to build a homology model of the human isoform (template 1HT5,[180] 89% sequence identity, Figures 30A and B).

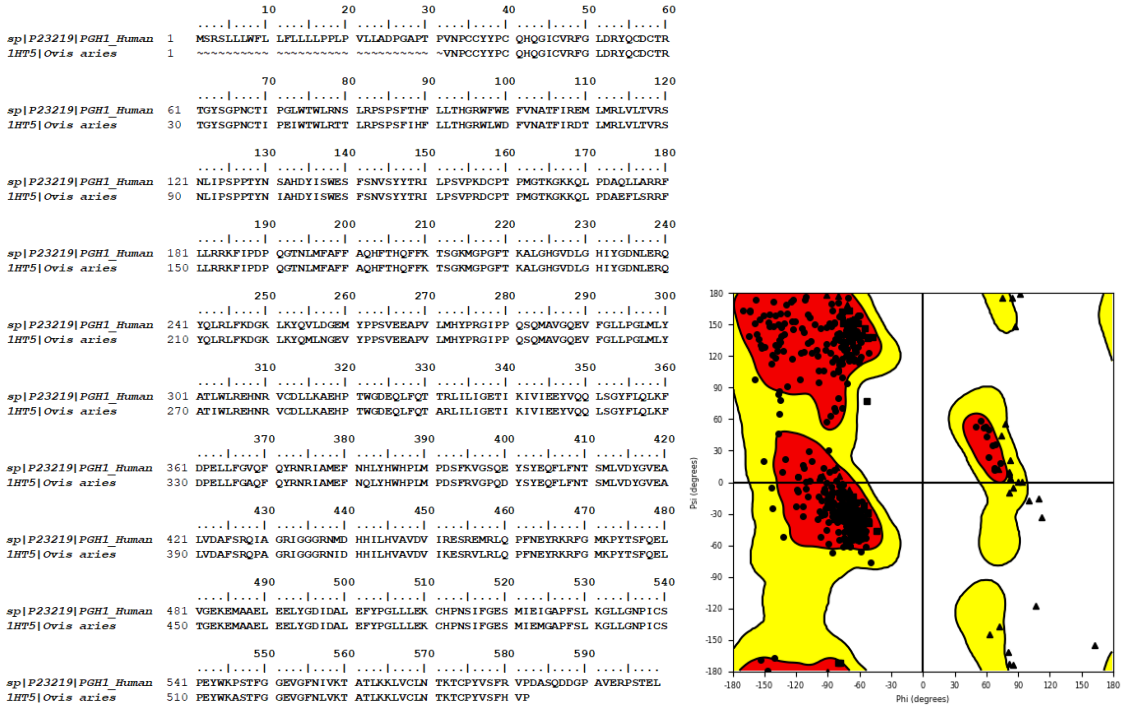

Figure 30. A) Sequence alignment between human and ovine COX-1 (PDB 1HT5), B) Ramachandran plot of hCOX-1 model.

The four ibuprofen derivatives **A22, A30, B6**, **B13**, which showed a greater action in the platelet aggregation inhibition test, were docked with COX-1 to assess whether the functionalization of ibuprofen carboxylic group with coumarin amines or alcohols enables or hinders the NSAID-like binding mode.

The binding mode of amides **A22**, **A30** and ibuprofen to the COX-1 active site is shown in Figure 31, while the interaction mode of esters **B6** and **B13** compared to the reference NSAID is depicted in Figure 32.

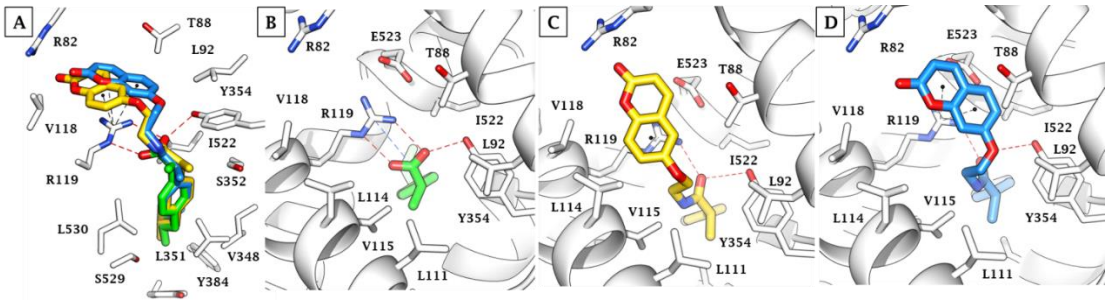

Figure 31. A) Superimposition of the predicted binding orientations of ibuprofen, **A22** and **A30** to hCOX-1 (homology model). Upper view of the COX-1 complex with B) ibuprofen, C) **A22** and D) **A30**.

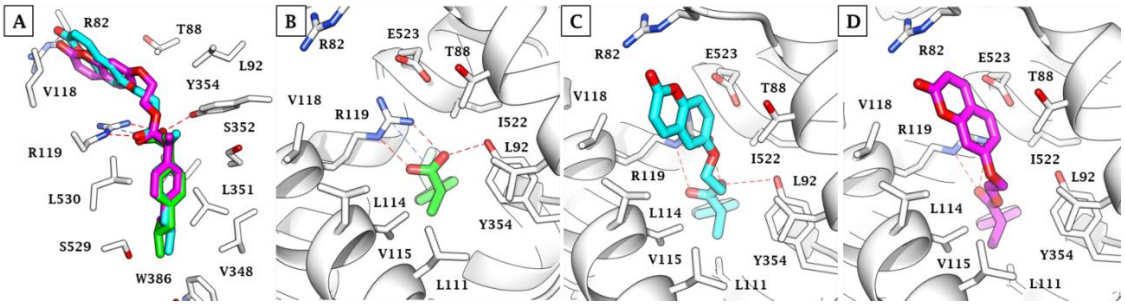

Figure 32. A) Superimposition of the predicted binding orientations of ibuprofen, **B6** and **B13** to hCOX-1 (homology model). Upper view of the COX-1 complex with B) ibuprofen, C) **B6** and D) **B13**.

The 4-isobutylphenyl group of the NSAID and the α-methyl group of ibuprofen accommodated in hydrophobic pockets lined by Y384, W386, V348, L351, S529, L530 and I522 (Figure 31A) and L111, L114 and L92 (Figure 31B), respectively.

The superimposition of the predicted binding orientations of ibuprofen and the amides **A22**, **A30** (Figure 31A) and the esters **B6**, **B13** (Figure 32A) suggested that the binding to the target is driven by the NSAID portion of the hybrids and that the interactions exploited by the carboxylic moiety of ibuprofen with R119 and Y354 are, as expected, missed in the ester and amide derivatives. However, the coumarin portion of these compounds may establishes additional hydrophobic, π-cation and dipolar interactions at the outer edge of the active site (Figures 31C-D and 32C-D).

In detail, the amide and ester groups of **B6**, **B13**, **A22** and **A30** were in H-bond distance with Y354 and R119 (Figures 31C-D and 32C-D), which additionally established π-cation interactions with the coumarin portion of amides **A22** and **A30**. Moreover, the aromatic scaffolds in **B6** and **B13** formed hydrophobic contacts with T88, V118 and L114 and polar interaction with R82 (Figure 32C-D).

The two ketoprofen esters **B5** and **B12,** which showed a greater PgE_2 production inhibition, were accordingly docked with hCOX-2, as well as their reference NSAID. Outcomes from docking (Figure 33A-B) showed that the position of the NSAID portion was substantially preserved with respect to the precursor carboxylic acid, with the obvious exception of the salt bridge with R120 (Figure 33B). However, the esters groups of **B5** and **B12** are still H-bonded with R120 and the coumarin portions (which are mutually 180° tilted) accommodated in the hydrophobic pocket lined by P86, V89, L93, Y115, V116 and were able to establish π-cation contacts with R120 (Figure 33A). Not

surprisingly, due to the 96% sequence identity of the binding sites, a completely similar binding mode was predicted for **B5** and **B12** with the murine COX-2 (data not shown).

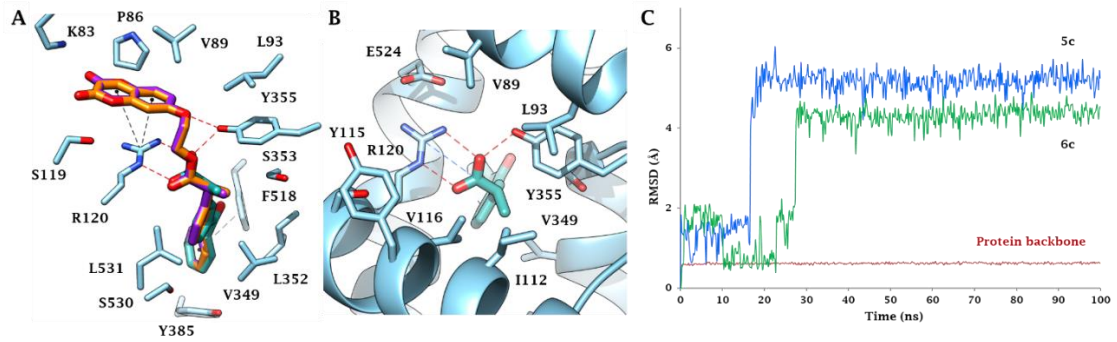

Figure 33. A) Superimposition of the predicted binding orientations of ketoprofen, **B5** and **B12** to hCOX-2 (PDB 5KIR). B) Upper view of the ketoprofen / hCOX-2. C) RMSD analysis of the protein backbone and ligands heavy atoms over the 100 ns MD.

The docking procedure was complemented with a 100 ns long molecular dynamic (MD) simulation performed on the predicted binding orientations of the *in vitro* most promising derivatives **B5** and **B12**. While the protein is subjected to small conformational variations, the plots in Figure 33 report intriguing dynamic evolution of the ligands complexed with hCOX-2 during the 100 ns.

The analysis of the simulation showed the stability of the positioning over 100 ns of the **B5** and **B12** NSAID portions and ethylenic linkers (Figure 33C).

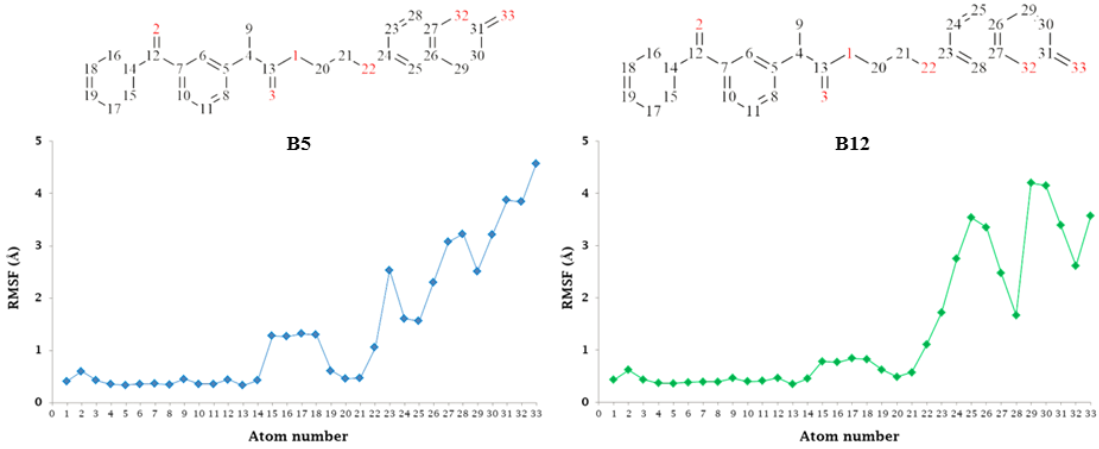

Figure 34. RMSF analysis of the heavy atoms of **B5** and **B12** along the MD course.

In contrast, the coumarin scaffolds of both ligands met significant changes, though at the different times along the course of the MD (Figure 33C and 34).

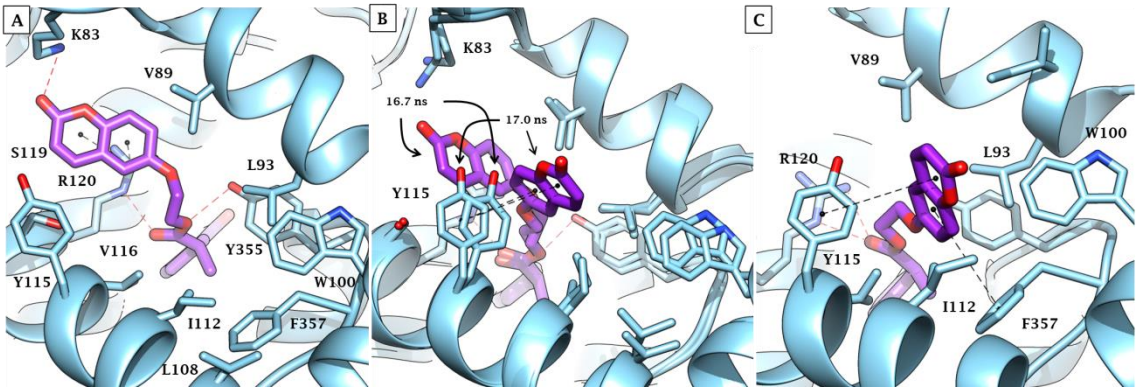

Figure 35. Dynamics evolution of **B5** binding mode to hCOX-2 over the course of 100 ns. A) Frame at t_0 after relaxation protocol of the ligand/target complex. B) Superimposition of frames at 16.7 and 17.0 ns. C) Frame at 100 ns.

The positioning of **B5** within the COX-2 active site was shown to be rather stable for the first 15 ns (Figure 35A), with RMDS fluctuating around 1.5 Å (Figure 33C). From that moment on, the coumarin ring progressively lost contacts with R120 and, aided by the concomitant displacement of the tyrosine residue Y115, reached a new position where it was stabilized by π-π interactions occurring with the aromatic side chain of the amino acid (Figure 35B). As the simulation progresses, the coumarin ring found a definite placing within the hydrophobic environment lined by V89, W100, V103, I112, L93, Y115 and F357 (Figure 35C).

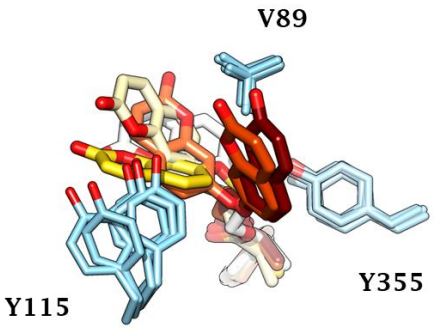

Figure 36. Dynamics evolution of **B12** binding mode to hCOX-2 over the course of 100 ns. The ligand colours darken over the dynamic simulation.

The evolution of **B12** binding to hCOX-2 turned out to be more complex (Figures 36 and 37). As already described for **B5**, the coumarin portion initially broke away from R120 (Figures 36 and 37B). However, after 20 ns it came back to its original positioning

(Figures 36 and 37A-C). Within the interval 10-25 ns, the ligand underwent a series of conformational changes driven by the repositioning of Y115 (Figure 37C), which culminated into the definitive settling of the coumarin portion within the hydrophobic area lined by V89, V103, I112, L93, I92, Y115 (Figure 37D).

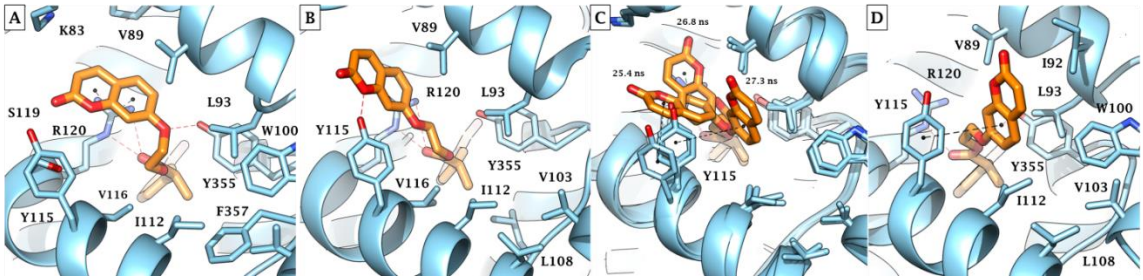

Figure 37. Dynamics evolution of **B12** binding mode to hCOX-2 (PDB 5KIR) over the course of 100 ns. A) Frame at t_0 after relaxation protocol of the ligand/target complex. B) Frame at 5 ns. C) Superimposition of frames at 25.4, 26.8 and 27.3 ns. C) Frame at 100 ns.

Data from MD testified the stability of the COX-2 / ligands adduct, although it turned out that the coumarin portion of the hybrids might occupy two different, but commonly hydrophobic environments within the active site, according to the movement of tyrosine residue Y115.

Gathering kinetic, stability, *in silico*, and *in vitro* data, ketoprofen ester derivatives **B5** and **B12** were chosen to move *in vivo*. The study was again conducted by Dr. Lorenzo Di Cesare Mannelli and Prof. Carla Ghelardini, Neurofarba Dept., University of Florence. The acute effects of **B5** and **B12** in a rat model of rheumatoid arthritis induced by the intra-articular injection of Complete Freund's Adjuvant. In Figure 38A, the hypersensitivity to a mechanical noxious stimulus (Paw pressure test) is shown. In the CFA + vehicle group (red line), the weight tolerated on the ipsilateral paw decreased to 40.1 ± 0.7 g in comparison to the control value of 68.5 ± 1.0 g recorded in vehicle + vehicle-treated animals (black line). These two groups, treated with 1% CMC, displayed a nociceptive threshold that was stable over the time course of the experiments (from 0 min to 60 min). Compound **B5** administered orally evoked an anti-hypersensitivity effect in a dose dependent manner; the higher dose of 30 mg kg^{-1} increased the pain threshold of the ipsilateral paw up to 53.8 ± 1.3 g 15 min after treatment, up to 64.4 ± 1.6 g after 30 min and up to 50.0 ± 0.5 g after 45 min. The effect disappeared at 60 min. Compound **B5** at 10 mg kg^{-1} partially increased the pain threshold at 15 min, fully counteracted the hypersensitivity of the ipsilateral paw induced by CFA injection 30 min after

administration and lost its efficacy at 45 min. The lower dose (3 mg kg^{-1}) slightly counteracted the hypersensitivity only 30 min after treatment reaching the value of 49.4 ± 0.6 g. Compound **B12** was tested only at 30 mg kg^{-1}, but was ineffective, similarly to its amide analogue (series A).[173] Higher doses of **B12** were not attempted due to the low solubility of the compound. Ketoprofen was used as reference drug at the dose of 30 mg kg^{-1}. This drug was effective in relieving hypersensitivity induced by CFA injection, and the pain threshold of the ipsilateral paw was increased 15 and 30 min after treatment without reaching the values of the control group (Figure 38A).

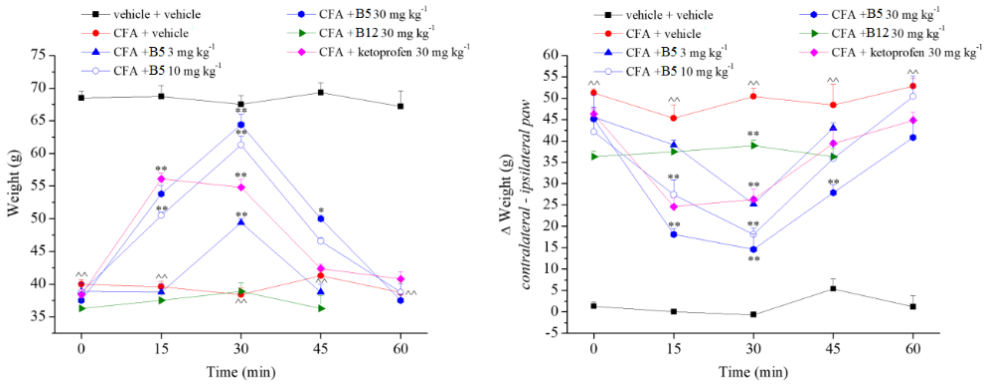

Figure 38. Acute pain-relieving effect of **B5** and **B12**. A) Paw pressure test was performed to evaluate the hypersensitivity to noxious mechanical stimuli. B) Incapacitance test was performed to evaluate the hind limb weight bearing alterations measured as postural imbalance related to pain. Data are expressed as the difference between the weight applied on the limb contralateral to the injury and the weight applied on the ipsilateral limb (Δ weight). Measurements were performed on day 14 after CFA intra-articular injection. Compounds were suspended in 1% CMC and orally acutely administered, evaluating the pain threshold over time. Ketoprofen 30 mg kg-1 was used as reference drug. Control animals were treated with vehicle. The values represent the mean of 10 rats performed in two different experimental sets. ^^P<0.01 vs vehicle + vehicle treated animals. *P<0.05 and **P<0.01 vs CFA + vehicle group.

Unilateral pain was also able to cause hind limb weight bearing alterations and the postural unbalance related to spontaneous pain was evaluated by incapacitance test (Figure 38B). The difference between the weight burdened on the contralateral and the ipsilateral paw was significantly increased in the CFA + vehicle treated animals compared with the control group (51.2 ± 1.0 g and 1.3 ± 1.0 g, respectively). This difference remained stable over the time course of the experiments (0 – 60 min). Compound **B5** significantly reduced the Δweight value in a dose dependent manner after a single administration. In particular, 30 mg kg^{-1} reduced the postural unbalance starting from 15 min and peaking 30 min after treatment. The effect lasted up to 45 min. The 10 mg kg^{-1}

dose was active from 15 min to 30 min while the dose of 3 mg kg^{-1} was effective only 30 min after **B5** administration. Compound **B12** was active only 30 min after treatment. Likewise, the results obtained by the Paw pressure test, ketoprofen (30 mg kg^{-1}) was effective in reducing postural unbalance 15 and 30 min after treatment (Figure 38B).

The effect of the reference drug ketoprofen at 30 mg kg^{-1} was comparable to **B5** at the same dose after 15 min after administration, but partially dropped after 30 min, whereas at this time the effect of **B5** was even increased at 10 mg kg^{-1}. In contrast to **B5**, the effect of ketoprofen did not last up to 45 min. In the incapacitance test (Figure 38B), ketoprofen at 30 mg kg^{-1} showed comparable effect with 1/3 of the dose of **B5** after 15 min post-administration. The effect of ketoprofen decreased after 30 min reaching an equal one with **B5** at 1/10 of the dose. Conversely the effect of **B5** increased at 30 min, lasting up to 45 min.

As it unexpectedly happened with several compounds of series A and B which were assayed *in vivo, - e.g.* its corresponding amide derivative - compound **B12** lacked pain-relieving effects in the used rat model. Because **B5** and **B12** show almost superimposable kinetic and *in vitro* profiles, further unevaluated processes take place which hinder **B12** pain-relieving efficacy. It should be stressed that even **A31**, that was shown to possess a valuable COX-2 inhibition-based activity *in vitro*, had produced no pain-relieving action when assayed *in vivo*.[173]

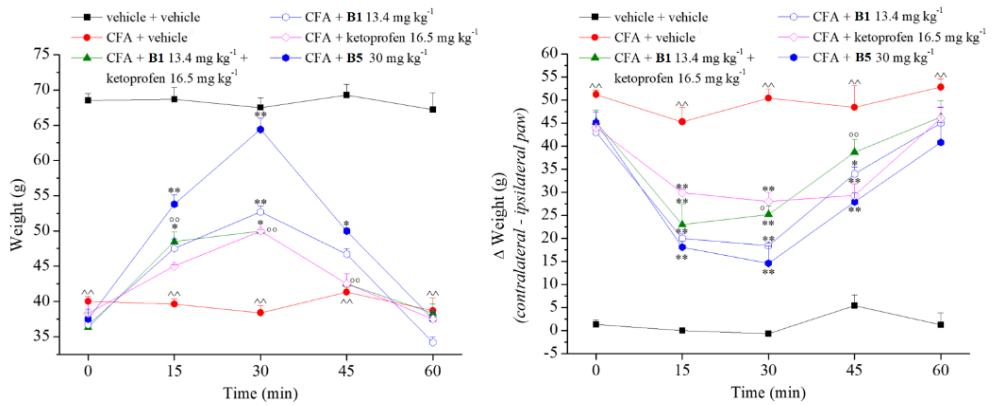

Figure 39. Comparison between the acute pain-relieving effect of **B5** 30 mg kg-1 and equimolar quantity of the CAI 3 (13.4 mg kg-1), ketoprofen (16.5 mg kg-1) and their co-administration **B1** + ketoprofen (13.4 mg kg-1 and 16.5 mg kg-1, respectively) in the A) Paw pressure test and B) Incapacitance test. Compounds were suspended in 1% CMC and orally acutely administered, evaluating the pain threshold over time. Control animals were treated with vehicle. The values represent the mean of 10 rats performed in two different experimental sets. ^^P<0.01 vs vehicle + vehicle treated animals; *P<0.05 and **P<0.01 vs CFA + vehicle group; °P<0.05 and °°P<0.01 vs CFA + **B5** treated group.[173]

Furthermore, the anti-hyperalgesic efficacy of 30 mg kg^{-1} of compound **B5** was compared to that evoked by the equimolar doses of the single drug CAI **B1** and ketoprofen (13.4 mg kg^{-1} and 16.5 mg kg^{-1}, respectively) as well as the equimolar co-administration of both (**B1**+ketoprofen) (Figure 39). The results were surprising. The 6-(2-hydroxyethoxy)coumarin **B1** showed to possess an unexpectedly marked anti-hyperalgesic action that started 15 min after injection and peaked at 30 min both in the Paw pressure and Incapacitance tests (reaching the values of 51.7 ± 0.8 g and 18.4 ± 0.5 g, respectively). The anti-hyperalgesic action was found to be significantly greater than that evoked by equimolar amount of ketoprofen, solely except for 45 min post-administration in the Incapacitance test. The action of coumarin **B1** was found to be even similar to the effect evoked by hybrid **B5** in the Incapacitance test uniquely at 15 min. However, the hybrid **B5** shows a significantly higher efficacy than equimolar doses of **B1**, ketoprofen and mainly their mixture in the Paw Pressure, and Incapacitance Test. These data indicate a significant synergistic effect of the hybrid in comparison to the mixture of single drugs which testifies the efficacy of the adopted multi-target strategy.

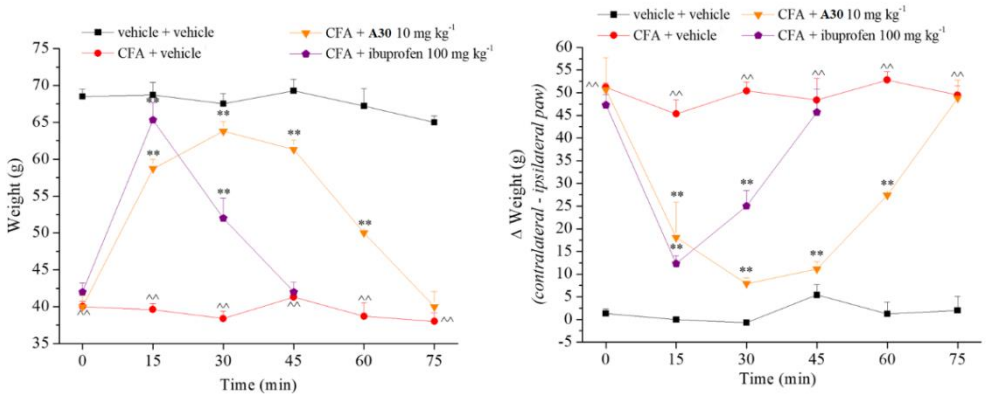

Figure 40. Acute pain-relieving effect of **A30** in comparison to ibuprofen in the A) Paw pressure test and B) Incapacitance test.[173]

To make a comparison between the ester and the amide best acting *in vivo*, the antihyperalgesic action of **A30** was reproduced in Figure 13 compared to the reference NSAID ibuprofen.[173] Compound **A30** had shown a similar pain-relieving trend during the experiments, but more potent than **B5**, because exerting a comparable effect at 1/3 of the dose (10 mg kg^{-1}). A full analgesic dose of ibuprofen (100 mg kg^{-1}) was found to be slightly more active than **A28** in the Paw pressure test after 15 min, but showed a rapid

drop of the effect, whereas **A30** continued to relieve pain up to 60 min. In contrast, the *in vitro* results showed that **A30** is weaker than ibuprofen in inhibiting platelet aggregation and reducing PGE_2 levels, implicating probable pharmacokinetics aspects which induce different *in vivo* behaviours.

As marked differences exist between the antihyperalgesic profiles of **B5** and the mixture **B1**+ketoprofen, the ester can be supposed to act also as multi-target integral agent in the target site and not only through the single portions after cleavage. Alternatively, the improved anti-inflammatory profile of the integral ester hybrid can be rationalized as an upgraded pharmacokinetics (as foreseen by the multi-target approach) which can enhance its absorption or drive the molecule to the target inflamed site, where the cleavage might occur and both single drugs act concomitantly and synergistically.

In contrast, it is reasonable to assume that the amides act uniquely as integral hybrids, possessing improved pharmacodynamics and pharmacokinetics with respect to the single drugs.

The successively acquired evidence of the plasma stability of amide-linked NSAID−CAI hybrid derivatives[175] aroused interest for gaining insights on their antinociceptive mechanism of action. Hence, we have here extended our studies on these multi-target agents for the management of rheumatoid arthritis[173,174] carrying out a bioisosteric substitution of the amide bond, which links the two inhibitory portions, to a more cleavable ester group. The new derivatives held and sometimes showed improved inhibitory profiles against the target CAs IV, IX and XII. Plasma stability studies showed the achievement of prodrug compounds because all derivatives reported a quick cleavage in rat plasma and some of them to be subjected to human plasma esterases according to the bore NSAID portion. A selection of derivatives, from both amides and esters series, was assayed *in vitro* to evaluate COX-1 (platelet aggregation inhibition) and COX-2 inhibition (reduction of PgE_2 production).[178-180] Interestingly, the ketoprofen ester derivatives **B5** and **B12** experience a small decrease of COX-1 related anti-inflammatory effect than the reference NSAID, maintaining a comparable PgE_2 level reducing activity. According to the amides and esters behavior in plasma and *in vitro*, the binding mode of some such derivatives to COX-1 and COX-2 was studied *in silico*, showing that the functionalization of the carboxylic group did not hinder the NSAID-like mode of action.

Data from MD with COX-2 revealed that the coumarin portion of the hybrids occupies two different, but commonly hydrophobic environments within the active site. The most promising compounds, **B5** and **B12**, were evaluated by the paw-pressure and incapacitance tests using an *in vivo* RA model. Of note, compounds **B5** showed a significantly major efficacy than equimolar doses of **B1**, ketoprofen and mainly their co-administration (**B1**+ketoprofen). These new studies allowed a more comprehensive understanding of the pharmacodynamics and pharmacokinetics of this class of multi-target derivatives. In fact, as marked differences exist between the antihyperalgesic profiles of **B5** and the mixture **B1**+ketoprofen, the ester can be supposed to also act as multi-target integral agent in the target site and not only through the single drugs after cleavage. Alternatively, the improved anti-inflammatory profile of the integral ester hybrid can be rationalized as an upgraded pharmacokinetic (as foreseen by the multi-target approach) which can enhance its absorption or drive the whole molecule to the target inflamed site, where the cleavage might occur and both single drugs act concomitantly and synergistically.

In contrast, it is reasonable to assume that the amides act uniquely as integral hybrids, possessing improved pharmacodynamics and pharmacokinetics with respect to the single drugs.

Finally, the pain-relieving action of **B5** has to be credited mainly to COX-2 over COX-1 inhibition, as shown by the NSAID and hybrid anti-inflammatory profiles measured *in vitro*. Hence, though the slightly minor analgesic effect of **B5** with respect to **A30**, a minor set of side effects should be expected which could induce a better tolerability of the pain-relieving treatment.

The experimental procedures are reported in Chapter 5.

3.4 Discovery of β-adrenergic receptors blocker - carbonic anhydrase inhibitor hybrids for multitargeted anti-glaucoma therapy (Series C)

Glaucoma is a leading cause of irreversible visual impairment and blindness, affecting more than 55 million people worldwide with a discouraging estimate of 80 million in 2020.[181-184] Glaucoma consists of a group of diseases characterized by a retinal and optic neuropathy, where progressive visual field loss is often associated with chronic elevation of intraocular pressure (IOP).[181,185]

The increase in IOP results from the malfunction of ciliary processes and the trabecular meshwork in the anterior chamber of the eye. These tissues physiologically support an adequate pressure in the eye by regulating aqueous humor secretion and its drainage. The main ionic constituent of the aqueous humor is bicarbonate. This fluid is present in the region between cornea and the lens (Figure 41), and its secretion and flow from the ciliary body to the anterior chamber leads to the homeostatic control of the IOP.[181,182] Glaucoma occurs when an increase in IOP occurs, which is due to either an excessive retention of aqueous humor within the anterior chamber or to an excessive secretion of the fluid (Figure 41).[34,181,185,186] Open-angle glaucoma (OAG) and angle-closure glaucoma (ACG) are the two most common types of primary glaucoma, with OAG being the most common in the Americas and Europe.[187,188] ACG is due to the impaired drainage of the aqueous humor from the anterior chamber. Conversely, this angle is constitutively open in OAG, but the drainage of the humor is diminished. The cause of the altered flow is unknown in OAG and under extensive investigation.[181,182,185] Because of the asymptomatic nature of chronic glaucoma, up to 50% of people in the industrialized world are unaware of their diagnosis and do not receive the required treatment.[186]

Multiple treatments for glaucoma exist and are chiefly separated into pharmacologic, laser, and surgical therapies.[185-189] In most individuals, pharmacologic therapy is the first therapy of choice for IOP reduction and generally includes the use of topically acting agents, such as eye drops, that reduce aqueous humor production, as well as agents that raise the outflow facility.[34,187-189] Lowering IOP is the cornerstone of glaucoma therapy, since each additional millimeter of mercury IOP increase can lead to an 11% increase in the risk of glaucoma progression.[190]

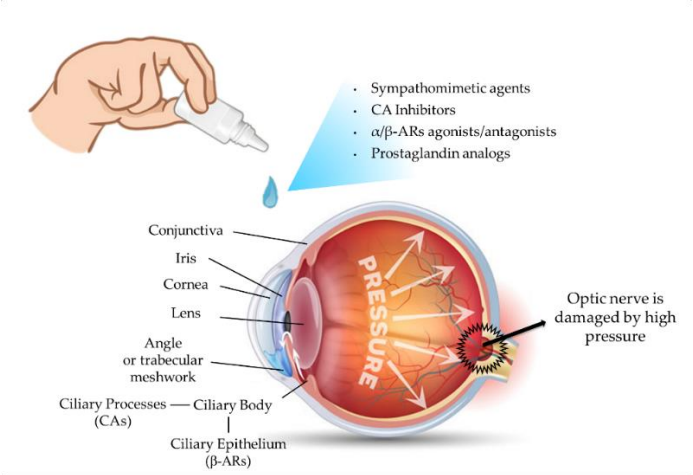

Figure 41. Mechanism and available pharmacologic treatments for glaucoma.[191]

The clinically available drugs include sympathomimetic stimulants (epinephrine), parasympathomimetic agents (pilocarpine), β-blockers (timolol), CAI (acetazolamide and dorzolamide), and prostaglandin derivatives (latanoprost and travoprost) (Figure 42). These classes of drugs can be used alone or in various combinations.[34,187-192]

β-Blockers reduce IOP via blockade of the sympathetic nerve endings in the ciliary epithelium, reducing the production of aqueous humour.[193] Among the topically-acting β-blockers available for the treatment of glaucoma, there are non-selective agents, which target both β_1- and β_2-adrenoceptors, and cardio-selective drugs, which block only the β1-receptors.[192] In the past, β-blockers were the most common first line topical glaucoma medication, however the use of more efficient prostaglandin analogues became the primary course of treatment during the 1990s.[189]

When monotherapy alone is not effective in controlling IOP, other drugs with different mechanisms of action can replace or be added in conjunction with beta-blockers or prostaglandin analogues.[192] Commonly used second-line agents include topical CAIs. Inhibition of CAs in the ciliary processes reduces aqueous humor secretion, probably by slowing the rate of bicarbonate production and therefore reducing the transport of water and osmotically obligated sodium within the fluid. As a result, the aqueous humour secretion decreases, leading to a reduction of IOP up to 25-30%.[176,183,184] If necessary, CAIs such as acetazolamide, methazolamide, ethoxzolamide, and dichlorophenamide can still be used as systemic antiglaucoma drugs, though they may show a wide range of undesired side effects in some patients.[194,195]

Compliance is the major challenge with adding multiple drops. It has been demonstrated that increasing the number of drop bottles to a patient's treatment results into a negative influence on patient adherence.[192] Fixed combination therapies have been developed and are currently available in the clinic. For example, the combination of a β-blocker (timolol) and CAI (dorzolamide, DZA) represents one of the most used therapeutic options.[192]

The current therapies are often inadequate given that topical glaucoma therapy is burdened by the need for multiple classes of medications to control IOP,[196] undesired side effects,[10] and barriers such as patient compliance[197] and difficulty with proper drop instillation.[198] New needed pharmacotherapies for glaucoma should exhibit favourable benefit-risk profiles and alternative mechanisms of action relative to current therapies.[187] This can be achieved by either increasing efficacy (ocular hypotensive efficacy), decreasing adverse events, or both.

In this third project, we proposed a multi-targeted approach for the treatment of glaucoma by design, synthesis, and biological *in vitro/vivo* evaluation of a series hybrid drugs which concomitantly affect the β-adrenergic receptors and carbonic anhydrases in the eye.

Therefore, an approach consisting of single-molecule, multi-targeted compounds was chosen over the co-administration of single drugs due to potential therapeutic benefits.[140,141,199,200] The hybrid drug strategy has been previously applied to target glaucoma by carbonic anhydrase inhibition. CAI – nitric oxide (*NO*) donor hybrids stood out amongst the most effective topically active agents.[200-202] Since hypertensive glaucoma patients show a decreased content of *NO*/cGMP in the aqueous humor, it has been shown that *NO*-donors can decrease IOP in normal and pathological conditions. One such compounds was twofold more efficient than dorzolamide to reduce high IOP characteristic of this disease in an animal model.[201]

The herein reported derivatives feature a benzene sulfonamide moiety, representing the CA inhibitory fragment, and the aryloxy-2-hydroxypropylamine portion of β-blockers such as propranolol and timolol (Figure 42).

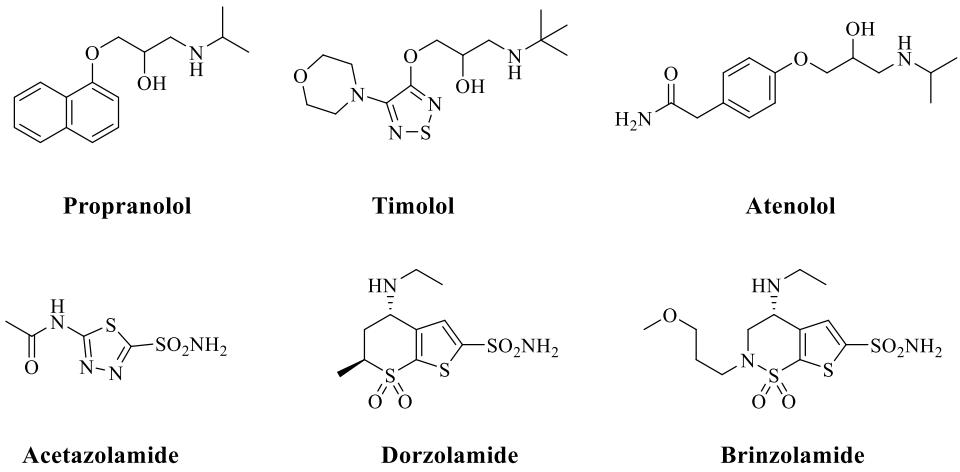

Figure 42. Molecular structures of clinically used β-blockers and anti-glaucoma CAI drugs.

Primary sulfonamides (Figure 42), such as **AAZ** or **BRZ**, have represented the first-generation CAIs and have been clinically used for almost 70 years as anti-glaucoma agents.[1,203] Dorzolamide, a second-generation CAI, was the first topically acting sulfonamide used clinically as an anti-glaucoma medication. It is indicated for the reduction of elevated IOP in patients with open-angle glaucoma or ocular hypertension that do not sufficiently respond to β-blockers.[34,194,195]

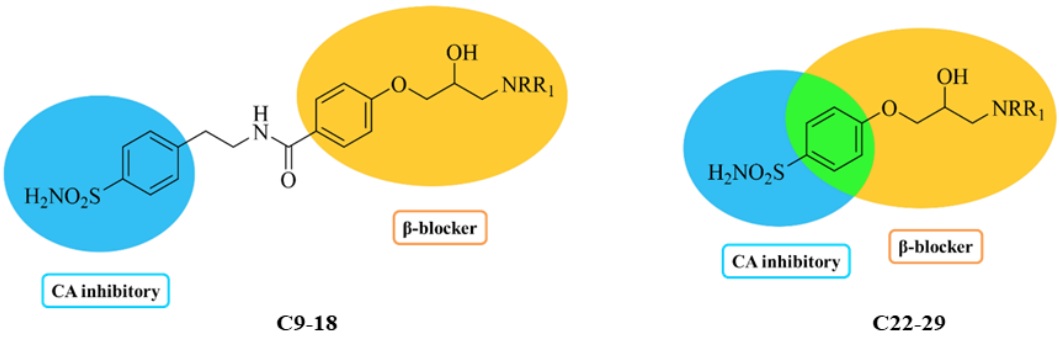

Figure 43. Design of aryloxy-2-hydroxypropylamine sulfonamides dual-targeted agents.

Modulation of the β-ARs was investigated by swapping the substituents appended at the aryloxy-2-hydroxypropylamine moiety, which is a rather common hallmark of β-blockers and thus maintained in the hybrids structure (Figure 43). The aryloxy-2-hydroxypropylamine portion was directly appended at the benzenesulfonamide scaffold (derivatives **C22-29**) or alternatively detached by means of an ethylbenzamide spacer (derivatives **C9-18**). In this second case, uniquely small aliphatic amines were considered in the β-blocker portion, owing to the hydrophobic nature of the spacer.

The incorporation of such 2-hydroxypropilamine moieties at the benzenesulfonamide scaffold (both direct and spaced) represents an application of the CAI "tail approach",[96, 204,205] the most common method to develop isoform selective inhibitors within the zinc-binders class. This approach explores the modulation of moieties appended at the aromatic/heterocyclic ring present in the scaffold of the CAIs in order to selectively promote interactions with isoform unique residues at the entrance of the active site cavity.

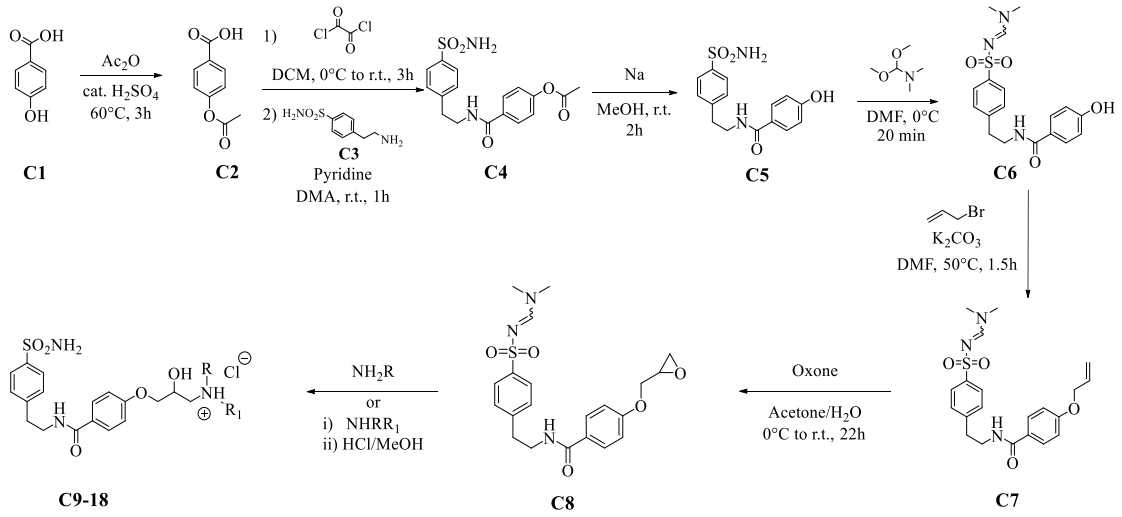

Scheme 5. General synthetic procedure for compounds **C9-18**.

I participated in the two synthetic strategies planned to obtain these hybrid compounds. Preparation of the first series molecules **C9-18** shared a common key epoxy intermediate **C8,** for which the synthetic route is illustrated in Scheme 5. Coupling of ethylamminobenzenesulfonamide **C2** with freshly prepared 4-acetoxybenzoyl chloride **C2** generated amide **C4**, which was therefore deacetylated with sodium methoxide and protected on the sulfonamide group with *N,N*-dimethylformamide dimethyl acetal. Reaction of the resulting phenol **C6** with allyl bromide followed by epoxidation of the olefinic function in presence of Oxone and acetone provided for intermediate **C8.** Epoxide ring opening (**C8**) to afford 2-hydroxypropylamine derivatives **C9-18** was achieved by treatment with an excess of varied primary and secondary amines. Reaction with primary amines occurred with an additional and unexpected cleavage of the sulfonamide protecting group, resulting directly in the 2-hydroxypropylamine derivatives **C9-16**. Because secondary amines were not able to carry out the deprotection process, treatment in acidic media was necessary to free the sulfonamide group and generate compounds **C17-18**.

In a similar manner, preparation of the second series of molecules **C22-29** (Scheme 6) shared the common epoxy intermediate **C21**, which was obtained by reacting the N-protected 4-hydroxybenzenesulfonamide **C20** with epibromohydrin in presence of Cs_2CO_3. Epoxide **C21** was reacted with different amines and subsequently treated in acidic media in the case of secondary amines to give the 2-hydroxypropylamine derivatives **C22-29**. These synthetic strategies were adopted to provide **C9-18** and **C22-29** as racemates, since the mixture of both enantiomers was deemed more suitable to initially seek for biological activity.

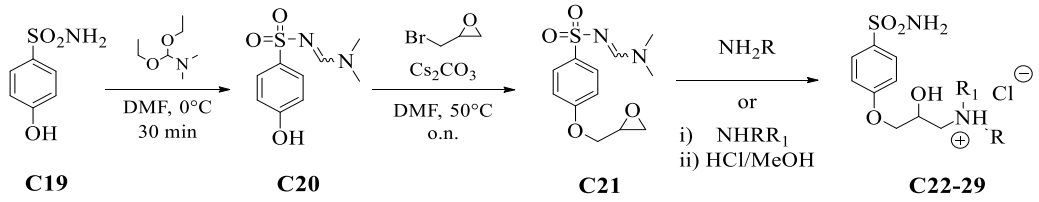

C19 **C20** **C21** **C22-29**

Scheme 6. General synthetic procedure for compounds **C22-29**.

Therefore, I evaluated the CA inhibition profiles of compounds of this third project in addition to **AAZ** as standard inhibitor, against four physiologically relevant isoforms, hCA I II, IX, and XII. The choice of these isoforms was based upon: hCA II and XII are upregulated in the eyes of glaucoma patients[1,34,185] and might be responsible for increased blood flow and thus the oxygen supply in hypoxic neovascular retinic tissues; hCA IX has been found to be upregulated in the hypoxia-suffering cells of the retinal pigment epithelium;[1,2,203] and hCA I is the main off-target isoform for the therapeutic application of CAIs in the reported ocular diseases.[1] The following SAR can be gathered from the inhibition data reported in Table 6.

(i) The cytosolic isoform hCA I was effectively inhibited by most of the sulfonamides of the first series with inhibition constants ranging in the low nanomolar range, between 6.6 and 59.1 nM. Conversely, the benzenesulfonamides directly bearing the 2-hydroxypropylamine (**C22-29**) moieties were found to act as weaker inhibitors with K_Is spanning between 74.5 and 750.8 nM. The sec-butyl and benzyl bearing derivatives **C24** and **C26** stood out from the others with K_Is less than 100 nM. All the first series compounds and **C24, C26-28** from the second series were stronger inhibitors compared to the clinically used **AAZ** (K_I value of 250 nM).

Table 6. Inhibition data of human CA isoforms hCA I, II, IX and XII with sulfonamides **C9-18**, **C22-29** reported here and the standard sulfonamide inhibitor acetazolamide (**AAZ**) by a stopped flow CO_2 hydrase assay.[169]

			K_I (nM)[a]			
Cmpd	**R**	**R_1**	**hCA I**	**hCA II**	**hCA IX**	**hCA XII**
C9	-CH_3	H	20.2	14.1	1.7	1.5
C10	-CH_2CH_3	H	9.3	48.8	22.1	1.9
C11	-$CH_2CH_2CH_3$	H	52.2	18.4	7.4	1.5
C12	-$CH(CH_3)_2$	H	8.9	3.0	61.8	18.1
C13	-$CH(CH_3)_3CH_2CH_3$	H	45.8	55.7	53.6	2.8
C14	-$C(CH_3)_3$	H	59.1	16.1	83.1	23.8
C15	-CH_2Ph	H	35.6	1.9	74.7	2.4
C16	-CH_2CH_2OH	H	33.2	16.6	5.8	27.7
C17	-$CH_2CH_2OCH_2CH_2$-		6.9	1.5	7.0	4.1
C18	- $CH(CH_3)_2$	- $CH(CH_3)_2$	6.6	1.2	6.0	1.6
C22	-CH_3	H	750.8	1174.3	23.4	4.9
C23	-$CH(CH_3)_2$	H	350.4	155.5	47.6	44.4
C24	- $CH(CH)_3CH_2CH_3$	H	74.5	240.6	107.7	58.6
C25	-$C(CH_3)_3$	H	234.3	174.1	95.4	41.9
C26	-CH_2Ph	H	85.4	44.1	93.1	72.4
C27	-CH_2CH_2Ph	H	145.6	75.0	59.2	39.8
C28	-CH_2CH_2OPh	H	183.1	15.2	84.6	82.2
C29	-$(CH_2CH_2)N(CH_3)(CH_2CH_2)$-		230.6	48.9	126.5	164.1
AAZ	-	-	250	12	25	5.7
DZA[b]	-	-	50000	9	52	3.5

a. Mean from 3 different assays, by a stopped flow technique (errors were in the range of ± 5-10 % of the reported values). b. From ref. 1

(ii) The physiologically dominant isoform hCA II was strongly inhibited by all reported sulfonamides (K_I values ranging between 1.5 and 75.0 nM, Table 6), apart from the second series compounds incorporating small substituents (methyl, isopropyl, sec-butyl and tert-butyl) on the amine moiety (**C22-25**), whose K_Is spanned from 155.5 to 1174.3 nM. The hCA II inhibition profiles showed the efficacy of the spacer-containing compounds. It is worth mentioning that the bulkiest derivatives of the first seriess **C15** (benzylamine, K_I 1.9 nM), **C17** (morpholine, K_I 1.5 nM) and **C18** (diisopropylamine, K_I 1.2 nM) as well as those of the second series **C26-29** (K_Is ranging between 15.2 and 75.0 nM) exhibited the strongest hCA II inhibition profiles within each subset. Despite a

generally comparable efficacy with the standard **AAZ** (K_I value of 12 nM), only compounds **C12**, **C15, C17** and **C18** exhibited a stronger effectiveness.

(iii) The data in Table 6 depicted similar inhibitory trends against the membrane-associated isoforms hCA IX and XII, which were strongly inhibited by most derivatives. In detail, the K_Is for the first series of derivatives against hCA IX spanned from 1.7 (**C9**, methylamine) to 83.1 nM (**C14**, *tert*-butylamine), whereas the efficacy of compounds **C22-29** was weaker with inhibition constants ranging between 23.4 (**C22**, methylamine) and 126.5 nM (**C29**, *N*-methylpiperazine), not permitting a rationale for a SAR. Again, only compounds **C9-11**, **C16-18** among the benzamide-bearing derivatives and compound **C22** in series two were found to possess at least comparable efficacy to the **AAZ** (K_I of 25 nM).

(iv) Most of the spacer-supplied compounds demonstrated strong hCA XII inhibitory effectiveness (K_Is ranging between 1.5 and 4.1 nM), except for **C12** (isopropylamine), **C14** (*tert*-butylamine) and **C16** (ethanolamine), which showed a 10-fold diminished activity (K_Is of 18.1-27-8 nM). Among the spacer-devoid derivatives, compound **C22**, that incorporated a methyl group on the amine moiety, exhibited low nanomolar efficacy (K_I of 4.9 nM), whereas the remaining compounds were significantly weaker with inhibition constants ranging between 39.8 and 164.1 nM.

(v) Noteworthy, the first series of derivatives were shown to be generally more efficacious against the hCAs in comparison to the directly linked dual-derivatives, to a greater extent against the cytosolic isozymes hCA I and II. The second series compounds **C22** and **C23**, which bear a methyl and isopropyl group appended at the amine moiety, were able to target hCA IX and XII with selectivity over the cytosolic isozymes (selectivity ratio hCA II / IX of 50.2 and 3.2 and hCA II / XII of 240.5 and 3.5, respectively). The inhibition profiles of compounds **C22** and **C23** indicate a potential to target several CAs-associated diseases without causing the typical side-effects of non-selective inhibitors in systematically administered treatments.

The β-adrenergic receptors (β-ADRs) binding properties of compounds **C9-18** and **C22-29** were evaluated, in addition to propranolol and atenolol[206,207] as standard β-blockers, against the human cloned β_1- and β_2-ADRs receptors expressed in HEK293T cell membranes. The study was conducted by Dr. Rosanna Matucci, Neurofarba Dept.,

University of Florence.The following remarks can be drawn from the data reported in Table 7.

Table 7. Inhibition binding constants (pK_i) of the tested compounds for human cloned β_1- and β_2-ADRs expressed in HEK293T cell membranes.

Cmpd	R	R_1	pK_i[a]	
C9	$-CH_3$	H	<4	<4
C10	$-CH_2CH_3$	H	<4	<4
C11	$-CH_2CH_2CH_3$	H	<4	<4
C12	$-CH(CH_3)_2$	H	<4	<4
C13	$-CH(CH)_3CH_2CH_3$	H	<4	<4
C14	$-C(CH_3)_3$	H	<4	<4
C15	$-CH_2Ph$	H	<4	<4
C16	$-CH_2CH_2OH$	H	<4	<4
C17	$-(CH_2CH_2)O(CH_2CH_2)-$		<4	<4
C18	$-CH(CH_3)_2$	$-CH(CH_3)_2$	<4	<4
C22	$-CH_3$	H	<4	<4
C23	$-CH(CH_3)_2$	H	4.98±0.06	4.50±0.05
C24	$-CH(CH)_3CH_2CH_3$	H	4.81±0.03	4.52±0.13
C25	$-C(CH_3)_3$	H	4.87±0.06	5.30±0.08
C26	$-CH_2Ph$	H	4.10±0.03	<4
C27	$-CH_2CH_2Ph$	H	4.57±0.02	4.40±0.02
C28	$-CH_2CH_2OPh$	H	5.18±0.05	4.55±0.03
C29	$-(CH_2CH_2)N(CH_3)(CH_2CH_2)-$		<4	<4
Propranolol [b]	-		7.93±0.03	8.76±0.02
Atenolol [b]	-		5.82±0.14	5.02±0.20
Timolol [c]	-		8.27±0.08	9.68±0.02

a. Values are reported as mean ± SEM of 3-5 experiments, each one performed in duplicate; b. Racemate; c. From ref. 195,196.

The competition binding experiments did not show striking affinities of the multi-targeted derivatives. The data in Table 7 highlight the absence of binding affinity reported towards both the β_1 and β_2-ADRs for the spacer-endowed derivatives **C9-18**, which were not able to compete with [^{3}H]-CGP12177 at the receptor subtypes below 100 μM. Conversely, interesting pK_i values can be gathered from the binding curves measured for the second series compounds (**C22-29).** Most derivatives were found to exhibit low micromolar affinities for both β-ADRs subtypes (except **C22** and **C29**).

When the *tert*-butylamine bearing **C25** showed approximately a three-fold β_2/β_1 selectivity (below 10 μM for the β_2-AR subtype), the remaining derivatives showed preferential affinity for the β_1-AR, with the highest selectivity (over four-fold) reported for **C28** (Figure 44). The incorporation of a simple methyl group or *N*-methylpiperazine moiety in the 2-hydroxylpropyl portion deprives respectively **C22** and **C29** of any affinity for both receptors subtypes up to 100 μM.

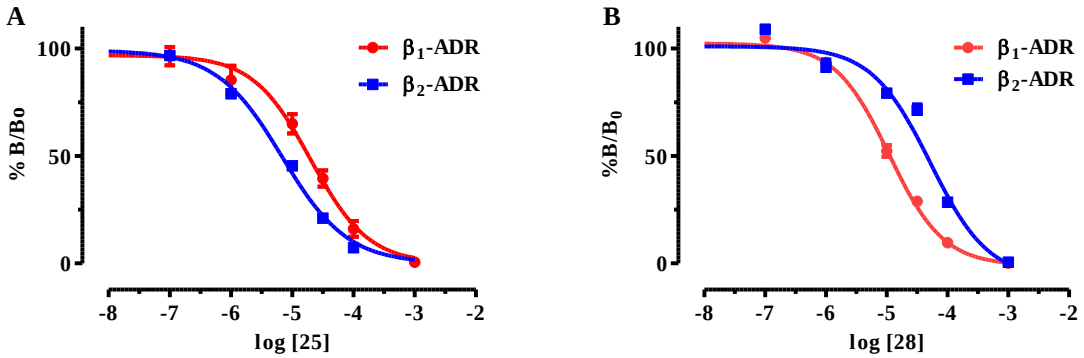

Figure 44. Inhibition of [^{3}H]-CGP12177 specific binding to membrane homogenates of HEK293T cells which stably express the β_1- and β_2-adrenergic receptors by increasing concentration of compound (A) **C25** and (B) **C28**. The curves were fitted using the standard four parameter logistic equation and are the mean ± S.E.M. from 3-4 independent experiments. Non- specific binding was determined in the presence of 10 μM propranolol. Y-axis: normalized Bound/Total bound.

The K_I values measured for most compounds **C23-28** were comparable to the racemic standard β-blocker atenolol (low micromolar range).[206-209] Moreover, the K_I of **C25** against the β_2-subtype exceed that reported for the clinically used drug. Such results are of interest in terms of single enantiomer binding constants evaluation for future developed derivatives.

Although the similarity between derivatives **C22-29** (sulfonamide-bearing) and clinically used β-blockers, such as atenolol, practolol and celiprolol (which possess an amide or urea group appended at the same position of the aromatic scaffold) indicates analogue functional tendency, further investigations with this respect are currently ongoing.

The X-ray crystal structure of hCA II was determined in complex with compounds **C12** and **C23** (Table 8). The crystallographic study was conducted by Dr. Carrie Lomelino and Prof. Robert McKenna, Dept. of Biochemistry and Molecular Biology, University of Florida. Compounds **C12** (*R* enantiomer) and **C23** (*S* enantiomer) were observed to bind directly to the active site zinc and displace the catalytic water, as is expected for sulfonamide-based compounds (Figure 45A, 45B). Hydrogen bonds were

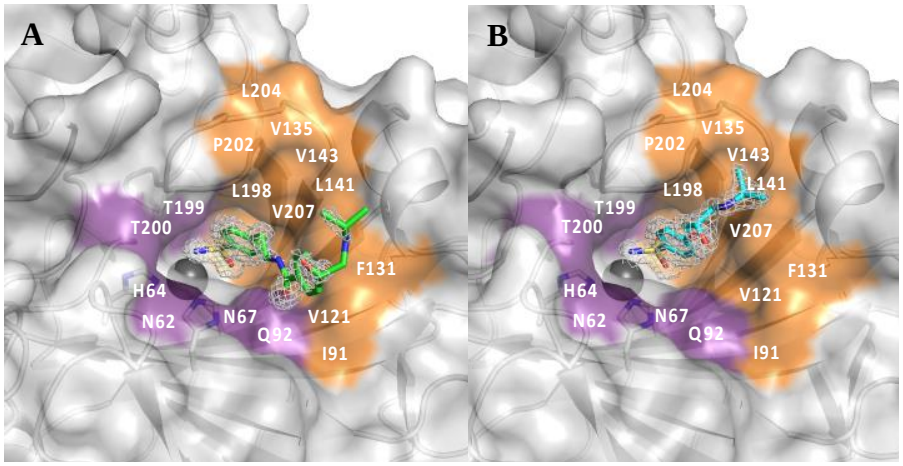

Figure 45. Surface representation of hCA II in complex with A. compound **C12** (represented as green sticks) and B. compound **C23** (represented as cyan sticks).

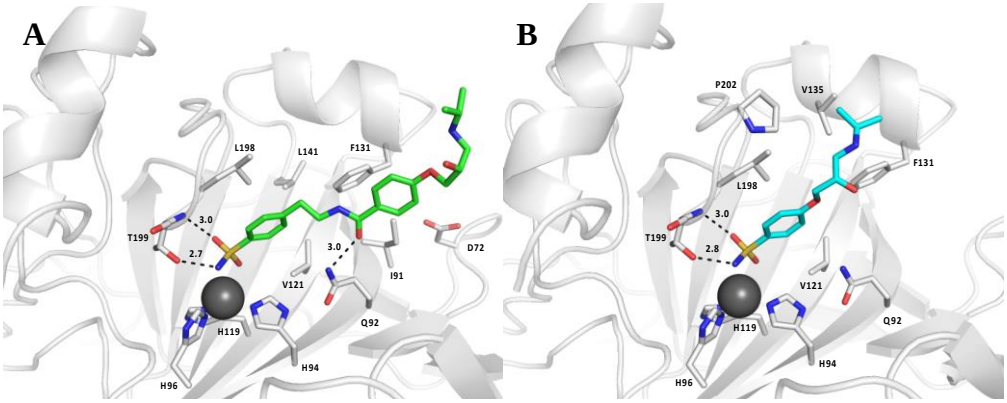

Figure 46. Active site view of hCA II in complex with A. compound **C12** (green) and B. compound **C23** (cyan). Hydrogen bonds are represented as black dashes with distances labelled in angstroms.

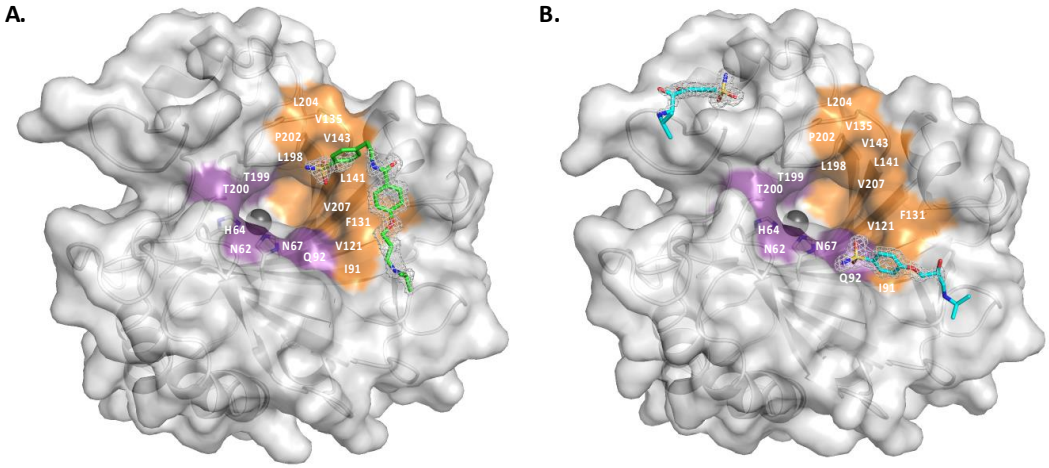

Figure 47. Surface representation of hCA II in complex with crystal contact inhibitors. hCA II in complex with A. compound **C12** (green) and B. compound **C23** (cyan). Hydrophobic and hydrophilic residues are labeled and colored (orange and purple, respectively).

observed between the nitrogen and oxygen atoms of the sulfonamide and Thr199 (2.7-2.8 and 3.0Å, respectively) (Figure 45A, 45B).

The presence of the spacer in compound **C12** resulted in the formation of an additional hydrogen bond between the carbonyl and Q92 side chain (3.0Å). This observation rationalizes the stronger binding affinity of compound **C12** for CA II in relation to the direct compound **C23** (Figure 42A). Both inhibitors were further stabilized by van der Waals interactions with active site residues I91, V121, F131, L141, and L198 in the case of compound **C12** and residues Q92, V121, F131, V135, L198, and P202 for compound **C23** (Figure 46A, 46B).

Steric hindrance between the benzene ring in spacer-containing compound **C12** and F131 shifted the tail of this compound toward the interface between the hydrophobic and hydrophilic regions of the active site, allowing a second molecule to bind between monomers within the crystal lattice (Figure 47).

This secondary inhibitor molecule interacts directly with hCA II through hydrogen bonding with D72 (2.6 and 2.7Å) and is further stabilized through an interaction with the *NH* group of the active site-bound **C12** (2.9Å) (Figure 48). Similarly, two additional molecules of compound **C23** were observed to bind outside the hCA II active site, thought to bind due to crystal packing (Figure 47).

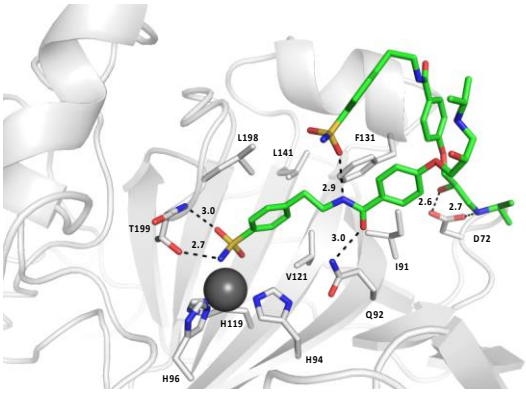

Figure 48. hCA II (gray) in complex with a secondary **C12** (green) molecule due to crystal packing. Hydrogen bonds are represented as black dashes with distances labeled in angstroms.

Table 8. X-ray crystallography statistics.

Sample	CA II_C12	CA II_C23
PDB Accession Code	**5WLV**	**5WLT**
Space Group Cell Dimensions	$P2_1$ a = 42.6, b = 41.6, c = 72.5; β = 104.3	$P2_1$ a = 42.7, b = 41.6, c = 72.7; β = 104.5
Resolution (Å)	30.8 - 1.4 (1.42 - 1.40)	40.3 - 1.6 (1.60 - 1.57)
Total Reflection	69.038	53.038
I/Iσ	21.3 (2.8)	17.1 (2.2)
Redundancy	3.2 (3.1)	4.0 (4.0)
Completeness (%)	99.4 (99.5)	90.2 (92.7)
Rcryst (%)	14.5 (22.3)	14.5 (18.9)
Rfree (%)	16.7 (25.5)	17.6 (25.0)
Rsym (%)	5.2 (40.4)	6.8 (54.8)
Rpim	3.4 (27.6)	3.5 (28.7)
# of Protein Atoms	2099	2094
# of Water Molecules	234	213
# of Ligand Atoms	60	76
Ramachandran stats (%): Favored, allowed, generously allowed	97.3, 2.7, 0	96.9, 3.1, 0
Avg. B factors (Å^2): Main-chain, Side-chain, Ligand	15.2, 19.5, 40.0	14.4, 18.7, 41.3
rmsd for bond lengths, angles (Å,°)	0.006, 0.939	0.006, 0.918

In spite of not striking β-ADR-binding affinities, several molecules within the second series demonstrated a multi-targeted action and excellent and suitable water solubility to be formulated as 1% eye drops at the neutral pH value. We investigated the intraocular pressure lowering properties of some of these compounds, more precisely, **C23** (iso-propylamine, for which the X-ray crystal structure in complex with hCA II was reported), **C25** (tert-butylamine) and **C27** (phenethylamine) in a rabbit model of glaucoma. The morpholine-bearing compound **C17** of the first subset was included in the study to evaluate the IOP lowering efficacy of a uniquely CA inhibitory derivative.[208,209] **DZA** hydrochloride and timolol, as well as their combination (1% + 0.25%, in the clinically used *ratio*) were used for comparison as standard drugs, with a control using the vehicle (hydroxypropylcellulose at 0.05%). The 1% compounds eye drops were administered to rabbits with high IOP, induced by the injection of 0.1 mL of hypertonic

saline solution (5% in distilled water) into the vitreous of both eyes. The benzamide derivative **C17** was a strong, low nanomolar inhibitor for hCA II, IX and XII (K_Is of 1.5, 7.0 and 4.1 nM), but lacked activity on the β-ADR. On the contrary, compounds **C23**, **C25** and **C27** showed a significant, low micromolar action against the β_1- and β_2-ADR, at the expense of a weaker efficacy against target hCAs (Figure 49).

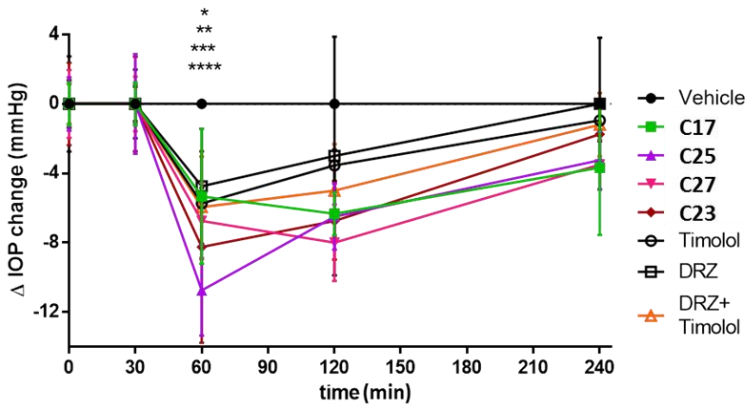

Figure 49. Drop of intraocular pressure (ΔIOP, mmHg) versus time (min) in hypertonic saline-induced ocular hypertension in rabbits, treated with 50 µL of 1 % solution of compounds **C17**, **C23**, **C25**, **C27**. **Timolol** 0.25%, **DRZ** 1% and their association (**DRZ+timolol**) were used as reference drugs. Data are analysed with 2way Anova followed by Dunnett's multiple comparison test. * p<0.05 **C17** and **DRZ** *vs* vehicle at 60'; ** p<0.005 **timolol** and **DRZ+timolol** *vs* vehicle at 60'; *** p<0.001 **C27** *vs* vehicle at 60'; ****p< 0.0001 **C23** and **C25** *vs* vehicle at 60'.

The dual agents **C23**, **C25**, **C27** were more effective than standard **DRZ** and timolol with IOP decreases of 8.25, 10.75 and 6.75 mmHg at 60 min post-administration, respectively (Figure 49). Compound **C25** stood out as the most efficient one, with a twofold enhanced efficacy in comparison to **DRZ** and timolol, which caused an IOP decrease of 4.75 mmHg and 5.73 at 60 min post-administration, respectively. Noteworthy, 1% eye drops of the multi-targeted derivatives were more effective than the combination of the CAI and β-blocker leads in the ratio 1% + 0.25%. CAI **C17** showed to lower IOP at 60 min post-administration in a comparable manner to the standards. Compounds **C17**, **C23** and **C25** showed similar IOP lowering effectiveness after 2 h post-administration in the range 6.33-6.75 mmHg, with **C27** excelling among the others producing an IOP drop of 8.0 mmHg. The IOP drops produced by all assayed derivatives were greater that those occurring using the standard drugs and their combination (3.0, 3.54, 5.0 mmHg, respectively). When compounds **C23** and **C25** were more active after 60 min post-administration, compounds **C17** and **C27** reached the greater efficacy after 120 min.

Derivatives **C17**, **C23** and **C25** maintained IOP lowering action at 4 h post-administration (3.25-3.67 mmHg), when timolol and the drugs combination were barely active and **DRZ** lost its efficacy. A significant enhancement in the IOP lowering efficacy of dual-agents **C23**, **C25**, **C27** with respect to **C17** (that uniquely inhibit the CAs) was observed at 60 min post-administration, whereas the range thinned after 2-hours, with the multi-target **C27** standing out anyhow as the most efficient compound. It is worth stressing that **C17** inhibits hCA II and XII much more potently (K_Is of 1.5 and 4.1 nM) than the **C23**, **C25**, **C27 (**K_Is in the range 75.0-174.1 and 39.8-44.4 nM, respectively). As a result, it is reasonable to ascribe the powerful IOP lowering efficacy of **C17**, that did not possess a dual action, to the orders of magnitude greater hCA II and XII inhibition than **C23**, **C25**, **C27**. Hence, the more effectual IOP lowering action of the hybrids compounds, in spite of a remarkably weaker CA inhibition than derivative **C17**, witnesses the concomitant, although unbalanced (nanomolar *vs* micromolar) modulation of two physiological systems, namely CAs and β-ADRs.

With the incidence of glaucoma steadily growing because of both demographic expansion and population aging, new pharmacologic therapies that possess more favourable benefit-risk profiles are needed. These can be achieved by either increasing efficacy (ocular hypotensive efficacy), decreasing adverse events, or both. The combination of a β-blocker and a CAI included in eye drops is one of the clinically-available options to treat glaucoma and is extensively used. In the present project, a novel single molecule, multi-targeted approach was chosen over the co-administration of single drugs due to varied potential therapeutic benefits, such as an improved effect onto the intricate biochemical processes involved in disease pathology. Concomitant modulation of β-adrenergic and CA systems present in the eye was achieved by combining benzenesulfonamide fragments of classical CAIs with 2-hydroxypropylamine fragments of known, clinically used β-blockers, such as propranolol or timolol. The resulting two series of molecules, which differ by the spacer incorporated between the pharmacophores, were investigated for their inhibitory activity against target (hCA II, IX and XII) and off-target (hCA I) hCAs as well as for their effectiveness to modulate the β_1- and β_2-ARs. A first subset of derivatives reported no multi-targeted modulatory efficacy, with a remarkable CA inhibitory potency at the expense of a void affinity to β-ADRs. The second subset of hybrid molecules exhibited a slightly worsening of CA

inhibition profiles, with the affinity to β-ADRs raising to micromolar range, which is comparable to racemic β-blocker atenolol.

The X-ray crystal structure of hCA II was determined in complex with compounds **C12** and **C23**, namely the isopropyl-substituted derivatives of both series. Multi-target derivatives **C23**, **C25**, **C27** were shown to possess more effective IOP lowering properties than the lead, clinically used dorzolamide and timolol, and their combination based onto the balanced multi-targeted modulation. The reported evidence supports the proof-of-concept of adrenergic receptors blocker - carbonic anhydrase inhibitor hybrids for anti-glaucoma therapy with an innovative mechanism of action. These spread the way of the research of more effective anti-glaucoma agents acting on the two systems in a more powerful and balanced manner. Identification of eutomers within the racemic mixtures will be of help in enhancing efficacy into β-ADRs without significantly affecting the compounds CA inhibitory activity.

The experimental procedures are reported in Chapter 5 and the data and results of this research were published in Alessio Nocentini, et al. J. *Med. Chem*. **2018**, *61*, 5380-5394.

3.5 Multi-potent hybrids assembled by CA inhibitors and *NO*-donors as antitumor and anti-infective drugs: synthesis and kinetic evaluation (Series D)

In this context of cancer growth, invasion and metastatization, *NO* also plays a crucial role.[210] *NO* is a key mediator with important functions in mammalian physiology and pathophysiology. High levels of *NO* and its metabolic derivatives, the reactive nitrogen species (RNS) and reactive oxygen species (ROS), have profound effects on tumor cells proliferation, angiogenesis and metastasis.[210] Recently, Bao N. et al. and Huang Z. et al. showed that the production of this gasotransmitter by *NO*-releaser compounds provokes cytotoxicity against human carcinoma cells *in vitro* and anti-metastatic activity *in vivo*.[211,212] *NO*-donors, such as the furoxans, are stable in acidic and basic conditions, and produce high levels of NO which lead to a potent cytotoxic action against several types of cancer cells.[210]

Since 1990, a number of *NO*-donor hybrids based on the benzofuroxan scaffold have been produced and tested in various disease models. Hybrids that incorporate a benzofuroxan *NO*-donor portion might possess a multitude of pharmacological activities and low toxicity.[213] The initial application of *NO*-donor hybrids limited to cardiovascular and inflammatory disorders has been considerably gradually extended to other fields, such as in the treatment of infections, neurodegenerative and gastrointestinal disorders, and cancer. Indeed, literature is plenty of hybrid derivatives constituted by a *NO*-donor portion combined with NSAIDs, H_2-antagonists, Ca^{2+}-channel blockers, α_1 and β_1 antagonists.[213,214]

In search of alternative anticancer multi-target strategies based on CA IX/XII inhibition, we designed and synthesized of new type of hybrid which incorporates in a single molecule a CA inhibitory portion and a *NO*-donor fragment (Figure 46). This multi-target strategy based on a benzofuroxan scaffold endowed with CA inhibitory action was additionally scheduled with a view to anti-infective drugs.[203-206] In fact, benzofuroxans were shown to possess anti-*Trypanosoma cruzi*, antitubercular and anti-*Leishmania* activity, whereas CAs from pathogens are known to be often crucial for the microorganism life and their inhibition to impair the growth.[215-217]

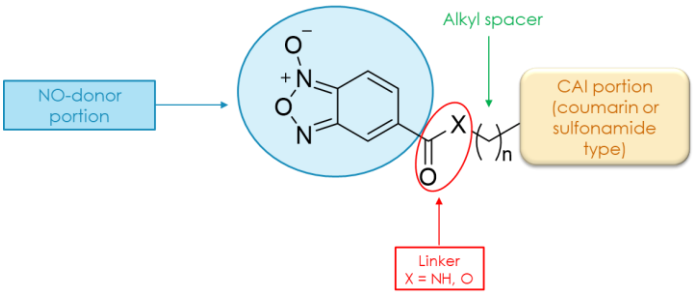

Figure 50. General Structures of hybrid compounds CAI-NO donors.

The chemistry of benzofuroxans is widely described in literature.[213] These scaffolds are intensively used in organic chemistry as intermediates in the synthesis of several chemotypes.[213]

Herein, the hybrids compounds were designed and produced by connecting a CA inhibiting moiety of the sulfonamide or coumarin type with the benzofuroxan by amide or ester bonds. Several spacers separating the two portions of the hybrid were investigated (Figure 50).

The synthetic strategy for the preparation of the final compounds includes **D2** as key intermediate (Scheme 7). Oxidation of 4-amino-3-nitrobenzoic acid **D1** by an excess of commercial hypochlorite solution in alkaline medium at 0°C provides an easier, efficient and rapid method to produce the carboxylic acid **D2**. The latter was reacted with sulfonamides **D3-D13** or coumarins **D14-D20**, with possess primary/secondary amine or alcoholic groups for coupling reaction to yield hybrids **D21-D26**, **D27-D31** and **D32-D38**. 1-(3-Dimethylaminopropyl)-3-ethylcarbodiimide hydrochloride and 1-hydroxy-7-azabenzotriazole and/or 4-dimethylaminopyridine and/or *N*-hydroxysuccinimide were used as coupling agents. Two distinct chemotypes for CA inhibition were chosen for thoroughly exploring the SAR against target/off-target CA isoforms. In particular, the subset of coumarin derivatives was prepared to yield a selective inhibition of the tumor-associated CA IX and XII, of interest for the anticancer application. In contrast, the subset of sulfonamide compounds was produced to investigate the anticancer effect of a promiscuous CA inhibition, however searching for a certain degree of selectivity for the target CAs activity, achieved exploring multiple kinds and combinations of tails appended to the inhibitory chemotype (Scheme 7). Further, the subset of NO-donor sulfonamides was scheduled for testing against CAs from pathogens which are not

affected by coumarin CAIs. Compounds **D21-D26**, **D27-D31** and **D32-D38** were fully characterized by spectroscopic and physicochemical methods.

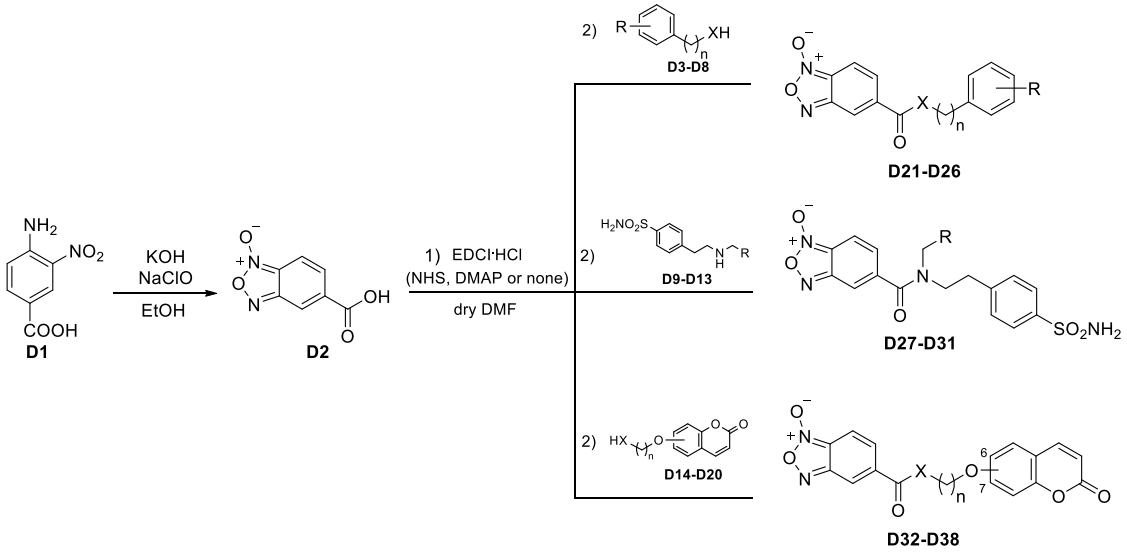

D3, D21: X=NH; n=0; R= *m*-SO_2NH_2
D4, D22: X=NH; n=0; R= *p*-SO_2NH_2
D5, D23: X=NH; n=0; R= *o*-OH, *m*-SO_2NH_2
D6, D24: X=NH; n=1; R= *p*-SO_2NH_2
D7, D25: X=NH; n=2; R= *p*-SO_2NH_2
D8, D26: X=O; n=0; R= *p*-SO_2NH_2

D9, D27: R= C_6H_5
D10, D28: R= 4-F-C_6H_4
D11, D29: R= 2-furyl
D12, D30: R= $CH_2C_6H_5$
D13, D31: R= CH_2CN

D14, D32: X=NH; n=2; 6-*subst*
D15, D33: X=NH; n=2; 7-*subst*
D16, D34: X=O; n=0; 6-*subst*
D17, D35: X=O; n=0; 7-*subst*
D18, D36: X=O; n=2; 7-*subst*
D19, D37: X=O; n=3; 6-*subst*
D20, D38: X=O; n=3; 7-*subst*

Scheme 7. General synthetic procedure for compounds **D21-38**.

All the newly synthesized *NO*-donor derivatives (**D2**, **D21-D38**) were evaluated for the inhibition of the cytosolic off-target isozymes hCA I and II and membrane-bound target isoforms hCA IX and XII by using Stopped-flow CO_2 hydrase assay method. Acetazolamide was used as reference drug. The results are reported in Table 9.

(i) All tested sulfonamides were found to be feeble inhibitors of the cytosolic isoform hCA I with K_Is in the range of 83.1–7658.8 nM. The comparison with the reference drug **AAZ** revealed that only compound **D24** was found to better inhibit hCA I (off-target for designing antitumor agents) than **AAZ**. The carboxylic acid **D2** showed no activity against the ubiquitous isoform. As expected, coumarins **D32-D38** do not inhibit hCA I below 10 μM.

(ii) Sulfonamides **D21-D31** showed efficient to moderate activity against the physiologically dominant isoform hCA II with K_Is ranging from 38.0 to 946.8 nM, whereas uniquely **D23** reported a micromolar K_I of 6.9 μM. As **D23**, which shows the

aromatic sulfonamide group in meta to the linker, the 3-substituted **D21** reported the second worst inhibition with a K_I of 946.8 nM.

Table 9. Inhibition data of human CA isoforms I, II, IX, XII with compounds **D21-38** and the standard inhibitor acetazolamide (**AAZ**) by a Stopped Flow CO_2 Hydrase Assay.[169]

Cmpd	K_I* (nM)			
	hCA I	hCA II	hCA IX	hCA XII
D2	>10000	732.8	1651.2	88.9
D21	7658.8	946.8	41.5	66.3
D22	791.5	38.0	69.7	0.98
D23	8447.8	6909.6	61.1	5.4
D24	83.1	53.5	37.9	48.8
D25	445.1	90.1	12.6	26.1
D26	736.0	52.8	38.7	20.3
D27	617.5	462.8	10.4	8.5
D28	416.7	67.9	2.5	4.8
D29	601.6	88.1	23.1	6.3
D30	831.4	453.9	14.9	6.4
D31	622.9	64.7	20.3	77.7
D32	>10000	>10000	23.6	7.0
D33	>10000	>10000	86.6	25.0
D34	>10000	>10000	15.8	3.9
D35	>10000	>10000	303.8	7.7
D36	>10000	>10000	111.7	19.8
D37	>10000	>10000	48.5	8.6
D38	>10000	>10000	36.3	33.0
AAZ	250.0	12.5	25.0	5.7

*Mean from 3 different assays, by a stopped flow technique (errors were in the range of ± 5-10 % of the reported values).

The carboxylate **D2** also weakly affected hCA II activity with a K_I of 732.8 nM. The best hCA II inhibitor in the seriess was **D22** (K_I = 38.0 nM), which has no spacer between the two fragments and the primary sulfonamide group is placed at the *para* position of the aromatic ring, while its ester analogue **D26** showed a weaker K_I of 52.8 nM. It is curious to note that the introduction of a methylene spacer in **D22** structure as in the compound **D24**, caused a slight deterioration of activity leading to a K_I of 53.5 nM. Analogy in the hCA II inhibition was found between **D28** (K_I of 67.9 nM) and **D31** (K_I of 64.7 nM), though they differ for the substituent at the amide linker which include a third aromatic ring in **D28** and a 2-CN-ethyl group in **D31**. The removal of the fluorine atom of **D28** resulted in a 6.8-fold worsening of the inhibitory activity for compound **D27**, which

showed a K_I of 88.1 nM. Compounds **D27** and **D30** reported very similar K_Is (462.8 and 453.9 nM, respectively), showing that the length of the R spacer has no incidence on the hCA II inhibitory capacity. Finally, the coumarin derivatives **D32-D38** did not report any inhibitory activity below 10 μM.

(iii) The target hCA IX was considerably inhibited indistinctly by the reported sulfonamides and coumarins with K_Is in the range 2.5 – 1651.2 nM. Among them, compounds **D21**, **D27**, **D28**, **D30**, **D31**, **D32** and **D34** showed better activity than the standard **AAZ**. In particular, the best inhibitor was compound **D28**, with a K_I of 2.5 nM. The derivative unsubstituted on the phenyl ring, **D27**, and the phenethyl **D30** reported a worsening of the hCA II inhibitory capacity (K_Is = 10.4 and 14.9 nM, respectively). The sulfonamide position at the aromatic ring did not significantly affect the inhibitory capacity, as it is possible to notice from the K_Is of compounds **D21** (K_I = 41.5 nM) and **D22** (K_I = 69.7 nM). In contrast, the switch from methylene (**D24** with K_I of 37.9 nM) to ethylene spacer led to a 3-fold inhibition increase (compound **D25** with K_I of 12.6 nM). It is worth noting that the best K_Is in the coumarins subset were reported by the 6-substituted heterocycles; in fact, compounds **D32** and **D34** (K_Is = 23.6 and 15.8 nM) showed better K_Is than their 7-substituted analogues **D33** and **D35** (K_Is = 86.6 and 303.8 nM). However, the introduction of a propylenic spacer in compounds **D37** (6-substituted) and **D38** (7-substituted) reversed this observed trend as they showed K_Is of 36.3 and 48.5 nM respectively. Carboxylate **D2** inhibited hCA IX in a low micromolar range (K_I of 1651.2 nM). In general, the sulfonamides turned out to be better inhibitors against CA IX than the assayed coumarins, though the latter reconfirmed their IX/II selectivity.

(iv) hCA XII was also effectively inhibited by all derivatives with K_Is starting from 0.98 nM, and a slight inhibition worsening exhibited uniquely by compounds **D2**, **D21** and **D31** (K_I = 88.9, 66.3 and 77.7 nM, respectively). Carboxylate **D2** was the worse hCA XII inhibitory benzofuroxan of the series with a K_I of 88.9 nM. Sulfonamide **D22** was instead the best inhibitor of the series with a subnanomolar K_I of 0.98 nM. It is certainly interesting to note that in the first subset (**D21-D26**), the best K_Is were reported by compounds which did not have spacer (**D21-D23** and **D26**) to connect the fragments, in comparison to compounds **D24** and **D25** with methylene and ethylene spacers, respectively. The sulfonamide group at the *para* position of phenyl ring was once again preferred over the replacement in *meta* position. Unexpectedly, the bulky compounds

(**D27-D31**) reported better inhibitory activity compared to the other sulfonamide derivatives of the first set (**D21-D26**). Except for compound **D31**, the other compounds showed K_I less than 10.0 nM. The presence of the fluorine atom in compound **D28** produced an excellent K_I of 4.8 nM. Similar K_Is were found for **D27**, **D29** and **D30** (K_Is = 8.5, 6.3 and 6.4 nM, respectively). Also, in the coumarin subset, compound **D34** showing the coumarin portion substituted at the 6-position and directly linked to the NO-donor scaffold showed a K_I of 3.9 nM, whereas the inhibition was 2-fold worsened by the introduction of a propylenic spacer as in the compound **D37** (K_I of 8.6 nM). The replacement of the amide linker (compounds **D32** and **D33**) with an ester did not have a considerable influence on the inhibitory potency of these compounds against CA XII.

This project is currently under further and detailed investigations. The promising CAs inhibition results led us to proceed measuring the hybrids *NO*-releasing profiles and to assess their anticancer action. Screening against CAs from *Leishmania* and *Trypanosoma cruzi* strains have been also scheduled to address the potential anti-infective action residing in this type of multi-target derivatives.

The experimental procedures are reported in Chapter 5.

3.6 "A Sweet Combination": an expansion of saccharin and acesulfame K based compounds for selectively targeting tumor-associated carbonic anhydrases IX and XII (Series E)

The main challenge encountered in the design of anticancer CAIs has been the lack of isoform-selectivity exhibited by the most classical inhibitory chemotypes, namely the sulfonamides and their bioisosteres.[3,91] A comparison of the 12 catalytically active human CAs shows a high homology between the active sites that complicates the design of disease-associated selective inhibitors.[218] Nonetheless, a plethora of strategies have been developed to overcome this issue, including the optimization of classical CAIs (i.e. the tail approach, which led to **SLC-0111**, the first-in-class CAI entering clinical trials for the treatment of hypoxic tumors)[3] or the use of alternative chemotypes adopting different mechanisms of enzymatic inhibition.[3,91]

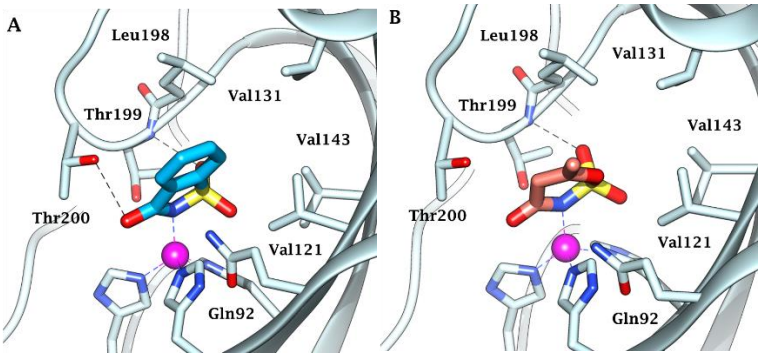

Figure 51. Active site view of the CA IX adduct with A) **SAC** (PDB: 4RIV) and B) **ACE** (PDB 5WGP).

The cyclic sulfonamide saccharin (**SAC**), the oldest artificial sweetener, has recently entered this topic. SAC, which is 450 times sweeter than sucrose, was shown to selectively discriminate among the diverse isoforms, distinctly from classical CAIs such as **AAZ**.[219] It is, in particular, a selective nanomolar inhibitor of CA IX, showing weaker, micromolar inhibition of the ubiquitous CA I and II (60-fold II/IX selectivity).[219] It is cyclic acylsulfonamide, which is much more acidic than primary sulfonamides, functions as a zinc binding group (ZBG) within the CA active site (Figure 51). X-ray and neutron crystallography studies pointed out that alternative interactions with residue Gln67 (leading to remodelling of H-bonds and water orientations) contributed to the CA IX

preferential binding of **SAC** compared to CA II (that reports an Asn in position 67).[220,221] A **SAC** derivative, called **SGC** (saccharin-glucose conjugate), was designed utilizing the tail approach with a polar carbohydrate linked by a triazole as the tail moiety of the CA inhibitor.[220] It showed even further enhanced selectivity for CA IX over both CA I and CA II (>1000-fold), with the specificity of binding explained by evident differences in interacting active site residues between CA II and CA IX.

Another FDA approved food additive, acesulfame K (**ACE**, a cyclic acylsulfamate), was recently kinetically and structurally characterized with CAs.[222] Interestingly, **ACE** induced no inhibition of CA I, II and XII while inhibiting CA IX in the low micromolar range, with its weak inhibition being likely due to the absence of the aromatic core (Figure 51). Furthermore, it exhibits different active site binding modes between isoforms, namely coordinating the Zn(II) ion via the aromatic nitrogen in the case of CA IX, and anchoring to zinc-bound water molecule/hydroxide ion in CA II. This behaviour is reflected by **ACE** demonstrating measurable inhibition toward CA IX but not to other CA isoforms.[222] This study showed the value of **ACE** as a lead compound for designing new CA IX specific inhibitors.

In this context, libraries of *N*- and/or *O*-substituted **SAC** and **ACE** derivatives have been recently reported as potent and selective inhibitors of CA IX and XII.[130,223] Nonetheless, this type of functionalization decoupled these chemotypes away from a zinc-binder character (or water-anchoring) promoting likely alternative binding modes, which have not yet been elucidated.

Here a new series of **SAC**- and **ACE**-based derivatives is reported by combining and developing the lead chemotypes structures to produce cyclic ureidosulfonamides, namely 2H-benzo[e][1,2,4]thiadiazin-3(4H)-one 1,1-dioxides (**BTD**), which preserve a zinc-binding group and include another foothold for ligand/target interactions and/or functionalization (Figure 52).

Although sulfimides have been long deemed to possess no or weak CA inhibitory action, in 2007 **SAC** was shown to induce the selective inhibition of the tumor-associated CAs over ubiquitous isoforms.[223] Successive X-ray and neutron crystallography studies supplied significant insights about the CAs inhibition profiles of **SAC**, and in 2018 even the 6-membered cyclic acylsulfamate sweetener **ACE** was kinetically and structurally proved to display a CA IX selective inhibitory action.[224,225] To methodically explore the

chemical space that induces cyclic acylsulfonamides or sulfamates to yield specific inhibition of CA IX and XII, an approach to merge **SAC** and **ACE** structures was developed and is here reported, producing a series of cyclic ureidosulfonamides **E18-E37**. The redesigned scaffold **BTD** preserves the zinc-binding group of **SAC** and **ACE** and includes another interaction and/or functionalization point (the *NH* between the carbonyl and the aromatic ring).

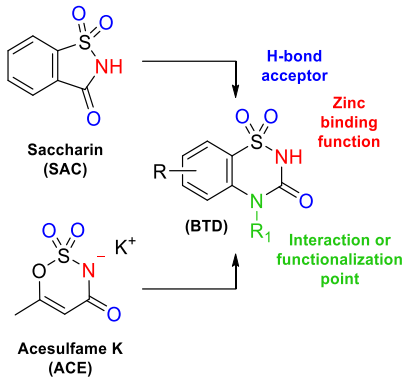

Figure 52. Rational development of benzothiadiazin-3-one 1,1-dioxides (**BTD**), based on the structures and inhibition profiles of **SAC** and **ACE**.

In order to identify new CA inhibitory scaffolds, previous screens of a library of chemotypes[167] included the unsubstituted 2H-benzo[e][1,2,4]thiadiazin-3(4H)-one 1,1-dioxide **E18,** further supporting the production of such a series as this derivative was shown to hold selectivity for CA IX/XII over CAs I and II. Here an extended SAR study was worked out by appending a wealth of substituents both in R and R_1 position (Figure 2) by exploiting a more versatile synthetic procedure than that reported by Bozdag M. et al. for **E18**.[167] Instead of treating *o*-aminobenzenesulfonamide with phosgene, which does not allow accessible **BTD** functionalization, a forward strategy recently proposed by Zhang and Kornahrens (for providing new classes of aldose reductase and irreversible serine hydrolase inhibitors, respectively)[224,225] is here applied and extended.

The adopted synthetic procedure is depicted in Scheme 8. Chlorosulfonyl isocyanate (**CSI**) was treated at -40°C with commercially available variously substituted anilines (**E1-E14**), N-methylanilines (**E15**, **E16**) and indoline (**E17**) using nitromethane or nitroethane as solvent to yield the intermediates chlorosulfamoylureas **β_{a-q}**. Thus, aluminium trichloride ($AlCl_3$) was added and temperature risen to 110°C to promote a Friedel-Crafts-like core cyclization. The absence of a base and a very low temperature are

important to avoid reaction of the aniline with the sulfamoyl portion of **CSI**. In contrast, the choice of nitromethane or nitroethane is driven by the necessity to use a polar aprotic solvent which can span from markedly under-zero temperatures to over 100°C without solidifying or boiling. Reaction attempts with markedly electron-poor anilines of the nitro-, sulfonamido- or polyhalo-substituted types crashed with their low reactivity in both reaction steps.

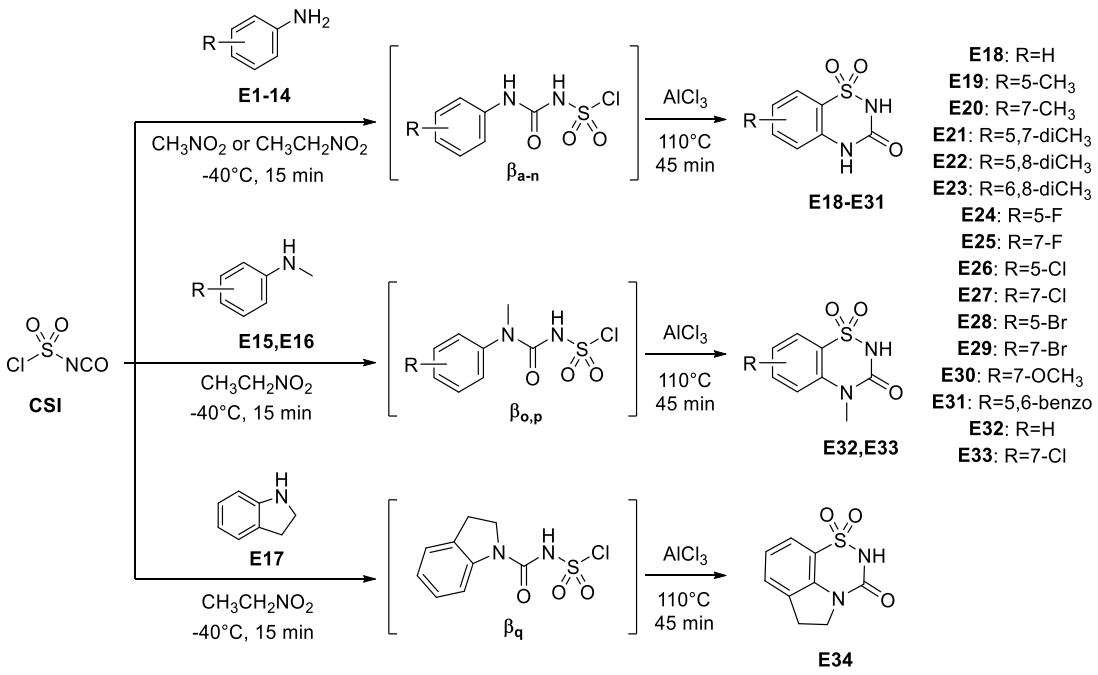

Scheme 8. Synthesis of 2H-benzo[e][1,2,4]thiadiazin-3(4H)-one 1,1-dioxides **E18-E34**.

The 5- and 7-methyl derivatives **E19** and **E20** were also oxidized with potassium permanganate to give benzoic acids **E35** and **E36** respectively, as illustrated in Scheme 10. The 7-methoxy-**BTD** underwent demethylation by treatment with 1.0 M BBr_3 in DCM to produce alcohol **E37** (Scheme 9).

Compounds **E18-E37** were obtained in high yields and characterized by means of ^{1}H-, ^{13}C-, ^{19}F-NMR spectroscopy and HRMS. Compounds used in biological assays were >95% pure, as determined by HPLC (see Chapter 5 for details). Sodium salts, thereof, were in case produced by treating **BTD** derivatives with NaOH in methanol.

Compounds **E18-E37** were assayed *in vitro* for their inhibitory action against six physiologically relevant human hCA isoforms – *i.e.* the cytosolic I, II (ubiquitous isoforms) and VII (defined as a CNS-associated isozyme) and the membrane associated IV (overexpressed in some CNS tumors), IX and XII - by means of a Stopped-Flow CO_2

hydrase assay using the clinically used drug **AAZ** as a standard.[169] The following SAR can be assembled from the data reported in Table 10.

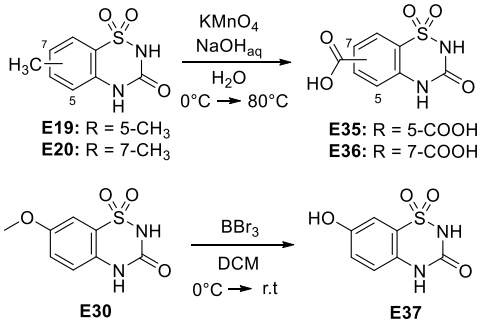

Scheme 9. Synthesis of derivatives **E35-E37**.

Table 10. Inhibition data of human CA isoforms I, II, IV, VII, IX, XII with compounds **E18-E37** and the standard inhibitor acetazolamide (AAZ) by a Stopped Flow CO_2 Hydrase Assay.[169]

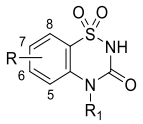

Cmpd	R	R_1	K_I (nM)[a]					
			hCA I	hCA II	hCA IV	hCA VII	hCA IX	hCA XII
E18[b]	H	H	866.0	150.3	675.3	465.8	78.7	53.1
E19	5-CH_3	H	968.7	143.8	1228	975.3	63.9	69.3
E20	7-CH_3	H	1066	871.7	896.6	956.0	45.8	74.3
E21	5,7-	H	1274	763.5	1637	690.9	25.8	38.3
E22	5,8-	H	2541	2192	1427	1899	367.6	458.7
E23	6,8-	H	1920	2936	2692	1790	408.5	764.0
E24	5-F	H	546.7	140.1	461.0	125.5	58.4	42.7
E25	7-F	H	1289	533.6	708.6	435.5	19.1	24.9
E26	5-Cl	H	930.2	685.5	1031	389.3	28.2	42.5
E27	7-Cl	H	1864	1141	1748	1178	56.9	70.8
E28	5-Br	H	2324	526.9	853.6	620.3	73.3	75.8
E29	7-Br	H	4403	2362	1557	467.8	31.0	96.6
E30	7-OCH_3	H	3809	1922	1945	1364	35.8	64.5
E31	5,6-	H	2071	483.6	2674	3949	60.2	104.9
E32	H	CH_3	3406	853.1	3459	7507	139.5	181.5
E33	7-Cl	CH_3	>10000	2337	5885	3238	188.9	325.7
E34	5-CH_2-CH_2-		6857	1060	3894	1282	273.4	247.2
E35	5-	H	5783	2445	379.8	2796	91.2	27.0
E36	7-	H	>10000	6775	76.1	4965	98.7	15.5
E37	7-OH	H	1894	3024	452.4	2565	88.1	34.6
SAC[c]	-		>10000	5950	7920	10	103	633
SCG[d]	-		>10000	>10000	n.d.	n.d.	50	600
ACE[e]	-		>10000	>10000	n.d.	n.d.	2400	>10000
AAZ	-		250	12.5	74.0	2.5	25.0	5.7

a. Mean from 3 different assays, by a stopped flow technique (errors were in the range of ± 5-10 % of the reported values);
b. data in agreement with ref. 153; c. data from ref. 215; d. data from ref. 216; e. data from ref. 218.

Most compounds among **E18-E37** inhibited the ubiquitous off-target CA I in the micromolar range with K_I spanning between 1066 and over 10000 nM, whereas the unsubstituted (**E18**), 5-CH_3 (**E19**), 5-F (**E24**) and 5-Cl (**E26**) derivatives were high nanomolar inhibitors (K_Is in the range 546.7-968.7 nM).

The physiologically dominant CA II was shown to be slightly more inhibited by **BTDs** than CA I as a minor number of compounds acted in the micromolar range, from 1060 to 6775 nM (**E27**, **E29**, **E30**, **E33-E37**) and most displayed medium to high nanomolar K_Is (in the range 140.1-871.7 nM). The unsubstituted (**E18**), 5-CH_3 (**E19**) and 5-F (**E24**) derivatives resulted to be the most potent CA II inhibitors of the series with K_Is of 150.3, 143.8 and 140.1 nM), showing that the CA II active site efficiently tolerates solely small substituents appended at the 5-position of the scaffold.

CA IV was inhibited in a comparable range with CA I by **BTDs E18-E37** with most compounds functioning with K_Is between 1031 and 5885 nM, and a small subset (**E18**, **E20**, **E24**, **E25**, **E28**) acting in the high nanomolar range (461.0-896.6 nM). Of note is the case of derivatives bearing hydrophilic groups on the aromatic ring, that are **E35-E37**, which showed enhanced CA IV inhibitory properties such as the 76.1 nM K_I of the 7-carboxy-**BTD E36**. The presence of a markedly hydrophilic pocket is a unique hallmark of CA IV active site structure that might account for the inhibition data shown by **E35-E37**.[205]

The other cytosolic isoform CA VII showed, in contrast, an inhibition profile that resembled that of CA II, according significant similarities existing between their active sites.[224] Nonetheless, the 5-F-**BTD E24** solely displayed a K_I below 200 nM (125.5 nM) and the halogen swapping with a chlorine atom produced the second best CA VII inhibitor with a K_I of 389.3 nM. Also, the unsubstituted (**E18**), 7-F (**E25**) and 7-Br (**E29**) derivatives reported K_Is minor than 500 nM (435.5-467.8 nM), whereas the 5-CH_3-derivative **E19** showed a worsening of CA VII inhibition when compared to CA II (from 143.8 to 975.3 nM).

In agreement with the planned drug-design, the inhibitory profiles measured against CA IX for **BTDs E18-E37** deviate from those of the other assayed isoforms. The compounds K_I values spanned between 19.1 and 473.4 nM. A rather flat inhibition trend can be seen from data in Table 10 for derivatives acting on CA IX below 100 nM, as K_Is lie in the

range 31.0-98.7 nM, except for the 5,7-diCH_3 (**E21**), 7-F (**E25**) and 5-Cl (**E26**) derivatives which resulted to be the best CA IX inhibitor of the study with K_Is of 25.8, 19.1 and 28.2 nM, respectively. A subset of compounds, among which the 5,8-diCH_3 (**E22**) and 6,8-diCH_3 (**E23**) derivatives and the *N*-substituted **E32-E34** reported, in contrast, over 100 nM K_Is which spanned from 139.5 and 408.5 nM.

Again, structural similarities between CA IX and XII active sites yielded analogies in the inhibitory profiles of the two isoforms with **BTDs E18-E37**.[224] CA XII was, in fact, efficiently inhibited by most derivatives with K_Is settling in the range 15.5-764.0 nM. While the 7-F derivative **E25** retained one of the most efficient activities with a K_I of 24.9 nM, a worsening can be observed for **E21** and **E26** (K_I of 38.3 and 42.5 nM). In contrast, an inhibition increase with respect to CA IX was shown by the carboxy and hydroxy derivatives **E35-E37 (**K_Is in the range 15.5-34.6 nM), with the 7-carboxy **E35** resulting the best CA XII inhibitor of the series. It should be stressed that one of the dissimilarities in the active site architectures of the tumor-associated CAs is the presence of a set of Thr and Ser residues uniquely in CA XII, which might produce H-bond networks accounting for the **E35-E37** inhibition potency. Again, the 5,8-diCH_3 (**E22**) and 6,8-diCH_3 (**E23**) derivatives and the N-substituted **E32-E34** reported the weakest CA XII inhibition.

Overall, most compounds of the **BTD** series showed significantly improved CA IX and XII inhibitory action than the lead **SAC** (K_Is of 103 and 633 nM) and **ACE** (K_Is of 2400 and >10000 nM), but also reported an increased binding to CA I, II and IV with respect to the leads. A marked drop of efficacy was instead displayed by **E18-E37** against CA VII compared to **SAC** (K_Is of 10 nM).

As for the selectivity of action of the newly reported CAIs, the selectivity index (*SI*) for CA IX and XII over the remaining isoforms are reported in Table 11. It is noteworthy that all derivatives are selective inhibitors of the tumor-related CAs over off-target ones, with the unique exception of compound **E36** in the IV/IX *ratio* (*SI* = 0.8). Almost all substitution patterns on the **BTD** scaffold induced better II/IX and II/XII *SI* than the unsubstituted **E18** (1.9 and 2.8, respectively), ranging from 2.3 to 68.6 and 2.1 to 437.1, respectively. While *SI* calculated for CA VII settle in a comparable range with CA II, those reported for CA I, II and IV are markedly greater, reaching a value major than 645.2 for **E36** in the I/XII *ratio*.

While *SI* calculated for the clinically used **AAZ** are easily exceeded by **BTDs E18-E37**, it is reasonable to comment on their comparison with *SI* measured for **SAC**, **SCG** and **ACE**. In spite of a more efficient inhibition of off-target CAs by the **BTDs** than the leads, comparable or even more favourable *SI* could be extrapolated for many compounds of the series from the inhibition data of Table 11. In fact, depending on the substitution pattern on the main scaffold some derivatives, such as **E29**, **E30** and **E36** in the II/IX *ratio* and many more in the II/XII *ratio*, showed increased selectivity than the lead **SAC**, with the **ACE** *SI* being difficult to comment because of its weak CA inhibition. A subset of derivatives might even compete with **SCG** in terms of I/XII and II/XII specificity of action.

Table 11. Selectivity index (*SI*) calculated for human CA IX and XII over off-targets isoforms as *ratio* between K_Is.

Cmpd	R	R_1	Selectivity index (*SI*)							
			I/IX	II/IX	IV/IX	VII/I	I/XII	II/XII	IV/XI	VII/XI
E18[b]	H	H	11.0	1.9	8.6	5.9	16.3	2.8	12.7	8.8
E19	5-CH_3	H	15.2	2.3	19.2	15.3	14.0	2.1	17.7	14.1
E20	7-CH_3	H	23.3	19.0	19.6	20.9	14.3	11.7	12.1	12.9
E21	5,7-diCH_3	H	49.4	29.6	63.4	26.8	33.2	19.9	42.7	18.0
E22	5,8-diCH_3	H	6.9	6.0	3.9	5.2	5.5	4.8	3.1	4.1
E23	6,8-diCH_3	H	4.7	7.2	6.6	4.4	2.5	3.8	3.5	2.3
E24	5-F	H	9.4	2.4	7.9	2.1	12.8	3.3	10.8	2.9
E25	7-F	H	67.5	27.9	37.1	22.8	51.8	21.4	28.5	17.5
E26	5-Cl	H	32.9	24.3	36.5	13.8	21.9	16.1	24.3	9.2
E27	7-Cl	H	32.8	20.1	30.7	20.7	26.3	16.1	24.7	16.6
E28	5-Br	H	31.7	7.2	11.6	8.5	30.7	7.0	11.3	8.2
E29	7-Br	H	142.0	76.2	50.2	15.1	45.6	24.5	16.1	4.8
E30	7-OCH_3	H	106.4	53.7	54.3	38.1	59.1	29.8	30.2	21.1
E31	5,6-benzo	H	34.4	8.0	44.4	65.6	19.7	4.6	25.5	37.6
E32	H	CH	24.4	6.1	24.8	53.8	18.8	4.7	19.1	41.4
E33	7-Cl	CH	>52.9	12.4	31.2	17.1	>30.7	7.2	18.1	9.9
E34	5-CH_2-CH_2-		25.1	3.9	14.2	4.7	27.7	4.3	15.8	5.2
E35	5-COOH	H	63.4	26.8	4.2	30.7	214.2	90.6	14.1	103.6
E36	7-COOH	H	>101.	68.6	0.8	50.3	>645.	437.1	4.9	320.3
E37	7-OH	H	21.5	34.3	5.1	29.1	54.7	87.4	13.1	74.1
SAC[c]	-		>97.1	57.8	76.9	0.1	>15.8	9.4	12.5	<0.1
SCG[d]	-		>200.	>200.	n.d.	n.d.	>16.7	>16.7	n.d.	n.d.
ACE[e]	-		>4.2	>4.2	n.d.	n.d.	n.d.	n.d.	n.d.	n.d.
AAZ	-		10.0	0.5	3.0	0.1	43.9	2.2	13.0	0.4

Crystal structures of CA II and CA IX-mimic in complex with cyclic ureidosulfonamide inhibitors **E18**, **E21**, **E25**, **E26**, and **E32** were determined in order to analyse compound binding and rationalize the observed inhibition profiles. The crystallographic study was conducted by Dr. Carrie Lomelino and Prof. Robert McKenna, Dept. of Biochemistry and Molecular Biology, University of Florida. Overall, these compounds bind similarly to the lead compounds **SAC** and **ACE** (bound in CA IX) (Figure 53).

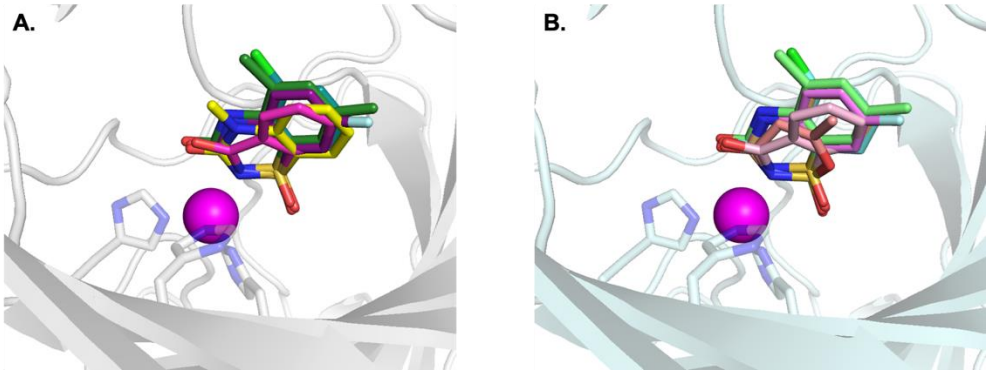

Figure 53. Overlay of ureidosulfonamide compounds **E18** (orange), **E21** (green), **E25** (purple), **E26** (blue), **E32** (yellow) and lead compounds **SAC** (pink, PDBs: 2Q1B in CA II, 4RIV in CA IX-mimic) and **AC**E (salmon) (CA IX-mimic only, PDB:5WGP) in **A.** CA II and **B.** CA IX-mimic.

As such, the aromatic *N* interacts directly with the zinc, displacing the zinc-bound water that is essential for catalytic activity, in addition to DW and W1 of the proton wire, which facilitate the transfer of a proton to bulk solvent during catalysis. Inhibitor binding was determined to be stabilized by the formation of hydrogen bonds between the compound carbonyl and T199 side chain hydroxyl in addition to inhibitor sulfonamide and T199 backbone amide. Binding is further supported by VDW interactions with active site residues such as V121, F131 (CA II), V135, L141, V143, L198, T200, P202, and W209 (Figure 54).

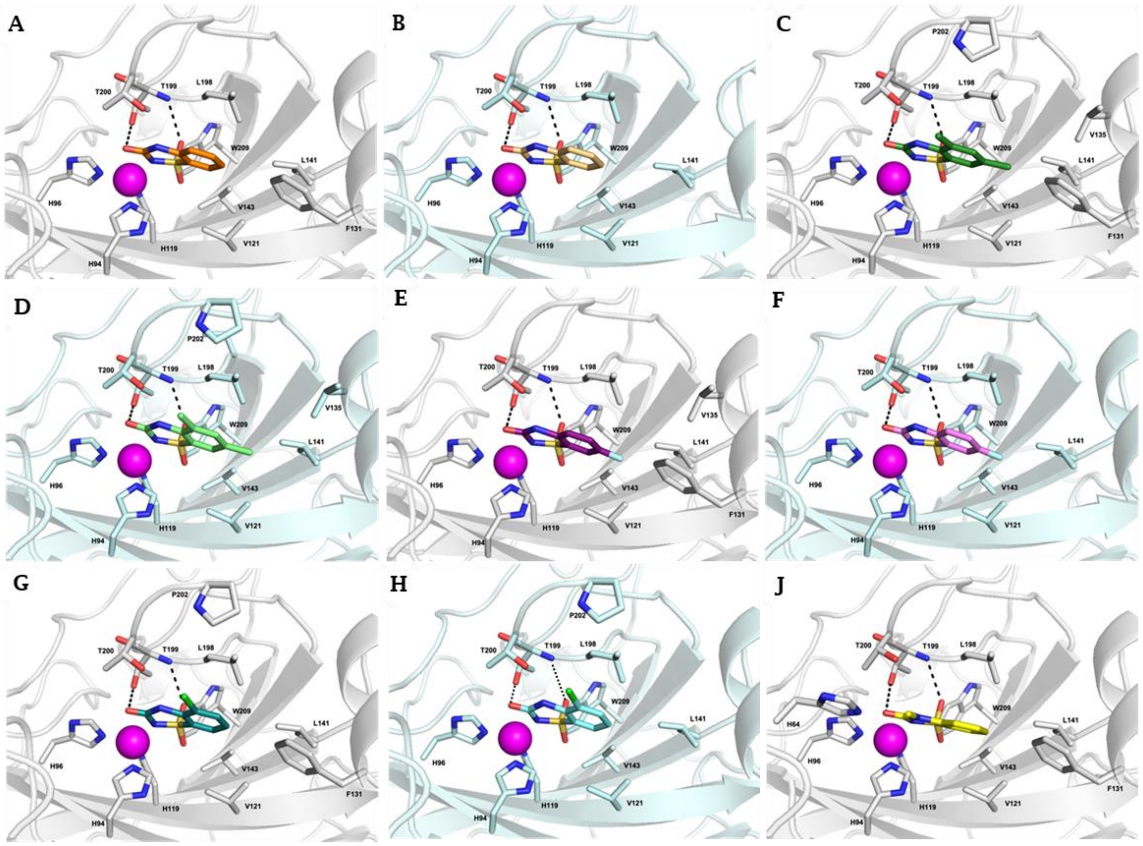

Figure 54. Binding of ureidosulfonamide compounds displayed in the active sites of CA II (gray) and CA IX-mimic (pale cyan). Hydrophobic residues are shaded orange and hydrophilic residues purple. The **E18** (panel A and B, PDBs 6U4Q and 6U4T), **E21** (panel C and D, PDBs 6UGN and 6UGO), **E25** (panel E and F, PDBs 6UGR and 6UGZ), **E26** (panel G and H, PDBs 6UGP and 6UGQ), and **E32** (panel J, PDB 6UH0) inhibitors are shown as orange, green, purple, blue, and yellow sticks, respectively.

These five compounds all exhibit a greater affinity for CA IX over the off-target, ubiquitous CA II. Interestingly, an overlay of each inhibitor bound in CA II and CA IX demonstrates that these inhibitors bind in a similar orientation in both isoforms (Figure 55) (excluding **E32** which was only determined in CA II), which has also been previously observed for **SAC** binding. Therefore, the observed specificity for CA IX is likely attributed to the feasibility of inhibitor movement and entry into the active site. CA IX has a larger hydrophobic pocket, along which substrate and many inhibitors travel, due to residue V131 in place of F131 in CA II. The decrease in steric hindrance of this residue at the opening of the active site facilitates the binding of bulkier, aromatic compounds such as these ureidosulfonamides.

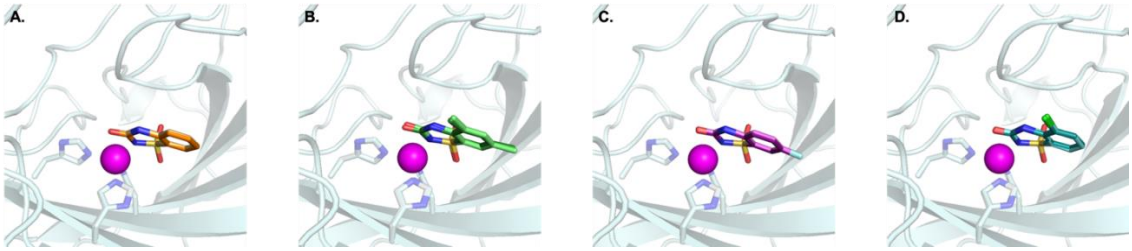

Figure 55. Overlay of inhibitors bound in CA II and CA IX-mimic. Inhibitors are displayed in the active site of CA IX-mimic as sticks. **A. E18** (orange), **B. E21** (green), **C. E25** (purple), and **D. E26** (blue).

Compounds **E21**, **E25**, **E26** have similar affinities for CA IX that are approximately 3- and 7-fold higher than those of **E18** and **E32**, respectively. Generally, the affinity of the inhibitor is observed to increase with the hydrophobicity of substitutions. Substitution of two positions or the addition of a halogen increases the number and/or strength of VDW and hydrophobic interactions with surrounding active site residues. Although the structure of **E32** was not determined in complex CA IX-mimic, an overlay of the five compounds in CA II shows that **E32** is shifted, reflecting the weakest affinity observed for both CA II and CA IX. This observation can be attributed to steric hindrance of the addition methyl group on the *N* with the side chain of T200, likely forcing the compound to bind in a less energetically favorable orientation.

The *in vitro* anti-proliferative potential of the five BTDs (**E18**, **E21**, **E25**, **E26**, **E32**) was examined toward three human cancer cell lines, namely A549 (lung), PC-3 (prostate) and HCT-116 (colon)[226-229] cancer cell lines using MTT reduction assay as described by T. Mosmann[230] and utilizing staurosporine as a reference anticancer drug. The five BTDs were evaluated under both normoxic and hypoxic conditions, where the cobalt (II) chloride hexahydrate was adopted as chemical inducer of HIF-1α to establish the hypoxic condition.[231] The results are expressed as IC_{50} values and listed in Table 12.
The presented IC_{50} (Table 12) revealed that the examined BTDs (**E18**, **E21**, **E25**, **E26**, **E32**) exhibited excellent to moderate growth inhibitory activity toward the tested cancer cell lines (A549, PC-3 and HCT-116). In particular, the assayed BTDs were more effective toward colon HCT-116 cells than A549 and PC-3 cells, except BTDs **E21** and **E26** which displayed an enhanced growth inhibitory activity against PC-3 cells under the hypoxic condition.

Table 12. *In vitro* anti-proliferative activity of compounds **E18**, **E21**, **E25**, **E26**, **E32** against lung A549, prostate PC-3 and colon HCT116 cancer cell lines under normoxic and hypoxic conditions.

Compound	IC_{50} (μM)[a]					
	A549		PC-3		HCT116	
	Normoxia	Hypoxia	Normoxia	Hypoxia	Normoxia	Hypoxia
E18	3.53±0.16	2.68±0.31	13.95±0.75	12.25±1.1	1.30±0.06	1.50±0.53
E21	4.77±0.22	5.74±0.28	6.31±0.41	0.82±0.06	3.85±0.22	4.18±0.27
E25	18.32±1.3	15.01±0.92	11.98±1.2	6.53±0.43	3.86±0.19	2.73±0.14
E26	10.88±0.73	7.35±0.36	16.23±0.92	3.52±0.24	5.26±0.36	7.57±0.51
E32	19.86±0.97	16.34±2.1	23.76±1.92	16.93±0.99	10.88±0.41	7.13±0.38
Staurosporine	7.47±0.39	13.22±0.82	4.91±0.17	5.92±0.24	8.86±0.33	16.15±0.57

a. IC_{50} values are the mean ± S.D. of three separate experiments.

As for the activity against HCT-116, the data displayed in Table 12 ascribed to all the examined **BTDs** excellent efficacy in inhibiting the growth of the cells under both normoxic (IC_{50} in the range 1.30 – 10.88 μM) and hypoxic (IC_{50} in the range 1.50 – 7.57 μM) conditions. In particular, compounds **E18** and **E25** were found to be the most potent of the series against HCT-116 cells under hypoxic conditions with IC_{50} values of 1.50±0.53 and 2.73±0.14 μM, respectively. In contrast, compounds **E18** and **E21** emerged as the most potent derivatives against A549 cells under both normoxic (IC_{50} = 3.53±0.16 and 4.77±0.22 μM, respectively) and hypoxic (IC_{50} = 2.68±0.31 and 5.74±0.28 μM, respectively) conditions. Compoun **E21**, instead, showed the best growth inhibitory activity against PC-3 cells with IC_{50} values of 6.31±0.41 and 0.82±0.06 μM under normoxic and hypoxic conditions, respectively.

The SAR outcomes illustrate that the substituents on the **BTD** scaffold such as in **E21**, **E25** and **E26** increase the growth inhibition action against prostate PC-3 cells compared to the unsubstituted **E18**. On the other hand, *N*-4 methylation (**E32**), produced a worsening of effectiveness against the three tested cancer cell lines in comparison to *N*-4 unsubstituted analogue **E18**. Notably, such methylation decreased the CA IX and XII inhibitory activities as well.

The ability of **E18** and **E25** to provoke apoptosis in colon HCT-116 cells was assessed by measuring the expression levels of apoptosis hallmark parameters upon treatment with the compounds at their IC_{50} concentrations (1.30 and 3.86 μM, respectively) (Figure 51, Tables 13 and 14). The exposure of HCT-116 cells to **E18** and

E25 induced a significant down-regulation of the expression levels of the anti-apoptotic protein Bcl-2 by approximately 59% and 42%, respectively, with a concurrent 8.12- and 4.73-fold increase, respectively, in the expression of the pro-apoptotic protein Bax, compared to the control. Accordingly, the Bax/Bcl-2 ratio was calculated to be boosted by 21.4- and 8.6-fold, respectively, in comparison to the control (Figure 56, Table 13).

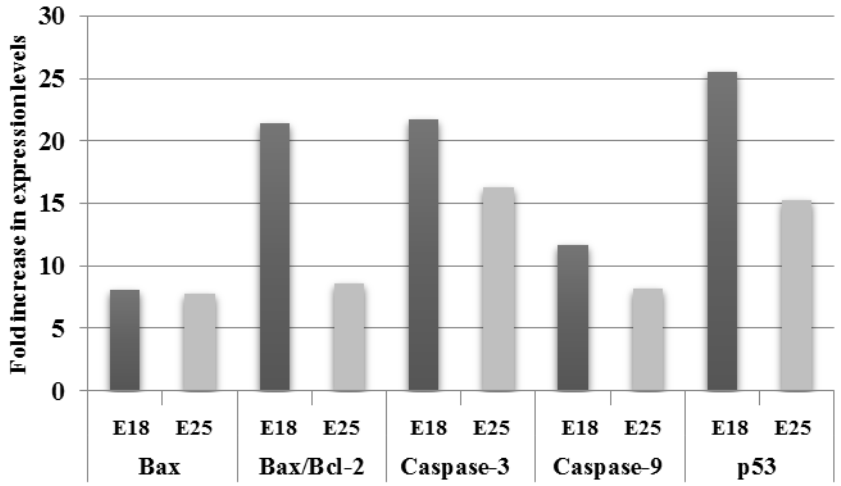

Figure 56. The numbers of fold increase in Bax/Bcl-2 ratio and expression levels of Bax, caspase-3, caspase-9, and p53 in HCT116 cancer cells upon treatment with **BTDs E18** and **E25**, in comparison to the control.

Thereafter, the expression levels of active caspase-3, caspase-9 and p53 tumor suppressor protein were evaluated. Treatment of HCT-116 cells with **E18** and **E25** led to a significant increase in the expression levels of the pro-apoptotic caspase-3 (by 21.7- and 16.3-fold, respectively), caspase-9 (by 11.7- and 8.2-fold, respectively), and p53 (by 25.5- and 15.3-fold, respectively), compared to control (Figure 56, Table 14).

After their kinetical and structural characterization as selective inhibitors of the tumor-associated CAs IX and XII, the sweeteners **SAC** and **ACE** have entered the topic of anticancer CAIs. Here, a drug design strategy over the structures of **SAC** and **ACE** was reported which produced a new series of 2H-benzo[e][1,2,4]thiadiazin-3(4H)-one 1,1-dioxides. Many such derivatives showed enhanced potency (CA IX K_Is in the range 19.1-473.4 nM; CA XII K_Is in the range 15.5-764.0 nM) and in some cases selectivity (II/IX selectivity index between 2 and 76; II/XII selectivity index between 2 and 440) when compared to the leads against the target CA IX and XII over off-target isoforms. A thorough X-ray crystallographic study conducted on 5 derivatives with both CA II and

IX-mimic enabled to speculate that the larger hydrophobic pocket in CA IX than CA II, along which substrate and many inhibitors travel, facilitates the binding of bulkier, aromatic compounds such as these ureidosulfonamides. A subset of compounds selected for the *in vitro* evaluation of their anticancer properties (**E18**, **E21**, **E25**, **E26** and **E32**) exhibited a greater efficacy against colon HCT-116 than A549 and PC-3 cells, except **E21** and **E26** which displayed an enhanced growth inhibitory action against PC-3 cells under the hypoxic conditions. In particular, BTDs **E18** and **E25** (IC_{50} against HCT-116 cells of 1.30±0.06 and 3.86±0.19 μM in normoxia, and 1.50±0.53 and 2.73±0.14 μM in hypoxia, respectively) were selected for further assessing their effect on apoptosis markers in HCT-116 cells. Treatment with **E18** and **E25** led to a significant increase in the expression levels of the pro-apoptotic proteins Bax, caspase-3, caspase-9, and p53 and a down-regulation of the anti-apoptotic protein Bcl-2. These outcomes indicate that **SAC** and **ACE**, widely used as sweeteners might be used for designing promising leads for the development of new anticancer drugs.

Table 13. Effect of **BTDs E18** and **E25** on the expression levels of Bcl-2 and Bax in HCT116 cancer cells treated with each compound at its IC_{50} concentration.

Compound	Bax (pg/mg of Total Protein	Bcl-2 (ng/mg of Total Protein)	Bax/Bcl-2
E18	348 ± 18.4	2.326 ± 0.12	0.15
E25	202.7 ± 8.55	3.295 ± 0.17	0.06
Control	42.85 ± 3.17	5.735 ± 0.29	0.007

Table 14. Effect of **BTDs E18** and **E25** on the expression levels of active caspases-3 and -9, and p53 in HCT116 cancer cells treated with each compound at its IC_{50} concentration.

Compound	Caspase-3 (ng/mg)	Caspase-9 (ng/mg)	p53 (pg/mg)
E18	514.7 ± 18.3	24.99 ± 1.52	1124 ± 42.1
E25	387.1 ± 12.8	17.44 ± 0.96	672.6 ± 22.6
Control	23.73 ± 2.17	2.13 ± 0.17	44.04 ± 2.91

The experimental procedures are reported in Chapter 5.

Chapter 4. Kinetic Characterization of Carbonic Anhydrases from the pathogenic protozoan *Entamoeba histolytica* and from the coral *Stylophora pistillata*

During my Ph.D. period I performed a multitude of kinetic studies with inhibitors and activators of several isoforms of CA belonging to the classes α, β, γ, δ, ζ, η and θ. The kinetic assessments were conducted by a Stopped Flow Assay.[169] These studies allowed to draw up the inhibition or activation profiles of hundreds of derivatives from collaborators of us.

Of note, I performed the *ex novo* complete kinetic characterization of the CA isoforms identified in the protozoan human parasite *Entamoeba histolytica* and in the coral *Stylophora pistillata*. These CAs were produced by Prof. Seppo Parkkila from Tampere University and Dr. Clemente Capasso from the Istitute of Biosciences and Bioresources, CNR of Naples, respectively.

4.1 *Entamoeba histolytica*

Entamoeba histolytica is a pathogenic protozoan human parasite causing amebiasis, which can be expressed as colitis or abscess of intestines or liver.[232,233] The common symptoms are diarrhea, colitis, and dysentery, but the majority of infections are asymptomatic.[232,233] *E. histolytica* is ingested with contaminated food or water as mature cysts, which excystate in the small intestine. The released trophozoites will then invade the large intestine.[232] *E. histolytica* is capable of lysing human tissues, killing immune effector cells by contact-dependent cytolysis.[232,234] The parasite has many virulence mechanisms, as it can adhere to host cells with multi-subunit GalGalNAc lectins, degrade the host extracellular matrix with cysteine proteases, and lyses target cells with amoebapores.[235] The invasive forms of the infection generally include cyst formation in the liver, which can lead to complications such as pleural effusion, due to the rupture of the cyst.[232] Rarely, they also disseminate through other extraintestinal organs (e.g. the brain or pericardium).[232,233] Although there are effective medications for treating *E. histolytica*, therapies for the invasive forms produce many adverse side effects,[232,233] and there are additional limitations to such therapies, among which is an increasing

prevalence of resistance to commonly used drugs, which emphasizes the need for new drug targets against this protozoan.[233,235] Thus, the research group of Prof. Seppo Parkkila decided to clone and investigate in detail the β-CA present in this pathogenic protozoan.

On my side, I performed the complete kinetic evaluation of the catalytic activity, and anion and sulfonamides inhibition profile of the recombinant enzyme identified in the genome of the pathogenic protozoan *E. histolytica*, denominated EhiCA.

EhiCA has been produced by the *E. coli* production system[236] and characterized with mass spectrometry (MS) and SDS-PAGE. Furthermore, atomic absorption spectroscopy allowed the Parkkila's group to determine the presence of one zinc ion per polypeptide chain (data not shown), which confirmed the MS data. The catalytic activity of the recombinant EhiCA was measured and compared to those of other such enzymes, belonging to the α-class, such as hCA I and II. Table 15 shows that EhiCA has a significant catalytic activity (for the physiologic reaction, CO_2 hydration to bicarbonate and protons), with a k_{cat} of 6.7 x 10^5 s^{-1} and a k_{cat}/K_m of 8.9 x 10^7 M^{-1} x s^{-1}, being thus 1.8 times more effective as a catalyst, compared to the slow human isoform hCA I (considering the k_{cat}/K_m values). Furthermore, like most enzymes belonging to the CA superfamily, EhiCA was inhibited by AAZ, with a K_I of 509 nM (Table 15).[1,14,48]

Table 15. Kinetic parameters for the CO_2 hydration reaction catalyzed by the human cytosolic isozymes hCA I and II (α-class CAs) at 20 °C and pH 7.5 in 10 mM HEPES buffer and 20 mM Na_2SO_4, and the β-CA EhiCA form *E. histolytica* measured at 20 °C, pH 8.3 in 20 mM TRIS buffer and 20 mM $NaClO_4$. Inhibition data with the clinically used sulfonamide acetazolamide are also provided.[169]

Enzyme	Activity Level	Class	k_{cat} (s^{-1})	K_m (mM)	k_{cat}/K_m (M^{-1} x s^{-1})	K_I Acetazolamide (nM)
hCA I	Moderate	α	2 x 10^5	4.0	5.0 x 10^7	250
hCA II	Very high	α	1.4 x 10^6	9.3	1.5 x 10^8	12
EhiCA	High	β	6.7 x 10^5	7.5	8.9 x 10^7	509

As seen in Figure 57, EhiCA (as all β-CAs investigated to date) has the conserved three zinc(II) ligands, Cys50, His103, and Cys106 (the fourth ligand is presumably a water molecule/hydroxide ion), as well as the catalytic dyad constituted by the pair Asp52–Arg54 (also conserved in all enzymes belonging to this class),[237–245] which contributes to the enhancement of the nucleophilicity of the water coordinated to the metal ion. The presence of these conserved amino acids, and all the structural elements connected to them, may explain the catalytic activity of EhiCA reported in this chapter (Table 15).

Figure 57. Multi-alignment of the amino acid sequences of the β-CAs from *M. tuberculosis* (isoform MTCA1_MYCTU), *Synechocystis sp.* (SYNY3), *V. cholerae* (VIBCL), *H. influenzae* (HAEIN), *E. coli* (ECOLI), *S. typhimurium* (SALTY), *E. histolytica* (ENTHI), and *M. tuberculosis* (isoform MTCA2_ MYCTU). Conserved amino acids depicted by an asterisk (*), semiconserved ones by (.) or (:).

4.1.1 Inhibition

4.1.1.1 Anions

The inhibition of EhiCA was assessed with a set of inorganic simple and complex anions, as well as small organic molecules known[238–245] to interact with CAs, such as diethyl-dithiocarbamate, sulfamide, sulfamic acid, phenyboronic and phenylphosphonic acid, among others (Table 16).

The following observations can be made from the inhibition data shown in Table 16: (i) The anions which did not show inhibitory activity against EhiCA were fluoride, chloride, and, surprisingly, cyanide and azide, which are highly effective inhibitors of α-CAs such as hCA I and II;[246] pyrodiphosphate and divanadate; perchlorate, tetrafluroborate, hexafluorophosphate, and triflate (which usually do not significantly inhibit any CA);[246] and, again surprisingly, sulfamic acid. All these compounds did not show significant inhibition up to a 100 mM concentration in the assay system.

Table 16. Inhibition constants of anionic inhibitors against the α-CA isoforms hCA II and hCA I, as well as the β-class protozoan enzyme EhiCA, for the CO_2 hydration reaction at 20 °C.[169]

	K_I(mM)[a]		
Anion[b]	**hCA I**	**hCA II**	**EhiCA**
F^-	>300	>300	>100
Cl^-	200	6.0	>100
Br^-	63	4.1	36.8
I^-	26	0.3	7.4
CNO^-	0.03	0.0007	0.77
SCN^-	1.6	0.2	7.9
CN^-	0.02	0.0005	>100
N_3^-	1.51	0.0012	>100
HCO_3^-	85	12	0.28
CO_3^{2-}	73	15	2.4
NO_3^-	35	7.0	3.6
NO_2^-	63	8.4	1.7
HS^-	0.04	0.0006	6.9
HSO_3^-	89	18	11.5
SO_4^{2-}	>200	63	21.6
SnO_3^{2-}	0.83	0.57	0.51
SeO_4^{2-}	112	118	6.0
TeO_4^{2-}	0.92	0.66	0.61
$P_2O_7^{4-}$	48.50	25.8	>100
$V_2O_7^{4-}$	0.57	0.54	>100
$B_4O_7^{2-}$	0.95	0.64	0.29
ReO_4^-	0.75	0.11	7.1
RuO_4^-	0.69	0.10	7.0
$S_2O_8^{2-}$	0.084	0.11	8.4
$SeCN^-$	0.086	0.085	0.87
CS_3^{2-}	0.0088	0.0087	6.0
$Et_2NCS_2^-$	3.1	0.00079	0.51
ClO_4^-	>200	>200	>100
BF_4^-	>200	>200	>100
FSO_3^-	0.46	0.79	0.086
PF_6^-	>200	>200	>100
$CF_3SO_3^-$	>200	>200	>100
$NH(SO_3)_2^{2-}$	0.76	0.31	2.2
$H_2NSO_2NH_2$	1.13	0.31	0.028
H_2NSO_3H	0.39	0.021	>100
$PhB(OH)_2$	23.1	38.6	0.047
$PhAsO_3H_2$	49.2	31.7	0.038

a. Errors were in the range of 3–5% of the reported values, from three different assays. b. Sodium salt.

(ii) The most effective EhiCA inhibitors were sulfamide (which is structurally highly similar to sulfamic acid, except that the pK_a of the two compounds is highly

different)[247,248] and fluorosulfonate, as well as phenylboronic acid and phenylarsonic acid, which showed K_Is in the range of 28–86 μM. As seen in Table 16, many of these small molecules/anions also act as inhibitors of hCA I and II, but with a rather different efficacy.[247]

(iii) Several anions, such as cyanate, selenocyanate, bicarbonate, stannate, tellurate, tetraborate, and *N*,*N*-diethyl-dithiocarbamate were also sub-millimolar EhiCA inhibitors, with K_Is in the range of 0.28–0.87 mM. Some of these compounds are typical metal complexing agents (cyanate, selenocyanate, *N*,*N*-diethyt-dithiocarbamate), and their propensity to bind the zinc ion in this β-CA explains these inhibitory activities. However, others, (among which are bicarbonate, stannate, tellurate, and tetraborate) show less affinity to act as metal complexing anions.[246] The inhibitory action of bicarbonate, one of the reaction products/substrates of the CA, is particularly interesting, possibly indicating that the enzyme is not acting as a highly efficient bicarbonate dehydratase, but instead that the CO_2 hydratase activity might be crucial during the life cycle of this protozoan. However, this speculation needs careful validation.

(iv) Many anions acted as low millimolar EhiCA inhibitors. They include iodide, thiocyanate, carbonate, nitrate, nitrite, hydrogensulfide, selenite, perrhenate, perruthenate, peroxydisulfate, trithiocarbonate, and imidosulfonate (K_Is in the range of 1.7–8.4 mM).

(v) Anions with a less effective inhibitory action against EhiCA were bromide, bisulfite, and sulfate, with K_Is in the range of 11.5–365.8 mM (Table 16).

The experimental procedures are reported in Chapter 5 and the data and results of this research were published in Susanna Haapanen, et al. *Molecules*. **2018**, *23*, pii: E3112.

4.1.1.2 Sulfonamides

Therefore, the inhibition of EhiCA was evaluated with a series of sulfonamide/sulfamate derivatives, some of which are clinically used drugs like diuretics, antiglaucoma, antiepileptics, antiobesity or antitumor agents[249–252] (Figure 58, 59 and Table 17). The structures of the sulfonamides/sulfamates included in our study are shown in Figure 53. They include acetazolamide **AAZ**, methazolamide **MZA**, ethoxzolamide **EZA** and dichlorophenamide **DCP** (the classical, systemically acting antiglaucoma CA

inhibitors),[1,14] dorzolamide **DZA** and brinzolamide **BRZ**, topically-acting antiglaucoma drugs, benzolamide **BZA**, topiramate **TPM**, zonisamide **ZNS**, and sulthiame **SLT**.[1,14,249-253] Sulpiride **SLP**, indisulam **IND**, celecoxib **CLX**, and valdecoxib **VLX**, as well as saccharin and the diuretic hydrochlorothiazide **HCT** were also included in the assay.[1,20,48] The simpler sulfonamides **F1–24** are known to possess CA inhibitory properties against many mammalians and prokaryotic such enzymes[254] and are also the building blocks for obtaining more complex CAIs.[247,255]

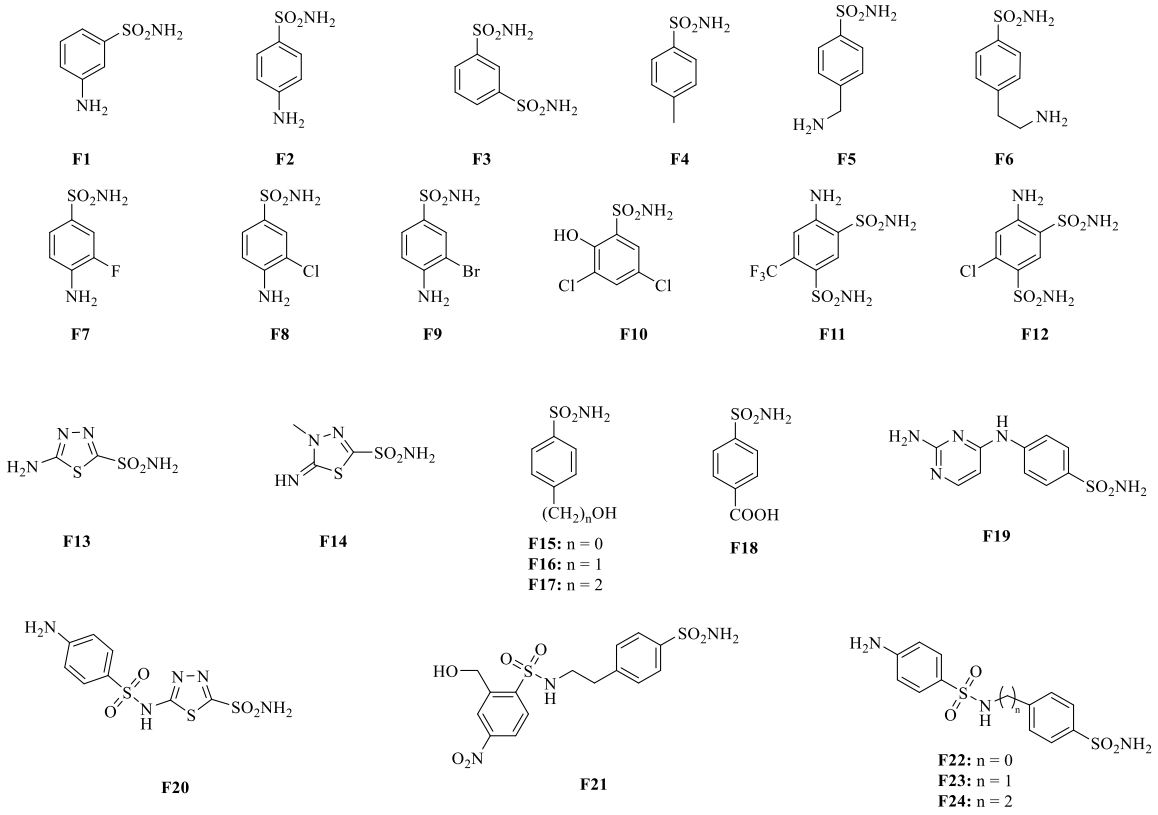

Figure 58. Sulfonamide (**F1–24**) investigated as *Entamoeba histolytica* (EhiCA) inhibitors in the present project.

The following SAR can be drawn from the data of Table 17:

(i) The most effective EhiCA inhibitors were the two simple compounds **F16** and **F17**, 4-hydroxymethyl/ethyl-benzenesulfonamides, which showed K_Is ranging between 36 and 89 nM, with the longer linker derivative (**F17**) being a more effective CAI compared to the hydroxymethyl one **F16**. It should also be noted that **F17** is a weaker hCA II inhibitor (K_I of 125 nM) and a quite ineffective hCA I inhibitor (K_I of 21 nM), making it a slightly ameba-CA-selective compound.

(ii) Several sulfonamides were slightly less effective as EhiCA inhibitors, with K_Is ranging between 285 and 521 nM. They include **F18–24** and acetazolamide **AAZ** (Table 17). Apart from **F18** (4-carboxy-benzenesulfonamide) and **F19** (a pyrimidinylamino-benzenesulfonamide), the remaining derivatives **F20–24** belong to the sulfanilyl-sulfonamide class of CAIs, which possess an elongated molecule, shown to interact favorably with many other CAs belonging to the β-class[238,242,256] and, thus, leading to effective inhibitors. For the homologous series of **F22–24**, the efficacy as EhiCA inhibitors increases with the increase of the linker between the two aromatic rings. **AAZ** and **F20** contain the 1,3,4-thiadiazole-2-sulfonamide motif present in many potent CAIs. In this case, aminobenzolamide **F20** is a more effective EhiCA inhibitor compared to **AAZ**. It is interesting to note that **BZA**, lacking the amino moiety present in **F20**, but with an identical scaffold, is a very weak CAI, with a K_I of 2471 nM (whereas it is a very potent hCA I and II inhibitor). Thus, minor structural changes in the molecule of the inhibitor lead to drastic effects on their inhibitory profiles against various CAs, including the one form the parasitic protozoan investigated here.

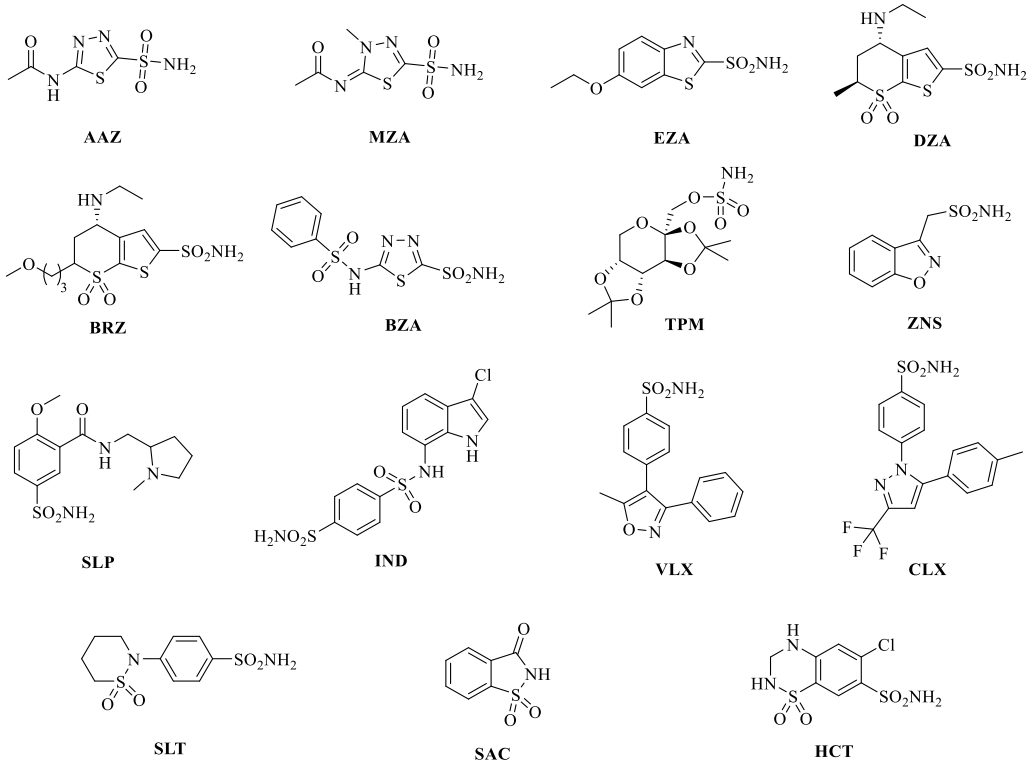

Figure 59. Sulfonamide/sulfamate derivatives (**AAZ–HCT**) investigated as *Entamoeba histolytica* (EhiCA) inhibitors in the present project.

Table 17. Inhibition of human isoforms hCA I and hCA II, and ***Entamoeba Histolytica*** (**EhiCA**) with sulfonamides **F1-24** and the clinically used drugs **AAZ – HCT** by a stopped-flow CO_2 hydrase assay.

	K_I* (nM)		
Cmpd	**CA I**	**CA I**	**EhiCA**
F1	28	300	2363
F2	25	240	6011
F3	79[c]	8	951
F4	785	320	833
F5	25	170	567
F6	21	160	798
F7	8300	60	>10000
F8	9800	110	>10000
F9	6500	40	>10000
F10	7300	54	4656
F11	5800	63	742
F12	8400	75	1911
F13	8600	60	821
F14	9300	19	579
F15	5500	80	772
F16	9500	94	89
F17	21	125	36
F18	164	46	383
F19	109	33	521
F20	6	2	385
F21	69	11	368
F22	164	46	331
F23	109	33	290
F24	95	30	285
AAZ	250	12	509
MZA	50	14	845
EZA	25	8	746
DZA	50	9	6444
BRZ	45	3	3051
BZA	15	9	2471
TPM	250	10	3100
ZNS	56	35	9595
SLP	1200	40	>10000
IND	31	15	822
VLX	54	43	>10000
CLX	50	21	>10000
SLT	374	9	6727
SAC	18540	5959	>10000
HCT	328	290	3402

*Errors in the range of 5 – 10 % of the reported data, from 3 different assays (data not shown).

(iii) The following compounds showed modest EhiCA inhibitory properties: **F3–6**, **F11**, **F13–15**, **MZA**, **EZA**, **DCP**, and **IND**, with K_Is ranging between 567 and 951 nM. They belong to heterogeneous classes of sulfonamides, most of them being benzenesulfonamides (apart **F13** and **F14** which are the deacetylated precursors of **AAZ** and **MZA**, thus, heterocyclic derivatives). A special mention regards **F15**, which is structurally related to the most effective EhiCA inhibitors detected here, compounds **F16** and **F17**. Indeed, **F15** is 9–20 times a weaker EhiCA inhibitor compared to **F16** and **F17**,

although they differ only by one or two CH_2 functionalities. From these data, it is again obvious that SAR is very sensitive to small changes in the molecule of the inhibitor and that the 4-hydroxyalkyl-substituted-benzenesulfonamides may lead to highly effective and isoform-selective CAIs targeting the enzyme from this parasite.

(iv) Weak, micromolar inhibition against EhiCA was observed with **F1**, **F2**, **F10**, **F12**, **DZA**, **BRZ**, **BZA**, **TPM**, **ZNZ**, **SLT**, and **HCT** (K_Is ranging between 1.91–9.59 μM) as discussed earlier. In addition, these derivatives belong to heterogeneous classes of derivatives, but overall one may observe that they possess a bulkier scaffold and more substituents on the aromatic/heterocyclic ring compared to the effective EhiCA inhibitors described above.

(v) The ineffective compounds as EhiCA inhibitors (K_I > 10 μM) detected here were **F7–9** (halogenated sulfanilamide derivatives), sulpiride **SLP**, the COX-2 inhibitors **CLX** and **VLX** (possessing a bulky, Y-shaped molecule), and saccharin **SAC**, the only acylated, secondary sulfonamide included in the project.

(vi) The inhibition profile of EhiCA with sulfonamides/sulfamates is very different from those of the human isoforms hCA I and II, but only two compounds, **F16** and **F17** showed selectivity for the protozoan over the human isoforms (Table 17).

The experimental procedures are reported in Chapter 5 and the data and results of this research were published in Silvia Bua, et al. *Int. J Mol. Sci.* **2018**, *19*, pii: E3946.

4.1.2 Activators

Additionally, we studied for the first time the activation of the β-CA from *E. histolytica* with a panel of amines and amino acid derivatives. As CAAs have poorly been investigated for their interaction with protozoan CAs, our study may be relevant for an improved understanding of the role of this enzyme in the life cycle of *E. histolytica*.

The kinetic measurements were performed in the presence of the amine and amino acid activators shown in Figure 60, such as for example L-Trp. Data of Table 18 show that the presence of L-Trp does not change the K_M, both for the α-class enzymes hCA I/II as well as the β-CA, EhiCA, investigated here. Interestingly, it influences the k_{cat}, which at 10-

μM concentration of activator leads to a 2.83 times enhancement of the kinetic constant for the protozoan enzyme, from 6.7 x 10^5 s^{-1} to 1.9 x 10^6 s^{-1} (Table 18).

Table 18. Activation of human carbonic anhydrase (hCA) isozymes I, II, and EhiCA with L-Trp at 25 °C for the CO_2 hydration reaction.[169]

Isozyme	k_{cat}* (s^{-1})	(k_{cat}) L-Trp** (s^{-1})	$K_{A\ L\text{-}Trp}$ ***(μM)
hCA I[a]	2.0 x 10^5	3.4 x 10^5	44.0
hCA II[a]	1.4 x 10^6	4.9 x 10^6	27.0
EhiCA[b]	6.7 x 10^5	1.9 x 10^6	5.24

* Observed catalytic rate without activator. K_M values in the presence and the absence of activators were the same for the various CAs (data not shown).; ** Observed catalytic rate in the presence of 10 M activator; *** The activation constant (K_A) for each enzyme was obtained by fitting the observed catalytic enhancements as a function of the activator concentration. Mean from at least three determinations by a stopped-flow, CO_2 hydrase method.[169] Standard errors were in the range of 5–10% of the reported values (data not shown); a. Human recombinant isozyme, from ref. 257; b. Protozoan recombinant enzyme.

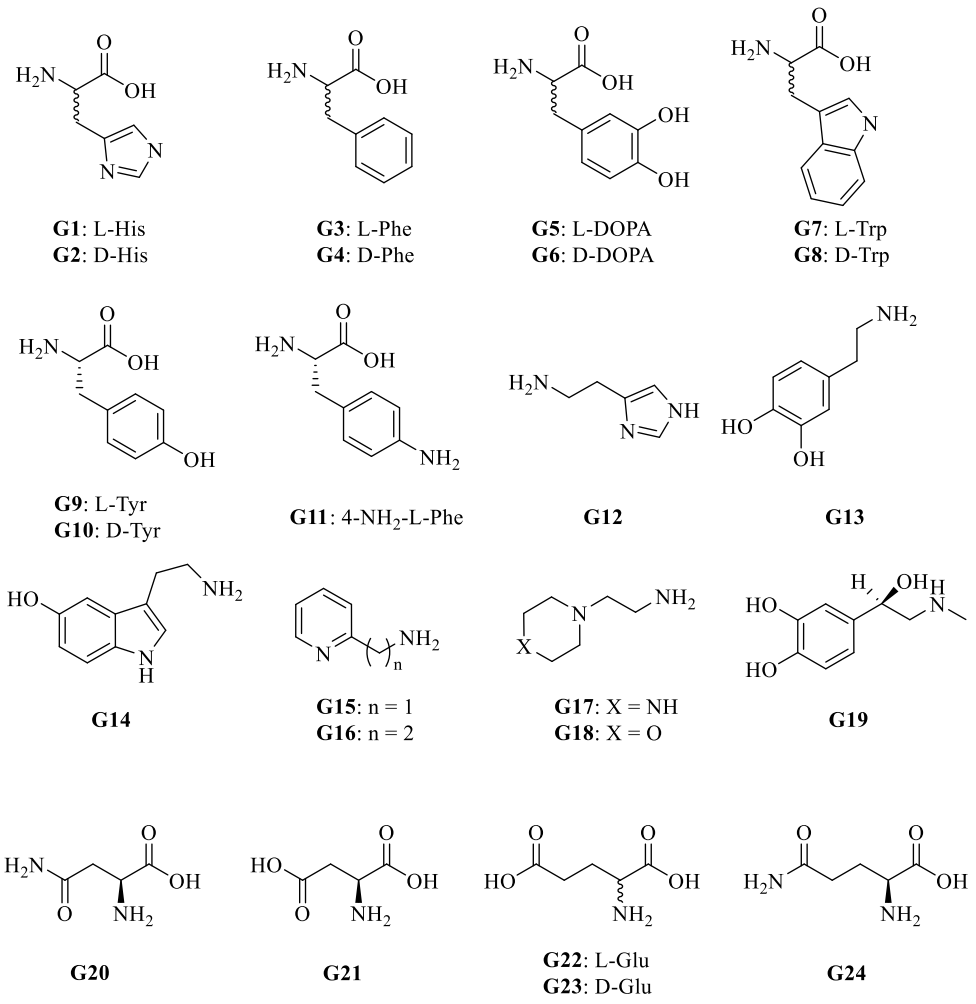

Figure 60. CAAs of type **G1-24** used in the present study.

Dose response curves of the activation of EhiCA in the presence of increasing concentrations of activators were performed in order to determine the activation constants K_As (see Chapter 5 for details). These activation data are reported in Table 19, in which, for comparison reasons, the activation of the human isoforms hCA I and II and of the protozoan β-CA from *Leishmania donovani chagasi* (LdcCA) are also presented.

Table 19. Activation constants of hCA I, hCA II and the protozoan enzymes LdcCA and EhiCA with amino acids and amines **1–24**. Data for hCA I and II are from 257 and for LdcCA from 258.

No.	Compound	K_A* (mM)			
		hCA I[a]	hCA II[a]	LdcCA[b]	EhiCA
1	L-His	0.03	10.9	8.21	78.7
2	D-His	0.09	43	4.13	9.83
3	L-Phe	0.07	0.013	9.16	16.5
4	D-Phe	86	0.035	3.95	10.1
5	L-DOPA	3.1	11.4	1.64	16.6
6	D-DOPA	4.9	7.8	5.47	4.05
7	L-Trp	44	27	4.02	5.24
8	D-Trp	41	12	6.18	4.95
9	L-Tyr	0.02	0.011	8.05	4.52
10	D-Tyr	0.04	0.013	1.27	1.07
11	4-H_2N-L-Phe	0.24	0.15	15.9	8.12
12	Histamine	2.1	125	0.74	7.38
13	Dopamine	13.5	9.2	0.81	30.8
14	Serotonin	45	50	0.62	4.94
15	2-Pyridyl-methylamine	26	34	0.23	>100
16	2-(2-Aminoethyl)pyridine	13	15	0.012	>100
17	1-(2-Aminoethyl)-piperazine	7.4	2.3	0.009	43.8
18	4-(2-Aminoethyl)-morpholine	0.14	0.19	0.94	>100
19	L-Adrenaline	0.09	96	4.89	25.6
20	L-Asn	11.3	>100	4.76	23.8
21	L-Asp	5.2	>100	0.3	23.9
22	L-Glu	6.43	>100	12.9	25.5
23	D-Glu	10.7	>100	0.082	30.3
24	L-Gln	>100	>50	2.51	20.1

*Mean from three determinations by a stopped-flow, CO_2 hydrase method.[169] Standard errors were in the range of 5–10% of the reported values (data not shown). A. Human recombinant isozymes, from ref. 257; b. Protozoan recombinant enzyme, from ref. 258.

The SAR for the activation of EhiCA with compounds **G1–24** revealed the following observations:

(i) Some heterocyclic-alkyl amines, such as 2-pyridyl-methyl/ethyl-amine **G15**, **G16** and 4-(2-aminoethyl)-morpholine, were devoid of EhiCA activating properties up to 100 μM

concentration of activator in the assay system. All these compounds are structurally related, possessing a heterocyclic ring and aminomethyl/aminoethyl moieties in their molecules.

(ii) L-His, dopamine, 1-(2-aminoethyl)-piperazine and D-Glu were poor EhiCA activators, with activation constants ranging between 30.3 and 78.7 μM (Table 19). There is no strong structural correlation between these three compounds.

(iii) Many of the compounds investigated here showed medium potency efficacy as EhiCA activators, with K_As ranging between 16.5 and 25.6 μM. They include L-Phe, L-DOPA, L-adrenaline, L-Asn, L-Asp, L-Glu and L-Gln. It may be observed that there are no remarkable differences of activity between the pairs L-Asp/L-Asn and L-Glu/L-Gln, whereas D-Glu was more ineffective compared to L-Glu. This is in fact the exception, as for other L-/D-enantiomeric amino acids investigated here, the D-enantiomer was the most effective activator (see later in the text).

(iv) Effective EhiCA activating properties were detected for the following amino acids/amines: D-His, D-Phe, D-DOPA, L- and D-Trp, L- and D-Tyr, 4-amino-L-Tyr, histamine and serotonin, which showed K_As ranging between 1.07 and 10.1 μM. The best activator was D-Tyr (K_A of 1.07 μM). In fact, for all aromatic amino acids investigated here, the D-enantiomer was more effective as EhiCA activator compared to the corresponding L-enantiomer. For the Phe-Tyr-DOPA subseries, the activity increased by hydroxylation of the Phe, achieving a maximum for Tyr and then slightly decreased with the introduction of an additional OH moiety in DOPA, but always the D-enantiomers were better activators compared to the L-ones. The loss of the carboxyl moiety, such as in histamine and serotonin, did not lead to important changes of activity compared to the corresponding D-amino acids, but in the case of dopamine, the activating efficacy was much lower compared to those of both L- and D-DOPA.

(v) The activation profile of EhiCA with amino acid and amine derivatives is rather different from those of other CAs, among which the protozoan β-CA from LdcCA or the α-class human CAs, isoforms hCA I and II. For example, **G17** was a nanomolar activator for LdcCA whereas its affinity for EhiCA was of only 43.8 μM. For the moment, no EhiCA-selective activators were detected.

As CAAs have poorly been investigated for their interaction with protozoan CAs, our study may be relevant for an improved understanding of the role of this enzyme in the life cycle of *E. histolytica*.[259,260]

The experimental procedures are reported in Chapter 5 and the data and results of this research were published in Silvia Bua, et al. *Metabolites*. **2019**, *9*, pii: E26.

4.2 *Stylophora pistillata*

Carbonic anhydrases also play a role in essential processes of coral physiology. In fact, CAs are involved in the carbon supply for calcium carbonate precipitation (formation of skeletons) as well as in carbon-concentrating mechanisms for symbiont photosynthesis.[261] In corals, most of the available results on CAs were obtained by measuring the CA activity in crude tissue extracts using non-specific CA inhibitors or antibodies raised against human isoforms.[262-266] Recently, the development of molecular biology tools allowed the isolation and full characterization of several CA isoforms in different coral species, such as *Lobactis scutaria*,[267] *Stylophora pistillata*,[268,269] and *Acropora millepora*.[270] In particular, analyzing the molecular data in the branching coral *Stylophora pistillata* 16 α-CA isoforms in the transcriptome and genome of this scleractinian coral were identified.[261,268,269,271–280] Among them, two α-CAs were isolated (STPCA and STPCA-2, here, indicated as SpiCA1 and SpiCA2, respectively) and have been localized in the coral-calcifying cells, within the epithelium facing the skeleton.[268,269] It has been proposed that SpiCA1 catalyzes the inter-conversion between the different inorganic forms of dissolved inorganic carbon at the site of calcification, whereas SpiCA2 is an intracellular enzyme, which is found as an organic matrix protein incorporated in the skeleton.[281,282] Beyond isoforms SpiCA1 and SpiCA2, the research group of Dr. Clemente Capasso from CNR of Naples also cloned, expressed, purified and characterized a new α-CA, named SpiCA3, which is intracellular (cytoplasmic) and ubiquitously expressed in all the cell layers including the calcifying cells and the symbiotic endodermal cells.

The recombinant SpiCA3 was produced as a fusion protein with a His-Tag tail in the cytoplasm of the *E. coli* BL21 DE3 cells. After appropriate purification, SpiCA3 was

aligned with the amino acid sequences of SpiCA1 and SpiCA2, previously identified in *S. pistillata* and the two human isoforms, hCA I and II, in order to identify the presence of salient features of SpiCA3 (Figure 61).

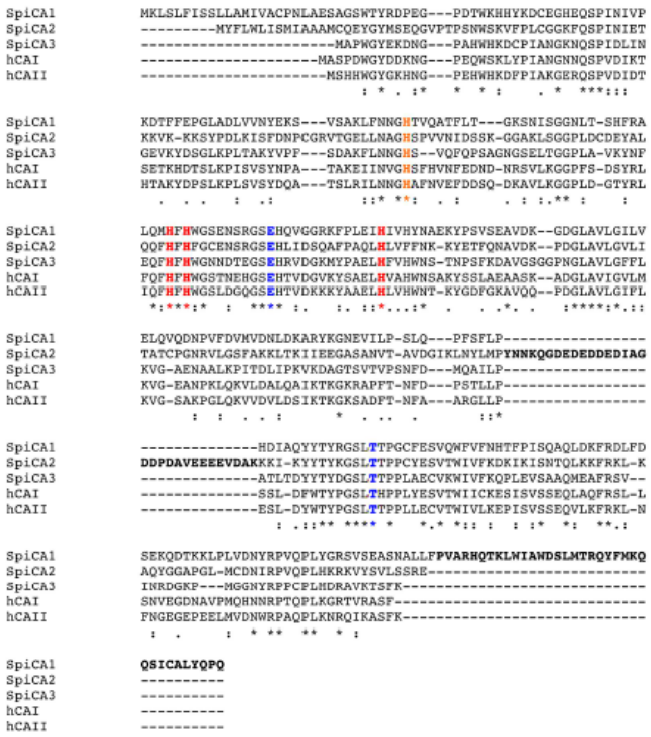

Figure 61. Multialignment of the α-CA amino acid sequences from human (hCAI and II) and *S. pistillata* (SpiCA1, SpiCA2 and SpiCA3). Multialignment was performed with the program Muscle. hCAI numbering system was used. Legend: zinc ligands, in red bold; "gate-keeper" residues, in blue bold; histidine proton shuttle, in orange bold; long stretches of 31 and 35 amino acid residues, in black bold; (*), indicates identity at a position; (:), designates conserved substitutions; (.) indicates semi-conserved substitutions.

Figure 55 shows a multi-alignment of the three α-CA isoforms encoded by the genome *S. pistillata* and investigated up until now. It is readily apparent that the three coral isoforms show the main features of a typical mammalian α-CAs. They possess the conserved: (i) Three His ligands, which coordinate the Zn(II) ion crucial for catalysis, (His94, His96, and His119, hCA I numbering system); (ii) the two gate-keeping residues (Glu106 and Thr199), which are implicated in the substrate orientation and the binding of the inhibitors; and (iii) the proton shuttle residue (His64), which is involved in the transfer of the proton (H^+) from the water coordinated to the Zn(II) ion to the environment, influencing and making very fast the rate of the catalytic reaction. Furthermore, SpiCA3, diversely from the other two coral isoforms, is a cytoplasmic protein. SpiCA1 and

SpiCA2 are, in fact, secreted proteins characterized by the presence of a signal peptide at the N-terminal of their amino acid sequences (Figure 61). Interesting, the insertions and deletions of a relatively extended number of amino acid residues along the polypeptide chain, which affect the three coral isoforms (Figure 61), may influence the kinetic and inhibition behavior of the coral enzymes, probably because of significant alterations of their three-dimensional structure. For example, SpiCA3 showed a $k_{cat} = 10^6$ s^{-1}, which is one order of magnitude higher than the k_{cat} (10^5 s^{-1}) of the other two isoforms.

In detail, this isoform showed a catalytic activity 1.14-times higher than human CA II (Table 20) and is one of the most effective CO_2 catalysts among all CAs known to date with a k_{cat} of 1.6 x 10^6 s^{-1} and a k_{cat}/K_M of 1.5 x 10^8 M^{-1} s^{-1}.

Table 20. Kinetic parameters for the CO_2 hydration reaction catalyzed by the human cytosolic α-hCA isozymes I-II, and the coral enzymes **SpiCA1-3**, at 20°C and pH 7.5 in 10 mM HEPES buffer, and their inhibition data with **AAZ**, a clinically used drug.

Isozyme	Activity Level	k_{cat} (s^{-1})	k_{cat}/K_M (M^{-1} s^{-1})	K_I (AAZ) (nM)
hCA I	Moderate	2.0 x 10^5	5.0 x 10^7	250
hCA II	Very high	1.4 x 10^6	1.5 x 10^8	12
SpiCA1	Moderate	3.1 x 10^5	4.6 x 10^7	16
SpiCA2	High	5.6 x 10^5	8.3 x 10^7	74
SpiCA3	Very high	1.6 x 10^5	1.5 x 10^8	737

Intriguingly, the three coral CAs (SpiCA1, SpiCA2, and SpiCA3) differ significantly in their catalytic activity and susceptibility to inhibition with anions.[269,276] Therefore, in this project, I measured the inhibition profiles of SpiCA3 and compared it with those obtained for SpiCA1 and SpiCA2 in the presence of inorganic anions, sulfonamides and other small molecules known to interfere with the metalloenzymes.[14,257,277-279]

4.2.1 Inhibition

4.2.1.1 Anions

The inhibition constants of a set of inorganic simple and complex anions, against SpiCA3 and other α-CAs, such as the two human isoforms hCAI and II, and the two *S. pistillata* isoforms, SpiCA1 and SpiCA2 are given in Table 21. From this table it can be noted that the most efficient inhibitors of SpiCA3 were sulfamide, diethylthiocarbamate, azide and cyanide, which showed a K_I in the range of 0.7–80 μM. Interestingly, sulfamide was also

an efficient inhibitor of SpiCA1 (K_I = 10 μM) and SpiCA2 (K_I = 57 μM), but less efficient for hCAI (K_I = 310 μM) and hCAII (K_I = 1130 μM). Compared to human isoforms, poor inhibitory properties were also detected for the following anions: fluoride, chloride, bromide, iodide, cyanate, thiocyanate, bicarbonate, carbonate, nitrate, nitrite, hydrogensulfide, bisulfite, stannate, selenate, tetraborate, perruthenate, selenocyanate, trithiocarbonate, triflate, fluorosulfonate and iminodisulfonate, which showed inhibition constants in the range of 0.23–12.8 mM. Among these, bromide and iodide resulted in the most efficient inhibitor of SpiCA1 with a K_I = 9.0 and 9.7 μM. Bicarbonate, which is one of the substrates of the CAs, shows a similar K_I for the coral isoforms SpiCA1 (K_I = 450 μM) and SpiCA3 (K_I = 400 μM) and a very low affinity for SpiCA2 (K_I = 7.81 mM). Only the K_I of SpiCA2 is in the range of K_I observed for the human isoforms (K_I in the range of 12–85 mM). Concerning carbonate, the three coral isoforms show different characteristics. This inhibitor is 23.6- and 566-fold more effective for SpiCA2 (K_I = 240 μM) and SpiCA1 (K_I = 10 μM) respectively than for SpiCA3 (K_I = 5660 μM). Only the K_I of SpiCA3 is in the range of K_I observed for the human isoforms (K_I in the range of 15–73 mM). Many other investigated anions did not significantly inhibit SpiCA3, such as tellurate, pyrophosphate, divanadate, perrhenate, peroxydisulfate, perchlorate, sulfamate, phenylboronic acid, phenylarsonic acid. All of them showed K_I > 100 mM against SpiCA3. Moreover, tetrafluoroborate and perchlorate showed a K_I > 200 mM against all the enzymes used in the present study. The inhibition pattern of the three coral enzymes shows how different the behavior of SpiCA1, SpiCA2 and SpiCA3 is towards these small anionic molecules. The dissimilar inhibition profile may be attributed to the different binding modes that each isoform has for the anions investigated, such as the different interactions of the amino acid residues and the metal ion at the active site with the inhibitors. For example, although anions were generally reported to directly coordinate to the metal ion form the enzyme active site,[246,280] for a β-CA from the alga *Coccomyxa*,[280] iodide was observed anchored to the zinc-coordinated water molecule, possessing thus a distinct inhibition mechanism. Such diverse inhibitory activity as the one observed here may in fact be ascribed to such putative, diverse interactions with the metal ion and its surrounding, but no detailed X-ray studies are available so far. In the branching coral *Stylophora pistillata* the genome encodes for 16 CAs[281] but only three of them have been fully characterized for their chemical properties. Our results, which show that the

sensitivity to anions varies between the three isoforms, suggest that the coral uses the CA isoforms to satisfy its physiological functions in different physicochemical microenvironments.

Table 21. Inhibition constants of anionic inhibitors against isozymes hCA I, II and VI (human, α-CA class enzymes), and the CA from the coral *Stylophora pistillata*, SpiCA1–SpiCA3, for the CO_2 hydration reaction, at 20 °C.[169]

Anion	K_I* (mM)				
	hCA I	**hCA II**	**SpiCA1[a]**	**SpiCA2[a]**	**SpiCA3[c]**
F^-	>300	>300	0.62	0.92	0.48
Cl^-	6	200	0.50	0.53	0.51
Br^-	4	63	0.0097	0.96	0.23
I^-	0.3	26	0.0090	33.0	0.56
CNO^-	0.0007	0.03	0.59	0.69	2.41
SCN^-	0.2	1.6	0.68	0.51	2.53
CN^-	0.0005	0.02	0.58	0.86	0.050
N_3^-	0.0012	1.5	0.52	4.68	0.080
HCO_3^-	12	85	0.45	7.81	0.40
CO_3^{2-}	15	73	0.010	0.24	5.66
NO_3^-	7	35	0.56	0.99	12.8
NO_2^-	8.4	63	0.77	3.15	0.45
HS^-	0.0006	0.04	0.58	3.94	0.34
HSO_3^-	18	89	0.41	0.43	5.20
SO_4^{2-}	63	>200	0.91	0.33	0.61
SnO_3^{2-}	0.57	0.83	nt	nt	2.96
SeO_4^{2-}	118	112	nt	nt	5.14
TeO_4^{2-}	0.66	0.92	nt	nt	>100
$P_2O_7^{4-}$	25.8	48.5	nt	nt	>100
$V_2O_7^{4-}$	0.54	0.57	nt	nt	>100
$B_4O_7^{2-}$	0.64	0.95	nt	nt	0.84
ReO_4^-	0.11	0.75	nt	nt	>100
RuO_4^-	0.10	0.69	nt	nt	0.76
$S_2O_8^{2-}$	0.11	0.084	nt	nt	>100
$SeCN^-$	0.085	0.086	nt	nt	0.15
CS_3^{2-}	0.0087	0.0088	nt	nt	0.47
$Et_2NCS_2^-$	0.00079	3.1	nt	nt	0.044
ClO_4^-	>200	>200	>200	>200	>200
BF_4^-	>200	>200	>200	>200	>200
FSO_3^-	nt	nt	nt	nt	0.55
PF_6^-	nt	nt	nt	nt	nt
$NH(SO_3)_2^{2-}$	nt	0.76	nt	nt	0.48
$H_2NSO_2NH_2$	0.31	1.13	0.010	0.057	0.0007
H_2NSO_3H	0.021	0.39	0.81	0.085	>100
Ph-$B(OH)_2$	58.6	23.1	0.68	0.081	>100
Ph-AsO_3H_2	31.7	49.2	0.78	0.067	>100

* Mean from three different assays. a. Coral recombinant enzyme, data from Reference 271 and 272. B. This work. nt = not tested.

The experimental procedures are reported in Chapter 5 and the data and results of this research were published in Sonia Del Prete, et al. *Int. J. Mo.l Sci.* **2018**, *19*, pii: E2128.

4.2.1.2 Sulfonamides

Therefore, the inhibition profile of SpiCA3 was evaluated with a series of sulfonamide/sulfamate derivatives (Figure 58 and 59) and compared to that of SpiCA1, SpiCA2 and human α-CAs I and II (Table 22).[269,272] The following should be noted regarding the inhibition of the three coral enzymes with the compounds investigated in this study (Table 22):

(i) High potency inhibitors: most of the tested sulfonamides were effective inhibitors of the coral isoform SpiCA1 with a K_I in the range of 16–92 nM. This is the case of the compounds **F5**, **F7**, **F8**, **F14**, **F18**, **F19**, **F20**, **AAZ**, **MZA**, **EZA**, **DZA**, **BRZ**, **BZA**, **TMP**, **VLX**, **CLX**, **SLT**, and **SAC**. Intriguingly, most of these compounds were moderate inhibitors of SpiCA2 and SpiCA3 showing a K_I > 100 nM. The SpiCA2 inhibition profile showed only one compound (**AAZ**) with a K_I < 100 nM; while SpiCA3 was well inhibited by compounds **F17**, **F19**, **F20**, **F21**, **F23**, **F24**, and **IND**.

(ii) Medium potency inhibitors: a large number of simple aromatic sulfonamides, such as derivatives **F2–20**, and the pharmacological sulfonamides **AAZ**, **MZA**, **EZA**, **DZA**, **BRZ**, **BZA**, **ZNS**, **TMP**, **SLP**, **IND**, **CLX**, **SLT**, and **SAC** showed moderate SpiCA2 inhibitory properties with a K_I in the range 105–868 nM. Intriguing, the sulfonamide inhibition profile of SpiCA2 was characterized mainly by moderate inhibitors (Table 22). The compounds, which resulted in effective and moderate inhibitors of SpiCA1 or moderate inhibitors of SpiCA2, such as **F2**, **F5**, **F6**, **F7**, **F8**, **TMP**, **ZNS**, **SLP**, **CLX**, and **SAC** resulted in the worst inhibitors for the coral isoform SpiCA3. Most of these derivatives are benzenesulfonamides with one or two simple substituents in *ortho*, *para*, or the 3,4-positions of the aromatic ring with respect to the sulfamoyl zinc-binding moiety.

(iii) Ineffective inhibitors: many sulfonamides, such as derivatives **F1**, **F2**, **F5**, **F6**, **F7**, **F8**, **F10**, **TPM**, **ZNS**, **SLP**, **VLX**, **CLX**, and **SAC** were weak inhibitors of SpiCA3 showing a K_I > 1000 nM. Interesting, the coral isoform SpiCA2 showed only one ineffective derivative (**VLX**), while the SpiCA1 was the isoform better inhibited by all the compounds used in the present study.

Table 22. Inhibition of human α-CAs (hCA I and hCA II) and the three-recombinant enzyme from *Stylophora pistillata* (SpiCA1, SpiCA2, and SpiCA3) with sulfonamides **F1–24** and the clinically used drugs **AAZ—HCT** reported in Figure 58 and 59.

Inhibitor	K_I* (nM)				
	hCA I[a]	hCA II[a]	SpiCA1[a]	SpiCA2[a]	SpiCA3
F1	28000	300	nt	nt	5059
F2	25000	240	364	300	4276
F3	79	8	nt	nt	667
F4	78500	320	614	516	694
F5	25000	170	83	508	7871
F6	21000	160	94	577	7828
F7	8300	60	75	493	3318
F8	9800	110	88	551	1815
F9	6500	40	104	540	918
F10	7300	54	nt	nt	2532
F11	5800	63	367	481	856
F12	8400	75	295	840	430
F13	8600	60	105	361	275
F14	9300	19	92	357	578
F15	5500	80	nt	nt	487
F16	9500	94	nt	nt	199
F17	21000	125	770	701	66
F18	164	46	30	661	241
F19	109	33	25	868	83
F20	6	2	28	333	74
F21	69	11	nt	nt	53
F22	164	46	nt	nt	568
F23	109	33	nt	nt	62
F24	95	30	nt	nt	46
AAZ	250	12	16	74	737
MZA	50	14	21	132	821
EZA	25	8	39	105	56
DZA	50000	9	18	113	354
BRZ	45000	3	48	169	250
BZA	15	9	20	214	394
TPM	250	10	29	367	5828
ZNS	56	35	259	645	5513
SLP	1200	40	430	415	>10000
IND	31	15	163	394	92
VLX	54000	43	29	5710	2918
CLX	50000	21	34	690	9102
SLT	374	9	45	123	251
SAC	18540	5959	40	104	>10000
HCT	328	290	nt	nt	243

* Errors in the range of 5–10% of the reported data, from 3 different assays (data not shown). a Human recombinant isozymes and coral recombinant isoforms, stopped flow CO_2 hydrase assay method, from references 271 and 282. nt = not tested.

(iv) Human isoforms versus coral enzymes: the comparison of the inhibition profile of the human isoforms with those of the coral enzymes showed that SpiCA1 resulted very similar to the isoform hCAII. Furthermore, the isoform hCAI was not inhibited by most of the derivatives indicated with the numbers **F1**, **F2**, and those of the range **F4–17** (K_I > 1000 nM). Moreover, the clinically used agents, among which **DZA**, **BRZ**, and **CLX** didn't affect the hCAI activity, while they were high potency inhibitors for hCAII and SpiCA1 and low potency inhibitors for SpCA2 and SpiCA3.
The gathering of coral CAs inhibition profiles may provide new insights to design tools aimed at a better understanding of the molecular mechanisms involved in coral biomineralization.

The experimental procedures are reported in Chapter 5 and the data and results of this research were published in Sonia Del Prete, et al. *Mar. Drugs*. **2019**, *17*, pii: E146.

Additionally, as stated above I conducted kinetic experiments with hundreds of derivatives, among which both inhibitors and activators, from collaborators of us. The data, which allowed to draw up the CA inhibition or activation profiles of several series of compounds, are published in:

Leonardo E. Riafrecha, et al. *Bioorg Med Chem Lett.* **2016**, *26*, 3892-5.
Rajiv Kumar, et al. *Bioorg Med. Chem.* **2017**, *25*, 1286-1293.
Wagdy M. Eldehna, et al. *Eur J Med Chem.* **2017**, *27*, 521-530.
Gillian M. Fisher, et al. *Int J Parasitol Drugs Drug Resist.* **2017**, *7*, 61-70.
Menshawy A. Mohamed, et al. *Bioorg Med Chem.* **2017**, *25*, 2524-2529.
Yeganeh Entezari Heravi, et al. *Bioorg Med Chem.* **2017**, *25*, 2577-2582.
Murat Bozdag, et al. *J Enzyme Inhib Med Chem.* **2017**, *32*, 885-892.
Emanuela Berrino, et al. *Molecules.* **2017**, *22*(7).
Rajiv Kumar, et al. *J Enzyme Inhib Med Chem.* **2017**, *32*, 1187-1194.
Alessio Nocentini, et al. *ACS Med Chem Lett.* **2017**, *8*, 1314-1319.
Leonardo E. Riafrecha, et al. *Bioorg Chem.* **2018**, *76*, 61-66.
Aikaterini Peperidou, et al. *Molecules.* **2018**, *23*(1).
Suleyman Akocak, et al. *Bioorg Chem.* **2018**, *77*, 245-251.
Nabih Lolak, et al. *Bioorg Chem.* **2018**, *77*, 542-547.
Shams-ul Mahmood, et al. *Bioorg Chem.* **2018**, *77*, 381-386.
Fadi M. Awadallah, et al. *J Enzyme Inhib Med Chem.* **2018**, *33*, 629-638.
Chandra Bhushan Mishra, et al. *J Med Chem.* **2018**, *61*, 3151-3165.
Alessio Nocentini, et al. *ChemMedChem.* **2018**, *13*, 816-823.
Silvia Bua, et al. *J Enzyme Inhib Med Chem.* **2018**, *33*, 707-713.

Halise Inci Gul, et al. *Bioorg Chem.* **2018**, *78*, 290-297.
Niccolò Chiaramonte, et al. *Eur J Med Chem.* **2018**, *151*, 363-375.
Prashant Mujumdar, et al. *Bioorg Med Chem Lett.* **2018**, S0960-894, 30350-0.
Tanvi V. Wani, et al. *J Enzyme Inhib Med Chem.* **2018**, *33*, 962-971.
Alessio Nocentini, et al. *J Med Chem.* **2018,** *61*, 5380-5394.
Rajiv Kumar, et al. *Eur J Med Chem.* **2018**, *155*, 545-551.
Silvia Bua, et al. *J Enzyme Inhib Med Chem.* **2018**, *33*, 1125-1136.
Mehdi Bouchouit, et al. *J Enzyme Inhib Med Chem.* **2018**, *33*, 1150-1159.
Chandra Bhushan Mishra, et al. *Eur J Med Chem.* **2018**, *156*, 430-443.
Mahmoud F. Abo-Ashour, et al. *Eur J Med Chem.* **2018**, *157*, 28-36.
Peter Mikuš, et al. *Bioorg Chem.* **2018**, *81*, 241-252.
Nesrin Buğday, et al. *Bioorg Chem.* **2018**, *81*, 311-318.
Suleyman Akocak, et al. *J Enzyme Inhib Med Chem.* **2018**, *33*, 1575-1580.
Nabih Lolak, et al. *Bioorg Chem.* **2018**, *82*, 117-122.
Tanzeela Abdul Fattah, et al. *Bioorg Chem.* **2018**, *82*, 123-128.
Wagdy M. Eldehna, et al. *Eur J Med Chem.* **2019**, *162*, 147-160.
Vikas Sharma, et al. *Bioorg Chem.* **2019**, *85*, 198-208.
Suleyman Akocak, et al. *Bioorg Med Chem.* **2019**, *27*, 800-804.
Silvia Bua, et al. *Bioorg Chem.* **2019**, *86*, 39-43.
Silvia Bua, et al. *Bioorg Chem.* **2019**, *86*, 183-186.
Nabih Lolak, et al. *Bioorg Med Chem.* **2019**, *27*, 1588-1594.
Kerem Buran, et al. *Int J Mol Sci.* **2019**, *20*, pii: E1208.
Alaa A.-M.Abdel-Aziz, et al. *Bioorg Chem.* **2019**, *87*, 425-431.
Prashant Mujumdar, et al. *J Med Chem.* **2019,** *62*, 4174-4192.
Mahmoud F. Abo-Ashour, et al. *Bioorg Chem.* **2019**, *87*, 794-802.
Kübra Demir-Yazıcı, et al. *Int J Mol Sci.* **2019**, *20*, pii: E2354.
Mohamed A. Abdelrahman, et al. *Int J Mol Sci.* **2019**, *20*, pii: E2484.
Suleyman Akocak, et al. *J Enzyme Inhib Med Chem.* **2019**, *34*, 1193-1198.
Wagdy M. Eldehna, et al. *Bioorg Chem.* **2019**, *90*, 103102.
Niccolò Chiaramonte, et al. *Bioorg Chem.* **2019**, *91*, 103130.
Adel S. El-Azab, et al. *Eur J Med Chem.* **2019**, *181*, 111573.
Mohammad M. Al-Sanea, et al. *J Enzyme Inhib Med Chem.* **2019**, *34*, 1457-1464.
Murat Bozdag, et al. *Eur J Med Chem.* **2019**, *182*, 111600.
Adel S. El-Azab, et al. *Bioorg Chem.* **2019**, *92*, 103225.
Cem Yamali, et al. *Bioorg Chem.* **2019**, *92*, 103222.
Ciro Milite, et al. *J Enzyme Inhib Med Chem.* **2019**, *34*, 1697-1710.
Lalit Vats, et al. *Eur J Med Chem.* **2019**, *183*, 111698.
Victor Kartsev, et al. *Molecules.* **2019**, *24*, pii: E3580.
Mahmoud F.Abo-Ashour, et al. *Eur J Med Chem.* **2019**, *184*, 111768.
Vincenzo Alterio, et al. *J Mol Biol.* **2019**, *431*, 4910-4921.
Riham F. George, et al. *Bioorg Chem*. **2019**, *95*, 103514.
Mohamed A. Said, et al. *Eur J Med Chem*. **2020**, *185*, 111843.

Chapter 5. Experimental section

General Protocols

Chemistry

Anhydrous solvents and all reagents were purchased from Sigma-Aldrich, Alfa Aesar and TCI. All reactions involving air- or moisture-sensitive compounds were performed under a nitrogen atmosphere using dried glassware and syringes techniques to transfer solutions. Nuclear magnetic resonance (^{1}H-NMR, ^{13}C-NMR, ^{19}F-NMR) spectra were recorded using a Bruker Advance III 400 MHz spectrometer in DMSO-d_6 or $CDCl_3$. Chemical shifts are reported in parts per million (ppm) and the coupling constants (*J*) are expressed in Hertz (Hz). Splitting patterns are designated as follows: s, singlet; d, doublet; t, triplet; q, quadruplet; sept, septet; m, multiplet; bs, broad singlet; dd, double of doubles, appt, apparent triplet, appq, apparent quartet. The assignment of exchangeable protons (O*H* and N*H*) was confirmed by the addition of D_2O. Analytical thin-layer chromatography (TLC) was carried out on Merck silica gel F-254 plates. Flash chromatography purifications were performed on Merck Silica gel 60 (230-400 mesh ASTM) as the stationary phase and ethyl acetate/*n*-hexane or MeOH/DCM were used as eluents. Melting points (m.p.) were measured in open capillary tubes with a Gallenkamp MPD350.BM3.5 apparatus and are uncorrected. HPLC was performed by using a Waters 2690 separation module coupled with a photodiode array detector (PDA Waters 996) and as column, a Nova-Pak C18 4 μm 3.9 mm × 150 mm (Waters), silica-based reverse phase column. Sample was dissolved in acetonitrile 10%, and an injection volume of 45 μL was used. The mobile phase, at a flow rate of 1 mL/min, was a gradient of water + trifluoroacetic acid (TFA) 0.1% (A) and acetonitrile + TFA 0.1% (B), with steps as follows: (A% : B%), 0−10 min 90:10, 10−25 min gradient to 60:40, 26:28 min isocratic 20:80, 29−35 min isocratic 90:10. TFA 0.1% in water as well in acetonitrile was used as counterion. All compounds reported here were >96% HPLC pure. The solvents used in MS measures were acetone, acetonitrile (Chromasolv grade), purchased from Sigma-Aldrich (Milan - Italy), and mQ water 18 MΩ, obtained from Millipore's Simplicity system (Milan-Italy). The mass spectra were obtained using a Varian 1200L triple

quadrupole system (Palo Alto, CA, USA) equipped by Electrospray Source (ESI) operating in both positive and negative ions. Stock solutions of analytes were prepared in acetone at 1.0 mg mL^{-1} and stored at 4°C. Working solutions of each analyte were freshly prepared by diluting stock solutions in a mixture of mQ H_2O/ACN 1/1 (*v/v*) up to a concentration of 1.0 µg mL^{-1} The mass spectra of each analyte were acquired by introducing, via syringe pump at 10 µL min^{-1}, of the its working solution. Raw-data were collected and processed by Varian Workstation, version 6.8 software.

Carbonic Anhydrase Inhibition

α-CAs

An Applied Photophysics stopped-flow instrument has been used for assaying the CA catalysed CO_2 hydration activity.[169] Phenol red (at a concentration of 0.2 mM) has been used as a pH indicator, working at the absorbance maximum of 557 nm, with 20 mM Hepes (pH 7.5) as the buffer, and 20 mM Na_2SO_4 (for maintaining constant the ionic strength), following the initial rates of the CA-catalyzed CO_2 hydration reaction for a period of 10-100 s at 25°C.[169] The CO_2 concentrations ranged from 1.7 to 17 mM for the determination of the kinetic parameters and inhibition constants. For each inhibitor, at least six traces of the initial 5-10% of the reaction have been used for determining the initial velocity. The uncatalyzed rates were determined in the same manner and subtracted from the total observed rates. Stock solutions of inhibitor (0.1 mM) were prepared in distilled-deionized water and dilutions up to 0.01 nM were done thereafter with the assay buffer. Inhibitor and enzyme solutions were preincubated together for 15 min (sulfonamides) or 6h (coumarins) at room temperature prior to assay, in order to allow for the formation of the E-I complex. The inhibition constants were obtained by non-linear least-squares methods using PRISM 3 and the Cheng-Prusoff equation, as reported earlier,[169] and represent the mean from at least three different determinations. All hCA isofoms were recombinant ones obtained in-house as reported earlier,[1,2] while the α-CA SpiCA3, was obtained and purified by a diverse procedure as the one reported earlier in the thesis.

β-CAs

An Applied Photophysics stopped-flow instrument has been used for assaying the CA catalysed CO_2 hydration activity.[169] Bromothymol blue (at a concentration of 0.2 mM) has been used as a pH indicator, working at the absorbance maximum of 557 nm, with 10–20 mM TRIS (pH 8.3) as buffer, and 20 mM $NaBF_4$ for maintaining constant the ionic strength, following the initial rates of the CA catalysed CO_2 hydration reaction for a period of 10–100 s at 25°C. The CO_2 concentrations ranged from 1.7 to 17 mM for the

determination of the kinetic parameters and inhibition constants. For each inhibitor, at least six traces of the initial 5–10% of the reaction have been used for determining the initial velocity. The uncatalyzed rates were determined in the same manner and subtracted from the total observed rates. Stock solutions of inhibitor (10 mM) were prepared in distilled-deionized water and dilutions up to 0.01M were done thereafter with the assay buffer. Inhibitor and enzyme solutions were preincubated together for 15 min (sulfonamides) or 30 min (anions) at room temperature prior to assay, in order to allow for the formation of the E-I complex. The inhibition constants were obtained by non-linear least-squares methods using the Cheng-Prusoff equation whereas the kinetic parameters for the uninhibited enzymes from Lineweaver-Burk plots, as reported earlier,[169] and represent the mean from at least three different determinations. *Entamoeba histolytica* was a protein, obtained and purified by a diverse procedure as the one reported below in the thesis.

5.1 Design and Synthesis of Novel Nonsteroidal Anti-Inflammatory Drugs and Carbonic Anhydrase Inhibitor Hybrids for the Treatment of Rheumatoid Arthritis (Series A)

5.1.1 Chemistry

The general chemistry protocols are reported at the beginning of the experimental section.

*General procedure **1** for the synthesis of tert-butyl (2-((2-oxo-2H-chromen-6-yl)oxy)ethyl)carbamates **A19-26** and tert-butyl (2-((2-oxo-2H-chromen-7-yl)oxy)ethyl) carbamates **A27-34***

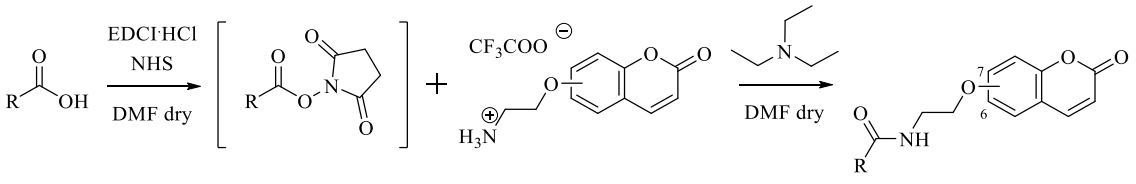

A1-8 **A9-16** **A17=6-*O*-alkyl** **A18=7-*O*-alkyl** **A19-26=6-*O*-alkyl** **A27-34=7-*O*-alkyl**

A1=Indometacin **A5**=Dichlofenac
A2=Sulindac **A6**=Flurbiprofen
A3=Ketoprofen **A7**=Naproxen
A4=Ibuprofen **A8**=Ketorolac

N-Hydroxysuccinimide (NHS) (1.5 eq.) and EDCI·HCl (1.5 eq.) were added to a solution of the appropriate carboxylic acid **A1-8** (0.5 g, 1.0 eq.) in dry DMF (3.0 mL) under a N_2 atmosphere. The reaction was stirred at r.t. until starting materials were consumed (TLC monitoring), followed by addition of 2-((2-oxo-2*H*-chromen-6-yl)oxy)ethan-1-ammoniun trifluoroacetate salt **A17** (1.0 eq.) or 2-((2-oxo-2*H*-chromen-7-yl)oxy)ethan-1-ammonium trifluoroacetate salt **A18** (1.0 eq.) and triethylamine (Et_3N) (1.0 eq.). The mixture was stirred at 60°C until starting materials were consumed (TLC monitoring), then quenched with H_2O (10 mL) to afford a precipitate which was collected by filtration or alternatively the reaction solution was extracted with EtOAc (3 x 10 mL). The combined organic layers were washed with H_2O (3 x 20 mL), dried over Na_2SO_4, filtered-off and concentrated under *vacuo* to give a solid that was purified by silica gel column

chromatography eluting with the appropriate mixture of EtOAc/*n*-hexane to afford the desired compounds **A19-34**.

*General procedure **2** for the synthesis of 2-((2-oxo-2H-chromen-6-yl)oxy)ethan-1-amonium trifluoroacetate salt **A17** and 2-((2-oxo-2H-chromen-7-yl)oxy)ethan-1-amonium trifluoroacetate salt **A18***

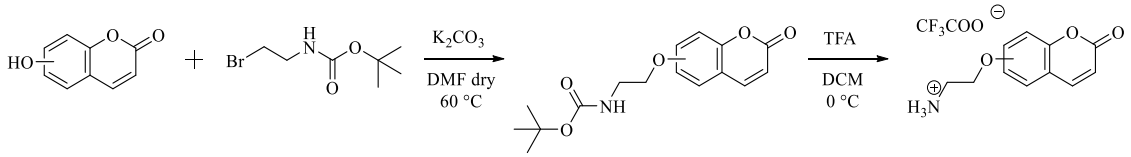

6-OH/7-OH Coumarin **A35** **A36,37** **A17,18**

Step 1: *tert*-Butyl (2-bromoethyl)carbamate **A35** (1.0 g, 1.0 eq.) was treated with 6-hydroxy-2*H*-chromen-2-one (**6-OH**) and K_2CO_3 (3.0 eq) in acetone or alternatively with 7-hydroxy-2*H*-chromen-2-one (**7-OH**) (1.0 eq.) was treated in the same conditions using dry *N*,*N*-dimethylformamide (5.0 mL) as solvent and under N_2 atmospheres. The reaction mixtures were stirred at 60 °C O.N. until consumption of starting materials (TLC monitoring), then cooled down to r.t. and treated respectively as follows.

i) The white precipitate was filtered-off and the obtained filtrate was concentrated under *vacuo* to afford the **A36** as an orange residue;

ii) The reaction was quenched with a 3.0 M aqueous hydrochloric acid solution to give a precipitate which was collected by filtration and triturated with diethyl ether to afford the **A37** as a white solid.

Step 2: *tert*-Butyl (2-((2-oxo-2*H*-chromen-6-yl)oxy)ethyl)carbamate **A36** (1.0 eq) and *tert*-butyl (2-((2-oxo-2*H*-chromen-7-yl)oxy)ethyl)carbamate **A37** (1.0 eq) were dissolved in DCM and TFA (6.0 eq) was added drop-wise to the suspension. The solution was stirred at 0°C and then at r.t. until starting materials were consumed (TLC monitoring). The solvent was evaporated and the obtained residue dried under *vacuo* to afford the titled compounds **A17** and **A18** as white solids.

2-((2-Oxo-2*H*-chromen-6-yl)oxy)ethan-1-aminium 2,2,2-trifluoroacetate A17: 20.0% yield; silica gel TLC R_f 0.55 (Ethyl acetate/*n*-hexane 50% *v/v*); δ_H (400 MHz, DMSO-d_6) 3.30 (2H, q, *J* 5.2, CH_2NH-), 4.25 (2H, t, *J* 5.0, CH_2O), 6.54 (1H, d, *J* 9.2, Ar-*H*), 7.29 (1H, d, *J* 3.2, Ar-*H*), 7.36 (1H, d, *J* 2.8, Ar-*H*), 7.41 (1H, d, *J* 8.8, Ar-*H*), 8.06 (1H, d, *J*

9.2, Ar-*H*); δ_C (100 MHz, DMSO-d_6) 39.3, 66.0, 112.7, 117.7, 118.5, 120.2, 121.0, 144.9, 149.2, 155.1, 161.1; δ_F (376 MHz, DMSO-d_6) -74.84.

2-((2-Oxo-2*H*-chromen-7-yl)oxy)ethan-1-aminium 2,2,2-trifluoroacetate A18: 61.3% yield; silica gel TLC R_f 0.50 (Ethyl acetate/*n*-hexane 50% *v/v*); δ_H (400 MHz, DMSO-d_6) 3.31 (2H, q, *J* 5.2, CH_2NH-), 4.31 (2H, t, *J* 5.16, CH_2O), 6.36 (1H, d, *J* 9.02, Ar-*H*), 7.03 (1H, dd, *J* 8.6, 2.5, Ar-*H*), 7.07 (1H, d, *J* 2.3, Ar-*H*), 7.70 (1H, d, *J* 8.66, Ar-*H*), 8.05 (1H, d, *J* 9.2, Ar-*H*); δ_C (100 MHz, DMSO-d_6) 38.2, 65.2, 101.5, 112.8, 112.9, 113.0, 129.7, 144.4, 115.3, 160.3, 160.9; δ_F (376 MHz, DMSO-d_6) -74.23.

*General procedure **3** for the synthesis of acids **A4**, **A5**, **A7** and **A8***

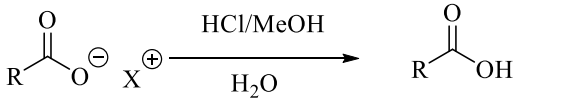

A4, A5, A7, A8

A4; R= Ibuprofene; X=Na
A5; R= Diclofenac; X= Na
A7; R= Naprossene; X= NaKetorolac; X= Trometamina
A8; R= Ketorolac; X= Trometamina

The appropriate carboxylic acid salt was treated with a 6.0 M or 12.0 M aqueous solution of hydrochloric acid. The reaction was vigorously stirred at 0°C, warmed up to r.t. until starting material was consumed (TLC monitoring). The obtained white precipitate was collected by filtration, dried under *vacuo* to afford the title compounds **A4, A5, A7** and **A8** as white solids.

Synthesis of (±)-2-(4-isobutylphenyl)propanoic acid ((±)-Ibuprofen) **(A4)**

(±)-Ibuprofen acid **A4** was obtained according to the general procedure **3** earlier reported using a 6.0 M aqueous solution of hydrochloric acid and (±)-Ibuprofen sodium salt (0.5 g, 1.0 eq).

(±)-Ibuprofen acid A4: 89.3% yield; silica gel TLC R_f 0.81 (Ethyl acetate/*n*-hexane 60% *v/v*); δ_H (400 MHz, DMSO-d_6) 0.89 (6H, d, *J* 6.8, 2 x CH_3), 1.37 (3H, d, *J* 6.8, CH_3), 1.83 (1H, m, CH_3C*H*), 3.36 (2H, s, CH_2), 3.65 (1H, m, $(CH_3)_2$C*H*), 7.13 (2H, d, *J* 8.0, Ar-*H*), 7.22 (2H, d, *J* 8.0, Ar-*H*), 12.29 (1H, m, exchange with D_2O, COO*H*).

Synthesis of 2-(2-((2,6-dichlorophenyl)amino)phenyl)acetic acid (Diclofenac) **(A5)**

Diclofenac acid **A5** was obtained according to the general procedure **3** earlier reported using a 12.0 M aqueous solution of hydrochloric acid and Diclofenac sodium salt (0.5 g, 1.0 eq).

Diclofenac acid A5: 70% yield; silica gel TLC R_f 0.45 (Ethyl acetate/*n*-hexane 30% *v/v*); δ_H (400 MHz, DMSO-d_6) 3.74 (2H, s, COCH_2), 6.32 (1H, d, *J* 7.2, Ar-*H*), 6.89 (1H, m, Ar-*H*), 7.10 (1H, m, Ar-*H*), 7.24 (3H, m, Ar-*H*), 7.57 (2H, d, *J* 8.0, Ar-*H* and N*H*), 12.70 (1H, m, exchange with D_2O, COO*H*).

Synthesis of (S)-2-(6-methoxynaphthalen-2-yl)propanoic acid ((S)-(+)-Naproxen) **(A7)**

Three tablets of Momendol® containing 0.220 g each of Naproxen sodium salt were crushed and the obtained powder was dissolved in EtOAc and treated with a 6.0 M aqueous solution of hydrochloric acid. The mixture was vigorously stirred at r.t. until consumption of starting materials (TLC monitoring). The mixture was filtered-off and the filtrate was extracted with EtOAc (3 x 10 mL). The combined organic layers were washed with H_2O (3 x 20 mL), dried over Na_2SO_4, filtered-off and concentrated under *vacuo* to give a pale-yellow oil that was purified by silica gel column chromatography eluting with EtOAc/*n*-hexane 30% *v/v* to afford the titled compound **A7** as a white solid.

(*S*)-(+)-Naproxen acid A7: 82.2% yield; silica gel TLC R_f 0.61 (Ethyl acetate/*n*-hexane 50% *v/v*); δ_H (400 MHz, DMSO-d_6) 1.48 (3H, d, *J* 7.6, CH_3), 3.83 (1H, q, *J* 7.2, CH_3C*H*), 3.90 (3H, s, OCH_3), 7.18 (1H, dd, *J* 8.8 3.8, Ar-*H*), 7.32 (1H, s, Ar-*H*), 7.44 (1H, d, *J* 7.2, Ar-*H*), 7.74 (1H, s, Ar-*H*), 7.82 (2H, t, *J* 9.6, Ar-H), 12.34 (1H, m, exchange with D_2O, COO*H*).

Synthesis of (±)-5-benzoyl-2,3-dihydro-1H-pyrrolizine-1-carboxylic acid ((±)-Ketorolac) **(A8)**

(±)-Ketorolac acid **A8** was obtained according to the general **3** procedure earlier reported using a 12.0 M aqueous solution of hydrochloric acid and (±)-Ketorolac tris salt (0.3 g, 1.0 eq.).

(±)-Ketorolac acid A8: 83.6% yield; silica gel TLC R_f 0.31 (Ethyl acetate/*n*-hexane 50% *v/v*); δ_H (400 MHz, DMSO-d_6) 2.78 (2H, q, *J* 7.2, 2 x CH_{ax}), 4.12 (1H, t, *J* 7.4, COC*H*), 4.33 (1H, m, CH_{eq}), 4.44 (1H, m, CH_{eq}), 6.12 (1H, d, *J* 3.8, pyrrole-*H*), 6.81 (1H, d, *J*

3.8, pyrrole-*H*), 7.55 (2H, t, *J* 7.6, Ar-*H*), 7.64 (1H, t, *J* 7.2, Ar-*H*), 7.79 (2H, d, *J* 7.6, Ar-*H*), 12.65 (1H, m, exchange with D_2O, COO*H*).

Synthesis of tert-butyl (2-bromoethyl)carbamate **(A35)**

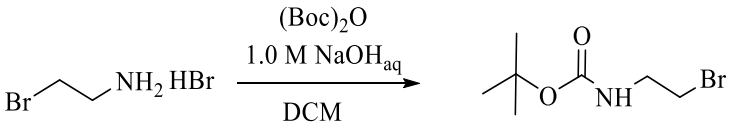

A35

2-Bromoethan-1-amine hydrobromide salt (1.0 g, 1.0 eq.) was dissolved in dichloromethane (DCM) (5.0 ml) and treated with a 1.0 M NaOH aqueous solution and di-*tert*-butyl dicarbonate $(Boc)_2O$ (1.0 eq.). The mixture was vigorously stirred at r.t. until consumption of starting materials (TLC monitoring). The reaction was quenched with a 1.0 M hydrochloric acid aqueous solution and extracted with EtOAc (3 x 15 mL). The combined organic layers were washed with H_2O (3 x 20 mL), dried over Na_2SO_4, filtered-off, and concentrated under *vacuo* to give the titled product **A35** as a colourless oil.

***tert*-Butyl (2-bromoethyl)carbamate A35:** 91% yield; silica gel TLC R_f 0.78 (Ethyl acetate/*n*-hexane 50% *v/v*); δ_H (400 MHz, DMSO-d_6) 1.42 (9H, s, 3 x CH_3), 3.32 (2H, q, *J* 6.2, NHCH_2), 3.46 (2H, t, *J* 6.4, BrCH_2), 7.13 (1H, t, *J* 5.2,exchange with D_2O, CON*H*).

Synthesis of 2-(1-(4-chlorobenzoyl)-5-methoxy-2-methyl-1H-indol-3-yl)-N-(2-((2-oxo-2H-chromen-6-yl)oxy)ethyl)acetamide **(A19)**

2-(1-(4-Chlorobenzoyl)-5-methoxy-2-methyl-1*H*-indol-3-yl)-*N*-(2-((2-oxo-2*H*-chromen-6-yl)oxy)ethyl)acetamide **A19** was obtained according to the general procedure **1** earlier reported using NHS (1.5 eq) and EDCI·HCl (1.5 eq.) in a solution of Indometacin **A1** (0.3 g, 1.0 eq.) in dry DMF (3.0 mL) under a N_2 atmosphere. The reaction mixture was stirred at r.t. until the formation of the activated ester intermediate **A** (TLC monitoring, not isolated). Then 2-((2-oxo-2*H*-chromen-6-yl)oxy)ethan-1-amonium trifluoroacetate salt **A17** and triethylamine (Et_3N) were added to the mixture, which was stirred at 60 °C until starting materials were consumed (TLC monitoring), followed by quenching with H_2O (10 mL). The formed brown precipitate was filtered-off, dried under *vacuo* to give a

residue that was purified by silica gel column chromatography eluting with EtOAc/*n*-hexane 50% *v/v* to afford the titled compound **A19** as a white solid.

2-(1-(4-Chlorobenzoyl)-5-methoxy-2-methyl-1H-indol-3-yl)-*N*-(2-((2-oxo-2H-chromen-6-yl)oxy)ethyl)acetamide A19: 65.8% yield; m.p.181-183°C; silica gel TLC R_f 0.35 (Ethyl acetate/*n*-hexane 90% *v/v*); δ_H (400 MHz, DMSO-d_6) 2.24 (3H, s, CH_3), 3.51 (2H, q, *J* 6.3, CH_2NH-), 3.58 (2H, s, CH_2CO), 3.78 (3H, s, OCH_3), 4.09 (2H, t, *J* 5.2, OCH_2), 6.53 (1H, d, *J* 9.4, Ar-*H*), 6.73 (1H, dd, *J* 8.0 2.4, Ar-*H*), 6.98 (1H, d, *J* 8.8, Ar-*H*), 7.15 (1H, d, *J* 2.0, Ar-*H*), 7.19 (1H, dd, *J* 8.0 2.4, Ar-*H*), 7.29 (1H, d, *J* 2.8, Ar-*H*), 7.36 (1H, d, *J* 8.8, Ar-*H*), 7.65 (2H, d, *J* 8.4, Ar-*H*), 7.71 (2H, d, *J* 8.4, Ar-*H*), 8.01 (1H, d, *J* 9.4, Ar-*H*), 8.34 (1H, t, *J* 6.3, exchange with D_2O, CON*H*); δ_C (100 MHz, DMSO-d_6) 13.5, 31.2, 38.5, 55.5, 67.1, 102.0, 111.3, 111.6, 114.3, 114.6, 116.7, 117.4, 119.3, 119.9, 129.1, 130.4, 130.9, 131.2, 134.3, 135.3, 137.6, 144.1, 148.0, 154.8, 155.7, 160.2, 167.9, 169.9; *m/z* (ESI positive) 545.1 $[M+H]^+$.

Synthesis of (Z)-2-(5-fluoro-2-methyl-1-(3-(methylsulfinyl)benzylidene)-1H-inden-3-yl)-N-(2-((2-oxo-2H-chromen-6-yl)oxy)ethyl)acetamide **(A20)**

(*Z*)-2-(5-Fluoro-2-methyl-1-(3-(methylsulfinyl)benzylidene)-1*H*-inden-3-yl)-*N*-(2-((2-oxo-2*H*-chromen-6-yl)oxy)ethyl)acetamide **A20** was obtained according **1** to the general procedure earlier reported using NHS (1.5 eq.) and EDCI·HCl (1.5 eq.) in a solution of Sulindac **A2** (0.3 g, 1.0 eq.) in dry DMF (3.0 mL) under a N_2 atmosphere. The reaction mixture was stirred at r.t. until the formation of the activated ester intermediate **B** (TLC monitoring, not isolated). 2-((2-oxo-2*H*-chromen-6-yl)oxy)ethan-1-amonium trifluoroacetate salt **A17** and triethylamine (Et_3N) were added to the mixture, which was stirred at 60 °C O.N. followed by 80 °C for 3hrs. Then the reaction mixture was quenched with H_2O (10 mL) and the formed precipitate was filtered-off and concentrated under *vacuo* to give a yellow precipitate that was triturated with acetone to afford the titled compound **A20** as a yellow solid.

(Z)-2-(5-Fluoro-2-methyl-1-(3-(methylsulfinyl)benzylidene)-1*H*-inden-3-yl)-*N*-(2-((2-oxo-2*H*-chromen-6-yl)oxy)ethyl)acetamide A20: 54.7% yield; m.p. 152-153°C; silica gel TLC R_f 0.19 (Ethyl acetate 100%); δ_H (400 MHz, DMSO-d_6) 2.21 (3H, s, CH_3), 2.85 (3H, s, SOCH_3), 3.51 (4H, m, CH_2CO and NHCH_2), 4.09 (2H, t, *J* 5.4, OCH_2), 6.53 (1H, d, *J* 9.6, Ar-*H*), 6.71 (1H, dt, *J* 8.2 8.0, Ar-*H*), 7.18 (3H, m, Ar-*H*), 7.31 (1H, s, Ar- *H*),

7.36 (2H, s, Ar-*H*), 7.75 (2H, d, *J* 8.1, Ar-*H*), 7.82 (2H, d, *J* 8.1, Ar-*H*), 8.02 (1H, d, *J* 9.6, Ar-*H*), 8.46 (1H, t, *J* 5.0, exchange with D_2O, CON*H*); δ_C (100 MHz, DMSO-d_6) 10.5, 32.8, 38.6, 43.2, 67.1, 106.2, 110.4 ($J^2_{C\text{-}F}$ 23), 111.6, 116.7, 117.4, 119.3, 119.9, 123.1 ($J^2_{C\text{-}F}$9), 124.0, 129.3, 129.5 ($J^3_{C\text{-}F}$ 3), 130.0, 133.7, 137.9, 138.7, 140.6, 144.1, 146.3, 147.3 ($J^2_{C\text{-}F}$ 9), 148.0, 154.9, 160.2, 162.6 ($J^1_{C\text{-}F}$ 243), 169.3; δ_F (376 MHz, DMSO-d_6) -113.49 (1F, s); *m/z* (ESI positive) 544.1 $[M+H]^+$.

Synthesis of (±)-2-(3-benzoylphenyl)-N-(2-((2-oxo-2H-chromen-6-yl)oxy)ethyl)propanamide **(A21)**

(±)-2-(3-Benzoylphenyl)-*N*-(2-((2-oxo-2*H*-chromen-6-yl)oxy)ethyl)propanamide **A21** was obtained according to the general procedure **1** earlier reported using NHS (1.5 eq.) and EDCI·HCl (1.5 eq.) in a solution of (±)-Ketoprofen **A3** (0.3 g, 1.0 eq.) in dry DMF (3.0 mL) under a N_2 atmosphere. The reaction mixture was stirred at r.t. until the formation of the activated ester intermediate **C** (TLC monitoring, not isolated). 2-((2-Oxo-2*H*-chromen-6-yl)oxy)ethan-1-amonium trifluoroacetate salt **A17** and triethylamine (Et_3N) were added to the mixture and that was stirred at 60 °C until starting materials were consumed (TLC monitoring), followed by quenching with H_2O (10 mL) and the mixture was extracted with EtOAc (3 x 10 mL). The combined organic layers were washed with H_2O (3 x 20 mL), dried over Na_2SO_4, filtered-off and concentrated under *vacuo* to give a yellow bright semisolid that was purified by silica gel column chromatography eluting with an increasing amount of EtOAc/*n*-hexane from 50% to 70% *v/v* to afford the titled compound **A21** as a white solid.

(±)-2-(3-Benzoylphenyl)-*N*-(2-((2-oxo-2H-chromen-6-yl)oxy)ethyl)propanamide A21: 38.4% yield; m.p. 101-103°C; silica gel TLC R_f 0.23 (Ethyl acetate/*n*-hexane 90% *v/v*); δ_H (400 MHz, DMSO-d_6) 1.39 (3H, d, *J* 6.8 CH_3), 3.46 (2H, q, *J* 5.6, CH_2NH), 3.79 (1H, q, *J* 6.8), 4.04 (2H, t, *J* 5.6, OCH_2), 6.51 (1H, d, *J* 9.6, Ar-*H*), 7.15 (1H, dd, *J* 9.2 3.2, Ar-*H*), 7.27 (1H, d, *J* 2.8 Ar-*H*), 7.32 (1H, d, *J* 9.2, Ar-*H*), 7.51 (1H, t , *J* 7.6, Ar-*H*), 7.56 (1H, s, Ar-*H*), 7.59 (2H, dd, *J* 8.0 3.0, Ar-*H*), 7.67 (1H, t, *J* 6.8, Ar-*H*), 7.70 (1H, s, Ar-*H*), 7.71 (3H, d, *J* 1.2 Ar-*H*), 7.99 (1H, d, *J* 9.6, Ar-*H*), 8.38 (1H, t, *J* 5.4 exchange with D_2O, CON*H*). δ_C (100 MHz, DMSO-d_6) 18.6, 38.4, 44.8, 67.1, 111.7, 116.7, 117.4, 119.3, 119.9, 128.2, 128.5, 128.60, 128.63, 129.7, 131.7, 132.8, 136.9, 137.1, 142.8, 144.1, 147.9, 154.8, 160.2, 173.4, 195.8; *m/z* (ESI positive) 442.1 $[M+H]^+$.

Synthesis of (±)-2-(4-isobutylphenyl)-N-(2-((2-oxo-2H-chromen-6-yl)oxy)ethyl)propanamide **(A22)**

(±)-2-(4-Isobutylphenyl)-*N*-(2-((2-oxo-2*H*-chromen-6-yl)oxy)ethyl)propanamide **A22** was obtained according to the general procedure **1** earlier reported using NHS (1.5 eq.) and EDCI·HCl (1.5 eq.) in a solution of (±)-Ibuprofen **A4** (0.58 g, 1.0 eq.) in dry DMF (3.0 mL) under a N_2 atmosphere. The reaction mixture was stirred at r.t. until the formation of the activated ester intermediate **D** (TLC monitoring, not isolated). 2-((2-Oxo-2*H*-chromen-6-yl)oxy)ethan-1-amonium trifluoroacetate salt **A17** and triethylamine (Et_3N) were added to the mixture which was stirred at 60°C until starting materials were consumed (TLC monitoring), followed by quenching with H_2O (10 mL), extracted with EtOAc (3 x 10 mL) and the combined organic layers were washed with H_2O (3 x 20 mL), dried over Na_2SO_4, filtered-off and concentrated under *vacuo* to give a white semisolid that was purified by silica gel column chromatography eluting with EtOAc/*n*-hexane 50% *v/v* to afford the titled compound **A22** as a white solid.

(±)-2-(4-Isobutylphenyl)-*N*-(2-((2-oxo-2H-chromen-6-yl)oxy)ethyl)propanamide

A22: 25.3% yield; m.p. 99-101°C; silica gel TLC R_f 0.24 (Ethyl acetate/*n*-hexane 50% *v/v*); δ_H (400 MHz, DMSO-d_6) 0.85 (6H, d, *J* 6.8, 2 x CH_3), 1.33 (3H, d, *J* 7.2, CH_3), 1.78 (1H, sept, CH(CH_3)$_2$), 2.40 (2H, d, *J* 7.2, CH_2), 3.46 (2H, q, *J* 5.6, NHCH_2), 3.62 (1H, q, *J* 7.0, CHCH_3), 4.04 (2H, t, *J* 5.6, OCH_2), 6.52 (1H, d, *J* 9.6, Ar-*H*), 7.05 (2H, d, *J* 8.0, Ar-*H*), 7.16 (1H, dd, *J* 8.8 3.0, Ar-*H*), 7.23 (2H, d, *J* 8.0, Ar-*H*), 7.29 (1H, d, *J* 2.8, Ar-*H*), 7.35 (1H, d, *J* 8.8, Ar- *H*), 8.02 (1H, d, *J* 9.6, Ar-*H*), 8.25 (1H, t, *J* 5.6 exchange with D_2O, CON*H*); δ_C (100 MHz, DMSO-d_6) 18.6, 22.1, 22.2, 29.7, 38.4, 44.3, 44.7, 67.1, 111.6, 116.6, 117.4, 119.3, 119.9, 127.0, 128.8, 139.2, 139.5, 144.1, 147.9, 154.8, 160.2, 173.9; *m/z* (ESI positive) 394.2 $[M+H]^+$.

Synthesis of 2-(2-((2,6-dichlorophenyl)amino)phenyl)-N-(2-((2-oxo-2H-chromen-6-yl)oxy)ethyl)acetamide **(A23)**

2-(2-((2,6-Dichlorophenyl)amino)phenyl)-*N*-(2-((2-oxo-2*H*-chromen-6-yl)oxy)ethyl)acetamide **A23** was obtained according to the general procedure **1** earlier reported using NHS (1.5 eq.) and EDCI·HCl (1.5 eq.) in a solution of Diclofenac **A5** (0.3 g, 1.0 eq.) in dry DMF (3.0 mL) under a N_2 atmosphere. The reaction mixture was stirred

at r.t. until the formation of the activated ester intermediate **E** (TLC monitoring, not isolated). 2-((2-Oxo-2*H*-chromen-6-yl)oxy)ethan-1-amonium trifluoroacetate salt **A17** and triethylamine (Et_3N) were added to the mixture which was stirred at 60°C until starting materials were consumed (TLC monitoring), followed by quenching with H_2O (10 mL). The formed precipitate was filtered-off and dried under *vacuo* to give a white residue which was triturated with acetone to afford the title compound **A23** as a white solid.

2-(2-((2,6-Dichlorophenyl)amino)phenyl)-*N*-(2-((2-oxo-2H-chromen-6-yl)oxy)ethyl)acetamide A23: 34.8 % yield; m.p. 176-178 °C; silica gel TLC R_f 0.33 (Ethyl acetate/*n*-hexane 50% *v/v*); δ_H (400 MHz, DMSO-d_6) 3.52 (2H, q, *J* 4.8, NHCH_2), 3.65 (2H, s, CH_2), 4.11 (2H, t, *J* 5.0, OCH_2), 6.32 (1H. d, *J* 8.0, Ar-*H*), 6.53 (1H, d, *J* 9.6, Ar-*H*), 6.87 (1H, appt, *J* 7.4, Ar-*H*), 7.07 (1H, appt, *J* 8.2, Ar-*H*), 7.20 (3H, m, Ar-*H*), 7.35 (2H, m, Ar-*H*), 7.52 (2H, d, *J* 8.0, Ar-*H*), 8.02 (1H, d, *J* 9.6, Ar-*H*), 8.34 (1H, s, exchange with D_2O, N*H*), 8.71 (1H, t, *J* 4.8, exchange with D_2O, CON*H*); δ_C (100 MHz, DMSO-d_6) 39.5, 40.4, 67.9, 112.6, 116.9, 117.6, 118.3, 120.2, 120.9, 121.6, 126.0, 126.3, 128.2, 130.1, 130.4, 131.4, 138.1, 143.9, 144.9, 148.9, 155.7, 161.1, 172.9; *m/z* (ESI positive) 483.0 $[M+H]^+$.

Synthesis of (±)-2-(2-fluoro-[1,1'-biphenyl]-4-yl)-N-(2-((2-oxo-2H-chromen-6-yl)oxy)ethyl)propanamide **(A24)**

(±)-2-(2-Fluoro-[1,1'-biphenyl]-4-yl)-*N*-(2-((2-oxo-2*H*-chromen-6-yl)oxy)ethyl)propanamide **A24** was obtained according to the general procedure **1** earlier reported using NHS (1.5 eq.) and EDCI·HCl (1.5 eq.) in a solution of (±)-Flurbiprofen **A6** (0.2 g, 1.0 eq.) in dry DMF (3.0 mL) under a N_2 atmosphere. The reaction mixture was stirred at r.t. until the formation of the activated ester intermediate **F** (TLC monitoring, not isolated). 2-((2-Oxo-2*H*-chromen-6-yl)oxy)ethan-1-amonium trifluoroacetate salt **A17** and triethylamine (Et_3N) were added to the mixture which was stirred at r.t. until starting materials were consumed (TLC monitoring), followed by quenching with H_2O (10 mL) and the mixture was extracted with EtOAc (3 x 10 mL). The combined organic layers were washed with H_2O (3 x 20 mL), dried over Na_2SO_4, filtered-off and concentrated under *vacuo* to give an orange oil that was purified by silica gel column

chromatography eluting with EtOAc/*n*-hexane 60% *v/v* to afford the titled compounds **A24** as a white solid.

(±)-2-(2-Fluoro-[1,1'-biphenyl]-4-yl)-*N*-(2-((2-oxo-2H-chromen-6-yl)oxy)ethyl)propanamide A24: 61.4% yield; m.p. 130-131 °C; silica gel TLC R_f 0.25 (Ethyl acetate/*n*-hexane 50% *v/v*); δ_H (400 MHz, DMSO-d_6) 1.39 (3H, d, *J* 6.8, CH_3), 3.46 (2H, q, *J* 5.4, NHCH_2), 3.75 (1H, q, *J* 7.1, C*H*CH$_3$), 4.06 (2H, t, *J* 5.4, OCH_2), 6.51 (1H, d, *J* 9.6, Ar-*H*), 7.20 (2H, dd, *J* 8.8 4.0, Ar-*H*), 7.28 (2H, m, Ar-*H*), 7.35 (1H, d, *J* 8.8, Ar-*H*), 7.41 (2H, d, *J* 6.4, Ar-*H*), 7.44 (1H, d, *J* 4.0, Ar-*H*), 7.47 (2H, d, *J* 4.0, Ar-*H*), 7.51 (1H, t, *J* 7.6, Ar-*H*), 8.01 (1H, d, *J* 9.6, Ar-*H*), 8.36 (1H, t, *J* 5.4, exchange with D_2O, CON*H*); δ_C (100 MHz, DMSO-d_6) 19.3, 39.3, 45.4, 67.9, 112.5, 115.7 ($J^2_{C\text{-}F}$ 23), 117.5, 118.3, 120.2, 120.8, 124.7 ($J^5_{C\text{-}F}$ 3), 127.2 ($J^5_{C\text{-}F}$ 3), 128.7, 129.5, 129.6 ($J^5_{C\text{-}F}$ 3), 131.4, 135.9, 145.0, 145.1 ($J^4_{C\text{-}F}$ 8), 148.9, 155.7, 159.0 ($J^1_{C\text{-}F}$ 245), 161.1, 174.1; δ_F (376 MHz, DMSO-d_6) -118.75 (1F, s); *m/z* (ESI positive) 432.0 $[M+H]^+$.

Synthesis of (S)-(+)-2-(6-methoxynaphthalen-2-yl)-N-(2-((2-oxo-2H-chromen-6-yl)oxy)ethyl)propanamide **(A25)**

(*S*)-(+)-2-(6-Methoxynaphthalen-2-yl)-*N*-(2-((2-oxo-2*H*-chromen-6-yl)oxy)ethyl)propanamide **A25** was obtained according to the general procedure **1** earlier reported using NHS (1.5 eq.) and EDCI·HCl (1.5 eq.) in a solution of (*S*)-(+)-Naproxen free acid **A7** (0.23 g, 1.0 eq.) in dry DMF (3.0 mL) under a N_2 atmosphere. The reaction mixture was stirred at r.t. until the formation of the activated ester intermediate **H** (TLC monitoring, not isolated). 2-((2-Oxo-2*H*-chromen-6-yl)oxy)ethan-1-amonium trifluoroacetate salt **A17** and triethylamine (Et_3N) were added to the mixture which was stirred at 60°C until starting materials were consumed (TLC monitoring), followed by quenching with H_2O (10 mL) and extracted with EtOAc (3 x 10 mL). The combined organic layers were washed with H_2O (3 x 20 mL), dried over Na_2SO_4, filtered-off and dried under *vacuo* to give an oil which was triturated with diethyl ether. The residue obtained was purified by silica gel column chromatography eluting with EtOAc/*n*-hexane 60% *v/v* to afford the titled compound **A25** as a white solid.

(S)-(+)-2-(6-Methoxynaphthalen-2-yl)-*N*-(2-((2-oxo-2H-chromen-6-yl)oxy)ethyl)propanamide A25: 43.2% yield; m.p. 126-128 °C; silica gel TLC R_f 0.22 (Ethyl acetate/*n*-hexane 60% *v/v*); δ_H (400 MHz, DMSO-d_6) 1.43 (3H, d, *J* 6.8, CH_3),

3.72 (2H, q, *J* 5.3, NHC*H*$_2$), 3.80 (1H, q, *J* 6.9, C*H*), 3.88 (3H, s, OC*H*$_3$), 4.04 (2H, t, *J* 5.6, OC*H*$_2$), 6.51 (1H, d, *J* 9.6, Ar-*H*), 7.15 (2H, m, Ar-*H*), 7.28 (3H, m), 7.46 (2H, d, *J* 8.8, Ar-*H*), 7.74 (2H, m, Ar-*H*), 7.97 (1H, d, *J* 9.6, Ar-*H*), 8.31 (1H, t, *J* 5.3, exchange with D_2O, CON*H*); δ_C (100 MHz, DMSO-d_6) 18.6, 38.4, 45.0, 55.2, 67.1, 105.7, 111.7, 116.6, 117.4, 118.6, 119.2, 119.9, 125.3, 126.5, 126.7, 128.4, 129.1, 133.2, 137.4, 144.1, 147.9, 154.8, 157.1, 160.2, 173.9; *m/z* (ESI positive) 418.1 $[M+H]^+$.

Synthesis of (±)-5-benzoyl-N-(2-((2-oxo-2H-chromen-6-yl)oxy)ethyl)-2,3-dihydro-1H-pyrrolizine-1-carboxamide **(A26)**

(±)-5-Benzoyl-*N*-(2-((2-oxo-2*H*-chromen-6-yl)oxy)ethyl)-2,3-dihydro-1*H*-pyrrolizine-1-carboxamide **A26** was obtained according to the general procedure **1** earlier reported using NHS (1.5 eq.) and EDCI HCl (1.5 eq.) in a solution of (±)-Ketorolac **A8** (0.17 g, 1.0 eq.) in dry DMF (3.0 mL) under a N_2 atmosphere. The reaction mixture was stirred at r.t. until the formation of the activated ester intermediate **G** (TLC monitoring, not isolated). 2-((2-Oxo-2*H*-chromen-6-yl)oxy)ethan-1-amonium trifluoroacetate salt **3a** and triethylamine (Et_3N) were added to the mixture which was stirred at 60°C until starting materials were consumed (TLC monitoring), followed by quenching with H_2O (10 mL), extracted with EtOAc (3 x 10 mL) and the combined organic layers were washed with H_2O (3 x 20 mL), dried over Na_2SO_4, filtered-off and concentrated under *vacuo* to give a brown residue that was purified by silica gel column chromatography eluting with EtOAc/*n*-hexane 80% *v/v* to afford the titled compound **A26** as a white solid.

(±)-5-Benzoyl-*N*-(2-((2-oxo-2H-chromen-6-yl)oxy)ethyl)-2,3-dihydro-1H-pyrrolizine-1-carboxamide A26: 33.9% yield; m.p. 198-199 °C; silica gel TLC R_f 0.25 (Ethyl acetate/*n*-hexane 80% *v/v*); δ_H (400 MHz, DMSO-d_6) 2.75 (2H, m, 2 x CHH_{ax}), 3.54 (2H, q, *J* 4.9, NHC*H*$_2$), 4.03 (1H, dd, *J* 8.8 4.8, C*H*), 4.11 (2H, t, *J* 5.6, OC*H*$_2$), 4.39 (2H, m, 2 x CHH_{eq}), 6.02 (1H, dd, *J* 4.0, pyrrole-*H*), 6.53 (1H, d, *J* 9.2, Ar-*H*), 6.75 (1H, d, *J* 4.0, pyrrole-*H*), 7.26 (2H, dd, *J* 9.0 4.0, Ar-*H*), 7.35 (1H, d, *J* 3.2, Ar-*H*), 7.40 (1H, d, *J* 8.8, Ar-*H*), 7.54 (2H, m), 7.62 (1H, m), 7.76 (1H, d, *J* 8.0, Ar-*H*), 8.05 (1H, d, *J* 9.6, Ar-*H*), 8.58 (1H, t, *J* 6.0, exchange with D_2O, CON*H*); δ_C (100 MHz, DMSO-d_6) 38.6, 42.8, 47.9, 67.0, 102.4, 111.7, 116.7, 117.5, 119.31, 119.33, 120.0, 124.5, 126.1, 128.4, 128.5, 131.5, 139.0, 144.1, 145.5, 148.0, 154.9, 160.2, 170.8, 183.5; *m/z* (ESI positive) 443.1 $[M+H]^+$.

Synthesis of 2-(1-(4-chlorobenzoyl)-5-methoxy-2-methyl-1H-indol-3-yl)-N-(2-((2-oxo-2H-chromen-7-yl)oxy)ethyl)acetamide **(A27)**

2-(1-(4-Chlorobenzoyl)-5-methoxy-2-methyl-1*H*-indol-3-yl)-*N*-(2-((2-oxo-2*H*-chromen-7-yl)oxy)ethyl)acetamide **A27** was obtained according to the general procedure **1** earlier reported using NHS (1.5 eq.) and EDCI·HCl (1.5 eq.) in a solution of Indometacin **A1** (0.5 g, 1.0 eq.) in dry DMF (3.0 mL) under a N_2 atmosphere. The reaction mixture was stirred at r.t. until the formation of the activated ester intermediate **A** (TLC monitoring, not isolated).2-((2-Oxo-2*H*-chromen-7-yl)oxy)ethan-1-amonium trifluoroacetate salt **A18** and triethylamine (Et_3N) were added to the mixture, which was stirred at 60°C until starting materials were consumed (TLC monitoring), followed by quenching with H_2O (10 mL) and the formed precipitate was filtered-off, dried under *vacuo* to afford the titled compound **A27** as a yellow solid.

2-(1-(4-Chlorobenzoyl)-5-methoxy-2-methyl-1H-indol-3-yl)-*N*-(2-((2-oxo-2H-chromen-7-yl)oxy)ethyl)acetamide A27: 79.2% yield; m.p. 157-158 °C; silica gel TLC R_f 0.26 (Ethyl acetate/*n*-hexane 70% *v/v*); δ_H (400 MHz, DMSO-d_6) 2.24 (3H, s, CH_3), 3.50 (2H, q, *J* 5.4, NHCH_2), 3.57 (2H, s, COCH_2), 3.74 (3H, s, OCH_3), 4.15 (2H, t, *J* 5.0, OCH_2), 6.33 (1H, d, *J* 9.6, Ar-*H*), 6.73 (1H, dd, *J* 9.0 3.87, Ar-*H*), 6.93 (1H, dd, *J* 8.8 3.73, Ar-*H*), 6.99 (2H, m, Ar-*H*), 7.14 (1H, d, *J* 2.4, Ar-*H*), 7.64 (1H, d, *J* 7.2, Ar-*H*), 7.65 (2H, d, *J* 8.72, Ar-*H*), 7.71 (2H, d, *J* 8.6, Ar-*H*), 8.02 (1H, d, *J* 9.6, Ar-*H*), 8.32 (1H, t, *J* 5.8, exchange with D_2O CON*H);* δ_c (100 MHz, DMSO-d_6) 13.5, 31.2, 38.3, 55.5, 67.1, 101.3, 102.0, 111.2, 112.5, 112.6, 112.7, 114.3, 114.6, 129.1, 129.6, 130.4, 131.0, 131.2, 134.3, 135.3, 137.6, 144.4, 155.4, 155.6, 160.4, 161.7, 168.0, 170.0; *m/z* (ESI positive) 545.0 $[M+H]^+$.

Synthesis of (Z)-2-(5-fluoro-2-methyl-1-(3-(methylsulfinyl)benzylidene)-1H-inden-3-yl)-N-(2-((2-oxo-2H-chromen-7-yl)oxy)ethyl)acetamide **(A28)**

(*Z*)-2-(5-Fluoro-2-methyl-1-(3-(methylsulfinyl)benzylidene)-1*H*-inden-3-yl)-*N*-(2-((2-oxo-2*H*-chromen-7-yl)oxy)ethyl)acetamide **A28** was obtained according to the general procedure **1** earlier reported using NHS (1.5 eq.) and EDCI·HCl (1.5 eq.) in a solution of Sulindac **A2** (0.5 g, 1.0 eq.) in dry DMF (3.0 mL) under a N_2 atmosphere. The reaction mixture was stirred at r.t. until the formation of the activated ester intermediate **B** (TLC

monitoring, not isolated). 2-((2-Oxo-2*H*-chromen-7-yl)oxy)ethan-1-amonium trifluoroacetate salt **A18** and triethylamine (Et_3N) were added to the mixture which was stirred at 60°C until starting materials were consumed (TLC monitoring), followed by quenching with H_2O (10 mL) and the formed precipitate was filtered-off, dried under *vacuo* to give a residue was purified by silica gel column chromatography eluting with EtOAc/*n*-hexane 80% *v/v* to afford the titled compound **A28** as a yellow solid.

(Z)-2-(5-Fluoro-2-methyl-1-(3-(methylsulfinyl)benzylidene)-1H-inden-3-yl)-*N*-(2-((2-oxo-2H-chromen-7-yl)oxy)ethyl)acetamide A28: 51.4% yield; m.p. 152-153 °C; silica gel TLC R_f 0.15 (Ethyl acetate/*n*-hexane 80% *v/v*); δ_H (400 MHz, DMSO-d_6) 2.21 (3H, s, C*H3*), 2.86 (3H, s, SOCH_3), 3.52 (4H, m, CH_2CO and NHCH_2), 4.17 (2H, t, *J* 5.2, OCH_2), 6.33 (1H, d, *J* 9.6, Ar-*H*), 6.71 (1H, dt, *J* 9.1 9.0, Ar-*H*), 6.97 (1H, dd, *J* 8.8 3.7, Ar-*H*), 7.01 (1H, d, *J* 2.4, Ar-*H*), 7.13 (1H, dd, *J* 9.30 3.9, Ar-*H*), 7.19 (1H, q, *J* 4.4, Ar-*H*), 7.38 (1H, s, Ar-*H*), 7.66 (1H, d, *J* 8.8, Ar-*H*), 7.75 (2H, d, *J* 8.2, Ar-*H*), 7.82 (2H, d, *J* 8.2, Ar-*H*), 8.03 (1H, d, *J* 9.6, Ar-*H*) 8.44 (1H, t, *J* 5.2, exchange with D_2O, CON*H*); δ_C (100 MHz, DMSO-d_6) 10.5, 32.8, 38.4, 43.2, 67.1, 101.4, 112.6, 112.7, 112.7, 124.0, 129.3, 129.5, 129.6, 129.6, 130.0, 133.6, 133.6, 133.6, 137.9, 138.7, 140.6, 144.4, 146.3, 146.3, 147.3, 147.4, 147.4, 155.5, 160.4, 161.7, 169.3; δ_F (376 MHz, DMSO-d_6) -113,52(1F, s); *m/z* (ESI positive) 544.0 $[M+H]^+$.

Synthesis of (±)-2-(3-benzoylphenyl)-N-(2-((2-oxo-2H-chromen-7-yl)oxy)ethyl)propanamide **(A29)**

(±)-2-(3-Benzoylphenyl)-*N*-(2-((2-oxo-2*H*-chromen-7-yl)oxy)ethyl)propanamide **A29** was obtained according to the general procedure **1** earlier reported using NHS (1.5 eq.) and EDCI·HCl (1.5 eq.) in a solution of (±)-Ketoprofen **A3** (0.5 g, 1.0 eq.) in dry DMF (3.0 mL) under a N_2 atmosphere. The reaction mixture was stirred at r.t. until the formation of the activated ester intermediate **C** (TLC monitoring, not isolated). 2-((2-Oxo-2*H*-chromen-7-yl)oxy)ethan-1-amonium trifluoroacetate salt A18 and triethylamine (Et_3N) were added to the mixture which was stirred at 60°C until starting materials were consumed (TLC monitoring), followed by quenching with H_2O (10 mL), extracted with EtOAc (3 x 10 mL) and the combined organic layers were washed with H_2O (3 x 20 mL), dried over Na_2SO_4, filtered-off and dried under *vacuo* to give a white residue that was

purified by silica gel column chromatography eluting with EtOAc/*n*-hexane 50% *v/v* to afford the titled compound **A29** as a white solid.

(±)-2-(3-Benzoylphenyl)-*N*-(2-((2-oxo-2H-chromen-7-yl)oxy)ethyl)propanamide A29: 44.7% yield; m.p. 116-118 °C; silica gel TLC R_f 0.16 (Ethyl acetate/*n*-hexane 50% *v/v*); δ_H (400 MHz, DMSO-d_6) 1.39 (3H, d, *J* 6.8, CH_3), 3.46 (2H, *J* 5.4, NHCH_2), 3.79 (1H, q, *J* 6.8, C*H*), 4.11 (2H, t, *J* 5.4, OCH_2), 6.31 (1H, d, *J* 9.6, Ar-*H*), 6.90 (1H, dd, *J* 8.6 3.6, Ar-*H*), 6.97 (1H, d, *J* 2.4, Ar-*H*), 7.66 (1H, d, *J* 7.2, Ar-H), 7.68 (9H, m, Ar-*H*), 7.99 (1H, d, *J* 9.6, Ar-*H*), 8.35 (1H, t, *J* 5.22, exchange with D_2O, CON*H*); δ_C (100 MHz, DMSO-d_6) 18.6, 38.2, 44.8, 67.1, 101.4, 112.5, 112.6, 112.7, 128.2, 128.5, 128.6, 128.7, 129.6, 129.7, 131.7, 132.7, 136.9, 137.1, 142.7, 144.4, 155.4, 160.4, 161.6, 173.4, 195.8; *m/z* (ESI positive) 442.0 $[M+H]^+$.

Synthesis of (±)-2-(4-isobutylphenyl)-N-(2-((2-oxo-2H-chromen-6-yl)oxy)ethyl)propanamide **(A30)**

(±)-2-(4-Isobutylphenyl)-*N*-(2-((2-oxo-2*H*-chromen-6-yl)oxy)ethyl)propanamide **A30** was obtained according to the general procedure **1** earlier reported using NHS (1.5 eq.) and EDCI·HCl (1.5 eq.) in a solution of (±)-Ibuprofen **A4** (0.09 g, 1.0 eq.) in dry DMF (3.0 mL) under a N_2 atmosphere. The reaction mixture was stirred at r.t. until the formation of the activated ester intermediate **D** (TLC monitoring, not isolated). 2-((2-Oxo-2*H*-chromen-7-yl)oxy)ethan-1-amonium trifluoroacetate salt **A18** and triethylamine (Et_3N) were added to the mixture which was stirred at 60 °C until starting materials were consumed (TLC monitoring), followed by quenching with H_2O (10 mL), extracted with EtOAc (3 x 10 mL) and the combined organic layers were washed with H_2O (3 x 20 mL), dried over Na_2SO_4, filtered-off and concentrated under *vacuo* to give a brown residue that was purified by silica gel column chromatography eluting with EtOAc/*n*-hexane 50% *v/v* to afford a colourless oil that was triturated with diethyl ether to afford the titled compound **A30** as a white solid.

(±)-2-(4-Isobutylphenyl)-*N*-(2-((2-oxo-2H-chromen-6-yl)oxy)ethyl)propanamide A30: 64.3% yield; m.p. 106-108°C; silica gel TLC R_f 0.25 (Ethyl acetate/*n*-hexane 50% *v/v*); δ_H (400 MHz, DMSO-d_6) 0.85 (6H, d, *J* 6.6, 2 x CH_3), 1.34 (3H, d, *J* 7.1, CH_3), 1.78 (1H, sept, C*H*(CH_3)$_2$), 2.40 (2H, d, *J* 7.2, CH_2), 3.46 (2H, q, *J* 5.5, NHCH_2), 3.62 (1H, q, *J* 6.7, C*H*CH_3), 4.11 (2H, t, *J* 5.4, OCH_2), 6.33 (1H, d, *J* 9.6, Ar-*H*), 6.95 (1H, dd, *J* 8.4

3.6, Ar-*H*), 6.99 (1H, d, *J* 2.4, Ar-*H*), 7.05 (2H, d, *J* 8.0, Ar-*H*), 7.23 (2H, d, *J* 8, Ar-*H*), 7.65 (1H, d, *J* 8.8, Ar-*H*), 8.02 (1H, d, *J* 9.6,Ar-*H*), 8.22 (1H, t, *J* 5.5, exchange with D_2O, CON*H*); δ_C (100 MHz, DMSO-d_6) 18.6, 22.2 (2 x *C*H3), 29.7, 38.2, 44.3, 44.7, 67.1, 101.4, 112.5, 112.6, 112.7, 127.0, 128.8, 129.6, 139.2, 139.5, 144.4, 155.4, 160.4, 161.7, 173.9; *m/z* (ESI positive) 394.1 $[M+H]^+$.

Synthesis of 2-(2-((2,6-dichlorophenyl)amino)phenyl)-N-(2-((2-oxo-2H-chromen-7-yl)oxy)ethyl)acetamide **(A31)**

2-(2-((2,6-Dichlorophenyl)amino)phenyl)-*N*-(2-((2-oxo-2*H*-chromen-7-yl)oxy)ethyl)acetamide **A31** was obtained according to the general procedure **1** earlier reported using NHS (1.5 eq.) and EDCI·HCl (1.5 eq.) in a solution of Diclofenac **A5** (0.25 g, 1.0 eq.) in dry DMF (3.0 mL) under a N_2 atmosphere. The reaction mixture was stirred at r.t. until the formation of the activated ester intermediate **E** (TLC monitoring, not isolated). 2-((2-Oxo-2*H*-chromen-7-yl)oxy)ethan-1-amonium trifluoroacetate salt **A18** and triethylamine (Et_3N) were added to the mixture which was stirred at 60°C until starting materials were consumed (TLC monitoring), followed by quenching with H_2O (10 mL), extracted with EtOAc (3 x 10 mL) and the combined organic layers were washed with H_2O (3 x 20 mL), dried over Na_2SO_4, filtered-off and concentrated under *vacuo* to give a white residue that was purified by silica gel column chromatography eluting with EtOAc/*n*-hexane 50% *v/v* to afford the titled compound **A31** as a white solid.

2-(2-((2,6-Dichlorophenyl)amino)phenyl)-*N*-(2-((2-oxo-2H-chromen-7-yl)oxy)ethyl)acetamide A31: 40.4% yield; m.p. 195-196°C; silica gel TLC R_f 0.30 (Ethyl acetate/*n*-hexane 50% *v/v*); δ_H (400 MHz, DMSO-d_6) 3.53 (2H, q, *J* 5.4, NHCH_2), 3.65 (2H, s, CH_2), 4.18 (2H, t, *J* 5.6, OCH_2), 6.32 (1H, d, *J* 8.0, Ar-*H*), 6.33 (1H, d, *J* 9.6, Ar-*H*), 6.87 (1H, appt, *J* 7.4, Ar-*H*) 6.98 (1H, dd, *J* 8.6 3.6, Ar-*H*), 7.03 (1H, d, *J* 2.0, Ar-*H*), 7.07 (1H, appt, *J* 7.4, Ar-*H*), 7.18 (1H, d, *J* 8.4, Ar-*H*), 7.22 (1H, t, *J* 5.4, Ar-*H*), 7,54 (2H, d, *J* 8.0, Ar-*H*), 7.65 (1H, d, *J* 8.8, Ar-*H*), 8.03 (1H, d, *J* 9.6, Ar-*H*), 8.30 (1H, s, N*H*), 8.69 (1H, t, *J* 5.4, exchange with D_2O, CON*H*). δ_C (100 MHz, DMSO-d_6) 38.4, 67.1, 101.5, 112.6, 112.7, 112.8, 116.0, 120.7, 125.2, 125.4, 127.3, 129.3, 129.6, 130.6, 137.3, 143.1, 144.4, 155.4, 160.4, 161.6, 172.1; *m/z* (ESI positive) 483.0 $[M+H]^+$.

Synthesis of (±)-2-(2-fluoro-[1,1'-biphenyl]-4-yl)-N-(2-((2-oxo-2H-chromen-7-yl)oxy)ethyl)propanamide **(A32)**

(±)-2-(2-Fluoro-[1,1'-biphenyl]-4-yl)-*N*-(2-((2-oxo-2*H*-chromen-7-yl)oxy)ethyl)propanamide **A32** was obtained according to the general procedure **1** earlier reported using NHS (1.5 eq.) and EDCI·HCl (1.5 eq.) in a solution of (±)-Flurbiprofen **A6** (0.5 g, 1.0 eq.) in dry DMF (3.0 mL) under a N_2 atmosphere. The reaction mixture was stirred at r.t. until the formation of the activated ester intermediate **F** (TLC monitoring, not isolated). 2-((2-Oxo-2*H*-chromen-7-yl)oxy)ethan-1-amonium trifluoroacetate salt **A18** and triethylamine (Et_3N) were added to the mixture which was stirred at 60°C until starting materials were consumed (TLC monitoring), followed by quenching with H_2O (10 mL), extracted with EtOAc (3 x 10 mL) and the combined organic layers were washed with H_2O (3 x 20 mL), dried over Na_2SO_4, filtered-off and concentrated under *vacuo* to give a residue that was purified by silica gel column chromatography eluting with EtOAc/*n*-hexane 50% *v/v* to afford the titled compound **A32** as a white solid.

(±)-2-(2-Fluoro-[1,1'-biphenyl]-4-yl)-*N*-(2-((2-oxo-2H-chromen-7-yl)oxy)ethyl)propanamide A32: 31.7% yield; m.p. 139-140 °C; silica gel TLC R_f 0.14 (Ethyl acetate/*n*-hexane 50% *v/v*); δ_H (400 MHz, DMSO-d_6) 1.40 (3H, d, *J* 6.8, CH_3), 3.50 (2H, q, *J* 5.4, NHCH_2), 3.75 (1H, q, *J* 6.8, C*H*CH$_3$), 4.14 (2H, t, *J* 5.6, OCH_2), 6.32 (1H, d, *J* 9.6, Ar-*H*), 6.95 (1H, dd, *J* 8.8 3.7, Ar-*H*), 7.01 (1H, d, *J* 2.0, Ar-*H)*, 7.25 (1H, s, Ar-*H*), 7.27 (1H, d, *J* 3.2, Ar-*H*), 7.46 (6H, m, Ar-*H*), 7.64 (1H, d, *J* 8.8, Ar-*H*), 8.01 (1H, d, *J* 9.6, Ar-*H*), 8.36 (1H, t, *J* 5.4, exchange with D_2O, CON*H)*; δ_C (100 MHz, DMSO-d_6) 19.3, 39.1, 45.4, 67.9, 102.3, 113.4, 113.5 ($J^4_{C\text{-}F}$ 6), 115.6, 115.9, 124.7 ($J^5_{C\text{-}F}$ 3), 127.3 ($J^5_{C\text{-}F}$ 13), 128.7, 129.5, 129.6, 130.5, 131.4 ($J^5_{C\text{-}F}$ 3), 135.9, 145.0 ($J^4_{C\text{-}F}$6), 145.2, 156.3, 157.4 ($J^1_{C\text{-}F}$ 245), 161.2, 162.6, 174.1; δ_F (376 MHz, DMSO-d_6) -118.75(1F, s); *m/z* (ESI positive) 432.1 $[M+H]^+$.

Synthesis of (S)-(+)-2-(6-methoxynaphthalen-2-yl)-N-(2-((2-oxo-2H-chromen-7-yl)oxy)ethyl)propanamide **(A33)**

(*S*)-(+)-2-(6-Methoxynaphthalen-2-yl)-*N*-(2-((2-oxo-2*H*-chromen-7-yl)oxy)ethyl)propanamide **A33** was obtained according to the general procedure **1** earlier reported using NHS (1.5 eq.) and EDCI·HCl (1.5 eq.) in a solution of (*S*)-(+)-Naproxen **A7** (0.23 g, 1.0 eq.) in dry DMF (3.0 mL) under a N_2 atmosphere. The reaction mixture

was stirred at r.t. until the formation of the activated ester intermediate **H** (TLC monitoring, not isolated). 2-((2-Oxo-2*H*-chromen-7-yl)oxy)ethan-1-amonium trifluoroacetate salt **A18** and triethylamine (Et_3N) were added to the mixture which was stirred at 60°C until starting materials were consumed (TLC monitoring), followed by quenching with H_2O (10 mL) and the formed precipitate was filtered-off and dried under *vacuo* to give a residue was purified by silica gel column chromatography eluting with EtOAc/*n*-hexane 60% *v/v* to afford the titled compound **A33** as a white solid.

(S)-(+)-2-(6-Methoxynaphthalen-2-yl)-*N*-(2-((2-oxo-2H-chromen-7-yl)oxy)ethyl)propanamide A33: 24% yield; m.p. 140-141 °C; silica gel TLC R_f 0.26 (Ethyl acetate/*n*-hexane 60% *v/v*); δ_H (400 MHz, DMSO-d_6) 1.44 (3H, d, *J* 7.0, CH_3), 3.48 (2H, q, *J* 5.5, NHCH_2), 3.79 (1H, q, *J* 6.9, C*H*), 3.89 (3H, s, OCH_3), 4.12 (2H, t, *J* 5.6, OCH_2), 6.32 (1H, d, *J* 9.6, Ar-*H*), 6.92 (1H, dd, *J* 8.6 3.6, Ar-*H*), 6.97 (1H, d, *J* 2.0, Ar-*H*), 7.13 (1H, dd, *J* 8.8 3.8, Ar-*H*), 7.27 (1H, d, *J* 2.4, Ar-*H*), 7.46 (1H, dd, *J* 8.0 3.3, Ar-*H*), 7.61 (1H, d, *J* 8.8, Ar-*H*), 7.74 (3H, m, Ar-*H*), 8.01 (1H, d, *J* 9.44, Ar-*H*), 8.29 (1H, t, *J* 5.6, exchange with D_2O, CON*H*); δ_C (100 MHz, DMSO-d_6) 19.5, 39.1, 45.9, 56.1, 67.9, 102.3, 106.6, 113.4, 113.5, 113.6, 119.5, 126.2, 127.4, 127.6, 129.3, 130.0, 130.4, 134.1, 138.3, 145.3, 156.3, 157.9, 161.3, 162.5, 174.8; *m/z* (ESI positive) 418.0 $[M+H]^+$.

Synthesis of (±)-5-benzoyl-N-(2-((2-oxo-2H-chromen-7-yl)oxy)ethyl)-2,3-dihydro-1H-pyrrolizine-1-carboxamide **(A34)**

(±)-5-Benzoyl-*N*-(2-((2-oxo-2*H*-chromen-7-yl)oxy)ethyl)-2,3-dihydro-1*H*-pyrrolizine-1-carboxamide **A34** was obtained according to the general procedure **1** earlier reported using NHS (1.5 eq.) and EDCI·HCl (1.5 eq.) in a solution of (±)-Ketorolac **A8** (0.2 g, 1.0 eq.) in dry DMF (3.0 mL) under a N_2 atmosphere. The reaction mixture was stirred at r.t. until the formation of the activated ester intermediate **G** (TLC monitoring, not isolated). 2-((2-Oxo-2*H*-chromen-7-yl)oxy)ethan-1-amonium trifluoroacetate salt **A18** and triethylamine (Et_3N) were added to the mixture which was stirred at 60°C until starting materials were consumed (TLC monitoring), followed by quenching with H_2O (10 mL) and the formed precipitate was filtered-off and dried under *vacuo* to give a residue was purified by silica gel column chromatography eluting with EtOAc/*n*-hexane 80% *v/v* to afford the titled compound **A34** as a white solid.

(±)-5-Benzoyl-*N*-(2-((2-oxo-2H-chromen-7-yl)oxy)ethyl)-2,3-dihydro-1H-pyrrolizine-1-carboxamide A34: 75.4% yield; m.p. 148-149 °C; silica gel TLC R_f 0.14 (Ethyl acetate/*n*-hexane 60% *v/v*); δ_H (400 MHz, DMSO-d_6) 2.76 (2H, m, 2 x CHH_{ax}), 3.55 (2H, q, *J* 5.4, NHCH_2), 4.03 (1H, q, J 4.8, C*H*), 4.18 (2H, t, *J* 5.1, OCH_2), 4.25 (2H, m, 2 x CHH_{eq}), 6.02 (1H, d, *J* 3.8, pyrrole-*H*), 6.34 (1H, d, *J* 9.6, Ar-*H*), 6.75 (1H, d, *J* 3.8, pyrrole-*H*), 7.01 (1H, dd, *J*, 8.8 4.4, Ar-*H*), 7.06 (1H, d, *J* 2.4, Ar-*H*), 7.54 (2H, m, Ar-*H*), 7.63 (1H, m, Ar-*H*), 7.68 (1H, d, *J* 8.4, Ar-*H*), 7.77 (2H, d, *J* 8.0, Ar-*H*), 8.04 (1H, d, *J* 9.6, Ar-*H*), 8.59 (1H, t, *J* 5.4, exchange with D_2O, CON*H*); δ_C (100 MHz, DMSO-d_6) 30.8, 38.4, 42.8, 47.8, 67.0, 101.4, 102.4, 112.6, 112.7, 112.8, 124.5, 126.1, 128.4, 128.5, 129.7, 131.5, 139.0, 144.4, 145.4, 155.5, 160.4, 161.7, 170.9, 183.5; *m/z* (ESI positive) 443.0 $[M+H]^+$.

5.1.2 Carbonic Anhydrase Inhibition

The CA inhibitory profiles of compounds belonging to series A were obtained according to the general procedures described at the beginning of the experimental section.

5.1.3 Pain Relief Efficacy Tests

5.1.3.1 Animals

Sprague Dawley rats (Harlan, Varese, Italy) weighing 200-250 g at the beginning of the experimental procedure were used. Animals were housed in the Centro Stabulazione Animali da Laboratorio (University of Florence) and used at least 1 week after their arrival. Four rats were housed per cage (size 26 cm × 41 cm); animals were fed a standard laboratory diet and tap water ad libitum and kept at 23 ± 1 °C with a 12 h light/dark cycle (light at 7 a.m.). All animal manipulations were carried out according to the European Community guidelines for animal care [DL 116/92, application of the European Communities Council Directive of November 24th 1986 (86/609/EEC)]. The ethical policy of the University of Florence complies with the Guide for the Care and Use of Laboratory Animals of the US National Institutes of Health (NIH Publication No. 85-23, revised 1996; University of Florence assurance number A5278-01). Formal approval to conduct the experiments described was obtained from the Animal Subjects Review Board

of the University of Florence. Experiments involving animals have been reported according to ARRIVE - Animal Research: Reporting of *in Vivo* Experiments – guidelines.[283] All efforts were made to minimize animal suffering and to reduce the number of animals used.

5.1.3.2 Complete Freund's adjuvant-induced arthritis

Articular damage was induced by injection of complete Freund's adjuvant (CFA; Sigma-Aldrich St Louis, MO, USA), containing 1 mg/ml of heat-killed and dried Mycobacterium tuberculosis in paraffin oil and mannide monooleate, into the tibiotarsal joint.[170,284,285] Briefly, the rats were lightly anesthetized by 2% isoflurane, the left leg skin was sterilized with 75% ethyl alcohol and the lateral malleolus located by palpation. A 28-gauge needle was then inserted vertically to penetrate the skin and turned distally for insertion into the articular cavity at the gap between the tibiofibular and tarsal bone until a distinct loss of resistance was felt. A volume of 50 µl of CFA was then injected (day 0). Control rats received 50 µl of saline solution (day 0) in the tibiotarsal joint. Behavioral experiments were performed 14 days after.

5.1.3.3 Administration of compounds

Compounds **A19**, **A28**, **A30**, **A32** and **A34** were suspended in a 1% solution of carboxymethylcellulose sodium salt (CMC) and administered per os (p.o.) once on day 14. All compounds were tested at the dose of 10 mg kg^{-1}, 5d was also administered at the dose of 1 mg kg^{-1}. Ibuprofen was administered p.o. at 10 mg kg^{-1}, the effectiveness of this dosage was previously demonstrated in the same model whereas the compound was ineffective when administered at 15 mg kg^{-1}.[170]

5.1.3.4 Paw-pressure test

The nociceptive threshold of rats was determined with an analgesimeter (Ugo Basile, Varese, Italy), according to the method described by Leighton et al.[286] Briefly, a constantly increasing pressure was applied to a small area of the dorsal surface of the

hind paw using a blunt conical probe by a mechanical device. Mechanical pressure was increased until vocalization or a withdrawal reflex occurred while rats were lightly restrained. Vocalization or withdrawal reflex thresholds were expressed in grams. Rats scoring below 40 g or over 75 g during the test before drug administration were rejected (25%). For analgesia measures, mechanical pressure application was stopped at 120 g.

5.1.3.5 Incapacitance test

Weight-bearing changes were measured using an incapacitance apparatus (Linton Instrumentation, Norfolk, UK) to detect changes in postural equilibrium after a hind limb injury.[287] Rats were trained to stand on their hind paws in a box with an inclined plane (65° from horizontal). This box was placed above the incapacitance apparatus. This allowed us to independently measure the weight that the animal applied on each hind limb. The value reported for each animal is the mean of five consecutive measurements. In the absence of hind limb injury, rats applied an equal weight on both hind limbs, indicating postural equilibrium, whereas an unequal distribution of weight on the hind limbs indicated a monolateral decreased pain threshold. Data are expressed as the difference between the weight applied to the limb contralateral to the injury and the weight applied to the ipsilateral limb (Δ Weight).

5.1.3.6 Statistical analysis

Behavioural measurements were performed on eight rats for each treatment carried out in two different experimental sets. Results were expressed as mean (S.E.M.) with one-way analysis of variance. A Bonferroni's significant difference procedure was used as a post hoc comparison. P-values <0.05 or <0.01 were considered significant. Data were analysed using the Origin 9 software (OriginLab, Northampton, MA, USA).

5.2 Bioisosteric development of multi-target NSAID - carbonic anhydrases inhibitor anti-arthritic agents: synthesis, enzyme kinetic, plasma stability and anti-inflammatory evaluation (Series B)

5.2.1 Chemistry

The general chemistry protocols are reported at the beginning of the experimental section.

*General procedure **4** for the synthesis of intermediates 6-(2-hydroxyethoxy)-2H-chromen-2-one **B1** and 7-(2-hydroxyethoxy)-2H-chromen-2-one **B2***

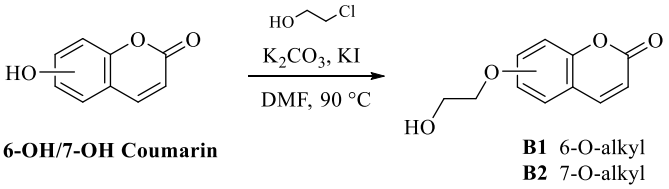

6-OH/7-OH Coumarin

B1 6-O-alkyl
B2 7-O-alkyl

2-Chloro-ethanol (1.5 eq.) was added to a suspension of 6-hydroxy-2H-chromen-2-one or 7-hydroxy-2H-chromen-2-one (1.0 g, 1.0 eq.), K_2CO_3 (1.2 eq.) and KI (1.0 eq.) in dry *N,N*-dimethylformamide (DMF) (4 mL) under a N_2 atmosphere. The reaction mixtures were stirred at 90 °C O.N. until consumption of starting materials (TLC monitoring), then cooled down to r.t. and quenched with H_2O (10 mL), the reaction solution was extracted with EtOAc (3 x 10 mL). The combined organic layers were washed with a saturated solution of K_2CO_3, brine and dried over Na_2SO_4, filtered-off and concentrated under *vacuo* to give an oil that was purified by silica gel column chromatography eluting with the appropriate mixture of EtOAc/n-hexane to afford **B1** or **B2** as white solids.

6-(2-Hydroxyethoxy)-2H-chromen-2-one (B1): 56% yield; m.p. 134-136°C; TLC: R_f = 0.14 (ethyl acetate/*n*-hexane 60% v/v); ^{1}H-NMR (DMSO-d_6, 400 MHz): δ 3.76 (2H, q, J = 12.0, 4.2, CH_2-OH), 4.06 (2H, t, J = 9.6, 4.8, O-CH_2-CH_2-OH), 4.94 (1H, t, J = 9.6, 4.8, CH$_2$-O*H*), 6.52 (1H, d, J = 9.6, Ar-*H*), 7.24 (1H, dd, J = 8.6, 3.6, Ar-*H*), 7.32 (1H, m, Ar-*H*), 7.37 (1H, d, J = 9.2, Ar-*H*), 8.03 (1H, d, J = 9.6, Ar-*H*); ^{13}C-NMR (DMSO-d_6, 100 MHz): δ 60.4, 71.1, 112.3, 117.4, 118.2, 120.1, 120.8, 145.0, 148.7, 155.9, 161.1; MS (ESI positive) m/z = 207.0 $[M + H]^+$.

7-(2-Hydroxyethoxy)-2H-chromen-2-one (B2): 50% yield; m.p. 85-87°C; TLC: R_f = 0.22 (ethyl acetate/*n*-hexane 50% v/v); ^{1}H-NMR (DMSO-d_6, 400 MHz): δ 3.77 (2H, q, CH_2-OH), 4.13 (2H, t, J = 9.6, 4.8, O-CH_2-CH_2-OH), 4.95 (1H, t, J = 11.2, 5.6, CH_2-O*H*), 6.32 (1H, d, J = 9.6, Ar-*H*), 7.99 (1H, dd, J = 8.6, 3.6, Ar-*H*), 7.02 (1H, d, J = 2.0, Ar-*H*), 7.66 (1H, d, J = 8.8, Ar-*H*), 8.02 (1H, d, J = 9.2, Ar-*H*); ^{13}C-NMR (DMSO-d_6, 100 MHz): δ 60.3, 71.3, 102.1, 113.2, 113.3, 113.7, 130.4, 145.3, 156.3, 161.2, 162.9; MS (ESI positive) m/z = 207.0 $[M + H]^+$.

*General procedure **5** for the synthesis of esters **B3-16***

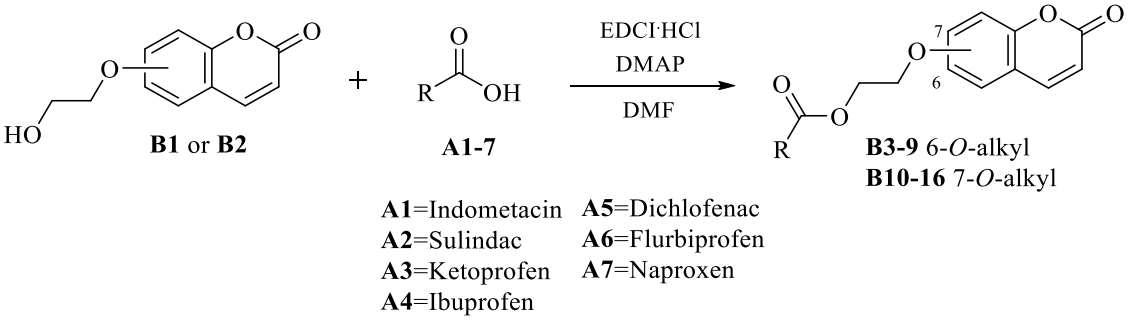

EDCI·HCl (1.2 eq.) and DMAP (0.03 eq.) were added to a solution of the appropriate NSAID **A1-7** (0.5 g, 1.0 eq.) and **B1** or **B2** in dry DMF (3.0 mL) under a N_2 atmosphere. The reaction was stirred at room temperature until starting materials were consumed (TLC monitoring), and then quenched with slush (10 mL). The mixture was extracted with EtOAc (3 x 10 mL) and the combined organic layers were washed with a saturated solution of K_2CO_3 (2 x 20 mL) and water (1 x 20 ml), dried over Na_2SO_4, filtered-off and concentrated under *vacuo* to give a crude residue that was purified by silica gel column chromatography eluting with the appropriate mixture of solvents.

Synthesis of 2-((2-oxo-2H-chromen-6-yl)oxy)ethyl 2-(1-(4-chlorobenzoyl)-5-methoxy-2-methyl-1H-indol-3-yl)acetate **(B3)**

Compound **B3** was obtained according to the general procedure earlier reported adding EDCI·HCl (1.8 eq.) and DMAP (0.03 eq.) to a solution of indometacin **A1** (0.15 g, 1.0 eq.) and 6-(2-hydroxyethoxy)-2H-chromen-2-one **B1** (0.11 g, 1.0 eq.) in dry DMF (2.0

mL). The crude compound was purified by silica gel column chromatography eluting with EtOAc/n-hexane 40% *v/v* to give **B3** as a white solid.

2-((2-Oxo-2H-chromen-6-yl)oxy)ethyl 2-(1-(4-chlorobenzoyl)-5-methoxy-2-methyl-1H-indol-3-yl)acetate B3: 47% yield; m.p. 175-177°C; silica gel TLC R_f 0.47 (ethyl acetate/*n*-hexane 40% *v/v*); δ_H (400 MHz, DMSO-d_6) 2.24 (3H, s, CH_3), 3.75 (3H, s, OCH_3), 3.85 (2H, s, CH_2CO), 4.27 (2H, t, *J* = 4.4, OCH_2), 4.46 (2H, t, *J* = 4.0, COOCH_2), 6.53 (1H, d, *J* = 9.6, Ar-*H*), 6.73 (1H, dd, *J* = 8.0 2.4, Ar-*H*), 6.96 (1H, d, *J* = 8.8, Ar-*H*), 7.07 (1H, d, *J* = 2.4, Ar-*H*), 7.17 (1H, dd, *J* = 8.0 2.4, Ar-*H*), 7.29 (1H, d, *J* = 2.8, Ar-*H*), 7.36 (1H, d, *J* = 9.2, Ar-*H*), 7.65 (4H, m, *J* = 8.4, Ar-*H*), 8.00 (1H, d, *J* = 9.6, Ar-*H*); δ_C (100 MHz, DMSO-d_6) 14.1, 30.2, 56.2, 63.8, 67.4, 102.5, 112.3, 112.5, 113.5, 115.5, 117.6, 118.3, 120.1, 120.6, 129.9, 131.1, 131.4, 132.0, 134.9, 136.3, 138.5, 144.9, 148.9, 155.4, 156.5, 161.0, 168.7, 171.4; ESI-HRMS (m/z) $[M+H]^+$: calculated for $C_{30}H_{25}ClNO_7$ 546.1314; found 546.1324.

Synthesis of 2-((2-oxo-2H-chromen-6-yl)oxy)ethyl(Z)-2-(5-fluoro-2-methyl-1-(4-(methylsulfinyl)benzylidene)-1H-inden-3-yl)acetate **(B4)**

Compound **B4** was obtained according to the general procedure earlier reported adding EDCI·HCl (2.0 eq.) and DMAP (0.03 eq.) to a solution of sulindac **A2** (0.27 g, 1.0 eq.) and 6-(2-hydroxyethoxy)-2H-chromen-2-one **B1** (0.2 g, 1.0 eq.) in dry DMF (2.0 mL) under a N_2 atmosphere. The crude residue was purified by silica gel column chromatography eluting with EtOAc/n-hexane 70% *v/v* to afford the titled compound **B4** as a yellow solid.

2-((2-Oxo-2H-chromen-6-yl)oxy)ethyl(Z)-2-(5-fluoro-2-methyl-1-(4-(methylsulfinyl)benzylidene)-1H-inden-3-yl)acetate B4: 47% yield; m.p. 131-133°C; silica gel TLC R_f 0.26 (MeOH/DCM 5% *v/v*); δ_H (400 MHz, DMSO-d_6) 2.19 (3H, s, CH_3), 2.86 (3H, s, SOCH_3), 3.76 (2H, s, CH_2CO), 4.27 (2H, m, OCH_2), 4.47 (2H, m, COOCH_2 Ar-*H*), 6.52 (1H, d, *J* = 9.6, Ar-*H*), 6.74 (1H, t, *J* = 8.0, Ar-*H*), 7.04 (1H, d, *J* = 8.0, Ar-*H*), 7.20 (2H, m, Ar-*H*), 7.35 (3H, m, Ar-*H*), 7.77 (4H, dd, *J* = 8.0 32.4, Ar-*H*), 8.0 (1H, d, *J* = 9.6, Ar-*H*); δ_C (100 MHz, DMSO-d_6) 11.2, 31.6, 31.7, 44.0, 63.8, 67.4, 111.4 ($J^2_{C\text{-}F}$ = 24), 112.6, 117.5, 118.3, 120.1, 120.6, 124.0, 124.1, 124.8, 130.2, 130.8, 132.6 ($J^3_{C\text{-}F}$ = 3), 139.3 ($J^3_{C\text{-}F}$ = 3), 141.1, 144.9, 147.3, 148.9, 155.4, 160.1, 163.4 ($J^1_{C\text{-}F}$ =

245), 164.6, 170.9; δ_F (376 MHz, DMSO-d_6) -113.36 (1F, s); ESI-HRMS (m/z) $[M+H]^+$: calculated for $C_{31}H_{26}FO_6S$ 545.1429; found 545.1421.

Synthesis of (±)-2-((2-oxo-2H-chromen-6-yl)oxy)ethyl 2-(3-benzoylphenyl)propanoate **(B5)**

Compound **B5** was obtained according to the general procedure earlier reported adding EDCI·HCl (2.0 eq.) and DMAP (0.03 eq.) to a solution of (±)-ketoprofen **A3** (0.145 g, 1.0 eq.) and 6-(2-hydroxyethoxy)-2H-chromen-2-one **B1** (0.15 g, 1.0 eq.) in dry DMF (2.0 mL). The crude residue was purified by silica gel column chromatography eluting with EtOAc/*n*-hexane from 50% *v/v* to give **B5** as a white solid.

(±)-2-((2-Oxo-2H-chromen-6-yl)oxy)ethyl 2-(3-benzoylphenyl)propanoate B5: 54% yield; m.p. 89-91°C; silica gel TLC R_f 0.50 (ethyl acetate/*n*-hexane 50% *v/v*); δ_H (400 MHz, DMSO-d_6) 1.46 (3H, d, *J* = 7.2 CH_3), 4.02 (1H, q, *J* = 6.8, C*H*), 4.22 (2H, t, *J* = 4.4, OCH_2), 4.45 (2H, q, *J* = 3.8, COOCH_2), 6.51 (1H, d, *J* = 9.6, Ar-*H*), 7.15 (1H, dd, *J* = 9.2, 3.2, Ar-*H*), 7.25 (1H, d, *J* = 3.2, Ar-*H*), 7.32 (1H, d, *J* = 9.2, Ar-*H*), 7.61 (9H, m, Ar-*H*), 7.98 (1H, d, *J* = 8.0, Ar-*H*); δ_C (100 MHz, DMSO-d_6) 19.4, 45.1, 63.8, 67.3, 112.6, 117.5, 118.2, 120.1, 120.6, 129.3, 129.4, 129.5, 129.7, 130.5, 132.6, 133.6, 137.8, 138.1, 141.9, 144.9, 148.9, 155.3, 161.0, 174.4, 196.4 ; ESI-HRMS (m/z) $[M+H]^+$: calculated for $C_{27}H_{23}O_6$ 443.1489; found 443.1496.

Synthesis of (±)-2-((2-oxo-2H-chromen-6-yl)oxy)ethyl 2-(4-isobutylphenyl)propanoate **(B6)**

Compound **B6** was obtained according to the general procedure earlier reported adding EDCI·HCl (1.8 eq.) and DMAP (0.03 eq.) to a solution of (±)-ibuprofen **A4** (0.17 g, 1.0 eq.) and 6-(2-hydroxyethoxy)-2H-chromen-2-one **B1** (0.2 g, 1.0 eq.) in dry DMF (2.0 mL). The crude residue was purified by silica gel column chromatography eluting with EtOAc/n-hexane from 40% *v/v* to give **B6** as a white solid.

(±)-2-((2-Oxo-2H-chromen-6-yl)oxy)ethyl 2-(4-isobutylphenyl)propanoate B6: 43% yield; m.p. 85-87°C; silica gel TLC R_f 0.65 (ethyl acetate/*n*-hexane 40% *v/v*); δ_H (400 MHz, DMSO-d_6) 0.85 (6H, d, *J* = 6.4, 2 x CH_3), 1.40 (3H, d, *J* = 7.2, CH_3), 1.76 (1H, sept, C*H*(CH_3)$_2$), 2.40 (2H, d, *J* = 6.8, CH_2), 3.80 (1H, q, *J* = 6.8, C*H*), 4.21 (2H, m, OCH_2), 4.42 (2H, t, *J* = 4.4, COOCH_2), 6.52 (1H, d, *J* = 9.6, Ar-*H*), 7.07 (2H, d, *J* = 8.0,

Ar-*H*), 7.17 (3H, m, Ar-*H*), 7.28 (1H, d, *J* = 2.8, Ar-*H*), 7.35 (1H, d, *J* = 9.2, Ar-*H*), 8.01 (1H, d, *J* = 9.6, Ar- *H*); δ_C (100 MHz, DMSO-d_6) 19.5, 23.0, 30.5, 45.0, 45.1, 63.6, 67.4, 112.6, 117.5, 118.3, 120.1, 120.8, 127.9, 129.9, 138.6, 140.6, 144.9, 148.9, 155.4, 161.0, 174.8; ESI-HRMS (m/z) $[M+H]^+$: calculated for $C_{24}H_{27}O_5$ 395.1853; found 395.1853.

Synthesis of 2-((2-oxo-2H-chromen-6-yl)oxy)ethyl,2-(2-((2,6-dichlorophenyl)amino)phenyl)acetate **(B7)**

Compound **B7** was obtained according to the general procedure earlier reported adding EDCI·HCl (1.8 eq.) and DMAP (0.03 eq.) to a solution of diclofenac **A5** (0.6 g, 1.0 eq.) and 6-(2-hydroxyethoxy)-2H-chromen-2-one **B1** (0.5 g, 1.0 eq.) in dry DMF (3.0 mL). The crude residue was purified by silica gel column chromatography eluting with EtOAc/*n*-hexane 50% *v/v* to give **B7** as a white solid.

2-((2-Oxo-2H-chromen-6-yl)oxy)ethyl,2-(2-((2,6-dichlorophenyl)amino)phenyl)acetate B7: 53% yield; m.p. 154-156°C; silica gel TLC R_f 0.50 (Ethyl acetate/*n*-hexane 50% *v/v*); δ_H (400 MHz, DMSO-d_6) 3.88 (2H, s, CH_2), 4.30 (2H, t, *J* = 4.8, OCH_2), 4.49 (2H, t, *J* = 4.0, COOCH_2), 6.28 (1H. d, *J* = 8.0, Ar-*H*), 6.53 (1H, d, *J* = 9.6, Ar-*H*), 6.85 (1H, appt, *J* = 6.8, Ar-*H*), 7.03 (1H, m, Ar-*H*), 7.08 (1H, appt, *J* = 8.2, Ar-*H*), 7.22 (3H, m, Ar-*H*), 7.45 (2H, m, Ar-*H*), 7.54 (2H, d, *J* = 8.0, Ar-*H*), 8.01 (1H, d, *J* = 9.6, Ar-*H*); δ_C (100 MHz, DMSO-d_6) 37.8, 64.0, 67.4, 112.6, 116.8, 117.5, 118.3, 120.1, 120.7, 121.5, 123.9, 126.9, 128.7, 130.0, 131.6, 131.8, 138.0, 143.8, 144.9, 148.9, 155.4, 161.0, 172.4; ESI-HRMS (m/z) $[M+H]^+$: calculated for $C_{25}H_{20}Cl_2NO_5$ 484.0713; found 484.0708.

Synthesis of (±)-2-((2-oxo-2H-chromen-6-yl)oxy)ethyl 2-(2-fluoro-[1,1'-biphenyl]-4-yl)propanoate **(B8)**

Compound **B8** was obtained according to the general procedure earlier reported adding EDCI·HCl (1.8 eq.) and DMAP (0.03 eq.) to a solution of (±)-flurbiprofen **A6** (0.14 g, 1.0 eq.) and 6-(2-hydroxyethoxy)-2H-chromen-2-one **B1** (0.15 g, 1.0 eq.) in dry DMF (3.0 mL). The reaction mixture was quenched with H_2O (10 mL) and the obtained precipitate was filtered-off and purified by silica gel column chromatography eluting with EtOAc/n-hexane 50% *v/v* to give **B8** as a white solid.

(±)-2-((2-Oxo-2H-chromen-6-yl)oxy)ethyl 2-(2-fluoro-[1,1'-biphenyl]-4-yl)propanoate B8: 64% yield; m.p. 122-124°C; silica gel TLC R_f 0.50 (ethyl acetate/*n*-hexane 50% *v/v*); δ_H (400 MHz, DMSO-d_6) 1.47 (3H, d, J = 7.2, CH_3), 3.98 (1H, q, J = 7.2, C*H*), 4.24 (2H, t, J = 4.4, OCH_2), 4.46 (2H, q, J = 4.0, COOCH_2), 6.51 (1H, d, J = 9.6, Ar-*H*), 7.20 (2H, dd, J = 8.8, 4.0, Ar-*H*), 7.26 (2H, m, Ar-*H*), 7.34 (1H, d, J = 9.2, Ar-*H*), 7.45 (6H, m, Ar-*H*), 7.98 (1H, d, J = 9.6, Ar-*H*); δ_C (100 MHz, DMSO-d_6) 19.2, 44.8, 63.8, 67.3, 112.6, 115.9 ($J^2_{C\text{-}F}$ = 23), 117.5, 118.3, 120.1, 120.7, 124.8 ($J^3_{C\text{-}F}$ = 3), 127.6 ($J^3_{C\text{-}F}$ = 3), 128.7, 129.6 ($J^3_{C\text{-}F}$ = 3), 131.6 ($J^3_{C\text{-}F}$ = 3), 135.7, 143.1 ($J^4_{C\text{-}F}$ = 8), 144.9, 148.9, 155.4, 158.6 ($J^1_{C\text{-}F}$ = 245), 174.2; δ_F (376 MHz, DMSO-d_6) -118.3 (1F, s); ESI-HRMS (m/z) $[M+H]^+$: calculated for $C_{26}H_{22}FO_5$ 433.1446; found 433.1451.

Synthesis of (S)-(+)-2-((2-oxo-2H-chromen-6-yl)oxy)ethyl 2-(6-methoxynaphthalen-2-yl)propanoate **(B9)**

Compound **B9** was obtained according to the general procedure earlier reported adding EDCI·HCl (1.8 eq.) and DMAP (0.03 eq.) to a solution of (*S*)-(+)-naproxen **A7** (0.18 g, 1.0 eq.) and 6-(2-hydroxyethoxy)-2H-chromen-2-one **B1** (0.2 g, 1.0 eq.) in dry DMF (2.0 mL). The crude residue was purified by silica gel column chromatography eluting with EtOAc/n-hexane 40% *v/v* to give **B9** as a white solid.

(S)-(+)-2-((2-Oxo-2H-chromen-6-yl)oxy)ethyl 2-(6-methoxynaphthalen-2-yl)propanoate B9: 55% yield; m.p. 100-102°C; silica gel TLC R_f 0.55 (ethyl acetate/*n*-hexane 50% *v/v*); δ_H (400 MHz, DMSO-d_6) 1.50 (3H, d, J = 7.1, CH_3), 3.89 (3H, s, OCH_3), 3.98 (1H, q, J = 7.1, C*H*), 4.21 (2H, t, J = 3.6, OCH_2), 4.44 (2H, m, COOCH_2), 6.51 (1H, d, J = 9.6, Ar-*H*), 7.12 (2H, m, Ar-*H*), 7.20 (1H, d, J = 3.0 Ar-*H*), 7.29 (2H, d, J = 9.1, Ar-*H*), 7.41 (1H, dd, J = 8.5, 1.8, Ar-*H*), 7.75 (3H, dd, J = 11.6, 4.5, Ar-*H*), 7.94 (1H, d, J = 9.6 Hz, Ar-*H*); δ_C (100 MHz, DMSO-d_6) 19.4, 45.3, 56.0, 63.6, 67.4, 106.6, 112.6, 117.5, 118.2, 119.6, 120.0, 120.6, 126.4, 127.1, 127.8, 129.2, 130.0, 134.2, 136.4, 144.8, 148.8, 155.3, 158.1, 161.0, 174.8; ESI-HRMS (m/z) $[M+H]^+$: calculated for $C_{25}H_{23}O_6$ 419.1489; found 419.1495.

Synthesis of 2-((2-oxo-2H-chromen-7-yl)oxy)ethyl 2-(1-(4-chlorobenzoyl)-5-methoxy-2-methyl-1H-indol-3-yl)acetate **(B10)**

Compound **B10** was obtained according to the general procedure earlier reported adding EDCI·HCl (1.2 eq.) and DMAP (0.03 eq.) to a solution of indometacin **A1** (0.27 g, 1.0 eq.) and 7-(2-hydroxyethoxy)-2H-chromen-2-one **B2** (0.2 g, 1.0 eq.) in dry DMF (2.0 mL). The crude residue was purified by silica gel column chromatography eluting with EtOAc/n-hexane 40% *v/v* to afford the titled compound **B10** as a yellow solid.

2-((2-Oxo-2H-chromen-7-yl)oxy)ethyl 2-(1-(4-chlorobenzoyl)-5-methoxy-2-methyl-1H-indol-3-yl)acetate B10:

82% yield; m.p. 143-145°C; silica gel TLC R_f 0.66 (ethyl acetate/*n*-hexane 60% *v/v*); δ_H (400 MHz, DMSO-d_6) 2.23 (3H, s, CH_3), 3.75 (3H, s, COCH_2), 3.84 (2H, s, OCH_3), 4.33 (2H, t, *J* = 4.4, OCH_2), 4.46 (2H, q, *J* = 3.6, COOCH_2), 6.33 (1H, d, *J* = 9.6, Ar-*H*), 6.72 (1H, d, *J* = 2.4, Ar-*H*), 6.90 (4H, m, Ar-*H*), 7.65 (5H, m, Ar-*H*), 8.02 (1H, d, *J* = 9.6, Ar-*H*); δ_c (100 MHz, DMSO-d_6) 14.1, 30.2, 56.3, 63.6, 67.6, 102.3, 102.6, 112.3, 113.5, 113.6, 113.7, 115.5, 130.0, 130.4, 131.2, 131.4, 132.1, 135.0, 136.4, 138.6, 145.2, 145.3, 156.3, 156.5, 161.2, 162.2, 168.8, 171.5 ; ESI-HRMS (m/z) $[M+H]^+$: calculated for $C_{30}H_{25}ClNO_7$ 546.1314; found 546.1309.

Synthesis of 2-((2-oxo-2H-chromen-7-yl)oxy)ethyl(Z)-2-(5-fluoro-2-methyl-1-(4-(methylsulfinyl)benzylidene)-1H-inden-3-yl)acetate **(B11)**

Compound **B11** was obtained according to the general procedure earlier reported adding EDCI·HCl (1.2 eq.) and DMAP (0.03 eq.) to a solution of sulindac **A2** (0.258 g, 0.95 eq.) and 7-(2-hydroxyethoxy)-2H-chromen-2-one **B2** (0.2 g, 1.0 eq.) in dry DMF (2.0 mL). The crude residue was purified by silica gel column chromatography eluting with EtOAc/n-hexane 80% *v/v* to afford **A11** as a yellow solid.

2-((2-Oxo-2H-chromen-7-yl)oxy)ethyl(Z)-2-(5-fluoro-2-methyl-1-(4-(methylsulfinyl)benzylidene)-1H-inden-3-yl)acetate B11: 42% yield; m.p. 155-157°C; silica gel TLC R_f 0.19 (ethyl acetate/*n*-hexane 80% *v/v*); δ_H (400 MHz, DMSO-d_6) 2.19 (3H, s, CH_3), 2.86 (3H, s, SOCH_3), 3.77 (2H, s, COCH_2), 4.35 (2H, d, *J* = 4.1, OCH_2), 4.47 (2H, m, COOCH_2), 6.33 (1H, d, *J* = 9.6, Ar-*H*), 6.74 (1H, dd, *J* = 12.4, 5.4 Ar-*H*), 7.00 (3H, m, Ar-*H*), 7.20 (1H, dd, *J* = 8.3, 5.2, Ar-*H*), 7.41 (1H, s, Ar-*H*), 7.66 (1H, d, *J* = 8.6, Ar-*H*), 7.78 (4H, dd, *J* = 30.9, 8.2, Ar-*H*), 8.02 (1H, d, *J* = 9.6, Ar-*H*); δ_C (100 MHz,

DMSO-d_6) 11.2, 31.6, 44.0, 63.6, 67.4, 102.2, 106.9 ($J^4_{C\text{-}F}$ = 24), 111.3 ($J^2_{C\text{-}F}$ = 24), 113.4, 113.5 ($J^4_{C\text{-}F}$ = 3), 113.6, 124.8, 130.2, 130.4, 130.8, 132.6 ($J^4_{C\text{-}F}$ = 3), 139.3 ($J^3_{C\text{-}F}$ = 8), 141.0, 145.1, 147.3, 147.5, 147.7 ($J^3_{C\text{-}F}$ = 8), 148.0, 156.2, 161.1, 163.2 ($J^1_{C\text{-}F}$ = 245), 170.8; δ_F (376 MHz, DMSO-d_6) -113,39 (1F, s); ESI-HRMS (m/z) $[M+H]^+$: calculated for $C_{31}H_{26}FO_6S$ 545.1429; found 545.1424.

Synthesis of (±)-2-((2-oxo-2H-chromen-7-yl)oxy)ethyl 2-(3-benzoylphenyl)propanoate **(B12)**

Compound **B12** was obtained according to the general procedure earlier reported adding EDCI·HCl (1.2 eq.) and DMAP (0.03 eq.) to a solution of (±)-ketoprofen **A3** (0.19 g, 1.0 eq.) and 7-(2-hydroxyethoxy)-2H-chromen-2-one **B2** (0.2 g, 1.0 eq.) in dry DMF (2.0 mL). The crude residue was purified by silica gel column chromatography eluting with EtOAc/n-hexane 40% *v/v* to afford the titled compound **B12**.

(±)-2-((2-Oxo-2H-chromen-7-yl)oxy)ethyl 2-(3-benzoylphenyl)propanoate B12: 47% yield; m.p. 108-110°C; silica gel TLC R_f 0.66 (ethyl acetate/*n*-hexane 60% *v/v*); δ_H (400 MHz, DMSO-d_6) 1.47 (3H, d, J = 7.1, CH_3), 4.04 (1H, dt, J = 14.2, 7.2, CH), 4.30 (2H, t, J = 4.2, OCH_2), 4.45 (2H, d, J = 3.4 Hz, COOCH_2), 6.32 (1H, d, J = 9.6, Ar-H), 6.90 (2H, m, Ar-H), 7.61 (10H, m, Ar-H), 8.00 (1H, d, J = 9.6, Ar-H); δ_C (100 MHz, DMSO-d_6) 19.4, 45.1, 63.6, 67.3, 102.2, 113.4, 113.5, 113.6, 129.3, 129.4, 129.7, 130.3, 130.4, 132.6, 133.6, 137.8, 138.0, 141.8, 145.1, 156.2, 161.1, 162.1, 174.5, 196.5 ; ESI-HRMS (m/z) $[M+H]^+$: calculated for $C_{27}H_{23}O_6$ 443.1489; found 443.1486.

Synthesis of (±)-2-((2-oxo-2H-chromen-7-yl)oxy)ethyl 2-(4-isobutylphenyl)propanoate **(B13)**

Compound **B13** was obtained according to the general procedure earlier reported adding EDCI·HCl (1.2 eq.) and DMAP (0.03 eq.) to a solution of (±)-ibuprofen **A4** (0.17 g, 1.0 eq.) and 7-(2-hydroxyethoxy)-2H-chromen-2-one **B2** (0.2 g, 1.0 eq.) in dry DMF (3.0 mL). The reaction mixture was purified by silica gel column chromatography eluting with EtOAc/n-hexane 50% *v/v* to afford the titled compound **B13** as an oil.

(±)-2-((2-Oxo-2H-chromen-7-yl)oxy)ethyl 2-(4-isobutylphenyl)propanoate B13: 57% yield; m.p. 96-98°C; silica gel TLC R_f 0.57 (ethyl acetate/*n*-hexane 50% *v/v*); δ_H (400 MHz, DMSO-d_6) 0.83 (6H, d, J = 6.8, 2 x CH_3), 1.40 (3H, d, J = 7.2, CH_3), 1.74 (1H, dp,

J = 13.5, 6.8, $CH(CH_3)_2$), 2.39 (2H, d, *J* = 6.8, CH_2), 3.81 (1H, q, *J* = 7.2, $CHCH_3$), 4.28 (2H, t, *J* = 4.4, OCH_2), 4.42 (2H, q, *J* = 3.6, $COOCH_2$), 6.33 (1H, d, *J* = 9.6, Ar-*H*), 6.93 (1H, dd, *J* = 8.4 3.6, Ar-*H*), 6.98 (1H, d, *J* 2.4, Ar-*H*), 7.06 (2H, d, *J* = 8.0, Ar-*H*), 7.19 (2H, d, *J* = 8.0, Ar-*H*), 7.65 (1H, d, *J* = 8.8, Ar-*H*), 8.03 (1H, d, *J* = 9.6, Ar-*H*); δ_C (100 MHz, DMSO-d_6) 15.0, 19.4, 23.0, 30.5, 44.9, 63.4, 67.4, 102.3, 113.5, 113.6, 127.9, 129.9, 130.4, 138.6, 140.6, 145.2, 156.2, 156.3, 161.2, 162.2, 174.8; ESI-HRMS (m/z) $[M+H]^+$: calculated for $C_{24}H_{27}O_5$ 395.1853; found 395.1849.

Synthesis of 2-((2-oxo-2H-chromen-7-yl)oxy)ethyl 2-(2-((2,6-dichlorophenyl)amino)phenyl)acetate **(B14)**

Compound **B14** was obtained according to the general procedure earlier reported adding EDCI·HCl (1.8 eq.) and DMAP (0.03 eq.) to a solution of diclofenac **A5** (0.6 g, 1.0 eq.) and 7-(2-hydroxyethoxy)-2H-chromen-2-one **B2** (0.25 g, 1.0 eq.) in dry DMF (3.0 mL). The crude residue was purified by silica gel column chromatography eluting with EtOAc/n-hexane 30% *v/v* to afford **B14** as a white solid.

2-((2-Oxo-2H-chromen-7-yl)oxy)ethyl 2-(2-((2,6-dichlorophenyl)amino)phenyl)acetate B14: 38% yield; m.p. 173-175°C; silica gel TLC R_f 0.36 (ethyl acetate/*n*-hexane 40% *v/v*); δ_H (400 MHz, DMSO-d_6) 3.89 (2H, s, $COCH_2$), 4.38 (2H, m, OCH_2), 4.49 (2H, m, $COOCH_2$), 6.28 (1H, d, *J* = 8.0, Ar-*H*), 6.34 (1H, d, *J* = 9.6, Ar-*H*), 6.86 (1H, m, Ar-*H*), 6.97 (1H, dd, *J* = 8.6, 2.4, Ar-*H*), 7.06 (3H, m, Ar-*H*), 7.23 (2H, dd, *J* = 11.1, 5.0, Ar-*H*), 7.54 (2H, d, *J* = 8.0, Ar-*H*), 7.65 (1H, d, *J* = 8.6, Ar-*H*), 8.02 (1H, d, *J* = 9.6, Ar-*H*); δ_C (100 MHz, DMSO-d_6) 37.8, 63.8, 67.4, 102.2, 113.4, 113.5, 113.6, 116.7, 121.5, 123.9, 126.8, 128.7, 130.0, 130.4, 131.7, 131.8, 138.0, 143.8, 145.2, 156.2, 161.2, 162.2, 172.4; ESI-HRMS (m/z) $[M+H]^+$: calculated for $C_{25}H_{20}Cl_2NO_5$ 484.0713; found 484.0704.

Synthesis of (±)-2-((2-oxo-2H-chromen-7-yl)oxy)ethyl 2-(2-fluoro-[1,1'-biphenyl]-4-yl)propanoate **(B15)**

Compound **B15** was obtained according to the general procedure earlier reported adding EDCI·HCl (1.5 eq.) and DMAP (0.03 eq.) to a solution of (±)-flurbiprofen **A6** (0.17 g, 1.0 eq.) and 7-(2-hydroxyethoxy)-2H-chromen-2-one **B2** (0.2 g, 1.0 eq.) in dry DMF (3.0

mL). The reaction mixture was purified by silica gel column chromatography eluting with EtOAc/n-hexane 50% *v/v* to afford the titled compound **B15** as a colourless oil.

(±)-2-((2-Oxo-2H-chromen-7-yl)oxy)ethyl 2-(2-fluoro-[1,1'-biphenyl]-4-yl)propanoate B15: 67% yield; m.p. 111-113°C; silica gel TLC R_f 0.56 (ethyl acetate/*n*-hexane 50% *v/v*); δ_H (400 MHz, DMSO-d_6) 1.47 (3H, d, J = 7.1, CH_3), 3.97 (1H, q, J = 7.1, CHCH$_3$), 4.32 (2H, t, J = 4.4, OCH_2), 4.47 (2H, m, COOCH_2), 6.32 (1H, d, J = 9.6, Ar-*H*), 6.94 (1H, dd, J = 8.6, 2.4, Ar-*H*), 7.00 (1H, d, J = 2.4, Ar-*H*), 7.25 (2H, m, Ar-*H*), 7.46 (6H, m, Ar-*H*), 7.64 (1H, d, J = 8.6, Ar-*H*), 8.00 (1H, d, J = 9.6, Ar-*H*); δ_C (100 MHz, DMSO-d_6) 19.2, 44.8, 63.6, 67.4, 102.2, 113.4, 113.5 ($J^4_{C\text{-}F}$ 8), 115.9, 116.1, 124.8 ($J^3_{C\text{-}F}$ = 3), 127.7 ($J^2_{C\text{-}F}$ = 13), 128.7, 129.5, 129.6 ($J^3_{C\text{-}F}$ = 3), 130.5, 131.6 ($J^3_{C\text{-}F}$ = 3), 135.7, 143.0 ($J^2_{C\text{-}F}$ = 8), 145.1, 156.2, 158.5 ($J^1_{C\text{-}F}$ = 245), 161.2, 162.2, 174.2; δ_F (376 MHz, DMSO-d_6) -118.30 (1F, s); ESI-HRMS (m/z) $[M+H]^+$: calculated for $C_{26}H_{22}FO_5$ 433.1446; found 433.1440.

Synthesis of (S)-(+)-2-((2-oxo-2H-chromen-7-yl)oxy)ethyl 2-(6-methoxynaphthalen-2-yl)propanoate **(B16)**

Compound **B16** was obtained according to the general procedure earlier reported adding EDCI·HCl (1.2 eq.) and DMAP (0.03 eq.) to a solution of (*S*)-(+)-naproxen **A7** (0.175 g, 1.0 eq.) and 7-(2-hydroxyethoxy)-2H-chromen-2-one **B2** (0.2 g, 1.0 eq.) in dry DMF (2.0 mL). The crude residue was purified by silica gel column chromatography eluting with EtOAc/n-hexane 50% *v/v* to afford the titled compound **B16** as a white solid.

(S)-(+)-2-((2-Oxo-2H-chromen-7-yl)oxy)ethyl 2-(6-methoxynaphthalen-2-yl)propanoate B16: 63% yield; m.p. 123-125°C; silica gel TLC R_f 0.64 (ethyl acetate/*n*-hexane 60% *v/v*); δ_H (400 MHz, DMSO-d_6) 1.50 (3H, d, J = 7.2, CH_3), 3.88 (3H, s, OCH_3), 3.95 (1H, q, J = 7.1, CH), 4.29 (2H, m, OCH_3), 4.43 (2H, dd, J = 3.4, 5.4, OCH_2), 6.32 (1H, d, J = 9.6, Ar-*H*), 6.87 (1H, dd, J = 3.6, 8.6, Ar-*H*), 6.93 (1H, d, J = 2.0, Ar-*H*), 7.13 (1H, dd, J = 3.8, 8.8, Ar-*H*), 7.27 (1H, d, J = 2.4, Ar-*H*), 7.39 (1H, dd, J = 3.3, 8.5, Ar-*H*), 7.59 (1H, d, J = 8.8, Ar-*H*), 7.74 (3H, m, Ar-*H*), 8.01 (1H, d, J = 9.0, Ar-*H*); δ_C (100 MHz, DMSO-d_6) 19.4, 45.3, 56.0, 63.5, 67.4, 102.2, 106.6, 113.4, 113.5, 113.6, 119.6, 126.4, 127.1, 127.8, 129.3, 129.9, 130.3, 134.2, 136.4, 145.1, 156.1, 158.1, 161.1, 162.1, 174.8; ESI-HRMS (m/z) $[M+H]^+$: calculated for $C_{25}H_{23}O_6$ 419.1489; found 419.1497.

5.2.2 Carbonic Anhydrase Inhibition

The CA inhibitory profiles of compounds belonging to Series B were obtained according to the general procedures described at the beginning of the experimental section.

5.2.3 Drug stability study

5.2.3.1 Chemicals

Acetonitrile (Chromasolv), formic acid (MS grade), NaCl, KCl, Na_2HPO_4 $2H_2O$, KH_2PO_4 (Reagent grade) and verapamil hydrochloride (analytical standard, used as internal standard), ketoprofen and enalapril (analytical standard) were purchased by Sigma-Aldrich (Milan, Italy). Ketoprofen Ethyl Ester (KEE) were obtained by Fisher's reaction from ketoprofen and ethanol. MilliQ water 18 MΩ cm was obtained from Millipore's Simplicity system (Milan - Italy).
Phosphate buffer solution (PBS) was prepared by adding 8.01 g L^{-1} of NaCl, 0.2 g L^{-1} of KCl, 1.78 g L^{-1} of Na_2HPO_4 $_2H_2O$ and 0.27 g L^{-1} of KH_2PO_4. Human plasma was collected from healthy male volunteer and the rat plasma was collected from Sprague Dawley male rats; each plasma batch was kept at -80 °C until use.

5.2.3.2 Instrumental

The LC-MS/MS analysis was carried out using a Varian 1200L triple quadrupole system (Palo Alto, CA, USA) equipped by two Prostar 210 pumps, a Prostar 410 autosampler and an Elettrospray Source (ESI) operating in positive ions. Raw-data were collected and processed by Varian Workstation vers. 6.8 software.
G-Therm 015 thermostatic oven was used to maintain the samples at 37 °C during the degradation test. ALC micro centrifugate 4214 was employed to centrifuge plasma samples.

5.2.3.3 Standard solutions and calibration curves

Stock solutions of analytes and verapamil hydrochloride (internal standard or ISTD) were prepared in acetonitrile at 1.0 mg mL^{-1} and stored at 4 °C. Working solutions of each analyte were freshly prepared by diluting stock solutions up to a concentration of 1.0 µg mL^{-1} and 0.1 µg mL^{-1} (working solution 1 and 2 respectively) in mixture of mQ water: acetonitrile 50:50 (*v/v*). The ISTD working solution was prepared in acetonitrile at 33.3 µg mL^{-1} (ISTD solution). The spiked solutions of each analyte were prepared separately, by diluting the respective stock solutions in mQ water:acetonitrile 80:20 (*v/v*) solution, to obtain a final concentration of 10 µM.

A six-level calibration curve was prepared by adding proper volumes of working solution (1 or 2) of each analyte to 300 µL of ISTD solution. The obtained solutions were dried under a gentle nitrogen stream and dissolved in 1.0 mL of 10 mM of formic acid in mQ water:acetonitrile 80:20 (*v/v*) solution. Final concentrations of calibration levels were: 2.5, 5.0, 10.0, 25.0, 50.0 and 100.0 ng mL-1 of analyte in the sample.

All calibration levels were analysed six times by LC-MS/MS system with the appropriate conditions.

The calibration curve parameters (slope, intercept and R2), limit of detection (LOD) and quantitation (LOQ) obtained for each tested compound did not reported in the thesis.

5.2.3.4 LC-MS/MS methods

The chromatographic parameters employed to analyse the samples were tuned to minimize the run time. The column used was a Pursuit XRs C18 30 mm length, 2 mm internal diameter and 3 µm particle size, at constant flow of 0.25 mL min^{-1}, employing a binary mobile phases elution gradient. The solvents used were 10 mM formic acid in water solution (solvent A) and 10 mM formic acid in acetonitrile (solvent B) according to the elution gradient as follows: initial at 90 % solvent A, which was then decreased to 10 % in 4.0 min, kept for 3.0 min, returned to initial conditions in 0.1 min and maintained for 3.0 min for reconditioning, to a total run time of 10.0 min.

The column temperature was maintained at 30 °C and the injection volume was 5 µL. The ESI source was operated in positive ion mode, using the following setting: 5 kV needle,

42 psi nebulizing gas, 600 V shield and 20 psi drying gas at 280 °C. The analyses were acquired in Multiple Reaction Monitoring (MRM) using 50 ms of dwell time.

5.2.3.5 Sample preparation

The sample was prepared adding 10 µL of spiked solution to 100 µL of tested matrix (PBS or human plasma or rat plasma) in microcentrifuge tubes. The obtained solutions correspond to 1 µM of analyte.
Each set of samples was incubated in triplicate at four different times 0, 30, 60 and 120 min at 37 °C. Therefore, the matrix stability profile of each analyte was represented by a batch of 12 samples (4 incubation times x 3 replicates). After the incubation, the samples were added with 300 µL of ISTD solution and centrifuged (room temperature for 5 min at 10000 rpm). The supernatants were transferred in autosampler vials and dried under a gentle stream of nitrogen. The dried samples were dissolved in 1.0 mL of 10 mM of formic acid in mQ water:acetonitrile 80:20 solution.
Following the procedure described above, the expected concentrations of the samples ranging about 40-50 ng mL^{-1} (depends by the MW of considered analyte), values on which the calibration curve was centered.

5.2.4 *In vitro* anti-inflammatory studies

The murine macrophage cell line RAW 264.7 was used to evaluated PGE_2 production. The cells were cultured in Dulbecco's modified Eagle's medium (DMEM) supplemented with 10% fetal bovine serum (FBS) and 1% penicillin (10000 IU/mL)-streptomycin (10000 µg/mL) at 37°C in a humidified incubator containing 5% CO_2. The cells were left to acclimate for 24h before any treatment.

5.2.4.1 Lipopolysaccharide induced inflammation in RAW264.7 and determination of PGE_2 production

RAW 264.-7 macrophage cell line ($2x10^4$cells/well) were cultivated on 12-well plates and treated with 100 nM, 1µM, 10 µM and 100 µM of each compound. One hour before the

cells were challenged with 1 μg/mL of *Escherichia coli* lipopolysaccharide (LPS) to induce inflammation.[288] At the end of the treatment, 18 hours later, cell-free supernatants were harvested, and cell lysates collected and stored at -80°C for further experiments. The concentrations of PGE_2 in the supernatants of RAW 264.7 cell cultures were determined using a PGE_2 ELISA kit (Cayman Chemical, Ann Arbor, MI, USA), according to the manufacturer's instructions.

5.2.4.2 Human platelet-rich plasm

Human platelet-rich plasma (PRP) was obtained from human whole blood from healthy donors, who signed an informed consent. The blood draw occurs with the addition of the anticoagulant citrate dextrose A (1:10 *v/v*) to prevent platelet activation prior to its use.
PRP was prepared with a process known as differential centrifugation, where acceleration force is adjusted to sediment certain cellular constituents based on different specific gravity.[289] Briefly, an initial centrifugation to separate red blood cells (RBC) was followed by a second centrifugation to concentrate platelets, which were suspended in the smallest final plasma volume. The first spin step was performed at constant acceleration to separate RBCs from the remaining WB volume. After the first spin step, the WB separates into three layers: an upper layer that contains mostly platelets and WBC, an intermediate thin layer that is known as the buffy coat and that is rich in WBCs, and a bottom layer that consists mostly of RBCs. For the production of pure PRP, upper layer and superficial buffy coat were transferred to an empty sterile tube. The second spin step was performed with an adequate *g* to obtain a soft pellet (erythrocyte platelet) at the bottom of the tube. The upper portion of the volume that is composed mostly of platelet poor plasma (PPP) was removed. Pellets are homogenized in lower 1/3rd (5 ml of plasma) to create the PRP.

5.2.4.3 Platelet aggregation

Turbidimetric platelet aggregation (PA) was used to measure agonist-induced PA. Platelet-rich plasma was stimulated with 10 μM ADP (Mascia Brunelli, Milan, Italy) using an APACT 4 aggregometer (Helena Laboratories Italia S.P.A, Milan, Italy).

Platelet aggregation was evaluated, according to Born's method, considering the maximal percentage of platelet aggregation in response to stimulus (ADP-PA) after 5 min, both in presence and in absence of the studied compounds at a concentration of 100 μM.[289] Platelet aggregation baseline: 77.74%, corresponding to 100% of aggregation.

5.2.4.4 Statistical Analysis

Data were reported as mean % of four independent experiments for inhibition of platelet aggregation study and mean values (± SEM) of eight independent experiments for PgE_2 production analysis. Significance of differences among the groups was assessed by one-way ANOVA followed by Newman-Keuls post hoc test for multiple comparisons. Calculations were made with Prism 5 statistical software (GraphPad Software, Inc., San Diego, CA, USA). The results were considered to be statistically significant when $p<0.05$.

5.2.5 *In silico* studies

The primary sequence of the human COX-1 was retrieved from UniProt. The crystal structures of ovine COX-1 (1HT5)[180] was downloaded from the Protein Data Bank and used as template in the homology modelling procedure. Prime module of the Schrödinger suite was used in the sequence alignment and model building procedures.[290a] Then, the models were submitted to loop refinements and the quality checked by the analysis of the Ramachandran plots and by the evaluation of the QMEAN value.

COX-1 (homology model) and COX-2 (5KIR)[180] were prepared using the Protein Preparation Wizard tool implemented in Maestro - Schrödinger suite, assigning bond orders, adding hydrogens, deleting water molecules, and optimizing H-bonding networks.[290] Energy minimization protocol with a root mean square deviation (RMSD) value of 0.30 was applied using an Optimized Potentials for Liquid Simulation (OPLS3e) force field. 3D ligand structures were prepared by Maestro [290b] and evaluated for their ionization states at pH 7.4 ± 0.5 with Epik.[290c] Uniquely the *S*-enantiomer (eutomer) of ibuprofen and ketoprofen was considered. OPLS3e force field in Macromodel [290d] was used for energy minimization for a maximum number of 2500 conjugate gradient

iteration and setting a convergence criterion of 0.05 kcal $mol^{-1}Å^{-1}$. The docking grid was centred on the center of mass of the co-crystallized ligands and Glide used with default settings. Ligands were docked with the standard precision mode (SP) of Glide [290e] and the best 5 poses of each molecule retained as output. The best pose for each compound, evaluated in terms of coordination, hydrogen bond interactions and hydrophobic contacts, was refined with Prime [290a] with a VSGB solvation model considering the target flexible within 3Å around the ligand.

The best scored binding poses of **B5** and **B12** to CA IX were submitted to a MD simulation using Desmond[291] and the OPL3e force field. Specifically, the system was solvated in an orthorhombic box using TIP4PEW water molecules, extended 15 Å away from any protein atom. It was neutralized adding a concentration of 0.15 M chlorine and sodium ions. The simulation protocol included a starting relaxation step followed by a final production phase of 50 ns. In particular, the relaxation step comprised the following: (a) a stage of 100 ps at 10 K retaining the harmonic restraints on the solute heavy atoms (force constant of 50.0 kcal mol^{-1} $Å^{-2}$) using the NPT ensemble with Brownian dynamics; (b) a stage of 12 ps at 10 K with harmonic restraints on the solute heavy atoms (force constant of 50.0 kcal mol^{-1} $Å^{-2}$), using the NVT ensemble and Berendsen thermostat; (c) a stage of 12 ps at 10 K and 1 atm, retaining the harmonic restraints and using the NPT ensemble and Berendsen thermostat and barostat; (f) a stage of 12 ps at 300 K and 1 atm, retaining the harmonic restraints and using the NPT ensemble and Berendsen thermostat and barostat; (g) a final 24 ps stage at 300 K and 1 atm without harmonic restraints, using the NPT Berendsen thermostat and barostat. The final production phase of MD was run using a canonical the NPT Berendsen ensemble at temperature 300 K. During the MD simulation, a time step of 2 fs was used while constraining the bond lengths of hydrogen atoms with the M-SHAKE algorithm. The atomic coordinates of the system were saved every 100 ps along the MD trajectory. Protein RMSD, ligand RMSD/RMSF, ligand torsions evolution and occupancy of intermolecular hydrogen bonds and hydrophobic contacts were investigated along the production phase of the MD simulation with the Simulation Interaction Diagram tools implemented in Maestro.

5.2.6 *In vivo* anti-hyperalgesic studies

The *in vivo* anti-hyperalgesic protocols are described in paragraph 5.1.3.

5.2.6.1 Administration of compounds

Compounds **B5** (3 – 30 mg kg^{-1}), **B12** (30 mg kg^{-1}) and **A30** (10 mg kg^{-1}) were suspended in a 1% solution of carboxymethylcellulose sodium salt (CMC) and acutely *per os* administered starting from day 14 after CFA intra-articular (i.a.) injection. Ketoprofen (30 mg kg^{-1}) and ibuprofen (100 mg kg^{-1}) were used as reference drug. The anti-hypersensitivity effects were evaluated over time by Paw pressure test and Incapacitance test.

5.3 Discovery of β-adrenergic receptors blocker - carbonic anhydrase inhibitor hybrids for multitargeted anti-glaucoma therapy (Series C)

5.3.1 Chemistry

The general chemistry protocols are reported at the beginning of the experimental section.

Synthesis of 4-acetoxybenzoic acid **(C2)**[292]

A suspension of 4-hydroxy benzoic acid **C1** (1.0 g, 1.0 eq.) in Ac_2O (5 ml, 7.3 eq.) was treated with four drops of H_2SO_4 95% and the obtained solution was stirred 3h at 60°C under a nitrogen atmosphere. The reaction mixture was cooled to r.t., quenched with slush (50g) and then stirred for 1.5 h to obtain a white precipitate, that was filtered and washed with water to afford the titled compound **C2**.

4-Acetoxybenzoic acid C2: 82% yield; silica gel TLC R_f 0.23 (EtOAc/*n*-Hex 50 % *v/v*); δ_H (400 MHz, DMSO-d_6): 2.34 (s, 3H, CH_3), 7.30 (d, J = 8.8, 2H, Ar), 8.02 (d, J = 8.8, 2H, Ar), 13.05 (bs, 1H, exchange with D_2O, COO*H*); δ_C (100 MHz, DMSO-d_6): 21.8, 123.0, 129.3, 131.8, 154.9, 167.6, 169.8.

Synthesis of 4-(2-(4-acetoxybenzamido)ethyl)benzenesulfonamide **(C4)**[293]

Oxalyl chloride (4.15 eq.) and DMF (0.02 eq.) were added to a solution 4-acetoxy benzoic acid **C2** (0.9 g, 1.0 eq.) in CH_2Cl_2 (18 ml), under a nitrogen atmosphere. The reaction mixture was stirred 0.5 h at r.t. and at reflux temperature for 2.5 h. The volatiles were removed under vacuum and the obtained viscous oil is dissolved in DMA (4 ml). Pyridine (10.0 eq) and 4-(2-aminoethyl)-benzensulfonamide **C3** (1.05 eq) were added to the obtained solution under a nitrogen atmosphere, the reaction mixture was stirred for 1h at r.t. and then was quenched with slush (30g). The pH was taken to 2 with HCl 6M, at ice bath temperature to obtain a precipitate that was filtered and washed with water and Et_2O to afford the titled compound **C4**.

4-(2-(4-Acetoxybenzamido)ethyl)benzenesulfonamide C4: 83% yield; silica gel TLC R_f 0.30 (MeO*H*/DCM 10 % *v/v*); δ_H (400 MHz, DMSO-d_6): 2.32 (s, 3H, CH_3), 2.97 (t, J = 7.2, 2H, CH_2), 3.55 (q, J = 7.2, 2H, CH_2), 7.25 (d, J = 8.4, 2H, Ar), 7.32 (s, 2H, exchange with D_2O, SO_2NH_2), 7.47 (d, J = 8.0, 2H, Ar), 7.78 (d, J = 8.0, 2H, Ar), 7.89

(d, *J* = 8.4, 2H, Ar), 8.64 (t, *J* = 5.2, 1H, N*H*CO); δ_C (100 MHz, DMSO-d_6): 21.8, 35.7, 41.4, 122.6, 126.6, 129.5, 130.1, 133.0, 143.0, 144.7, 153.5, 166.4, 169.9.

Synthesis of 4-Hydroxy-N-(4-sulfamoylphenethyl)benzamide **(C5)**[293]

4-(2-(4-Acetoxybenzamido)ethyl) benzenesulfonamide **C4** (1.35 g, 1.0 eq.) was added to a freshly prepared solution of sodium (1.0 eq.) in dry methanol (40 ml) under a nitrogen atmosphere and the resulting solution was stirred for 2h at r.t. The reaction mixture was quenched with slush (40 g) and acidified to pH 1-2 with HCl 6M, to obtain a precipitate that was filtered and washed with water and Et_2O to afford the titled compound **C5**.

4-Hydroxy-*N*-(4-sulfamoylphenethyl)benzamide C5: 82% yield; silica gel TLC R_f 0.22 (MeOH/DCM 10 % *v/v*); δ_H (400 MHz, DMSO-d_6): 2.94 (t, *J* = 7.2, 2H, CH_2), 3.51 (q, *J* = 7.2, 2H, CH_2), 6.81 (d, *J* = 8.8, 2H, Ar), 7.31 (s, 2H, exchange with D_2O, SO_2NH_2), 7.45 (d, *J* = 8.8, 2H, Ar), 7.71 (d, *J* = 8.8, 2H, Ar), 7.77 (d, *J* = 8.8, 2H, Ar), 8.35 (t, *J* = 5.2, 1H, N*H*CO), 9.97 (s, 1H, exchange with D_2O, O*H*); δ_C (100 MHz, DMSO-d_6): 35.9, 41.3, 115.7, 126.2, 126.7, 130.0, 130.1, 143.0, 144.9, 161.0, 166.9.

Synthesis of N-{2-[4-(1-dimethylamino-ethylidenesulfamoyl)-phenyl]-ethyl}-4-hydroxy-benzamide **(C6)**

N,N-Dimethylformamide dimethyl acetal (2.0 eq.) was added to a solution of 4-(2-(4-hydroxybemzamido)ethyl)benzenesulfonamide **C5** (0.94 g, 1.0 eq.) in DMF (5 ml) cooled to 0°C. The reaction mixture was stirred 20' at r.t. and then quenched with H_2O (40 ml) to obtain a precipitate, that was filtered and washed with water and Et_2O to afford the titled compound **C6**.

***N*-{2-[4-(1-Dimethylamino-ethylidenesulfamoyl)-phenyl]-ethyl}-4-hydroxy-benzamide C6:** 84% yield; silica gel TLC R_f 0.30 (MeOH/DCM 10 % *v/v*); δ_H (400 MHz, DMSO-d_6): 2.92 (m, 5H, CH_2 + CH_3), 3.17 (s, 3H, CH_3), 3.50 (q, *J* = 6,8 , 2H, CH_2), 6.81 (d, *J* = 8.8, 2H, Ar), 7.41 (d, *J* = 8.8, 2H, Ar), 7.71 (m, 4H, Ar), 8.23 (s, 1H), 8.35 (t, *J* = 5.2, 1H, N*H*CO), 9.97 (s, 1H, exchange with D_2O, O*H*); δ_C (100 MHz, DMSO-d_6): 35.8, 35.9, 41.3, 41.8, 115.7, 126.2, 126.9, 129.9, 130.1, 141.8, 144.8, 160.6, 161.0, 166.9.

Synthesis of 4-allyloxy-N-{2-[4-(1-dimethylamino-ethylidenesulfamoyl)-phenyl]-ethyl}-benzamide **(C7)**

K_2CO_3 (2.0 eq.) and allyl bromide (1.2 eq.) were added to a solution of N-{2-[4-(1-dimethylamino-ethylidenesulfamoyl)-phenyl]-ethyl}-4-hydroxy-benzamide **C6** (1.0 g, 1.0 eq) in dry DMA (4 ml) under a nitrogen atmosphere. The suspension was stirred for 1.5h at 50°C and then quenched with water (40 ml). The obtained solid was filtered and purified by silica gel chromatography eluting with 10% MeOH/DCM to afford the titled compound **C7**.

4-Allyloxy-*N*-{2-[4-(1-dimethylamino-ethylidenesulfamoyl)-phenyl]-ethyl}-benzamide C7: 74% yield; silica gel TLC R_f 0.50 (MeOH/DCM 10 % *v/v*); δ_H (400 MHz, DMSO-d_6): 2.93 (m, 5H, CH_2 + CH_3), 3.17 (s, 3H, CH_3), 3.51 (q, J = 6,8 , 2H, CH_2), 4.65 (d, J = 5.2, 2H, CH_2), 5.31 (dd, J = 1.6, 10.4, 1H, C*H*), 5.44 (dd, J = 2, 17.4, 1H, C*H*), 6.08 (m, 1H, C*H*), 7.02 (d, J = 8.4, 2H, Ar), 7.42 (d, J = 8.8, 2H, Ar), 7.72 (d, J = 8.4, 2H, Ar), 7.82 (d, J = 8.8, 2H, Ar), 8.24 (s, 1H), 8.46 (t, J = 5.2, 1H, N*H*CO); δ_C (100 MHz, DMSO-d_6): 35.8, 35.9, 41.3, 41.8, 69.2, 115.1, 118.6, 126.9, 127.8, 129.8, 130.1, 134.3, 141.8, 144.7, 160.6, 161.3, 166.6.

Synthesis of N-{2-[4-(1-dimethylamino-ethylidenesulfamoyl)-phenyl]-ethyl}-4-oxiranylmethoxy-benzamide **(C8)**[294]

$NaHCO_3$ (3.5 eq.) and oxone (1.0 eq.) were added to a solution of 4-allyloxy-N-{2-[4-(1-dimethylamino-ethylidenesulfamoyl)-phenyl]-ethyl}-benzamide **C7** (1.60 g, 1.0 eq.) in a mixture aceton/water 3:2 (40 ml) at 0°C and the resulting suspension was stirred 15' at the same temperature. Additional $NaHCO_3$ (3.5 eq.) and oxone (1.0 eq.) were added and the temperature was raised to r.t. The reaction mixture was stirred at r.t. for 4h, then the temperature was reduced again to 0°C and other two portions of $NaHCO_3$ (3.5 eq. x 2) and oxone (1.0 eq. x 2) were added, the second 15' after the first. The reaction mixture stirred at r.t. for 18h, then filtered to remove the undissolved salts and treated with an aqueous solution of $Na_2S_2O_4$ (5.0 eq.). The obtained suspension was concentrated in vacuum and then extracted with ethyl acetate (4 x 25 ml). The combined organic layers were dried over anhydrous Na_2SO_4 and concentrated under reduced pressure to give a residue purified by silica gel chromatography eluting with 10% MeOH/DCM to afford the titled compound **C8**.

***N*-{2-[4-(1-Dimethylamino-ethylidenesulfamoyl)-phenyl]-ethyl}-4-oxiranylmethoxy-benzamide C8:** 76% yield; silica gel TLC R_f 0.50 (MeOH/DCM 10 % *v/v*); δ_H (400 MHz, DMSO-d_6): 2.76 (dd, *J* = 2.6, 5.2, 1H, C*H*), 2.89 (t, *J* = 4.8, 1H, C*H*), 2.92 (m, 5H, CH_3 + CH_2), 3.17 (s, 3H, CH_3), 3.38 (m, 1H, C*H*), 3.52 (q, *J* = 6,8 , 2H, CH_2), 3.93 (dd, *J* = 6.6, 11.4, 1H, C*H*), 4.43 (dd, *J* = 2.7, 11.4, 1H, C*H*), 7.05 (d, *J* = 8.8, 2H, Ar), 7.42 (d, *J* = 8.4, 2H, Ar), 7.72 (d, *J* = 8.4, 2H, Ar), 7.82 (d, *J* = 8.8, 2H, Ar), 8.24 (s, 1H), 8.46 (t, *J* = 5.2, 1H, N*H*CO); δ_C (100 MHz, DMSO-d_6): 35.8, 35.9, 41.3, 41.8, 44.7, 50.5, 70.0, 114.9, 126.9, 128.0, 129.8, 130.1, 141.8, 144.7, 160.6, 161.4, 166.6.

*General synthetic procedure **6** of compounds 4-(3-alkylamino-2-hydroxy-propoxy)-N-[2-(4-sulfamoyl-phenyl)-ethyl]-benzamide **C9-18**, **C22-29***[295,296]

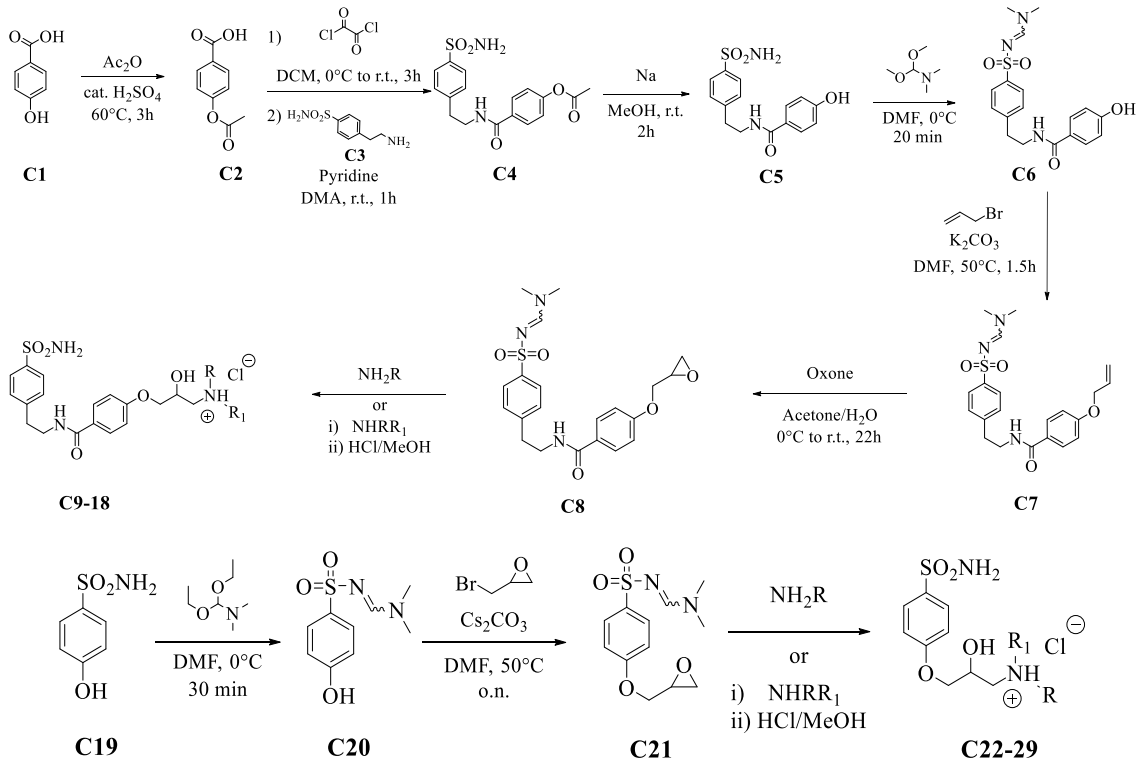

Procedure 6.1

The proper epoxide **C8** or **C21** (0.25 g, 1.0 eq.) was suspended in variable volume of primary amine or, alternatively in EtOH and treated with the appropriate primary amine (10 eq.), and the reaction mixture was stirred at r.t. or under heating until starting materials were consumed (TLC monitoring). EtOH and excess of amine were removed under vacuum and the residue was triturated with water (**C9-16**) or with Et_2O (**C22-26**).

A solution of the obtained deprotected free base in HCl 1.25M in MeOH was stirred at r.t. for 20' and then concentrated under vacuum to give a residue that was triturated with aceton to give the titled compounds **C9-16**, **C22-26**.

Procedure 6.2

The proper secondary amine (3 eq.) was added to a suspension of the proper epoxide **C8** or **C21** (0.25 g, 1.0 eq.) in EtOH (8 ml) and reaction mixture stirred at 70°C until starting materials were consumed (TLC monitoring). EtOH and excess of amine were removed under vacuum and the obtained residue was triturated with water (**C17-18**) or with Et_2O (**C27-29**). A solution of the resulting protected free base in HCl 1.25 in MeOH was stirred at 80 °C in a sealed tube until starting materials were consumed (TLC monitoring). The solvent was removed under vacuum and the obtained residue was triturated with aceton to give the titled compounds **C17-18**, **C27-29**.

Synthesis of 4-(2-hydroxy-3-methylamino-propoxy)-N-[2-(4-sulfamoyl-phenyl)-ethyl]-benzamide hydrochloride **(C9)**

Compound **C9** was obtained according the general **procedure 6.1** earlier reported. N-{2-[4-(1-Dimethylamino-ethylidenesulfamoyl)-phenyl]-ethyl}-4-oxiranylmethoxy-benzamide **C8** (0.25 g, 1.0 eq.) was suspended in EtOH and treated with a 35% aqueous solution of methylamine overnight at r.t. and then the obtained free base was treated with HCl 1.25M in MeOH (10 ml) to afford the corresponding hydrochloride salt **C9**.

4-(2-Hydroxy-3-methylamino-propoxy)-*N*-[2-(4-sulfamoyl-phenyl)-ethyl]-benzamide hydrochloride C9: 55% yield; silica gel TLC R_f 0.10 (TFA/MeO*H*/DCM 3/15/82% *v/v*); δ_H (400 MHz, DMSO-d_6): 2.64 (m, 3H, CH_3), 2.95 (t, J = 6.8, 2H, CH_2), 3.03 (m, 1H, C*H*), 3.15 (m, 1H, C*H*), 3.53 (q, J = 7.2, 2H, CH_2), 4.05 (d, J = 5.2, 2H, CH_2), 4.21 (m, 1H, C*H*), 5.95 (bs, 1H, exchange with D_2O, O*H*), 7.04 (d, J = 8.8, 2H, Ar), 7.33 (s, 2H, exchange with D_2O, SO_2NH_2), 7.46 (d, J = 8.4, 2H, Ar), 7.78 (d, J = 8.4, 2H, Ar), 7.85 (d, J = 8.8, 2H, Ar), 8.53 (t, J = 5.6, 1H, CON*H*), 8.73 (bd, exchange with D_2O, 2H, NH_2^+); δ_C (100 MHz, DMSO-d_6): 33.93, 35.78, 41.31, 51.79, 65.62, 70.78, 114.98, 126.61, 127.98, 129.89, 130.06, 142.95, 144.79, 161.42, 166.56; *m/z* (ESI positive) 408.2 $[M\text{-}Cl^-]^+$

Synthesis of 4-(2-hydroxy-3-(methylamino)propoxy)-N-(4-sulfamoylphenethyl)benzamide hydrochloride **(C10)**

Compound **C10** was obtained according the general **procedure 6.1** earlier reported. N-{2-[4-(1-Dimethylamino-ethylidenesulfamoyl)-phenyl]-ethyl}-4-oxiranylmethoxy-benzamide **C8** (0.25 g, 1.0 eq.) was treated with ethylamine in EtOH overnight at r.t. and then the obtained free base was treated with HCl 1.25M in MeOH (10 ml) to afford the corresponding hydrochloride salt **C10**.

4-(2-Hydroxy-3-(methylamino)propoxy)-N-(4-sulfamoylphenethyl)benzamide hydrochloride C10: 54% yield; silica gel TLC R_f 0.15 (TFA/MeO*H*/DCM 3/15/82% *v/v*);δ_H (400 MHz, DMSO-d_6): 1.27 (t, J = 7.2, 3H, CH_3), 2.95 (t, J = 6.8, 2H, CH_2), 3.03 (m, 3H, C*H* + CH_2), 3.17 (m, 1H, C*H*), 3.52 (q, J = 7.2, 2H, CH_2), 4.06 (d, J = 5.2, 2H, CH_2), 4.22 (m, 1H, C*H*), 5.95 (bs, 1H, exchange with D_2O, O*H*), 7.04 (d, J = 8.8, 2H, Ar), 7.33 (s, 2H, exchange with D_2O, SO_2NH_2), 7.46 (d, J = 8.4, 2H, Ar), 7.78 (d, J = 8.4 Hz, 2H, Ar), 7.85 (d, J = 8.8, 2H, Ar), 8.51 (t, J = 5.6, 1H, exchange with D_2O, CON*H*), 8.71 (bd, 2H, exchange with D_2O, NH_2^+); δ_C (100 MHz, DMSO-d_6): 11.70, 35.75, 41.28, 43.30, 49.80, 65.77, 70.78, 114.95, 126.59, 127.95, 129.87, 130.03, 142.93, 144.76, 161.40, 166.52; *m/z* (ESI positive) 422.2$[M\text{-}Cl^-]^+$.

Synthesis of 4-(2-Hydroxy-3-propylamino-propoxy)-N-[2-(4-sulfamoyl-phenyl)-ethyl]-benzamide hydrochloride **(C11)**

Compound **C11** was obtained according the general **procedure 6.1** earlier reported. N-{2-[4-(1-Dimethylamino-ethylidenesulfamoyl)-phenyl]-ethyl}-4-oxiranylmethoxy-benzamide **C8** (0.25 g, 1.0 eq) was treated with propylamine (8 ml) for 8h at 50°C and then the obtained free base was treated with HCl 1.25M in MeOH (10 ml) to afford the corresponding hydrochloride salt **C11**.

4-(2-Hydroxy-3-propylamino-propoxy)-*N*-[2-(4-sulfamoyl-phenyl)-ethyl]-benzamide hydrochloride C11: 64% yield; silica gel TLC R_f 0.24 (TFA/MeO*H*/DCM 3/15/82% *v/v*); δ_H (400 MHz, DMSO-d_6): 0.95 (t, J = 6.0, 3H, CH_3), 1.68 (m, 2H, CH_2), 2.94 (m, 4H, 2 x CH_2), 3.03 (m, 1H, C*H*), 3.17 (m, 1H, C*H*), 3.53 (m, 2H, CH_2), 4.06 (d, J = 5.2, 2H, CH_2), 4.21 (m, 1H, C*H*), 5.94 (bs, 1H, exchange with D_2O, O*H*), 7.04 (d, J = 8.8, 2H, Ar), 7.33 (s, 2H, exchange with D_2O, SO_2NH_2), 7.46 (d, J = 8.4, 2H, Ar), 7.77 (d, J = 8.4, 2H, Ar), 7.84 (d, J = 8.8, 2H, Ar), 8.50 (t, J = 5.6, 1H, CON*H*), 8.61 (bs, 2H,

exchange with D_2O, NH_2^+); δ_C (100 MHz, DMSO-*d*$_6$): 11.87, 19.68, 35.76, 41.30, 49.71, 50.28, 65.74, 70.80, 114.98, 126.61, 127.95, 129.89, 130.05, 142.94, 144.78, 161.44, 166.58; *m/z* (ESI positive) 436.2 $[M\text{-}Cl^-]^+$.

Synthesis of 4-(2-hydroxy-3-isopropylamino-propoxy)-N-[2-(4-sulfamoyl-phenyl)-ethyl]-benzamide hydrochloride **(C12)**

Compound **C12** was obtained according the general **procedure 6.1** earlier reported. N-{2-[4-(1-dimethylamino-ethylidenesulfamoyl)-phenyl]-ethyl}-4-oxiranylmethoxy-benzamide **C8** (0.25 g, 1.0 eq.) was treated with isopropylamine (5 ml) for 6h at 50°C and then the obtained free base was treated with HCl 1.25M in MeOH (10 ml) to afford the corresponding hydrochloride salt **C12**.

4-(2-Hydroxy-3-isopropylamino-propoxy)-*N*-[2-(4-sulfamoyl-phenyl)-ethyl]-benzamide hydrochloride C12: 54% yield; silica gel TLC R_f 0.40 (TFA/MeO*H*/DCM 3/15/82% *v/v*); δ_H (400 MHz, DMSO-*d*$_6$): 1.29 (t, *J* = 6.0, 6H, 2 x C*H*$_3$,), 2.96 (t, *J* = 7.2, 2H, C*H*$_2$,), 3.01 (m, 1H, C*H*), 3.16 (m, 1H, C*H*), 3.53 (q, *J* = 6.4, 2H, C*H*$_2$,), 4.08 (d, *J* = 5.2, 2H, C*H*$_2$,), 4.25 (m, 1H, C*H*), 5.95 (d, *J* = 5.2, 1H, exchange with D_2O, O*H*), 7.05 (d, *J* = 8.8, 2H, Ar), 7.33 (s, 2H, exchange with D_2O, SO_2NH_2), 7.46 (d, *J* = 8.4, 2H, Ar), 7.78 (d, *J* = 8.4, 2H, Ar), 7.85 (d, *J* = 8.8, 2H, Ar), 8.52 (t, *J* = 5.6, 1H, exchange with D_2O, CON*H*), 8.70 (bd, 2H, exchange with D_2O, NH_2^+); δ_C (100 MHz, DMSO-*d*$_6$): 24.01, 35.94, 49.27, 50.99, 69.42, 72.04, 115.05, 126.75, 126.97, 127.69, 129.96, 130.19, 143.09, 144.93, 162.07, 166.78; *m/z* (ESI positive) 436.2 $[M\text{-}Cl^-]^+$.

Synthesis of 4-(2-hydroxy-3-sec-butylamino-propoxy)-N-[2-(4-sulfamoyl-phenyl)-ethyl]-benzamide hydroclhoride **(C13)**

Compound **C13** was obtained according the general **procedure 6.1** earlier reported. N-{2-[4-(1-Dimethylamino-ethylidenesulfamoyl)-phenyl]-ethyl}-4-oxiranylmethoxy-benzamide **C8** (0.25 g, 1.0 eq.) was treated with sec-butylamine (8 ml) overnight at r.t. and then the obtained free base was treated with HCl 1.25M in MeOH (10 ml) to afford the corresponding hydrochloride salt **C13**.

4-(2-Hydroxy-3-sec-butylamino-propoxy)-*N*-[2-(4-sulfamoyl-phenyl)-ethyl]-benzamide hydroclhoride C13: 49% yield; silica gel TLC R_f 0.31 (TFA/MeO*H*/DCM 3/15/82% *v/v*); δ_H (400 MHz, DMSO-*d*$_6$): 0.94 (td, *J* = 2.0, 7.6, 3H, C*H*$_3$), 1.27 (t, *J* =

6.4, 3H, C*H*$_3$), 1.51 (m, H, C*H*), 1.82 (m, 1H, C*H*), 2.96 (t, *J* = 7.2, 2H, C*H*$_2$), 3.03 (m, 1H, C*H*), 3.17 (m, 2H, C*H*$_2$), 3.53 (q, *J* = 6.4, 2H, C*H*$_2$), 4.08 (d, *J* = 5.2, 2H, C*H*$_2$), 4.26 (m, 1H, C*H*), 5.94 (d, *J* = 2.4, 1H, exchange with D_2O, O*H*), 7.05 (d, *J* = 8.8, 2H, Ar), 7.33 (s, 2H, exchange with D_2O, SO_2NH_2), 7.46 (d, *J* = 8.4, 2H, Ar), 7.77 (d, *J* = 8.4, 2H, Ar), 7.84 (d, *J* = 8.8, 2H, Ar), 8.52 (t, *J* = 5.6, 1H, CON*H*), 8.77 (bt, exchange with D_2O, 2H, NH_2^+); δ_C (100 MHz, DMSO-*d*$_6$): 10.66, 15.89, 25.90, 35.77, 41.31, 47.51, 55.88, 65.97, 70.80, 114.98, 126.61, 127.94, 129.90, 130.05, 142.95, 144.79, 161.45, 166.55; *m/z* (ESI positive) 450.2 $[M\text{-}Cl^-]^+$.

Synthesis of 4-(2-hydroxy-3-t-butylamino-propoxy)-N-[2-(4-sulfamoyl-phenyl)-ethyl]-benzamide hydrochloride **(C14)**

Compound **C14** was obtained according the general **procedure 6.1** earlier reported. N-{2-[4-(1-Dimethylamino-ethylidenesulfamoyl)-phenyl]-ethyl}-4-oxiranylmethoxy-benzamide **C8** (0.25 g, 1.0 eq.) was treated with t-butylamine (8 ml) overnight at r.t. and then the obtained free base was treated with HCl 1.25M in MeOH (10 ml) to afford the corresponding hydrochloride salt **C14**.

4-(2-Hydroxy-3-t-butylamino-propoxy)-*N*-[2-(4-sulfamoyl-phenyl)-ethyl]-benzamide hydrochloride C14: 47% yield; silica gel TLC R_f 0.25 (TFA/MeO*H*/DCM 3/15/82% *v/v*); δ_H (400 MHz, DMSO-*d*$_6$): 0.94 (td, *J* = 2.0, 7.6, 3H, C*H*$_3$), 1.35 (s, 9H, 3 x C*H*$_3$), 2.96 (m, 3H, C*H* + C*H*$_2$), 3.17 (m, 1H, C*H*), 3.52 (q, *J* = 6.4, 2H, C*H*$_2$), 4.10 (d, *J* = 5.2 , 2H, C*H*$_2$), 4.26 (m, 1H, C*H*), 5.95 (d, *J* = 4.8, 1H, exchange with D_2O, O*H*), 7.06 (d, *J* = 8.8, 2H, Ar), 7.33 (s, 2H, exchange with D_2O, SO_2NH_2), 7.46 (d, *J* = 8.4, 2H, Ar), 7.78 (d, *J* = 8.4, 2H, Ar), 7.85 (d, *J* = 8.8, 2H, Ar), 8.53 (t, *J* = 5.6, 1H, CON*H*), 8.74 (bt, 2H, exchange with D_2O, NH_2^+); δ_C (100 MHz, DMSO-*d*$_6$): 25.90, 35.76, 41.29, 44.91, 57.31, 66.35, 70.76, 114.99, 126.60, 127.94, 129.88, 130.04, 142.94, 144.77, 161.44, 166.54; *m/z* (ESI positive) 450.2 $[M\text{-}Cl^-]^+$.

Synthesis of 4-(2-hydroxy-3-benzylamino-propoxy)-N-[2-(4-sulfamoyl-phenyl)-ethyl]-benzamide **(C15)**

Compound **C15** was obtained according the general **procedure 6.1** earlier reported. N-{2-[4-(1-Dimethylamino-ethylidenesulfamoyl)-phenyl]-ethyl}-4-oxiranylmethoxy-

benzamide **C8** (0.25 g, 1.0 eq.) was treated with benzylamine in EtOH for 7h at 50°C to afford the titled compound **C15** as a free base.

4-(2-Hydroxy-3-benzylamino-propoxy)-*N*-[2-(4-sulfamoyl-phenyl)-ethyl]-benzamide C15: 68% yield; silica gel TLC R_f 0.35 (TFA/MeO*H*/DCM 3/15/82% *v/v*); δ_H (400 MHz, DMSO-d_6): 2.19 (bs, 1H, exchange with D_2O, N*H*), 2.62 (m, 2H, CH_2), 2.95 (m, 2H, CH_2), 3.53 (q, *J* = 6.4, 2H, CH_2), 3.76 (s, 2H, CH_2), 3.97 (m, 2H, CH_2), 4.07 (m, 1H, C*H*), 5.04 (d, *J* = 4.4, 1H, exchange with D_2O , O*H*), 7.01 (d, *J* = 8.8, 2H, Ar), 7.32 (m, 7H, partial exchange with D_2O, Ar + SO_2NH_2), 7.46 (d, *J* = 8.4, 2H, Ar), 7.78 (d, *J* = 8.4, 2H, Ar), 7.81 (d, *J* = 8.8, 2H, Ar), 8.46 (t, *J* = 5.6, 1H, CON*H*); δ_C (100 MHz, DMSO-d_6): 35.79, 41.31, 52.62, 54.01, 69.07, 71.82, 114.90, 126.61, 127.43, 127.55, 128.80, 129.02, 129.82, 130.04, 141.82, 142.94, 144.79, 161.92, 166.64; *m/z* (ESI positive) 484.2 $[M+H]^+$.

Synthesis of 4-(2-hydroxy-3-((2-hydroxyethyl)amino)propoxy)-N-(4-sulfamoylphenethyl)benzamide hydrochloride **(C16)**

Compound **C16** was obtained according the general **procedure 6.1** earlier reported. N-{2-[4-(1-dimethylamino-ethylidenesulfamoyl)-phenyl]-ethyl}-4-oxiranylmethoxy-benzamide **C8** (0.25 g, 1.0 eq.) was treated with ethanolamine in EtOH overnight at r.t. and then the obtained free base was treated with HCl 1.25M in MeOH (10 ml) to afford the corresponding hydrochloride salt **C16**.

4-(2-Hydroxy-3-((2-hydroxyethyl)amino)propoxy)-*N*-(4-sulfamoylphenethyl)benzamide hydrochloride C16: 46% yield; silica gel TLC R_f 0.09 (TFA/MeO*H*/DCM 3/15/82% *v/v*) (MeOH/DCM 10 % *v/v*); δ_H (400 MHz, DMSO-d_6): 2.96 (t, *J* = 6.8, 2H, CH_2), 3.03 (m, 3H, C*H* + CH_2), 3.17 (m, 1H, C*H*), 3.52 (q, *J* = 7.2, 2H, CH_2), 3.74 (m, 2H, CH_2), 4.06 (d, *J* = 4.8, 2H, CH_2), 4.27 (m, 1H, C*H*), 5.30 (bs, 1H, exchange with D_2O, O*H*), 5.93 (bs, 1H, exchange with D_2O, OH,), 7.04 (d, *J* = 8.8, 2H, Ar), 7.33 (s, 2H, exchange with D_2O, SO_2NH_2), 7.46 (d, *J* = 8.4, 2H, Ar), 7.78 (d, *J* = 8.4, 2H, Ar), 7.85 (d, *J* = 8.8, 2H, Ar), 8.53 (t, *J* = 5.6, 1H, exchange with D_2O, CON*H*), 8.80 (bd, 2H, exchange with D_2O, NH_2^+); δ_C (100 MHz, DMSO-d_6): 35.75, 41.28, 50.27, 50.42, 65.65, 70.84, 114.96, 126.59, 127.93, 129.87, 130.03, 142.93, 114.76, 161.41, 166.53; *m/z* (ESI positive) 438.2 $[M-Cl^-]^+$.

Synthesis of 4-(2-hydroxy-3-morpholinopropoxy)-N-(4-sulfamoylphenethyl)benzamide hydrochloride **(C17)**

Compound **C17** was obtained according the general **procedure 6.2** earlier reported. N-{2-[4-(1-Dimethylamino-ethylidenesulfamoyl)-phenyl]-ethyl}-4-oxiranylmethoxy-benzamide **C8** (0.25 g, 1.0 eq.) was treated with morpholine in EtOH for 5h at 70°C and then the obtained protected free base was treated with HCl 1.25M in MeOH in sealed tube to afford the titled compound **C17** as hydrochloride salt.

4-(2-Hydroxy-3-morpholinopropoxy)-*N*-(4-sulfamoylphenethyl)benzamide hydrochloride C17: 43% yield; silica gel TLC R_f 0.20 (TFA/MeO*H*/DCM 3/15/82% *v/v*); δ_H (400 MHz, DMSO-d_6): 2.96 (t, *J* = 6.8, 2H, CH_2), 2.28 (m, 4H, 2 x CH_2), 3.17 (m, 1H, C*H*), 3.53 (m, 4H, 2 x CH_2), 3.85 (m, 2H, CH_2), 4.03 (m, 2H, CH_2), 4.06 (d, *J* = 4.8, 2H, CH_2), 4.43 (m, 1H, C*H*), 6.04 (bs, 1H, exchange with D_2O, O*H*), 7.04 (d, *J* = 8.8, 2H, Ar), 7.33 (s, 2H, exchange with D_2O, SO_2NH_2), 7.46 (d, *J* = 8.4, 2H, Ar), 7.78 (d, *J* = 8.4, 2H, Ar), 7.85 (d, *J* = 8.8, 2H, Ar), 8.51 (t, *J* = 5.6, 1H, exchange with D_2O, CON*H*), 10.37 (bs, 1H, exchange with D_2O, NH^+); δ_C (100 MHz, DMSO-d_6): 35.76, 51.93, 53.56, 59.69, 63.98, 64.32, 71.10, 115.01, 126.61, 128.02, 129.91, 130.05, 142.95, 144.78, 161.41, 166.54; *m/z* (ESI positive) 464.2 $[M\text{-}Cl^-]^+$.

Synthesis of 4-(2-hydroxy-3-diisopropylamino-propoxy)-N-[2-(4-sulfamoyl-phenyl)-ethyl]-benzamide hydrochloride **(C18)**

Compound **C18** was obtained according the general **procedure 6.2** earlier reported. N-{2-[4-(1-Dimethylamino-ethylidenesulfamoyl)-phenyl]-ethyl}-4-oxiranylmethoxy-benzamide **C8** (0.25 g, 1.0 eq.) was treated with diisopropylamine in EtOH for 24h at 70°C and then the obtained protected free base was treated with HCl 1.25M in MeOH in sealed tube to afford the titled compound **C18** as hydrochloride salt.

4-(2-Hydroxy-3-diisopropylamino-propoxy)-N-[2-(4-sulfamoyl-phenyl)-ethyl]-benzamide hydrochloride C18: 41% yield; silica gel TLC R_f 0.36 (TFA/MeO*H*/DCM 3/15/82% *v/v*); δ_H (400 MHz, DMSO-d_6): 1.30 (m, 12H, 4 x CH_3), 2.96 (t, *J* = 6.8, 2H, CH_2), 3.19 (m, 1H, C*H*), 3.33 (m, 1H, C*H*), 3.53 (m, 2H, CH_2), 3.74 (m, 2H, 2 x C*H*), 4.13 (m, 2H, CH_2), 4.27 (m, H, C*H*), 5.93 (d, *J* = 4.8, 1H, exchange with D_2O, O*H*), 7.06 (d, *J* = 8.8, 2H, Ar), 7.33 (s, 2H, exchange with D_2O, SO_2NH_2), 7.46 (d, *J* = 8.4, 2H, Ar), 7.78 (d, *J* = 8.4, 2H, Ar), 7.85 (d, *J* = 8.8, 2H, Ar), 8.51 (t, *J* = 5.6, 1H, exchange with

D_2O, CON*H*), 9.01 (bs, 1H, exchange with D_2O, NH^+); δ_C (100 MHz, DMSO-d_6): 17.07, 17.94, 35.76, 51.08, 55.70, 56.55, 66.53, 70.49, 114.95, 126.60, 128.01, 129.90, 130.03, 142.95, 144.76, 161.32, 166.52; *m/z* (ESI positive) 478.2 $[M\text{-}Cl^-]^+$.

Synthesis of N,N-dimethylaminomethylene-4-hydroxy-benzenesulfonamide **(C20)**[297]

N,N-Dimethylformamide diethyl acetal (1.2 eq.) was added to a solution of 4-hydroxybenzenesulfonamide **C19** (1.5 g, 1.0 eq.) in DMF (1.5 ml) at 0°C and that was stirred for 0.5h at r.t. The reaction mixture was treated with EtOAc (40ml) and the obtained solid was filtered and purified by silica gel chromatography eluting with 10% MeOH/DCM to afford the titled compound **C20.**

***N,N*-Dimethylaminomethylene-4-hydroxy-benzenesulfonamide C20:** 76% yield; silica gel TLC R_f 0.22 (MeOH/DCM 5 % *v/v*); δ_H (400 MHz, DMSO-d_6): 2.92 (s, 3H, CH_3), 3.16 (s, 3H, CH_3), 6.88 (d, *J* = 8.4. 2H, Ar), 7.61 (d, *J* = 8.4. 2H, Ar), 8.18 (s, 1H, exchange with D_2O, O*H*); δ_C (100 MHz, DMSO-d_6): 35.9, 41.7, 116.2, 129.1, 134.2, 160.3, 161.3.

Synthesis of N,N-dimethylaminomethylene-4-oxiranylmethoxy-benzenesulfonamide **(C21)**

Epibromohydrin (1.2 eq.) was added dropwise to a suspension of N,N-dimethylaminomethylene-4-hydroxy-benzenesulfonamide **C20** (0.5 g, 1.0 eq.) and Cs_2CO_3 (1.5 eq.) in dry DMF under a nitrogen atmosphere and that was stirred o.n. at 50°C. The reaction mixture was quenched with slush and extracted with EtOAc (2x20ml). The organic layers were washed with brine (4x15ml), dried over anhydrous Na_2SO_4 and concentrate under vacuum to give a residue that was triturated with Et_2O to afford the titled compound **C21**.

***N,N*-Dimethylaminomethylene-4-oxiranylmethoxy-benzenesulfonamide C21:** 76% yield; m.p. °C; silica gel TLC R_f 0.45 (MeOH/DCM 5 % *v/v*); δ_H (400 MHz, DMSO-d_6): 2.75 (dd, *J* = 2.6, 5.0, 1H, C*H*), 2.89 (t, *J* = 4.8, 1H, C*H*), 2.90 (s, 3H, CH_3), 2.92 (s, 3H, CH_3), 3.38 (m, 1H, C*H*), 3.93 (dd, *J* = 6.6, 11.4, 1H, C*H*), 4.45 (dd, *J* = 2.7, 11.4, 1H, C*H*), 7.11 (d, *J* = 7.0, 2H, Ar), 7.72 (d, *J* = 7.0, 2H, Ar); δ_C (100 MHz, DMSO-d_6): 35.9, 41.8, 44.7, 50.4, 70.2, 115.6, 128.9, 136.3, 160.5, 161.5.

Synthesis of 4-(2-hydroxy-3-methylamino-propoxy)-benzenesulfonamide hydrochloride **(C22)**

Compound **C22** was obtained according the general **procedure 6.1** earlier reported. *N*,*N*-dimethylaminomethylene-4-oxiranylmethoxy-benzenesulfonamide **C21** (0.25 g, 1.0 eq.) was suspended in EtOH and treated with a 35% aqueous solution of methylamine overnight at r.t. and then the obtained free base was treated with HCl 1.25M in MeOH (10 ml) to afford the corresponding hydrochloride salt **C22**.

4-(2-Hydroxy-3-methylamino-propoxy)-benzenesulfonamide hydrochloride C22: 42% yield; silica gel TLC R_f 0.12 (TFA/MeO*H*/DCM 3/15/82% *v/v*); δ_H (400 MHz, DMSO-d_6): 2.46 (s, 3H, CH_3), 2.95 (m, 1H, C*H*), 3.08 (m, 1H, C*H*), 4.02 (d, *J* = 4.4, 2H, CH_2), 4.16 (m, 1H, C*H*), 5.91 (bs, 1H, exchange with D_2O , O*H*), 7.07 (d, *J* = 7.8, 2H, Ar), 7.19 (s, 2H, exchange with D_2O, SO_2NH_2), 7.72 (d, *J* = 7.8, 2H, Ar), 8.83 (bd, 2H, exchange with D_2O, NH_2^+); δ_C (100 MHz, DMSO-d_6): 33.88, 51.71, 65.54, 70.98, 115.51, 128.59, 137.46, 161.56; *m/z* (ESI positive) 261.1 $[M\text{-}Cl^-]^+$.

Synthesis of 4-(2-hydroxy-3-isopropylamino-propoxy)-benzenesulfonamide hydrochloride **(C23)**

Compound **C23** was obtained according the general **procedure 6.1** earlier reported. N,N-Dimethylaminomethylene-4-oxiranylmethoxy-benzenesulfonamide **C21** (0.25 g, 1.0 eq.) was treated with isopropylamine (5 ml) for 6h at 50°C and then the obtained free base was treated with HCl 1.25M in MeOH (10 ml) to afford the corresponding hydrochloride salt **C23**.

4-(2-Hydroxy-3-isopropylamino-propoxy)-benzenesulfonamide hydrochloride C23: 40% yield; silica gel TLC R_f 0.24 (TFA/MeO*H*/DCM 3/15/82% *v/v*); δ_H (400 MHz, DMSO-d_6): 1.30 (t, *J* = 6.0, 6H, 2 x CH_3), 3.01 (m, 1H, C*H*), 3.16 (m, 1H, C*H*), 3.35 (m, 2H, 2 x C*H*), 4.12 (d, *J* = 4.4, 2H, CH_2), 4.29 (m, 1H, *CH*), 5.97 (bs, 1H, exchange with D_2O ,O*H*), 7.15 (d, *J* = 7.0, 2H, Ar), 7.27 (s, 2H, exchange with D_2O, SO_2NH_2), 7.80 (d, 2H, *J* = 7.0, Ar), 8.89 (bd, 2H, exchange with D_2O, NH_2^+); δ_C (100 MHz, DMSO-d_6): 19.11, 19.56, 47.51, 50.77, 65.93, 71.03, 115.52, 128.60, 137.45, 161.59; *m/z* (ESI positive) 289.1 $[M\text{-}Cl^-]^+$.

Synthesis of 4-(3-(sec-butylamino)-2-hydroxypropoxy)benzenesulfonamide hydrochloride **(C24)**

Compound **C24** was obtained according the general **procedure 6.1** earlier reported. *N,N*-Dimethylaminomethylene-4-oxiranylmethoxy-benzenesulfonamide **C21** (0.25 g, 1.0 eq.) was treated with sec-butylamine (5 ml) for 6h at 50°C and then the obtained free base was treated with HCl 1.25M in MeOH (10 ml) to afford the corresponding hydrochloride salt **C24**.

4-(3-(*Sec*-butylamino)-2-hydroxypropoxy)benzenesulfonamide hydrochloride C24: 40% yield; silica gel TLC R_f 0.32 (TFA/MeO*H*/DCM 3/12/85% *v/v*); δ_H (400 MHz, DMSO-d_6): 0.94 (t, *J* = 7.6, 3H, CH_3), 1.27 (t, *J* = 6.4, 3H, CH_3), 1.53 (m, H, C*H*), 1.87 (m, 1H, C*H*), 3.03 (m, 1H, C*H*), 3.17 (m, 2H, CH_2), 4.12 (d, *J* = 5.2, 2H, CH_2), 4.30 (m, 1H, C*H*), 5.97 (d, *J* = 2.4, 1H, exchange with D_2O, O*H*), 7.15 (d, *J* = 8.4, 2H, Ar), 7.27 (s, 2H, exchange with D_2O, SO_2NH_2), 7.80 (d, 2H, *J* = 8.4, Ar), 8.90 (bt, 2H, exchange with D_2O, NH_2^+); δ_C (100 MHz, DMSO-d_6): 10.7, 15.9, 25.9, 47.5, 55.9, 65.9, 71.0, 115.5, 128.6, 137.4, 161.6; *m/z* (ESI positive) 303.1 $[M\text{-}Cl^-]^+$.

Synthesis of 4-(3-(tert-butylamino)-2-hydroxypropoxy)benzenesulfonamide hydrochloride **(C25)**

Compound **C25** was obtained according the general **procedure 6.1** earlier reported. *N,N*-dimethylaminomethylene-4-oxiranylmethoxy-benzenesulfonamide **C21** (0.25 g, 1.0 eq.) was treated with tert-butylamine (5 ml) for 6h at 50°C and then the obtained free base was treated with HCl 1.25M in MeOH (10 ml) to afford the corresponding hydrochloride salt **C25**.

4-(3-(*tert*-Butylamino)-2-hydroxypropoxy)benzenesulfonamide hydrochloride C25: 43% yield; silica gel TLC R_f 0.30 (TFA/MeO*H*/DCM 3/12/85% *v/v*); δ_H (400 MHz, DMSO-d_6): 1.36 (s, 9H, 3 x CH_3), 2.97 (m, 1H, C*H*), 3.16 (m, 1H, C*H*), 4.15 (m, 2H, CH_2), 4.30 (m, 1H, C*H*), 5.98 (bs, 1H, exchange with D_2O, O*H*), 7.16 (d, *J* = 8.4, 2H, Ar), 7.28 (s, 2H, exchange with D_2O, SO_2NH_2), 7.80 (d, 2H, *J* = 8.4, Ar), 8.99 (bdt, 2H, exchange with D_2O, NH_2^+); δ_C (100 MHz, DMSO-d_6): 25.9, 45.0, 57.3, 66.3, 71.0, 115.5, 128.6, 137.4, 161.6; *m/z* (ESI positive) 303.1 $[M\text{-}Cl^-]^+$.

Synthesis of 4-(3-(benzylamino)-2-hydroxypropoxy)benzenesulfonamide hydrochloride **(C26)**

Compound **C26** was obtained according the general **procedure 6.1** earlier reported. *N*,*N*-dimethylaminomethylene-4-oxiranylmethoxy-benzenesulfonamide **C21** (0.25 g, 1.0 eq.) was treated with benzylamine (3 ml) for 8h at 50°C and then the obtained free base was treated with HCl 1.25M in MeOH (10 ml) to afford the corresponding hydrochloride salt **C26**.

4-(3-(Benzylamino)-2-hydroxypropoxy)benzenesulfonamide hydrochloride C26: 54% yield; silica gel TLC R_f 0.34 (TFA/MeO*H*/DCM 3/12/85% *v/v*); δ_H (400 MHz, DMSO-d_6): 2.97 (m, 1H, C*H*), 3.16 (m, 1H, C*H*), 4.09 (d, *J* = 5.2, 2H, CH_2), 4.24 (m, 2H, CH_2), 4.33 (m, 1H, C*H*), 5.98 (bs, 1H, exchange with D_2O ,O*H*), 7.12 (d, *J* = 7.0, 2H, Ar), 7.26 (s, 2H, exchange with D_2O, SO_2NH_2), 7.47 (m, 3H, Ar), 7.62 (m, 2H, Ar), 7.79 (d, 2H, *J* = 7.0, Ar), 9.43 (bd, 2H, exchange with D_2O, NH_2^+); δ_C (100 MHz, DMSO-d_6): 49.7, 51.1, 65.6, 70.9, 115.5, 128.5, 129.5, 129.8, 131.1, 132.6, 137.4, 161.5; *m/z* (ESI positive) 337.1 $[M\text{-}Cl^-]^+$.

Synthesis of 4-(2-hydroxy-3-(phenethylamino)propoxy)benzenesulfonamide hydrochloride **(C27)**

Compound **C27** was obtained according the general **procedure 6.2** earlier reported. *N*,*N*-dimethylaminomethylene-4-oxiranylmethoxy-benzenesulfonamide **C21** (0.25 g, 1.0 eq.) was treated with phenethylamine in EtOH for 6h at 70°C and then the obtained protected free base was treated with HCl 1.25M in MeOH in sealed tube to afford the corresponding hydrochloride salt **C27**.

4-(2-Hydroxy-3-(phenethylamino)propoxy)benzenesulfonamide hydrochloride C27: 35% yield; silica gel TLC R_f 0.37 (TFA/MeO*H*/DCM 3/12/85% *v/v*); δ_H (400 MHz, DMSO-d_6): 3.05 (m, 3H, CH_2 + C*H*), 3.24 (m, 3H, CH_2 + C*H*), 4.09 (d, *J* = 5.2, 2H, CH_2), 4.31 (m, 1H, C*H*), 6.02 (d, *J* = 4.8, 1H, exchange with D_2O, O*H*), 7.14 (d, *J* = 8.8, 2H, Ar), 7.29 (m, 6H, partial exchange with D_2O, SO_2NH_2 + Ar), 7.38 (m, 1H, Ar), 7.80 (d, 2H, *J* = 8.8, Ar), 9.19 (bs, 2H, exchange with D_2O, NH_2^+) ; δ_C (100 MHz, DMSO-d_6): 32.3, 49.1, 50.3, 65.7, 71.0, 115.5, 127.6, 128.6, 129.5, 129.6, 137.5, 138.3, 161.6; *m/z* (ESI positive) 351.1 $[M\text{-}Cl^-]^+$.

Synthesis of 4-(2-hydroxy-3-((2-phenoxyethyl)amino)propoxy)benzenesulfonamide hydrochloride **(C28)**

Compound **C28** was obtained according the general **procedure 6.2** earlier reported. *N,N*-dimethylaminomethylene-4-oxiranylmethoxy-benzenesulfonamide **C21** (0.25 g, 1.0 eq.) was treated with 2-(phenoxy)ethylamine in EtOH for 6h at 70°C and then the obtained protected free base was treated with HCl 1.25M in MeOH in sealed tube to afford the corresponding hydrochloride salt **C28**.

4-(2-Hydroxy-3-((2-phenoxyethyl)amino)propoxy)benzenesulfonamide hydrochloride C28: 29% yield; silica gel TLC R_f 0.35 (TFA/MeO*H*/DCM 3/12/85% *v/v*); δ_H (400 MHz, DMSO-d_6): δ_H (400 MHz, DMSO-d_6): 3.15 (m, 1H, C*H*), 3.32 (m, 1H, C*H*), 4.95 (m, 2H, CH_2), 4.12 (d, *J* = 5.2, 2H, CH_2), 4.34 (m, 3H, CH_2 + C*H*), 5.98 (d, *J* = 4.8, 1H, exchange with D_2O, O*H*), 7.02 (m, 3H, Ar), 7.14 (d, *J* = 8.8, 2H, Ar), 7.27 (s, 2H, exchange with D_2O, SO_2NH_2), 7.37 (t, *J* = 8.0, 1H, Ar), 7.81 (d, 2H, *J* = 8.8, Ar), 9.09 (bd, 2H, exchange with D_2O, NH_2^+) ; δ_C (100 MHz, DMSO-d_6): 47.1, 50.6, 64.1, 65.6, 71.0, 115.5, 115.6, 122.1, 128.6, 130.5, 137.5, 158.6, 161.5; ; *m/z* (ESI positive) 367.1 $[M\text{-}Cl^-]^+$.

Synthesis of 4-(2-hydroxy-3-(4-methylpiperazin-1-yl)propoxy)benzenesulfonamide **(C29)**

Compound **C29** was obtained according the general **procedure 6.2** earlier reported. *N,N*-dimethylaminomethylene-4-oxiranylmethoxy-benzenesulfonamide **C21** (0.25 g, 1.0 eq.) was treated with 1-methylpiperazine in EtOH for 6h at 70°C and then the obtained protected free base was treated with HCl 1.25M in MeOH in sealed tube. The di-hydrochloride salt of **C29** was washed with aceton and thus treated with a $NaHCO_{3(aq)}$ saturated solution, which was extracted with EtOAc (3x20ml) and the combined organic layers were dried over anhydrous Na_2SO_4 and concentrated under reduced pressure to give the titled compound **C29**.

4-(2-Hydroxy-3-(4-methylpiperazin-1-yl)propoxy)benzenesulfonamide C29: 36% yield; silica gel TLC R_f 0.08 (TFA/MeO*H*/DCM 3/12/85% *v/v*); δ_H (400 MHz, DMSO-d_6): 2.17 (s, 3H, CH_3), 2.38 (m, 4H, 2 x CH_2), 2.48 (m, 6H, 2 x CH_2 + 2 x C*H*), 3.96 (m, 2H, CH_2), 4.09 (m, 1H, C*H*), 4.93 (bs, 1H, exchange with D_2O ,O*H*), 7.12 (d, *J* = 8.8, 2H, Ar), 7.23 (s, 2H, exchange with D_2O, SO_2NH_2), 7.77 (d, 2H, *J* = 8.8, Ar); δ_C (100

MHz, DMSO-d_6): 46.7, 54.3, 55.7, 61.8, 67.3, 72.4, 115.4, 128.5, 137.0, 162.1; *m/z* (ESI positive) 330.1 $[M\text{-}Cl^-]^+$.

5.3.2 Carbonic Anhydrase Inhibition

The CA inhibitory profiles of compounds belonging to Series C were obtained according to the general procedures described at the beginning of the experimental section.

5.3.3 β-ADR -Binding assay

5.3.3.1 Plasmids

The coding region sequences (CDSs) of β_1 and β_2 adrenergic receptor were cloned inside AID-express-puro2 plasmid[298] replacing the coding sequence of Activation Induced Deaminase (AID). We used this plasmid for the presence of an Internal Ribosome Entry Site (IRES) sequence, which allows the expression of a reporter gene (GFP) under the same promoter of our CDS, producing only one mRNA but two different proteins; this let us analyze the presence and the amount of the β adrenergic receptors by FACS analysis for GFP positive cells.

The CDS of β_1 adrenergic receptor was cloned by digestion using BamHI and ApaI from pcDNA3 Flag β_1 adrenergic receptor (a gift from Robert Lefkowitz -Addgene plasmid # 14698); this fragment was then blunted (using Cloned Pfu DNA Polymerase AD from Agilent Technologies at 72ºC for 15min) and cloned inside AID-express-puro2 digested by NheI and BglII.

Differently, for β_2 adrenergic receptor we extracted RNA from HEK293T cells (using TRIzol – Thermo Fisher Scientific) to obtain cDNA using High Capacity cDNA Reverse Transcription Kits (Applied Biosystems). After, we amplified the receptor by PCR adding NheI and BamHI restriction sites to the ends of the fragment to clone it inside AID-express-puro2 digested by NheI and BglII (forward primer: aaaGCTAGCatggggcaacccgggaacg; reverse primer: aaaGGATCCttacagcagtgagtcattt). These plasmids were used to transfect HEK293T cells, for stably expression of β_1 and β_2 adrenergic receptors.

5.3.3.2 Cell culture and transfections

HEK293T cells were cultured at 37 °C, 5% CO_2, in Dulbecco's modified eagle medium (DMEM, EuroClone S.p.A Pero, Milano, Italy) supplemented with 10% fetal bovine serum (FBS; Carlo Erba Reagents, Cornaredo, Milano, Italy), 2 mM L -glutamine (Carlo Erba Reagents, Cornaredo, Milano, Italy), and 1 mM penicillin/streptomycin (Carlo Erba Reagents, Cornaredo, Milano, Italy). Transfections were performed in six-well plates (5 x 10^5 cells) using Lipofectamine LTX (Invitrogen, Carlsbad, CA, USA) or GeneJuice (Novagen s.r.l., Podenzano, Piacenza, Italy) according to the manufacturer's instructions. 48h after transfections cells were plated in 96-well plates in medium supplemented with puromycin (1.5 μg/ml), in several dilution to obtain single clones. Colonies were picked after 10–14 days and only wells bearing single colonies were expanded for FACS analysis for the presence of GFP. Clones GFP positive were then utilized for further analysis.

5.3.3.3 Membrane preparation

HEK293T cells stably expressing the human cloned β_1 and β_2 ADRs were grown at approximately 80% confluence. Then, they were harvested by scraping the culture plate with a cell scraper, washed by centrifugation at 500 g at room temperature and homogenized in ice-cold buffer (50 mM Tris HCl, pH 7.4) with an Ultra-Turrax (IKA Labortechnik, Staufen, Germany) twice for 20 s at half speed. The homogenates were centrifuged for 10 min at 50,000 g at 4°C in Avanti J-26XP centrifuge (Beckman Coulter S.p.A., Cassina de' Pecchi, Milano, Italy). The resultant membrane pellet was resuspended in buffer and stored frozen at -80°C. Protein concentration was determined colorimetrically using a commercial protein determination kit based on the BCA reaction (Thermo Scientific, Rockford, IL, USA).

5.3.3.4 Radioligand binding experiments

Saturation binding experiments were performed by incubating cell membranes (about 20 μg/ml of protein) in a total volume of 1 mL incubation buffer (50 mM Tris HCl pH 7.4),

containing increasing concentrations (approximately 0.03-0.1-0.3-1-3 nM) of [^{3}H]-CGP12177 (Perkin-Elmer Life and Analytical Science, Monza, Italy). Incubations were carried out at 25°C for 90 min. Non-specific binding was determined in the presence of 10 μM propranolol.

Reactions were terminated by rapid filtration through glass fiber filters grade MGB (Sartorius Italy S.r.l., Bagno a Ripoli, Firenze, Italy) that had been soaked for 60 min in 0.5% polyethyleneamine using a Brandell cell harvester (Biomedical Research and Development Laboratory, Inc Atlas Drive, Gaithersburg, MD, USA).

Filters were washed three times with 4 ml aliquots of ice-cold milliQ water and dried before the addition of 4.5 ml of scintillation cocktail (Filter Count, Perkin-Elmer Life and Analytical Science, Monza, Italy). The radioactivity bound to the filters was measured using TRICARB 1100 scintillation counter (Perkin-Elmer Life and Analytical Science, Monza, Italy).

Clones expressing about 29 pmol/mg protein and 12 pmol/mg protein of the β_1 and β_2 ADRs respectively were used for all subsequent experiments (Supplemental Figure 3). Competition experiments were performed by incubating 20 μg/ml of protein with increasing amounts of test compound (from 1 nM-100 μM) and 0.2 nM [^{3}H]-CGP12177 for β_1-ADR and β_2-ADR binding assay, in a final incubation volume of 250 μL in 96 well plates (Sarstedt s.r.l., Verona, Italy). Non-specific binding was determined in the presence of 10 μM propranolol. The incubations were terminated by rapid vacuum filtration over WhatmanGF/B using a FilterMate harvester (Perkin-Elmer Life and Analytical Science, Monza, Italy). Each filter was abundantly washed with ice-cold milliQ water.

Radioactivity adherent to the filters was quantified in a Topcount NXT Microplate Scintillation Counter (Perkin-Elmer Life and Analytical Science, Monza, Italy) using Microscint20 (Perkin-Elmer Life and Analytical Science, Monza, Italy) scintillator after 4 hours.

Stock solutions of tested compounds were made in DMSO, and dilutions were usually made in the incubation buffer. DMSO at the highest concentration used had no effect on binding.

5.3.3.5 Data analysis

All experiments are conducted in duplicate and data are presented as mean ± S.E.M., unless otherwise noted. Saturation radioligand binding experiments were analyzed by fitting rectangular hyperbolic to the experimental data to obtain Bmax (the maximal binding capacity) and Kd (the dissociation constant). Data from equilibrium binding studies were corrected for non-specific binding and were analyzed by computer-aided nonlinear regression analysis using a four-parameter logistic equation. IC_{50} values were converted to binding constants K_i using the Cheng-Prusoff correction. All curve fitting was performed using the Prism programme 5.02 (Graphpad Software, San Diego, CA, USA).

5.3.4 X-ray Crystallography

The expression and purification of hCA II and hCA IX-mimic were performed as previously described.[299] hCA IX-mimic is a molecule of hCA II with seven active site mutations (A65S, N67Q, E69T, I91L, F131V, K170E and L204A) to mimic the residues in wild type hCA IX. The hCA IX-mimic is utilized due to the ease of expression and crystallization in relation to wild type. Protein was expressed in BL21(DE3) competent cells and purified utilizing the affinity chromatography technique on a p-(aminomethyl)benzenesulfonamide column. Purity was verified via SDS-PAGE. The formation of the protein-inhibitor complex was initiated utilizing the co-crystallization technique. Crystals were grown via the hanging drop vaporization method with a 1:1 protein to precipitant solution ratio (1.6 M Na-Citrate, 50 mM Tris, pH 7.8) and growth was observed after 2 weeks. The crystals were additionally soaked in ~10mM inhibitor for 5 min prior to freezing.

X-ray diffraction data was collected on a Pilatus 6M detector at the Cornell High Energy Synchrotron Source (CHESS) F1 beamline with a wavelength of 0.977 Å. A crystal-to-detector distance of 270 mm, 1° oscillation angle, and exposure time of 2 sec per image were utilized to collect data. A total of 270 images were collected. The data was indexed, integrated, and scaled to the $P2_1$ monoclinic space group in *HKL2000*.[300] Molecular replacement (search model PDB: 3KS3) was used to determine phases. Refinement of the

structure and ligand restraint files were generated in *Phenix*.[301] Interactions between the inhibitor and protein were analysed in Coot and figures generated in *PyMol*.[302]

5.3.5 Hypertensive Rabbit IOP Lowering Studies

Male New Zealand albino rabbits weighing 1500−2000 g were used in these studies. Animals were anesthetized using zoletil (tiletamine chloride plus zolazepam chloride, 3 mg/kg body weight, im) and injected with 0.1 mL of hypertonic saline solution (5% in distilled water) into the vitreous of both eyes. IOP was determined using a Model 30™Pneumatonometer (Reichert Inc. Depew, NY, USA) prior to hypertonic saline injection (basal) at 1, 2, 3, and 4 h after administration of the drug. Vehicle (phosphate buffer pH 7.00 plus DMSO 2%) or drugs were instilled immediately after the injection of hypertonic saline. Eyes were randomly assigned to different groups. Vehicle or drug (0.50 mL) was directly instilled into the conjunctive pocket at the desired doses (1−2%). The IOP was followed for 4 h after drug administration. Four different animals were used for each tested compound. All animal manipulations were carried out according to the European Community guidelines for animal care [DL 116/92, application of the European Communities Council Directive of 24 November 1986 (86/609/EEC)]. The ethical policy of the University of Florence complies with the Guide for the Care and Use of Laboratory Animals of the US National Institutes of Health (NIH Publication No. 85-23, revised 1996; University of Florence assurance number A5278-01). Formal approval to conduct the experiments described was obtained from the Animal Subjects Review Board of the University of Florence. Experiments involving animals have been reported according to ARRIVE - Animal Research: Reporting of *in vivo* Experiments–guidelines.[283] All efforts were made to minimize animal suffering and to reduce the number of animals used.

5.4 Multi-potent hybrids assembled by CA inhibitors and *NO*-donors as antitumor and anti-infective drugs: synthesis and kinetic evaluation (Series D)

5.4.1 Chemistry

The general chemistry protocols are reported at the beginning of the experimental section.

Synthesis of 5-carboxybenzo[c][1,2,5]oxadiazole 1-oxide **(D2)**

To a solution of KOH (0.59 g, 2.1 eq.) in C_2H_5OH (57 mL) previously heated to 70°C was added 4-amino-3-nitrobenzoic acid **D1** (0.92 g, 1.0 eq.). The suspension was triturated for 15 min and then cooled to 0°C. A commercially available (≈2 M) solution of sodium hypochlorite (20 mL) was added dropwise at 0°C. The reaction was stirred at the same temperature for 15 min, poured into ice and acidified with a 6 N HCl solution until pH 1.0 was reached. The mixture was concentrated, and the resulting precipitate was filtered off, washed with H_2O, and then dried to yield 0.78 g (84%) of an orange solid. m.p. 128–129°C; silica gel TLC: R_f = 0.5 (ethyl acetate/*n*-hexane 80% *v/v*). IR (KBr): 3095-2539 (br), 1682, 1610, 1589, 1490, 1430, 1314 cm^{-1}; δ_H (400 MHz, DMSO-d_6): 8.00 (m, 3H, Ar-*H*), 13.00 (s, 1H, COO*H*).

*General procedure **7** for the Synthesis of 4-(2-(arylalkyl)amino)ethyl)benzenesulfonamides **D9-D13***

Procedure 7.1 To a solution of 4-(2-aminoethyl)benzenesulfonamide (9,99 mmol, 1.0 eq.) in dry MeOH (40 mL), the appropriate aldehyde (1.1 eq.) was added and the mixture was heated under stirring to reflux temperature for 0.5-4 h. Sodium borohydride (1.6 eq.) was added portion wise at 0°C and the reaction mixture was heated under stirring to reflux temperature for 0,5-3 h. The solvent was evaporated under *vacuo*, water was added (25 mL) and neutralized with HCl 1M. The suspension was filtered, and the collected powder was occasionally purified with flash chromatography (MeOH/DCM 5% *v/v*) to give the compounds **D9-D11**.

Procedure 7.2 To a solution of 4-(2-aminoethyl)benzenesulfonamide (9,99 mmol, 1.0 eq.) in dry DMF (5 mL), triethylamine (1.2 eq.) and the appropriate halide (1.1 eq.) were added at room temperature and the mixture was stirred at 60°C for 8 h (**D12**) or at room

temperature for 0,5 h (**D13**). The reaction mixture was quenched by addition of water (20 mL) and extracted with DCM (30 mL x 3). The organic layer was collected, washed with brine (40 mL x 3), dried over Na_2SO_4, filtered and evaporated under *vacuo* to give the compounds **D12**,**13** as white/yellow powder.

Synthesis of 4-(2-(benzylamino)ethyl)benzenesulfonamide **(D9)**

Compound **D9** was obtained according the general **procedure 7.1** earlier reported using 4-(2-aminoethyl)benzenesulfonamide (9.99 mmol, 1.0 eq.) and commercial benzaldehyde (1.1 eq.) in dry MeOH (40 mL). The reaction mixture was initially stirred to reflux temperature for 4 h and after addition of sodium borohydride (1.6 eq.) was stirred to reflux temperature for 2 h.

4-(2-(Benzylamino)ethyl)benzenesulfonamide D9: 96% yield; m.p. 173-175 °C; silica gel TLC: R_f = 0.08 (TFA/MeOH/DCM 3/5/92% *v/v*). ^{1}H-NMR (DMSO-d_6, 400 MHz): δ 7.76 (d, J = 8.1 Hz, 2H, Ar-*H*), 7.42 (m, 7H, Ar-*H*), 7.32 (s, 2H, exchange with D_2O, SO_2NH_2, overlap with signal at 7.42), 4.04 (s, 2H, CH_2), 3.07 (m, 2H, CH_2), 2.97 (m, 2H, CH_2). ^{13}C-NMR (DMSO-d_6, 100 MHz): δ 145.87, 142.74, 141.80, 129.99, 129.05, 128.86, 127.46, 126.55, 53.77, 50.91, 36.50. MS (ESI positive) *m/z* = 291.1 $[M + H]^+$.

Synthesis of 4-(2-((4-fluorobenzyl)amino)ethyl)benzenesulfonamide **(D10)**

Compound **D10** was obtained according the general **procedure 7.1** earlier reported using 4-(2-aminoethyl)benzenesulfonamide (9.99 mmol, 1.0 eq.) and 4-fluorobenzaldehyde (1.1 eq.) in dry MeOH (40 mL). The reaction mixture was initially stirred to reflux temperature for 2 h and after addition of sodium borohydride (1.6 eq.) was stirred to reflux temperature for 2 h.

4-(2-((4-Fluorobenzyl)amino)ethyl)benzenesulfonamide D10: 95% yield; m.p. 145-147 °C; silica gel TLC: R_f = 0.21 (TFA/ MeOH/DCM 3/5/92% *v/v*). ^{1}H-NMR (DMSO-d_6, 400 MHz): δ 7.73 (d, J = 8.2 Hz, 2H, Ar-*H*), 7.38 (m, 4H, Ar-*H*), 7.28 (s, 2H, exchange with D_2O, SO_2NH_2, overlap with signal at 7.38), 7.12 (t, J = 8.8 Hz, 2H, Ar-*H*), 3.73 (s, 2H, CH_2), 2.79 (m, 4H, 2 x CH_2). δF (376 MHz, DMSO-d6): -116.18. ^{13}C-NMR (DMSO-d_6, 100 MHz): δ 145.61, 142.94, 131.06, 130.98, 130.10, 126.73, 115.96, 115.75, 52.74, 50.62, 36.18. MS (ESI positive) *m/z* = 309.1 $[M + H]^+$.

Synthesis of 4-(2-((furan-2-ylmethyl)amino)ethyl)benzenesulfonamide **(D11)**

Compound **D11** was obtained according the general **procedure 7.1** earlier reported using 4-(2-aminoethyl)benzenesulfonamide (9.99 mmol, 1.0 eq.) and 2-furaldehyde (1.1 eq.) in dry MeOH (40 mL). The reaction mixture was initially stirred to reflux temperature for 4 h and after addition of sodium borohydride (1.6 eq.) was stirred to reflux temperature for 3 h.

4-(2-((Furan-2-ylmethyl)amino)ethyl)benzenesulfonamide D11: 88% yield; m.p. 133-135 °C; silica gel TLC: R_f = 0.19 (TFA/ MeOH/DCM 3/5/92% *v/v*). ^{1}H-NMR (DMSO-d_6, 400 MHz): δ 7.71 (d, J = 8.3 Hz, 2H, Ar-*H*), 7.56-7.49 (m, 1H, Ar-*H*), 7.37 (d, J = 8.3 Hz, 2H, Ar-*H*), 7.24 (s, 2H, exchange with D_2O, SO_2NH_2), 6.35 (dd, J = 3.1, 1.9 Hz, 1H, Ar-*H*), 6.20 (d, J = 3.1 Hz, 1H, Ar-*H*), 3.67 (s, 2H, CH_2), 2.75 (m, 4H, 2 x CH_2), 2.04 (bs, 1H, exchange with D_2O, N*H*). ^{13}C-NMR (DMSO-d_6, 100 MHz): δ 155.36, 145.73, 142.62, 129.93, 126.49, 126.48, 111.13, 107.47, 50.67, 46.21, 36.29. MS (ESI positive) *m/z* = 281.1 $[M + H]^+$.

Synthesis of 4-(2-(phenethylamino)ethyl)benzenesulfonamide **(D12)**

Compound **D12** was obtained according the general **procedure 7.2** earlier reported using 4-(2-aminoethyl)benzenesulfonamide (9.99 mmol, 1.0 eq.) and (2-bromoethyl)benzene (1.1 eq.) in dry DMF (5 mL) stirred at 60 °C for 8 h (yellow powder).

4-(2-(Phenethylamino)ethyl)benzenesulfonamide D12: 73% yield; m.p. 213-215 °C; silica gel TLC: R_f = 0.02 (TFA/ MeOH/DCM 3/5/92% *v/v*). ^{1}H-NMR (DMSO-d_6, 400 MHz): δ 7.78 (d, J = 8.2 Hz, 2H, Ar-*H*), 7.44 (d, J = 8.2 Hz, 2H, Ar-*H*), 7.34 (m, 3H, Ar-*H*), 7.26 (s, 2H, exchange with D_2O, SO_2NH_2, overlap with signal at 7.25), 7.25 (m, 1H, Ar-*H*), 2.89 (m, 8H, 4 x CH_2). ^{13}C-NMR (DMSO-d_6, 100 MHz): δ 145.71, 142.27, 141.02, 130.04, 129.47, 129.26, 126.88, 126.59, 51.35, 50.91, 36.29, 36.05. MS (ESI positive) *m/z* = 305.1 $[M + H]^+$.

Synthesis of 4-(2-((2-cyanoethyl)amino)ethyl)benzenesulfonamide **(D13)**

Compound **D13** was obtained according the general **procedure 7.2** earlier reported using 4-(2-aminoethyl)benzenesulfonamide (9.99 mmol, 1.0 eq.) and 3-chloropropionitrile (1.1 eq.) in dry DMF (5 mL) stirred at r.t. for 0.5 h (white powder).

4-(2-((2-Cyanoethyl)amino)ethyl)benzenesulfonamide D13: 85% yield; m.p. 85-87 °C; silica gel TLC: R_f = 0.15 (TFA/ MeOH/DCM 3/5/92% *v/v*). ^{1}H-NMR (DMSO-d_6, 400 MHz): δ 7.72 (d, J = 8.0 Hz, 2H, Ar-*H*), 7.41 (d, J = 8.0 Hz, 2H, Ar-*H*), 7.27 (s, 2H, exchange with

D_2O, SO_2NH_2), 2.76 (m, 6H, 3 x CH_2), 2.57 (t, J = 6.6 Hz, 2H, CH_2). ^{13}C-NMR (DMSO-d_6, 100 MHz): δ 145.72, 142.88, 130.14, 126.68, 121.19, 50.83, 45.66, 36.59, 18.88. MS (ESI positive) m/z = 254.0 $[M + H]^+$.

*General procedure **8** for the synthesis of amines **D14, D15***

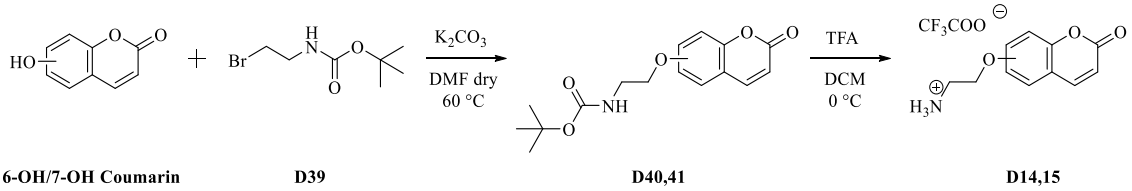

6-OH/7-OH Coumarin **D39** **D40,41** **D14,15**

Step 1. *tert*-Butyl (2-bromoethyl)carbamate **D39** (1.0 g, 1.0 eq.) was treated with 6-hydroxy-2H-chromen-2-one (6-OH) and K_2CO_3 (3.0 eq.) in acetone or alternatively with 7-hydroxy-2H-chromen-2-one (7-OH) (1.0 eq.) in the same conditions using dry *N*,*N*-dimethylformamide (5.0 mL) as solvent and under N_2 atmosphere. The reaction mixtures were stirred at 60 °C overnight until consumption of starting materials (TLC monitoring), then cooled to room temperature and treated respectively as follows.

(i) The white precipitate was filtered off, and the obtained filtrate was concentrated under vacuo to afford **D40** (tert-Butyl (2-((2-oxo-2H-chromen-6-yl)oxy)ethyl)carbamate) as an orange residue.

(ii) The reaction was quenched with a 3.0 M aqueous hydrochloric acid solution to give a precipitate which was collected by filtration and triturated with diethyl ether to afford **D41** (tert-butyl (2-((2-oxo-2H-chromen-7-yl)oxy)ethyl)-carbamate) as a white solid.

Step 2. **D40** (1.0 eq.) and **D41** (1.0 eq.) were dissolved in DCM, and TFA (6.0 eq.) was added dropwise to the suspension. The solution was stirred at 0 °C and then at room temperature until starting materials were consumed (TLC monitoring). The solvent was evaporated, and the obtained residue dried under vacuo to afford the title compounds **D14** and **D15** as white solids.

2-((2-Oxo-2*H*-chromen-6-yl)oxy)ethan-1-aminium 2,2,2-Tri-fluoroacetate D14: 20.0% yield; silica gel TLC R_f = 0.55 (ethyl acetate/n-hexane 50% *v/v*); δ_H (400 MHz, DMSO-d_6) 3.30 (2H, q, J = 5.2, CH_2NH-), 4.25 (2H, t, J = 5.0, CH_2O), 6.54 (1H, d, J = 9.2, Ar-*H*), 7.29 (1H, d, J = 3.2, Ar-*H*), 7.36 (1H, d, J = 2.8, Ar-*H*), 7.41 (1H, d, J = 8.8, Ar-*H*), 8.06 (1H, d, J

= 9.2, Ar-*H*); δ_C (100 MHz, DMSO-d_6) 39.3, 66.0, 112.7, 117.7, 118.5, 120.2, 121.0, 144.9, 149.2, 155.1, 161.1; δ_F (376 MHz, DMSO-d_6) −74.84.

2-((2-Oxo-2*H*-chromen-7-yl)oxy)ethan-1-aminium 2,2,2-Tri-fluoroacetate D15: 61.3% yield; silica gel TLC R_f = 0.50 (ethylacetate/n-hexane 50% *v/v*); δ_H (400 MHz, DMSO-d_6) 3.31 (2H, q, *J* = 5.2, C*H*$_2$NH-), 4.31 (2H, t, *J* = 5.16, C*H*$_2$O), 6.36 (1H, d, *J* = 9.02, Ar-*H*), 7.03 (1H, dd, *J* = 8.6, 2.5, Ar-*H*), 7.07 (1H, d, *J* = 2.3, Ar-*H*), 7.70 (1H, d, *J* = 8.66, Ar-*H*), 8.05 (1H, d, *J* = 9.2, Ar-*H*); δ_C (100 MHz, DMSO-d_6) 38.2, 65.2, 101.5, 112.8, 112.9, 113.0, 129.7, 144.4, 115.3, 160.3, 160.9; δ_F (376 MHz, DMSO-d_6) −74.23.

*General procedure **9** for the synthesis of alcohols **D18-D20***

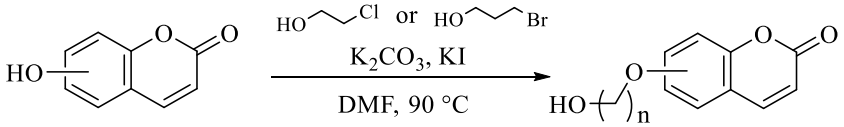

6-OH/7-OH Coumarin

D18: n=2; 7-*subst*
D19: n=3; 6-*subst*
D20: n=3; 7-*subst*

2-Chloro-ethanol (1.2 eq.) or 3-bromopropan-1-ol (1.5 eq.) was added to a suspension of 6-Hydroxy-2H-chromen-2-one (6-OH) (1.0 g, 1.0 eq.) or alternatively 7-hydroxy-2H-chromen-2-one (7-OH) (1.0 eq.), K_2CO_3 (1.2 eq.) and KI (1.0 eq.) in dry *N,N*-dimethylformamide (DMF) (4 mL) under N_2 atmospheres. The reaction mixture was stirred at 90°C O.N. until consumption of starting materials (TLC monitoring), then cooled down to r.t. and quenched with H_2O (10 mL) and was extracted with EtOAc (3 x 10 mL). The combined organic layers were washed with a saturated solution of K_2CO_3, brine and dried over Na_2SO_4, filtered-off and concentrated under *vacuo* to give an oil, that was triturated with diethyl ether and petroleum ether or purified by silica gel column chromatography eluting with the appropriate mixture of EtOAc/n-hexane to afford the titled compounds **D18-D20** as a white solid.

Synthesis of 7-(2-hydroxyethoxy)-2H-chromen-2-one **(D18)**

Compound **D18** was obtained according to the general procedure **9** earlier reported adding 2-Chloro-ethanol (1.2 eq.) to a suspension of 7-hydroxy-2H-chromen-2-one (7-OH) (1.0 eq.),

K_2CO_3 (1.2 eq.) and KI (1.0 eq.) in dry DMF (8.0 mL). The crude residue was triturated with diethyl ether and petroleum ether to give the titled compound **D18** as a white solid.

7-(2-Hydroxyethoxy)-2*H*-chromen-2-one D18: 50% yield; m.p. 85-87°C; silica gel TLC: R_f = 0.22 (ethyl acetate/*n*-hexane 50% *v/v*); ^{1}H-NMR (DMSO-d_6, 400 MHz): δ 3.77 (2H, q, CH_2-OH), 4.13 (2H, t, *J* = 9.6, 4.8, O-CH_2-CH$_2$-OH), 4.95 (1H, t, *J* = 11.2, 5.6, CH$_2$-O*H*), 6.32 (1H, d, *J* = 9.6, Ar-*H*), 7.99 (1H, dd, *J* = 8.6, 3.6, Ar-*H*), 7.02 (1H, d, *J* = 2.0, Ar-*H*), 7.66 (1H, d, *J* = 8.8, Ar-*H*), 8.02 (1H, d, *J* = 9.2, Ar-*H*); ^{13}C-NMR (DMSO-d_6, 100 MHz): δ 60.3, 71.3, 102.1, 113.2, 113.3, 113.7, 130.4, 145.3, 156.3, 161.2, 162.9; MS (ESI positive) *m/z* = 207.0 $[M + H]^+$.

Synthesis of 6-(3-hydroxypropoxy)-2H-chromen-2-one **(D19)**

Compound **D19** was obtained according to the general procedure **9** earlier reported adding 3-bromopropan-1-ol (2.0 eq.) to a suspension of 6-hydroxy-2H-chromen-2-one (6-OH) (1.0 g, 1.0 eq.), K_2CO_3 (1.2 eq.) and KI (1.0 eq.) in dry DMF (6.0 mL). The crude residue was purified by silica gel column chromatography eluting with EtOAc/n-hexane from 50%, then 60% and finally 80 % *v/v* to give the titled compound **D19** as a white solid.

6-(3-Hydroxypropoxy)-2*H*-chromen-2-one D19: 89% yield; m.p. 124-126 °C; silica gel TLC: R_f = 0.17 (ethyl acetate/*n*-hexane 60% *v/v*); ^{1}H-NMR (DMSO-d_6, 400 MHz): δ 1.92 (2H, m, CH$_2$-CH_2-CH$_2$-OH), 3.60 (2H, q, CH_2-OH), 4.11 (2H, t, *J* = 12.8, 6.4, CH_2-CH$_2$-CH$_2$-OH), 4.61 (1H, t, *J* = 10.4, 5.2, CH$_2$-O*H*), 6.52 (1H, d, *J* = 9.6, Ar-*H*), 7.24 (1H, dd, *J* = 8.6, 3.6, Ar-*H*), 7.32 (1H, d, *J* = 2.8, Ar-*H*), 7.36 (1H, m, Ar-*H*), 8.03 (1H, d, *J* = 9.6, Ar-*H*); ^{13}C-NMR (DMSO-d_6, 100 MHz): δ 32.9, 58.1, 66.2, 112.2, 117.4, 118.2, 120.1, 120.8, 145.0, 148.7, 155.9, 161.1; MS (ESI positive) *m/z* = 221.0 $[M + H]^+$.

Synthesis of 7-(3-hydroxypropoxy)-2H-chromen-2-one **(D20)**

Compound **D20** was obtained according to the general procedure **9** earlier reported adding 3-bromopropan-1-ol (1.0 eq.) to a suspension of 7-hydroxy-2H-chromen-2-one (7-OH) (1.0 eq.), K_2CO_3 (1.2 eq.) and KI (1.0 eq.) in dry DMF (8.0 mL). The crude residue was triturated with diethyl ether to give the titled compound **D20** as a white solid.

7-(3-Hydroxypropoxy)-2H-chromen-2-one D20: 27% yield; m.p. 75-77°C; silica gel TLC: R_f = 0.18 (ethyl acetate/*n*-hexane 60% *v/v*); ^{1}H-NMR (DMSO-d_6, 400 MHz): δ 1.92 (2H, m, CH$_2$-CH_2-CH$_2$-OH), 3.60 (2H, q, CH_2-OH), 4.18 (2H, t, *J* = 12.8, 6.4, CH_2-CH$_2$-CH$_2$-OH),

4.61 (1H, t, *J* = 10.4, 5.2, CH_2-O*H*), 6.31 (1H, d, *J* = 9.2, Ar-*H*), 6.98 (1H, dd, *J* = 8.6, 3.6, Ar-*H*), 7.00 (1H, d, *J* = 2.4, Ar-*H*), 7.65 (1H, d, *J* = 8.4, Ar-*H*), 8.02 (1H, d, *J* = 9.6, Ar-*H*); ^{13}C-NMR (DMSO-d_6, 100 MHz): δ 32.8, 58.0, 66.3, 102.0, 113.2, 113.3, 113.6, 130.4, 145.2, 156.3, 161.2, 162.8; MS (ESI positive) *m/z* = 221.0 $[M + H]^+$.

*General procedure **10** for the synthesis of hybrid compounds* **D21-D38**

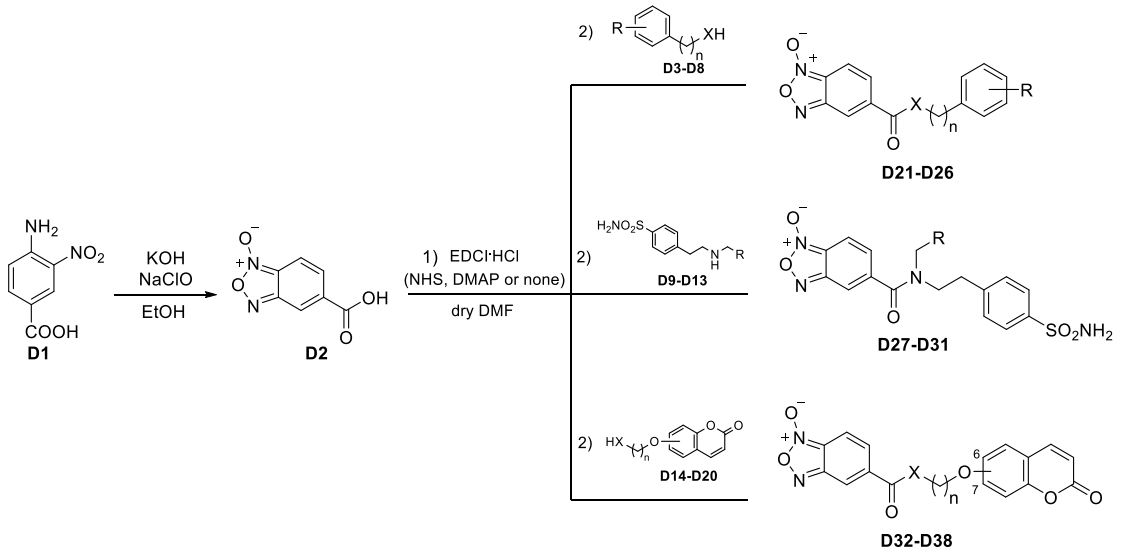

D3, D21: X=NH; n=0; R= *m*-SO_2NH_2
D4, D22: X=NH; n=0; R= *p*-SO_2NH_2
D5, D23: X=NH; n=0; R= *o*-OH, *m*-SO_2NH_2
D6, D24: X=NH; n=1; R= *p*-SO_2NH_2
D7, D25: X=NH; n=2; R= *p*-SO_2NH_2
D8, D26: X=O; n=0; R= *p*-SO_2NH_2

D9, D27: R= C_6H_5
D10, D28: R= 4-F-C_6H_4
D11, D29: R= 2-furyl
D12, D30: R= $CH_2C_6H_5$
D13, D31: R= CH_2CN

D14, D32: X=NH; n=2; 6-*subst*
D15, D33: X=NH; n=2; 7-*subst*
D16, D34: X=O; n=0; 6-*subst*
D17, D35: X=O; n=0; 7-*subst*
D18, D36: X=O; n=2; 7-*subst*
D19, D37: X=O; n=3; 6-*subst*
D20, D38: X=O; n=3; 7-*subst*

EDCI·HCl (1.5 eq.) and 1-hydroxy-7-azabenzotriazole (HOAt) and/or 4-dimethylaminopyridine (DMAP) and/or *N*-hydroxysuccinimide (NHS) (1.3 eq.) were added to a solution of the key intermediate **D2** (0.5 g, 1.0 eq.) in dry DMF (3.0 mL) under a N_2 atmosphere. The reaction was stirred at r.t. until the consumption of the starting material and, thereafter, the appropriate sulfonamide or coumarin bearing a NH_2 or OH group (1.1 eq.) was added to the reaction mixture. The latter was stirred at r.t. and checked by TLC monitoring to visualize the completion of the reaction, which was then quenched with slush and HCl 1M to afford a precipitate. The powder was collected by filtration or the suspension was extracted with ethyl acetate. The combined organic layers were washed with HCl 1M, brine, and dried over anhydrous Na_2SO_4, filtered-off, and concentrated under *vacuo* to give a residue that was triturated with Et_2O or purified by silica gel column chromatography eluting with the appropriate mixture of solvents to yield the titled compounds **D21-D38**.

Synthesis of 5-((3-sulfamoylphenyl)carbamoyl)benzo[c][1,2,5]oxadiazole 1-oxide **(D21)**

Compound **D21** was obtained according to the general procedure **10** earlier reported adding EDCI·HCl (1.5 eq.) and HOAt (1.5 eq.) to a solution of compound **D2** (0.3 g, 1.0 eq.) and commercial 3-aminobenzensulfonamide (1.1 eq.) in dry DMF (5.0 mL). After 20 min, 0.5 eq. of triethylamine (TEA) and 0.03 eq. of DMAP were added to the reaction mixture. The crude residue was collected by filtration and the precipitate washed with water to give **D21** as a yellow solid.

5-((3-Sulfamoylphenyl)carbamoyl)benzo[c][1,2,5]oxadiazole 1-oxide D21: 79% yield; m.p. 221-223 °C; silica gel TLC: R_f = 0.61 (ethyl acetate/*n*-hexane 70% *v/v*); ^{1}H-NMR (DMSO-d_6, 400 MHz): δ 7.45 (2H, s, exchangeable with D_2O, SO_2NH_2), 7.62 (2H, m, Ar-*H*), 7.92 (2H, m, Ar-*H*), 8.01 (1H, m, Ar-*H*), 8.38 (1H, s, Ar-*H*), 8.43 (1H, s, Ar-*H*), 10.86 (1H, s, exchangeable with D_2O, N*H*); MS (ESI negative) *m/z* = 333.1 $[M - H]^-$.

Synthesis of 5-((4-sulfamoylphenyl)carbamoyl)benzo[c][1,2,5]oxadiazole 1-oxide **(D22)**

Compound **D22** was obtained according to the general procedure **10** earlier reported adding EDCI·HCl (1.5 eq.) and HOAt (1.5 eq.) to a solution of compound **D2** (0.5 g, 1.0 eq.) and commercial sulfanilamide (1.1 eq.) in dry DMF (3.0 mL). After 20 min, 0.5 eq. of triethylamine (TEA) and 0.03 eq. of DMAP were added to the reaction mixture. The crude residue was collected by filtration to give **D22** as a yellow solid.

5-((4-Sulfamoylphenyl)carbamoyl)benzo[c][1,2,5]oxadiazole 1-oxide D22: 69% yield; m.p. 211-214 °C; silica gel TLC: R_f = 0.40 (ethyl acetate/*n*-hexane 60% *v/v*); ^{1}H-NMR (DMSO-d_6, 400 MHz): δ 7.34 (2H, s, exchangeable with D_2O, SO_2NH_2), 7.98 (6H, m, Ar-*H*), 8.51 (1H, s, Ar-*H*), 10.89 (1H, s, Ar-*H*); MS (ESI negative) *m/z* = 333.0 $[M - H]^-$.

Synthesis of 5-((2-hydroxy-5-sulfamoylphenyl)carbamoyl)benzo[c][1,2,5]oxadiazole 1-oxide **(D23)**

Compound **D23** was obtained according to the general procedure **10** earlier reported adding EDCI·HCl (1.5 eq.) and DMAP (0.03 eq.) to a solution of compound **D2** (0.5 g, 1.0 eq.) and commercial 2-Aminophenol-4-sulfonamide (1.2 eq.) in dry DMF (3.0 mL). The crude residue was collected by filtration and then was triturated with Et_2O for 24 h to give **D23** as an orange solid.

5-((2-Hydroxy-5-sulfamoylphenyl)carbamoyl)benzo[c][1,2,5]oxadiazole 1-oxide D23: 31% yield; m.p. 208-210 °C; silica gel TLC: R_f = 0.50 (ethyl acetate/*n*-hexane 80% *v/v*); ^{1}H-NMR (DMSO-d_6, 400 MHz): δ 7.09 (1H, d, J = 8.4, exchangeable with D_2O, -NH_2), 7.25 (2H, s, Ar-*H*), 7.58 (1H, dd, J = 8.4, 2.0, Ar-*H*), 7.93 (2H, s, Ar-*H*), 8.16 (1H, s, Ar-*H*), 8.37 (1H, s, Ar-*H*), 10.10 (1H, s, exchangeable with D_2O, -N*H*), 10.67 (1H, s, exchangeable with D_2O, -O*H*); MS (ESI negative) *m/z* = 348.8 $[M - H]^-$.

Synthesis of 5-((4-sulfamoylbenzyl)carbamoyl)benzo[c][1,2,5]oxadiazole 1-oxide **(D24)**

Compound **D24** was obtained according to the general procedure **10** earlier reported adding EDCI·HCl (1.7 eq.) and NHS (1.3 eq.) to a solution of compound **D2** (0.2 g, 1.0 eq.) in dry DMF (2.0 mL). After 2.5 h the starting materials were consumed and 1.2 eq. of commercial 4-Aminomethylbenzenesulfonamide hydrochloride was treated with TEA (1.0 eq.) and were added to the reaction mixture. The crude residue was collected by filtration, then was extracted with EtOAc (3 × 10 mL). The combined organic layers were washed with H_2O (3 × 20 mL), dried over Na_2SO_4, filtered off, and concentrated under *vacuo* to give an oil that was purified by silica gel column chromatography, eluting with the mixture of EtOAc/n-hexane 50% *v/v* to afford an solid that was also triturated with Et_2O to give **D24** as a yellow solid.

5-((4-Sulfamoylbenzyl)carbamoyl)benzo[c][1,2,5]oxadiazole 1-oxide D24: 21% yield; m.p. 200-202 °C; silica gel TLC: R_f = 0.38 (ethyl acetate/*n*-hexane 70% *v/v*); ^{1}H-NMR (DMSO-d_6, 400 MHz): δ 4.59 (2H, d, J = 5.6, CH_2), 7.34 (2H, s, exchangeable with D_2O, SO_2NH_2), 7.55 (2H, d, J = 8.4, Ar-*H*), 7.82 (2H, d, J = 8.4, Ar-*H*), 7.93 (2H, m, Ar-*H*), 8.24 (1H, s, Ar-*H*), 9.48 (1H, t, J = 5.6, exchangeable with D_2O, CON*H*); MS (ESI negative) *m/z* = 347.1 $[M - H]^-$.

Synthesis of 5-((4-sulfamoylphenethyl)carbamoyl)benzo[c][1,2,5]oxadiazole 1-oxide **(D25)**

Compound **D25** was obtained according to the general procedure **10** earlier reported adding EDCI·HCl (1.7 eq.) and NHS (1.3 eq.) to a solution of compound **D2** (0.1 g, 1.0 eq.) in dry DMF (1.0 mL). After 3 h the starting materials were consumed and 1.7 eq. of commercial 4-(2-aminoethyl)benzenesulfonamide was added to the reaction mixture. The crude residue was collected by filtration, then was washed with acid water (5 × 2 mL) to give **D25** as a white solid.

5-((4-Sulfamoylphenethyl)carbamoyl)benzo[c][1,2,5]oxadiazole 1-oxide D25: 89% yield; m.p. 206-208 °C; silica gel TLC: R_f = 0.18 (ethyl acetate/*n*-hexane 60% *v/v*); ^{1}H-NMR (DMSO-d_6, 400 MHz): δ 2.97 (2H, t, J = 7.4, NH-CH_2-CH_2), 3.58 (2H, q, J = 6.8, NH-CH_2-CH_2), 7.37 (2H, s, exchangeable with D_2O, SO_2NH_2), 7.48 (2H, d, J = 8.4, Ar-*H*), 7.78 (2H, d, J = 8.4, Ar-*H*), 7.85 (2H, s, Ar-*H*), 8.12 (1H, s, Ar-*H*), 8.97 (1H, t, J = 5.2, Ar-*H*); MS (ESI negative) *m/z* = 361.0 $[M - H]^-$.

Synthesis of 5-((4-sulfamoylphenoxy)carbonyl)benzo[c][1,2,5]oxadiazole 1-oxide **(D26)**

Compound **D26** was obtained according to the general procedure **10** earlier reported adding EDCI·HCl (1.8 eq.) and DMAP (0.03 eq.) to a solution of compound **D2** (0.5 g, 1.0 eq.) and commercial 4-Hydroxybenzensulfonamide (1.0 eq.) in dry DMF (3.0 mL). The crude residue was collected by filtration and then was purified by silica gel column chromatography, eluting with the mixture of methanol/dichloromethane 1% *v/v* to afford **D26** as a yellow solid.

5-((4-Sulfamoylphenoxy)carbonyl)benzo[c][1,2,5]oxadiazole 1-oxide D26: 98% yield; m.p. 202-204 °C; silica gel TLC: R_f = 0.78 (ethyl acetate/*n*-hexane 80% *v/v*); ^{1}H-NMR (DMSO-d_6, 400 MHz): δ 7.50 (2H, s, exchangeable with D_2O, NH_2), 7.61 (2H, d, J = 8.8, Ar-*H*), 7.98 (4H, m, Ar-*H*), 8.50 (1H, s, Ar-*H*); MS (ESI negative) *m/z* = 333.9 $[M - H]^-$.

Synthesis of 5-(benzyl(4-sulfamoylphenethyl)carbamoyl)benzo[c][1,2,5]oxadiazole 1-oxide **(D27)**

Compound **D27** was obtained according to the general procedure **10** earlier reported adding EDCI·HCl (2.0 eq.) and DMAP (0.03 eq.) to a solution of compound **D2** (0.3 g, 1.0 eq.) and sulfonamide intermediate **D9** (1.05 eq.) in dry DMF (4.0 mL). The crude residue was collected by filtration and then was purified by silica gel column chromatography, eluting with the mixture of EtOAc/n-hexane 50% *v/v* to afford **D27** as a yellow solid.

5-(Benzyl(4-sulfamoylphenethyl)carbamoyl)benzo[c][1,2,5]oxadiazole 1-oxide D27: 41% yield; m.p. 188-190 °C; silica gel TLC: R_f = 0.38 (ethyl acetate/*n*-hexane 60% *v/v*); ^{1}H-NMR (DMSO-d_6, 400 MHz): δ 2.82 (1H, m, CH_2-CH_2-Ph), 3.03 (1H, m, CH_2-CH_2-Ph), 3.53 (1H, m, CH_2-CH_2-Ph), 3.61 (1H, m, CH_2-CH_2-Ph), 4.52 (1H, s, N-CH_2-Ph), 4.83 (1H, s, N-CH_2-Ph), 6.88 (1H, s, Ar-*H*), 7.23 (2H, m, Ar-*H*), 7.44 (8H, m, SO_2NH_2, Ar-*H*), 7.70 (2H, d, J = 7.6, Ar-*H*), 7.80 (1H, d, J = 7.9, Ar-*H*), ; MS (ESI positive) *m/z* = 353.1 $[M + H]^+$.

Synthesis of 5-((4-fluorobenzyl)(4-sulfamoylphenethyl)carbamoyl)benzo[c][1,2,5]oxadiazole 1-oxide **(D28)**

Compound **D28** was obtained according to the general procedure **10** earlier reported adding EDCI·HCl (1.8 eq.) and DMAP (0.03 eq.) to a solution of compound **D2** (0.2 g, 1.0 eq.) and sulfonamide intermediate **D10** (1.0 eq.) in dry DMF (3.0 mL). The crude residue was extracted with EtOAc (3 × 10 mL). The combined organic layers were washed with H_2O (3 × 20 mL), dried over Na_2SO_4, filtered off, and concentrated under *vacuo* to give an oil that was purified by silica gel column chromatography, eluting with the mixture of EtOAc/n-hexane 50% *v/v* to give **D28** as a yellow solid.

5-((4-Fluorobenzyl)(4-sulfamoylphenethyl)carbamoyl)benzo[c][1,2,5]oxadiazole 1-oxide D28: 19% yield; m.p. 127-129 °C; silica gel TLC: R_f = 0.56 (ethyl acetate/*n*-hexane 70% *v/v*); ^{1}H-NMR (DMSO-d_6, 400 MHz): δ 2.92 (1H, m, CH_2-CH_2-Ph), 3.02 (1H, m, CH_2-CH_2-Ph), 3.53 (1H, m, CH_2-CH_2-Ph), 3.61 (1H, m, CH_2-CH_2-Ph), 4.51 (1H, s, N-CH_2-Ph), 4.81 (1H, s, N-CH_2-Ph), 6.87 (1H, s, Ar-*H*), 7.24 (5H, m, exchangeable with D_2O, SO_2NH_2, Ar-*H*), 7.36 (1H, m, Ar-*H*), 7.51 (2H, m, Ar-*H*), 7.70 (2H, d, *J* = 8.0, Ar-*H*), 7.80 (2H, d, *J* = 8.0, Ar-*H*); MS (ESI positive) *m/z* = 371.0 $[M + H]^+$.

Synthesis of 5-((furan-2-ylmethyl)(4-sulfamoylphenethyl)carbamoyl)benzo[c][1,2,5]oxadiazole 1-oxide **(D29)**

Compound **D29** was obtained according to the general procedure **10** earlier reported adding EDCI·HCl (1.8 eq.) and DMAP (0.03 eq.) to a solution of compound **D2** (0.2 g, 1.0 eq.) and sulfonamide intermediate **D11** (1.0 eq.) in dry DMF (3.0 mL). The crude residue was extracted with EtOAc (3 × 10 mL). The combined organic layers were washed with H_2O (3 × 20 mL), dried over Na_2SO_4, filtered off, and concentrated under *vacuo* to give an orange solid that was purified by silica gel column chromatography, eluting with the mixture of methanol/dichloromethane 1% *v/v* and the obtained oil was triturated with Et_2O to give **D29** as a yellow solid.

5-((Furan-2-ylmethyl)(4-sulfamoylphenethyl)carbamoyl)benzo[c][1,2,5]oxadiazole 1-oxide D29: 29% yield; m.p. 147-149 °C; silica gel TLC: R_f = 0.48 (ethyl acetate/*n*-hexane 80% *v/v*); ^{1}H-NMR (DMSO-d_6, 400 MHz): δ 2.92 (2H, m, CH_2-CH_2-Ph), 3.60 (2H, m, CH_2-CH_2-Ph), 4.53 (1H, s, CH_2-Furan), 4.83 (1H, s, CH_2-Furan), 6.52 (2H, m, Ar-*H*), 6.84 (1H, s,

Ar-*H*), 7.52 (9H, m, exchangeable with D_2O, SO_2NH_2, 7 x Ar-*H*); MS (ESI positive) *m/z* = 443.0 $[M + H]^+$.

Synthesis of 5-(phenethyl(4-sulfamoylphenethyl)carbamoyl)benzo[c][1,2,5]oxadiazole 1-oxide **(D30)**

Compound **D30** was obtained according to the general procedure **10** earlier reported adding EDCI·HCl (1.8 eq.) and DMAP (0.03 eq.) to a solution of compound **D2** (0.2 g, 1.0 eq.) and sulfonamide intermediate **D12** (1.0 eq.) in dry DMF (3.0 mL). The crude residue was collected by filtration and then was purified by silica gel column chromatography, eluting with the mixture of EtOAc/*n*-hexane 50% *v/v* to give **D30** as a yellow solid.

5-(Phenethyl(4-sulfamoylphenethyl)carbamoyl)benzo[c][1,2,5]oxadiazole 1-oxide D30: 37% yield; m.p. 196-198 °C; silica gel TLC: R_f = 0.42 (ethyl acetate/*n*-hexane 70% *v/v*); ^{1}H-NMR (DMSO-d_6, 400 MHz): δ 2.85 (2H, m, CH_2-CH_2-Ph), 3.04 (2H, m, CH_2-CH_2-Ph), 3.33 (2H, m, overlapped with the water peak, CH_2-CH_2-Ph), 4.13 (2H, m, CH_2-CH_2-Ph), 6.75 (1H, s, Ar-*H*), 6.95 (1H, s, Ar-*H*), 7.07 (1H, s, Ar-*H*), 7.26 (2H, m, exchangeable with D_2O, SO_2NH_2), 7.36 (4H, m, Ar-*H*), 7.56 (2H, d, *J* = 8.0, Ar-*H*), 7.69 (2H, d, *J* = 8.0, Ar-*H*), 7.83 (1H, d, *J* = 8.0, Ar-*H*); MS (ESI positive) *m/z* = 367.1 $[M + H]^+$.

Synthesis of 5-((2-cyanoethyl)(4-sulfamoylphenethyl)carbamoyl)benzo[c][1,2,5]oxadiazole 1-oxide **(D31)**

Compound **D31** was obtained according to the general procedure **10** earlier reported adding EDCI·HCl (1.8 eq.) and DMAP (0.03 eq.) to a solution of compound **D2** (0.4 g, 1.0 eq.) and sulfonamide intermediate **D13** (1.0 eq.) in dry DMF (3.0 mL). The crude residue was collected by filtration and then was purified by silica gel column chromatography, eluting with the mixture of methanol/dichloromethane 1% *v/v* to give a white solid that was triturated with Et_2O to afford **D31** as a white solid.

5-((2-Cyanoethyl)(4-sulfamoylphenethyl)carbamoyl)benzo[c][1,2,5]oxadiazole 1-oxide D31: 23% yield; m.p. 212-214 °C; silica gel TLC: R_f = 0.45 (ethyl acetate/*n*-hexane 80% *v/v*); ^{1}H-NMR (DMSO-d_6, 400 MHz): δ 2.94 (4H, m, CH_2-CH_2-Ph, CH_2-CH_2-CN), 3.62 (2H, m, CH_2-CH_2-Ph), 3.75 (1H, m, N-CH_2-CH_2-Ph), 3.84 (1H, s, N-CH_2-CH_2-Ph), 6.84 (1H, m, Ar-*H*), 7.44 (4H, m, Ar-*H*), 7.76 (4H, m, exchangeable with D_2O, SO_2NH_2, Ar-*H*); MS (ESI negative) *m/z* = 413.9 $[M - H]^-$.

Synthesis of 5-((2-((2-oxo-2H-chromen-6-yl)oxy)ethyl)carbamoyl)benzo[c][1,2,5]oxadiazole 1-oxide **(D32)**

Compound **D32** was obtained according to the general procedure **10** earlier reported adding EDCI·HCl (1.7 eq.) and NHS (1.3 eq.) to a solution of compound **D2** (0.1 g, 1.0 eq.) in dry DMF (1.0 mL). After 4 h, 1.0 eq. of triethylamine (TEA) and 1.0 eq. of **D14** were added to the reaction mixture. The crude residue was collected by filtration and washed with acid water to give **D32** as a yellow solid.

5-((2-((2-Oxo-2*H*-chromen-6-yl)oxy)ethyl)carbamoyl)benzo[c][1,2,5]oxadiazole 1-oxide D32: 36% yield; m.p. 212-214 °C; silica gel TLC: R_f = 0.30 (ethyl acetate/*n*-hexane 70% *v/v*); ^{1}H-NMR (DMSO-d_6, 400 MHz): δ 3.74 (2H, m, NH-CH_2), 4.25 (2H, t, J = 5.4, -OCH_2), 6.54 (1H, d, J = 9.6, Ar-*H*), 7.29 (1H, dd, J = 9.2, 2.4, Ar-*H*), 7.40 (2H, m, Ar-*H*), 7.88 (2H, m, Ar-*H*), 8.05 (1H, d, J = 5.6, Ar-*H*), 8.20 (1H, m, Ar-H), 9.12 (1H, s, exchangeable with D_2O, N*H*); MS (ESI negative) *m/z* = 366.0 $[M - H]^-$.

Synthesis of 5-((2-((2-oxo-2H-chromen-7-yl)oxy)ethyl)carbamoyl)benzo[c][1,2,5]oxadiazole 1-oxide **(D33)**

Compound **D33** was obtained according to the general procedure **10** earlier reported adding EDCI·HCl (1.7 eq.) and NHS (1.3 eq.) to a solution of compound **D2** (0.06 g, 1.0 eq.) in dry DMF (1.0 mL). After 5 h, 1.0 eq. of triethylamine (TEA) and 1.0 eq. of **D15** were added to the reaction mixture. The crude residue was collected by filtration and washed with acid water to give **D33** as a light brown solid.

5-((2-((2-Oxo-2*H*-chromen-7-yl)oxy)ethyl)carbamoyl)benzo[c][1,2,5]oxadiazole 1-oxide D33: 83% yield; m.p. 217-219 °C; silica gel TLC: R_f = 0.35 (ethyl acetate/*n*-hexane 70% *v/v*); ^{1}H-NMR (DMSO-d_6, 400 MHz): δ 3.73 (2H, m, NH-CH_2), 4.30 (2H, t, J = 5.4, -OCH_2), 6.33 (1H, d, J = 9.6, Ar-*H*), 7.02 (1H, dd, J = 9.2, 2.4, Ar-*H*), 7.07 (1H, m, Ar-*H*), 7.67 (1H, d, J = 8.4, Ar-*H*), 7.87 (2H, s, Ar-*H*), 8.02 (1H, d, J = 9.6, Ar-H), 8.16 (1H, s, Ar-*H*), 9.11 (1H, s, exchangeable with D_2O, N*H*); MS (ESI positive) *m/z* = 368.1 $[M + H]^+$.

Synthesis of 5-(((2-oxo-2H-chromen-6-yl)oxy)carbonyl)benzo[c][1,2,5]oxadiazole 1-oxide **(D34)**

Compound **D34** was obtained according to the general procedure **10** earlier reported adding EDCI·HCl (1.8 eq.) and DMAP (0.03 eq.) to a solution of compound **D2** (0.3 g, 1.0 eq.) and

commercial 6-Hydroxycoumarin (1.0 eq.) in dry DMF (2.0 mL). The crude residue was collected by filtration and then was triturated with Et_2O to afford **D34** as a yellow solid.

5-(((2-Oxo-2H-chromen-6-yl)oxy)carbonyl)benzo[c][1,2,5]oxadiazole 1-oxide D34: 49% yield; m.p. 225-227 °C; silica gel TLC: R_f = 0.75 (ethyl acetate/*n*-hexane 70% *v/v*); ^{1}H-NMR (DMSO-d_6, 400 MHz): δ 6.62 (1H, d, *J* = 9.2, Ar-*H*), 7.58 (1H, d, *J* = 8.8, Ar-*H*), 7.69 (1H, dd, *J* = 8.8, 2.4, Ar-*H*), 7.81 (1H, d, *J* = 2.4, Ar-*H*), 7.99 (2H, s, Ar-*H*), 8.12 (1H, d, *J* = 9.6, Ar-*H*), 8.50 (1H, s, Ar-*H*); MS (ESI negative) *m/z* = 324.9 $[M - H]^-$.

Synthesis of 5-(((2-oxo-2H-chromen-7-yl)oxy)carbonyl)benzo[c][1,2,5]oxadiazole 1-oxide **(D35)**

Compound **D35** was obtained according to the general procedure **10** earlier reported adding EDCI·HCl (1.8 eq.) and DMAP (0.03 eq.) to a solution of compound **D2** (0.3 g, 1.0 eq.) and commercial 7-hydroxycoumarin (1.0 eq.) in dry DMF (2.5 mL). The crude residue was collected by filtration and then was triturated with Et_2O to afford **D35** as a yellow solid.

5-(((2-Oxo-2*H*-chromen-7-yl)oxy)carbonyl)benzo[c][1,2,5]oxadiazole 1-oxide D35: 62% yield; m.p. 225-227 °C; silica gel TLC: R_f = 0.6 (ethyl acetate/*n*-hexane 70% *v/v*); ^{1}H-NMR (DMSO-d_6, 400 MHz): δ 6.56 (1H, d, *J* = 9.6, Ar-*H*), 7.43 (1H, d, *J* = 8.4, Ar-*H*), 7.57 (1H, s, Ar-*H*), 7.89 (1H, d, *J* = 8.4, Ar-*H*), 7.98 (2H, s, Ar-*H*), 8.15 (1H, d, *J* = 9.6, Ar-*H*), 8.51 (1H, s, Ar-*H*); MS (ESI negative) *m/z* = 324.9 $[M - H]^-$.

Synthesis of 5-((2-((2-oxo-2H-chromen-7-yl)oxy)ethoxy)carbonyl)benzo[c][1,2,5]oxadiazole 1-oxide **(D36)**

Compound **D36** was obtained according to the general procedure **10** earlier reported adding EDCI·HCl (1.8 eq.) and DMAP (0.03 eq.) to a solution of compound **D2** (0.3 g, 1.0 eq.) and intermediate **D18** (1.0 eq.) in dry DMF (2.0 mL). The crude residue was collected by filtration and then was washed with water to afford **D36** as a yellow solid.

5-((2-((2-Oxo-2*H*-chromen-7-yl)oxy)ethoxy)carbonyl)benzo[c][1,2,5]oxadiazole 1-oxide D36: 43% yield; m.p. 164-166 °C; silica gel TLC: R_f = 0.48 (ethyl acetate/*n*-hexane 60% *v/v*); ^{1}H-NMR (DMSO-d_6, 400 MHz): δ 4.54 (2H, m, COO-CH_2-CH_2-O), 4.72 (2H, t, *J* = 4.0, COO-CH_2-CH_2-OH), 6.33 (1H, d, *J* = 9.6, Ar-*H*), 7.05 (1H, dd, *J* = 8.8, 3.7, Ar-*H*), 7.12 (1H, d, *J* = 2.2, Ar-*H*), 7.67 (1H, d, *J* = 8.4, Ar-*H*), 7.85 (2H, s, Ar-*H*), 8.02 (1H, d, *J* = 9.6, Ar-*H*), 8.15 (1H, s, Ar-*H*); MS (ESI positive) *m/z* = 369.1 $[M + H]^+$.

Synthesis of 5-((3-((2-oxo-2H-chromen-6-yl)oxy)propoxy)carbonyl)benzo[c][1,2,5]oxadiazole 1-oxide **(D37)**

Compound **D37** was obtained according to the general procedure **10** earlier reported adding EDCI·HCl (1.8 eq.) and DMAP (0.03 eq.) to a solution of compound **D2** (0.1 g, 1.0 eq.) and intermediate **D19** (1.0 eq.) in dry DMF (3.0 mL). The crude residue was extracted with EtOAc (3 × 10 mL). The combined organic layers were washed with H_2O (3 × 20 mL), dried over Na_2SO_4, filtered off, and concentrated under *vacuo* to give a solid that was purified by silica gel column chromatography, eluting with the mixture of EtOAc/n-hexane 50% *v/v* to give **D37** as a yellow solid.

5-((3-((2-Oxo-2*H*-chromen-6-yl)oxy)propoxy)carbonyl)benzo[c][1,2,5]oxadiazole 1-oxide D37: 46% yield; m.p. 137-139 °C; silica gel TLC: R_f = 0.64 (ethyl acetate/*n*-hexane 80% *v/v*); ^{1}H-NMR (DMSO-d_6, 400 MHz): δ 2.27 (2H, m, CH_2-CH_2-CH_2), 4.25 (2H, t, *J* = 6.0, COO-CH_2-CH_2-CH_2-O), 4.54 (2H, t, *J* = 6.0, COO-CH_2-CH_2-CH_2-O), 6.52 (1H, d, *J* = 9.6, Ar-*H*), 7.25 (1H, dd, *J* = 8.8, 2.8, Ar-*H*), 7.34 (1H, d, *J* = 2.8, Ar-*H*), 7.36 (1H, d, *J* = 9.2, Ar-*H*), 7.86 (2H, s, Ar-*H*), 8.02 (1H, d, *J* = 9.6, Ar-*H*), 8.24 (1H, s, Ar-*H*); MS (ESI positive) *m/z* = 383.0 $[M + H]^+$.

Synthesis of 5-((3-((2-oxo-2H-chromen-7-yl)oxy)propoxy)carbonyl)benzo[c][1,2,5]oxadiazole 1-oxide **(D38)**

Compound **D38** was obtained according to the general procedure **10** earlier reported adding EDCI·HCl (1.8 eq.) and DMAP (0.03 eq.) to a solution of compound **D2** (0.3 g, 1.0 eq.) and intermediate **D20** (1.0 eq.) in dry DMF (2.0 mL). The crude residue was collected by filtration and then was washed with water to afford **D38** as a yellow solid.

5-((3-((2-Oxo-2*H*-chromen-7-yl)oxy)propoxy)carbonyl)benzo[c][1,2,5]oxadiazole 1-oxide D38: 37% yield; m.p. 176-178 °C; silica gel TLC: R_f = 0.76 (ethyl acetate/*n*-hexane 80% *v/v*); ^{1}H-NMR (DMSO-d_6, 400 MHz): δ 2.28 (2H, q, *J* = 6.0, CH_2-CH_2-CH_2), 4.32 (2H, t, *J* = 6.0, COO-CH_2-CH_2-CH_2-O), 4.52 (2H, t, *J* = 6.0, COO-CH_2-CH_2-CH_2-O), 6.31 (1H, d, *J* = 9.6, Ar-*H*), 7.00 (1H, dd, *J* = 8.8, 3.7, Ar-*H*), 7.05 (1H, d, *J* = 2.2, Ar-*H*), 7.65 (1H, d, *J* = 8.4, Ar-*H*), 7.88 (2H, s, Ar-*H*), 8.02 (1H, d, *J* = 9.6, Ar-*H*), 8.15 (1H, s, Ar-*H*); MS (ESI positive) *m/z* = 383.1 $[M + H]^+$.

5.4.2 Carbonic Anhydrase Inhibition

The CA inhibitory profiles of compounds belonging to Series D were obtained according to the general procedures described at the beginning of the experimental section.

5.5 "A Sweet Combination": an expansion of saccharin and acesulfame K based compounds for selectively targeting tumor-associated carbonic anhydrases IX and XII (Series E)

5.5.1 Chemistry

The general chemistry protocols are reported at the beginning of the experimental section.

*General procedure **11** for the synthesis of compounds **E18-E34***

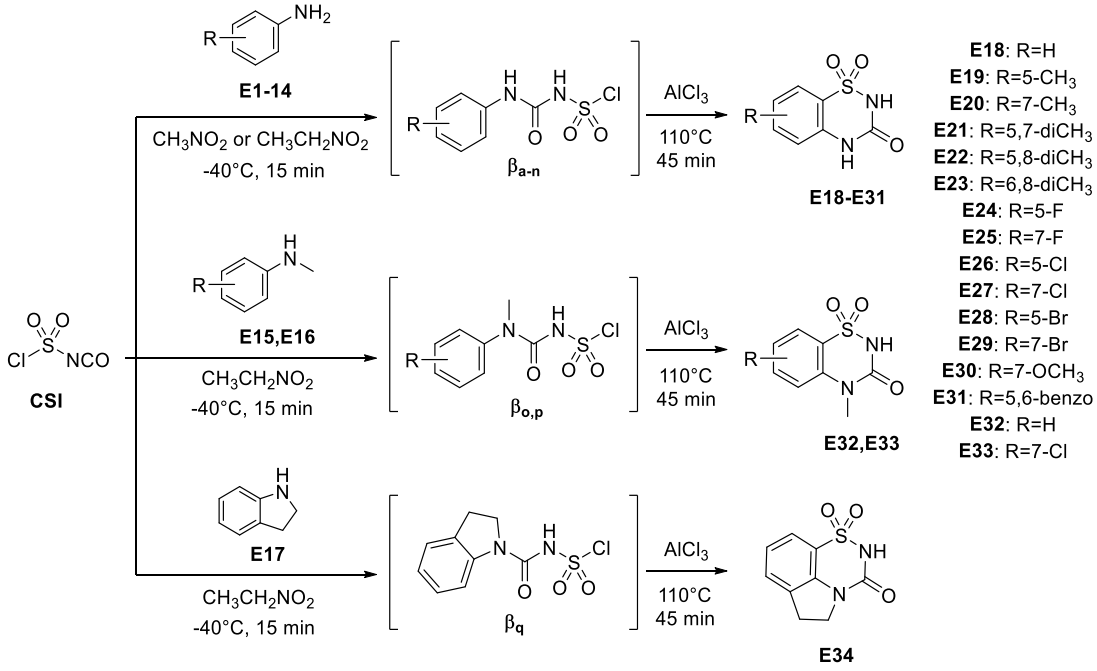

A solution of chlorosulfonyl isocyanate (0.48 mL, 1.1 eq.) in the proper solvent (nitromethane or nitroethane) was treated with a solution of the appropriate aromatic amine (1.0 eq.) in the same solvent (5 mL) at –40 °C. The reaction mixture was stirred for 15 min before $AlCl_3$(s) (1.0 eq.) was added and then it was warmed at 110 °C and stirred for 45 min. The resulting mixture was cooled and poured onto ice. The formed precipitate was collected by filtration and dried to obtain a powder that was purified by silica gel column chromatography eluting with appropriate mixture of solvents or alternatively by dissolution in a saturated solution of $NaHCO_3$ in 1:1 H_2O/MeOH, treatment with charcoal, filtration over Celite and re-acidification to pH 1. The precipitate was filtered *in*

vacuo to afford the titled compound (**E18-E34**) as a fine solid that was collected by filtration.

Synthesis of 2H-benzo[e][1,2,4]thiadiazin-3(4H)-one 1,1-dioxide **(E18)**

Compound **E18** was obtained according to the general procedure **11** earlier reported adding dropwise a solution of aniline **E1** (0.46 mL, 1.0 eq.) in nitromethane (6.0 mL) to a solution of chlorosulfonyl isocyanate (0.48 mL, 1.12 eq.) in nitromethane (6.0 mL). The crude compound was purified by dissolution in a saturated solution of $NaHCO_3$ in 1:1 H_2O/MeOH, treatment with charcoal, filtration over Celite and re-acidification to pH 1. The precipitate was filtered *in vacuo* to afford the title compound **E18**.

2*H*-Benzo[e][1,2,4]thiadiazin-3(4H)-one 1,1-dioxide E18: 31% yield; m.p. >300°C; TLC: R_f = 0.30 (methanol/dichloromethane 20% *v/v*); ^{1}H-NMR (DMSO-d_6, 400 MHz): δ 7.27 (2H, m, Ar-*H*), 7.64 (1H, t, *J* = 8.0, Ar-*H*), 7.78 (1H, d, *J* = 7.6, Ar-*H*), 11.09 (1H, s, exchange with D2O, CON*H*); ^{13}C-NMR (DMSO-d_6, 100 MHz): δ 117.7, 122.9, 123.5, 124.1, 134.6, 136.2, 151.9; ESI-HRMS (*m/z*) [M-H]$^-$: calculated for C7H5N2O3S 197.0021; found 197.0028.

Synthesis of 5-methyl-2H-benzo[e][1,2,4]thiadiazin-3(4H)-one 1,1-dioxide **(E19)**

Compound **E19** was obtained according to the general procedure **11** earlier reported adding dropwise a solution of *O*-toluidine **E2** (1.0 g., 1.0 eq.) in nitroethane (8.0 mL) to a solution of chlorosulfonyl isocyanate (0.89 mL, 1.1 eq.) in nitroethane (7.0 mL). The crude compound was purified by dissolution in a saturated solution of $NaHCO_3$ in 1:1 H_2O/MeOH, treatment with charcoal, filtration over Celite and re-acidification to pH 1. The precipitate was filtered *in vacuo* to afford **E19** as a green solid.

5-Methyl-2*H*-benzo[e][1,2,4]thiadiazin-3(4H)-one 1,1-dioxide E19: 26% yield; m.p. 292-293°C; TLC: R_f = 0.13 (methanol/dichloromethane 15% *v/v*); ^{1}H-NMR (DMSO-d_6, 400 MHz): δ 2.40 (3H, s, CH_3), 7.25 (1H, t, *J* = 7.6, Ar-*H*), 7.55 (1H, d, *J* = 7.6, Ar-*H*), 7.66 (1H, d, *J* = 7.6, Ar-*H*), 10.42 (1H, s, exchange with D_2O, CON*H*); ^{13}C-NMR (DMSO-d_6, 100 MHz): δ 18.4, 120.4, 124.1, 124.4, 127.3, 134.1, 136.1, 151.6; ESI-HRMS (*m/z*) [M-H]$^-$: calculated for C8H7N2O3S 211.0177; found 211.0181.

Synthesis of 7-methyl-2H-benzo[e][1,2,4]thiadiazin-3(4H)-one 1,1-dioxide **(E20)**

Compound **E20** was obtained according to the general procedure **11** earlier reported adding dropwise a solution of p-toluidine **E3**(1.0 g., 1.0 eq.) in nitromethane (9.7 mL) to a solution of chlorosulfonyl isocyanate (0.60 mL, 1.2 eq.) in nitromethane (6.4 mL). The crude compound was purified by dissolution in a saturated solution of $NaHCO_3$ in 1:1 H_2O/MeOH, treatment with charcoal, filtration over Celite and re-acidification to pH 1. The precipitate was filtered *in vacuo* to afford **E20** as a white solid.

7-Methyl-2*H*-benzo[e][1,2,4]thiadiazin-3(4H)-one 1,1-dioxide E20: 40% yield; m.p. 287-288°C; TLC: R_f = 0.30 (methanol/dichloromethane 30% *v/v*); ^{1}H-NMR (DMSO-d_6, 400 MHz): δ 2.38 (3H, s, CH_3), 7.17 (1H, d, *J* = 8.4, Ar-*H*), 7.49 (1H, dd, *J* = 8.0, 1.2, Ar-*H*), 7.63 (1H, s, Ar-*H*), 11.18 (1H, s, exchange with D_2O, CON*H*); ^{13}C-NMR (DMSO-d_6, 100 MHz): δ 21.0, 117.8, 122.4, 123.3, 133.6, 134.0, 135.6, 151.5; ESI-HRMS (*m/z*) $[M-H]^-$: calculated for C8H7N2O3S 211.0177; found 211.0169.

Synthesis of 5,7-dimethyl-2H-benzo[e][1,2,4]thiadiazin-3(4H)-one 1,1-dioxide (**E21)**

Compound **E21** was obtained according to the general procedure **11** earlier reported adding dropwise a solution of 2,4-dimenthylaniline **E4** (1.02 mL, 1.0 eq.) in nitromethane (5.0 mL) to a solution of chlorosulfonyl isocyanate (0.93 mL, 1.3 eq.) in nitromethane (5.0 mL). The crude compound was purified by dissolution in a saturated solution of $NaHCO_3$ in 1:1 H_2O/MeOH, treatment with charcoal, filtration over Celite and re-acidification to pH 1. The precipitate was filtered *in vacuo* to afford **E21** as a white solid.

5,7-Dimethyl-2*H*-benzo[e][1,2,4]thiadiazin-3(4H)-one 1,1-dioxide E21: 60% yield; m.p. 290-291°C; TLC: R_f = 0.23 (methanol/dichloromethane 20% *v/v*); ^{1}H-NMR (DMSO-d_6, 400 MHz): δ 2.35 (6H, d, *J* = 5.6, 2 x CH_3), 7.37 (1H, s, Ar-*H*), 7.48 (1H, s, Ar-*H*), 10.35 (1H, s, exchange with D_2O, CON*H*); ^{13}C-NMR (DMSO-d_6, 100 MHz): δ 18.3, 20.7, 119.9, 124.3, 127.1, 131.7, 133.7, 136.9, 151.5; ESI-HRMS (*m/z*) $[M-H]^-$: calculated for C9H9N2O3S 225.0334; found 225.0329.

Synthesis of 5,8-dimethyl-2H-benzo[e][1,2,4]thiadiazin-3(4H)-one 1,1-dioxide **(E22)**

Compound **E22** was obtained according to the general procedure **11** earlier reported adding dropwise a solution of 2,5-dimenthylaniline **E5** (1.03 mL, 1.0 eq.) in nitromethane (8.0 mL) to a solution of chlorosulfonyl isocyanate (0.93 mL, 1.3 eq.) in nitromethane

(7.0 mL). The crude compound was purified by dissolution in a saturated solution of $NaHCO_3$ in 1:1 H_2O/MeOH, treatment with charcoal, filtration over Celite and re-acidification to pH 1. The precipitate was filtered *in vacuo* to afford **E22** as a white solid. **5,8-Dimethyl-2*H*-benzo[e][1,2,4]thiadiazin-3(4H)-one 1,1-dioxide E22:** 66% yield; m.p. 297-298°C; TLC: R_f = 0.16 (methanol/dichloromethane 20% *v/v*); ^{1}H-NMR (DMSO-d_6, 400 MHz): δ 2.35 (3H, s, 5-CH_3), 2.57 (3H, s, 8-CH_3), 7.04 (1H, d, J = 7.6, Ar-*H*), 7.38 (1H, d, J = 8.0, Ar-*H*), 10.17 (1H, s, exchange with D_2O, CON*H*); ^{13}C-NMR (DMSO-d_6, 100 MHz): δ 18.4, 20.0, 123.2, 124.6, 126.7, 132.9, 134.4, 135.1, 151.2; ESI-HRMS (*m/z*) $[M-H]^-$: calculated for C9H9N2O3S 225.0334; found 225.0338.

Synthesis of 6,8-dimethyl-2H-benzo[e][1,2,4]thiadiazin-3(4H)-one 1,1-dioxide **(E23)**

Compound **E23** was obtained according to the general procedure **11** earlier reported adding dropwise a solution of 3,5-dimethylaniline **E6** (1.03 mL, 1.0 eq.) in nitromethane (5.0 mL) to a solution of chlorosulfonyl isocyanate (0.93 mL, 1.3 eq.) in nitromethane (5.0 mL). The crude compound was purified by dissolution in a saturated solution of $NaHCO_3$ in 1:1 H_2O/MeOH, treatment with charcoal, filtration over Celite and re-acidification to pH 1. The precipitate was filtered *in vacuo* to afford **E23** as a violet solid. **6,8-Dimethyl-2*H*-benzo[e][1,2,4]thiadiazin-3(4H)-one 1,1-dioxide E23:** 32% yield; m.p. 282-283°C; TLC: R_f = 0.11 (methanol/dichloromethane 20% *v/v*); ^{1}H-NMR (DMSO-d_6, 400 MHz): δ 2.32 (3H, s, 6-CH_3), 2.54 (3H, s, overlap with DMSO peak, 8-CH_3), 6.89 (1H, s, Ar-*H*), 6.95 (1H, s, Ar-*H*), 11.17 (1H, s, exchange with D2O, CON*H*); ^{13}C-NMR (DMSO-d_6, 100 MHz): δ 20.0, 21.9, 115.6, 119.7, 127.9, 135.5, 136.4, 144.2, 151.1; ESI-HRMS (*m/z*) $[M-H]^-$: calculated for C9H9N2O3S 225.0334; found 225.0341.

Synthesis of 5-fluoro-2H-benzo[e][1,2,4]thiadiazin-3(4H)-one 1,1-dioxide **(E24)**

Compound **E24** was obtained according to the general procedure **11** earlier reported adding dropwise a solution of 2-fluoroaniline **E7** (0.87 mL, 1.0 eq.) in nitroethane (5.0 mL) to a solution of chlorosulfonyl isocyanate (0.94 mL, 1.2 eq.) in nitroethane (5.0 mL). The crude compound was purified by dissolution in a saturated solution of $NaHCO_3$ in 1:1 H_2O/MeOH, treatment with charcoal, filtration over Celite and re-acidification to pH 1. The precipitate was filtered *in vacuo* to afford **E24** as a light brown solid.

5-Fluoro-2*H*-benzo[e][1,2,4]thiadiazin-3(4H)-one 1,1-dioxide E24: 10% yield; m.p. 277-278°C; TLC: R_f = 0.48 (ethyl acetate/*n*-hexane 70% *v/v*); ^{1}H-NMR (DMSO-d_6, 400 MHz): δ 7.34 (1H, m, Ar-*H*), 7.64 (2H, m, Ar-*H*), 11.31 (1H, s, exchange with D_2O, CON*H*); ^{13}C-NMR (DMSO-d_6, 100 MHz): δ 118.7 ($J^3_{C\text{-}F}$ = 4 Hz), 120.5 ($J^2_{C\text{-}F}$ = 18), 124.9 ($J^3_{C\text{-}F}$ = 6), 125.2 ($J^2_{C\text{-}F}$ = 15), 125.8, 150.2 ($J^1_{C\text{-}F}$ = 249), 151.5; ^{19}F-NMR (DMSO-d_6, 376 MHz) −125.93 (1F, s); ESI-HRMS (*m/z*) [M-H]$^-$: calculated for C7H4FN2O3S 214.9927; found 214.9935.

Synthesis of 7-fluoro-2H-benzo[e][1,2,4]thiadiazin-3(4H)-one 1,1-dioxide **(E25)**

Compound **E25** was obtained according to the general procedure **11** earlier reported adding dropwise a solution of 4-fluoroaniline **E8** (1.0 g., 1.0 eq.) in nitromethane (5.0 mL) to a solution of chlorosulfonyl isocyanate (1.02 mL, 1.3 eq.) in nitromethane (5.0 mL). The crude compound was purified by dissolution in a saturated solution of $NaHCO_3$ in 1:1 H_2O/MeOH, treatment with charcoal, filtration over Celite and re-acidification to pH 1. The precipitate was filtered *in vacuo* to afford **E25** as a grey solid.

7-Fluoro-2*H*-benzo[e][1,2,4]thiadiazin-3(4H)-one 1,1-dioxide E25: 38% yield; m.p. 288-289°C; TLC: R_f = 0.28 (methanol/dichloromethane 30% *v/v*); ^{1}H-NMR (DMSO-d_6, 400 MHz): δ 7.32 (1H, m, Ar-*H*), 7.59 (1H, m, Ar-*H*), 7.72 (1H, m, Ar-*H*), 11.41 (1H, s, exchange with D_2O, CON*H*); ^{13}C-NMR (DMSO-d_6, 100 MHz): δ 109.6 ($J^2_{C\text{-}F}$ = 26), 120.3 ($J^2_{C\text{-}F}$ = 8), 122.5 ($J^3_{C\text{-}F}$ = 23), 124.1 ($J^2_{C\text{-}F}$ = 7), 132.7 ($J^4_{C\text{-}F}$ = 2), 152.1, 158.3 ($J^1_{C\text{-}F}$ = 242); ^{19}F-NMR (DMSO-d_6, 376 MHz) −117.29 (1F, s); ESI-HRMS (*m/z*) [M-H]$^-$: calculated for C7H4FN2O3S 214.9927; found 214.9921.

Synthesis of 5-chloro-2H-benzo[e][1,2,4]thiadiazin-3(4H)-one 1,1-dioxide **(E26)**

Compound **E26** was obtained according to the general procedure **11** earlier reported adding dropwise a solution of 2-chloraniline **E9** (0.82 mL, 1.0 eq.) in nitroethane (6.0 mL) to a solution of chlorosulfonyl isocyanate (0.89 mL, 1.3 eq.) in nitroethane (6.0 mL). The crude compound was purified by dissolution in a saturated solution of $NaHCO_3$ in 1:1 H_2O/MeOH, treatment with charcoal, filtration over Celite and re-acidification to pH 1. The precipitate was filtered *in vacuo* to afford **E26** as a white solid.

5-Chloro-2*H*-benzo[e][1,2,4]thiadiazin-3(4H)-one 1,1-dioxide E26: 34% yield; m.p. 246-247°C; TLC: R_f = 0.08 (methanol/dichloromethane 10% *v/v*); ^{1}H-NMR (DMSO-d_6,

400 MHz): δ 7.36 (1H, t, J = 8.0, Ar-*H*), 7.85 (2H, m, Ar-*H*), 10.71 (1H, s, exchange with D_2O, CON*H*); ^{13}C-NMR (DMSO-d_6, 100 MHz): δ 121.5, 122.0, 125.4, 126.1, 133.1, 135.1, 151.4; ESI-HRMS (*m/z*) $[M-H]^-$: calculated for C7H4ClN2O3S 230.9631; found 230.9626.

Synthesis of 7-chloro-2H-benzo[e][1,2,4]thiadiazin-3(4H)-one 1,1-dioxide **(E27)**

Compound **E27** was obtained according to the general procedure **11** earlier reported adding dropwise a solution of 4-chloroaniline **E10** (1.0 g, 1.0 eq.) in nitroethane (6.0 mL) to a solution of chlorosulfonyl isocyanate (0.82 mL, 1.2 eq.) in nitroethane (6.0 mL). The crude compound was purified by dissolution in a saturated solution of $NaHCO_3$ in 1:1 H_2O/MeOH, treatment with charcoal, filtration over Celite and re-acidification to pH 1. The precipitate was filtered *in vacuo* to afford **E27** as a grey solid.

7-Chloro-2*H*-benzo[e][1,2,4]thiadiazin-3(4H)-one 1,1-dioxide E27: 48% yield; m.p. 285-286°C; TLC: R_f = 0.11 (methanol/dichloromethane 15% *v/v*); ^{1}H-NMR (DMSO-d_6, 400 MHz): δ 7.30 (1H, d, J = 8.8, Ar-*H*), 7.74 (1H, t, J = 8.0, 2.4, Ar-*H*), 7.86 (1H, d, J = 2.0, Ar-*H*), 11.47 (1H, s, exchange with D_2O, CON*H*); ^{13}C-NMR (DMSO-d_6, 100 MHz): δ 120.1, 122.6, 124.5, 128.1, 134.7, 135.0, 152.0; ESI-HRMS (m/z) $[M-H]^-$: calculated for C7H4ClN2O3S 230.9631; found 230.9636.

Synthesis of 5-bromo-2H-benzo[e][1,2,4]thiadiazin-3(4H)-one 1,1-dioxide **(E28)**

Compound **E28** was obtained according to the general procedure **11** earlier reported adding dropwise a solution of 2-bromoaniline **E11** (1.0 g, 1.0 eq.) in nitroethane (5.0 mL) to a solution of chlorosulfonyl isocyanate (0.61 mL, 1.2 eq.) in nitroethane (5.0 mL). The crude compound was purified by dissolution in a saturated solution of $NaHCO_3$ in 1:1 H_2O/MeOH, treatment with charcoal, filtration over Celite and re-acidification to pH 1. The precipitate was filtered *in vacuo* to afford **E28** as a grey solid.

5-Bromo-2*H*-benzo[e][1,2,4]thiadiazin-3(4H)-one 1,1-dioxide E28: 25% yield; m.p. 250-251°C; TLC: R_f = 0.19 (methanol/dichloromethane 15% *v/v*); ^{1}H-NMR (DMSO-d_6, 400 MHz): δ 7.29 (1H, t, J = 8.0, Ar-*H*), 7.86 (1H, d, J = 7.2 Ar-*H*), 8.00 (1H, dd, J = 8.4, 1.2, Ar-*H*), 10.28 (1H, s, exchange with D_2O, CON*H*); ^{13}C-NMR (DMSO-d_6, 100 MHz): δ 111.1, 122.6, 125.8, 126.2, 134.2, 138.4, 151.4; ESI-HRMS (*m/z*) $[M-H]^-$: calculated for C7H4BrN2O3S 274.9126; found 274.9120.

Synthesis of 7-bromo-2H-benzo[e][1,2,4]thiadiazin-3(4H)-one 1,1-dioxide **(E29)**

Compound **E29** was obtained according to the general procedure **11** earlier reported adding dropwise a solution of 4-bromoaniline **E12** (1.0 g., 1.0 eq.) in nitromethane (5.0 mL) to a solution of chlorosulfonyl isocyanate (0.60 mL, 1.2 eq.) in nitromethane (5.0 mL). The crude compound was purified by dissolution in a saturated solution of $NaHCO_3$ in 1:1 H_2O/MeOH, treatment with charcoal, filtration over Celite, re-acidification to pH 1. The precipitate was filtered *in vacuo* to afford **E29** as a white solid.

7-Bromo-2*H*-benzo[e][1,2,4]thiadiazin-3(4*H*)-one 1,1-dioxide E29: 30% yield; m.p. >300°C; TLC: R_f = 0.11 (methanol/dichloromethane 20% *v/v*); ^{1}H-NMR (DMSO-d_6, 400 MHz): δ 7.24 (1H, d, *J* = 8.8, Ar-*H*), 7.85 (1H, dd, *J* =8.8, 2.2, Ar-*H*), 7.95 (1H, d, *J* = 2.0, Ar-*H*), 11.46 (1H, s, exchange with D_2O, CON*H*); ^{13}C-NMR (DMSO-d_6, 100 MHz): 115.5, 120.3, 124.9, 125.2, 135.4, 137.4, 152.0; ESI-HRMS (*m/z*) $[M-H]^-$: calculated for C7H4BrN2O3S 274.9126; found 274.9130.

Synthesis of 7-methoxy-2H-benzo[e][1,2,4]thiadiazin-3(4H)-one 1,1-dioxide **(E30)**

Compound **E30** was obtained according to the general procedure **11** earlier reported adding dropwise a solution of p-anisidine **E13** (1.0 g, 1.0 eq.) in nitromethane (4.0 mL) to a solution of chlorosulfonyl isocyanate (0.78 mL, 1.1 eq.) in nitromethane (5.7 mL). The crude compound was purified by silica gel column chromatography eluting with from 1 to 15% *v/v* MeOH/DCM to give a purple solid. The obtained solid was further purified by dissolution in a saturated solution of $NaHCO_3$ in 1:1 H_2O/MeOH, treatment with charcoal, filtration over Celite, re-acidification to pH 1. The precipitate was filtered *in vacuo* to afford **E30** as a purple solid.

7-Methoxy-2*H*-benzo[e][1,2,4]thiadiazin-3(4*H*)-one 1,1-dioxide E30: 17% yield; m.p. 284-285°C; TLC: R_f = 0.15 (methanol/dichloromethane 5% *v/v*); ^{1}H-NMR (DMSO-d_6, 400 MHz): δ 3.85 (3H, s, CH_3), 7.26 (3H, m, Ar-*H*), 11.15 (1H, s, exchange with D_2O, CON*H*); ^{13}C-NMR (DMSO-d_6, 100 MHz): δ 56.9, 105.5, 119.7, 122.7, 123.9, 129.5, 151.8, 156.1; ESI-HRMS (*m/z*) $[M-H]^-$: calculated for C8H7N2O4S 227.0127; found 227.0122.

Synthesis of 1H-naphtho[1,2-e][1,2,4]thiadiazin-2(3H)-one 4,4-dioxide **(E31)**

Compound **E31** was obtained according to the general procedure **11** earlier reported adding dropwise a solution of 1-naphthylamine **E14** (1.0 g, 1.0 eq.) in nitroethane (5.0 mL) to a solution of chlorosulfonyl isocyanate (0.67 mL, 1.1 eq.) in nitroethane (5.0 mL). The crude compound was purified by dissolution in a saturated solution of $NaHCO_3$ in 1:1 H_2O/MeOH, treatment with charcoal, filtration over Celite and re-acidification to pH 1. The precipitate was filtered *in vacuo* to afford a green semisolid, that was purified by silica gel column chromatography eluting with 60 to 100% EtOAc/n-hexane to give a violet solid **E31**.

1*H*-Naphtho[1,2-e][1,2,4]thiadiazin-2(3*H*)-one 4,4-dioxide E31: 23% yield; m.p. 293-294°C; TLC: R_f = 0.15 (methanol/dichloromethane 15% *v/v*); ^{1}H-NMR (DMSO-d_6, 400 MHz): δ 7.76 (3H, m, Ar-*H*), 7.86 (1H, d, *J* = 8.8, Ar-*H*), 8.08 (1H, d, *J* = 7.6, Ar-*H*), 8.72 (1H, d, *J* = 8.0, Ar-*H*), 11.34 (1H, s, exchange with D_2O, CON*H*); ^{13}C-NMR (DMSO-d_6, 100 MHz): δ 118.4, 118.8, 122.6, 123.7, 124.7, 128.5, 129.7, 129.9, 133.1, 135.9, 152.2; ESI-HRMS (*m/z*) $[M-H]^-$: calculated for C11H7N2O3S 247.0177; found 247.0183.

Synthesis of 4-methyl-2H-benzo[e][1,2,4]thiadiazin-3(4H)-one 1,1-dioxide **(E32)**

Compound **E32** was obtained according to the general procedure **11** earlier reported adding dropwise a solution of *N*-methylaniline **E15** (1.01 mL, 1.0 eq.) in nitroethane (5.0 mL) to a solution of chlorosulfonyl isocyanate (0.90 mL, 1.1 eq.) in nitroethane (5.0 mL). The crude compound was purified by dissolution in a saturated solution of $NaHCO_3$ in 1:1 H_2O/MeOH, treatment with charcoal, filtration over Celite and re-acidification to pH 1. The precipitate was filtered *in vacuo* to afford **E32** as a brown solid.

4-Methyl-2*H*-benzo[e][1,2,4]thiadiazin-3(4*H*)-one 1,1-dioxide E32: 27% yield; m.p. 257-258°C; TLC: R_f = 0.20 (methanol/dichloromethane 15% *v/v*); ^{1}H-NMR (DMSO-d_6, 400 MHz): δ 3.47 (3H, s, CH_3), 7.42 (1H, t, *J* = 7.4, Ar-*H*), 7.56 (1H, d, *J* = 8.4, Ar-*H*), 7.81 (1H, m, Ar-*H*), 7.89 (1H, dd, *J* = 8.0, 1.2, Ar-*H*); ^{13}C-NMR (DMSO-d_6, 100 MHz): δ 32.5, 117.9, 122.7, 124.4, 126.1, 135.2, 137.9, 151.2; ESI-HRMS (*m/z*) $[M-H]^-$: calculated for C8H7N2O3S 211.0177; found 211.0182.

Synthesis of 7-chloro-4-methyl-2H-benzo[e][1,2,4]thiadiazin-3(4H)-one 1,1-dioxide **(E33)**

Compound **E33** was obtained according to the general procedure **11** earlier reported adding dropwise a solution of 4-chlor-*N*-methylaniline **E16** (0.86 mL, 1.0 eq.) in nitroethane (6.0 mL) to a solution of chlorosulfonyl isocyanate (0.74 mL, 1.2 eq.) in nitroethane (6.0 mL). The crude compound was purified by dissolution in a saturated solution of $NaHCO_3$ in 1:1 H_2O/MeOH, treatment with charcoal, filtration over Celite and re-acidification to pH 1. The precipitate was filtered *in vacuo* to afford **E33** as a white solid.

7-Chloro-4-methyl-2*H*-benzo[e][1,2,4]thiadiazin-3(4*H*)-one 1,1-dioxide E33: 29% yield; m.p. 254-255°C; TLC: R_f = 0.20 (methanol/dichloromethane 15% *v/v*); ^{1}H-NMR (DMSO-d_6, 400 MHz): δ 3.33 (3H, m, overlap with water peak, CH_3), 7.57 (1H, d, J = 9.2, Ar-*H*), 7.85 (1H, dd, J = 6.4, 2.4, Ar-*H*), 7.94 (1H, d, J = 2.4); ^{13}C-NMR (DMSO-d_6, 100 MHz): δ 32.8, 120.1, 122.2, 127.4, 128.4, 134.8, 137.1, 151.2; ESI-HRMS (*m/z*) [M-H]$^-$: calculated for C8H6ClN2O3S 244.9788; found 244.9782.

Synthesis of 5,6-dihydro-[1,2,4]thiadiazino[6,5,4-hi]indol-3(2H)-one 1,1-dioxide **(E34)**

Compound **E34** was obtained according to the general procedure **11** earlier reported adding dropwise a solution of indoline **E17** (0.94 mL, 1.0 eq.) in nitroethane (6.0 mL) to a solution of chlorosulfonyl isocyanate (0.95 mL, 1.3 eq.) in nitroethane (6.0 mL). The crude compound was purified by dissolution in a saturated solution of $NaHCO_3$ in 1:1 H_2O/MeOH, treatment with charcoal, filtration over Celite and re-acidification to pH 1. The precipitate was filtered *in vacuo* to afford **E34** as a grey solid.

5,6-Dihydro-[1,2,4]thiadiazino[6,5,4-hi]indol-3(2*H*)-one 1,1-dioxide E34: 68% yield; m.p. 252-253°C; TLC: R_f = 0.15 (methanol/dichloromethane 15% *v/v*); ^{1}H-NMR (DMSO-d_6, 400 MHz): δ 3.34 (2H, t, J = 8.6, CH_2), 4.17 (2H, t, J = 8.4, CH_2), 7.26 (1H, t, J = 7.6, Ar-*H*), 7.62 (2H, t, J = 8.6, Ar-*H*); ^{13}C-NMR (DMSO-d_6, 100 MHz): δ 28.0, 47.8, 119.6, 120.9, 124.9, 130.7, 133.4, 139.4, 149.2; ESI-HRMS (*m/z*) [M-H]$^-$: calculated for C9H7N2O3S 223.0177; found 223.0173.

Synthesis of 3-oxo-3,4-dihydro-2H-benzo[e][1,2,4]thiadiazine-5-carboxylic acid 1,1-dioxide **(E35)**

Compound **E19** (0.5 g, 1.0 eq.) was first suspended in H_2O (30 mL) and then dissolved during the addition of saturated aqueous NaOH (0.56 g). $KMnO_4$ (1.42 g, 3.8 eq.) was added portion wise at 0°C, and the reaction mixture was stirred at 80°C for 12 h. The insoluble material was removed by filtration, and the filtrate was acidified to pH 1 with concentrated HCl. The precipitate was collected by filtration, washed with Et_2O, and dried to yield the product **E35** as a white solid.

3-Oxo-3,4-dihydro-2*H*-benzo[e][1,2,4]thiadiazine-5-carboxylic acid 1,1-dioxide E35: 33% yield; m.p. 285-286°C; TLC: R_f = 0.14 (methanol/dichloromethane 20% *v/v*); ^{1}H-NMR (DMSO-d_6, 400 MHz): δ 7.26 (1H, t, *J* = 7.8, Ar-*H*), 7.97 (1H, d, *J* = 7.6, Ar-*H*), 8.18 (1H, dd, *J* = 8.0, 0.8, Ar-*H*), 10.58 (1H, s, exchange with D_2O, CON*H*), 14.01 (1H, s, exchange with D_2O, COO*H*); ^{13}C-NMR (DMSO-d_6, 100 MHz): δ 114.7, 122.1, 125.1, 128.8, 135.5, 139.0, 152.5, 169.3; ESI-HRMS (*m/z*) $[M-H]^-$: calculated for C8H5N2O5S 240.9919; found 240.9911.

Synthesis of 3-oxo-3,4-dihydro-2H-benzo[e][1,2,4]thiadiazine-7-carboxylic acid 1,1-dioxide **(E36)**

Compound **E20** (0.2 g, 1.0 eq.) was first suspended in H_2O (12 mL) and then dissolved during the addition of saturated aqueous NaOH (0.23 g). $KMnO_4$ (0.49 g, 3.3 eq.) was added portion wise at 0°C, and the reaction mixture was stirred at 80°C for 7 h. The insoluble material was removed by filtration, and the filtrate was acidified to pH 1 with concentrated HCl. The precipitate was collected by filtration, washed with acid water and Et_2O, and dried to yield the product **E36** as a white solid.

3-Oxo-3,4-dihydro-2*H*-benzo[e][1,2,4]thiadiazine-7-carboxylic acid 1,1-dioxide E36: 21% yield; m.p. >300°C; TLC: R_f = 0.17 (methanol/dichloromethane 20% *v/v*); ^{1}H-NMR (DMSO-d_6, 400 MHz): δ 7.37 (1H, d, *J* = 8.4, Ar-*H*), 8.19 (1H, m, Ar-*H*), 8.23 (1H, s, Ar-*H*), 11.64 (1H, s, exchange with D_2O, CON*H*), 13.38 (1H, s, exchange with D_2O, O*H*); ^{13}C-NMR (DMSO-d_6, 100 MHz): δ 118.3, 123.2, 124.4, 126.6, 135.4, 139.5, 151.8, 166.4; ESI-HRMS (*m/z*) $[M-H]^-$: calculated for C8H5N2O5S 240.9919; found 240.9923.

Synthesis of 7-hydroxy-2H-benzo[e][1,2,4]thiadiazin-3(4H)-one 1,1-dioxide **(E37)**

A solution of **E30** (0.2 g, 1.0 eq.) in dichloromethane (15 mL) was treated with BBr_3 (1.84 mL, 3.0 eq.) at –10 °C. The reaction mixture was stirred for 12 h at r.t. After

completion of the reaction, the mixture was quenched with ice and the dichloromethane was evaporated under *vacuum*. The suspended solid was filtered *in vacuo* to afford **E37** as a grey solid.

7-Hydroxy-2*H*-benzo[e][1,2,4]thiadiazin-3(4*H*)-one 1,1-dioxide E37: 42% yield; m.p. 284-285°C; TLC: R_f = 0.56 (methanol/dichloromethane 30% *v/v*); ^{1}H-NMR (DMSO-d_6, 400 MHz): δ 7.12 (3H, m, Ar-*H*), 10.03 (1H, s, exchange with D_2O, O*H*), 11.04 (1H, s, exchange with D_2O, CON*H*), 12.67 (1H, s, exchange with D_2O, SO_2N*H*); ^{13}C-NMR (DMSO-d_6, 100 MHz): 107.3, 119.6, 122.8, 124.0, 127.9, 151.7, 154.2; ESI-HRMS (*m/z*) $[M-H]^-$: calculated for C7H5N2O4S 212.9970; found 212.9974.

5.5.2 High resolution mass spectrometry (HR-MS) analysis

HR-MS was performed with a Thermo Finnigan LTQ Orbitrap mass spectrometer equipped with an electrospray ionization source. Analysis were carried out in negative ion mode monitoring the [M-H]- species, and a proper dwell time acquisition was used to achieve 60,000 units of resolution at Full Width at Half Maximum (FWHM). Elemental composition of compounds was calculated on the basis of their measured accurate masses, accepting only results with an attribution error less than 5 ppm and a not integer RDB (double bond/ring equivalents) value, in order to consider only the deprotonated species.[303] None of the screened derivatives reported PAINS alerts determined by SwissADME server (www.swissadme.ch).

5.5.3 Carbonic anhydrases inhibition

The CA inhibitory profiles of compounds belonging to series E were obtained according to the general procedures described at the beginning of the experimental section.

5.5.4 X-ray crystallography

CA II and CA IX-mimic were expressed and purified as previously described.[304] The CA IX-mimic was produced by mutating 7 residues in the active site of CA II in order to mimic the active site of CA IX, resulting in a construct that is more easily expressed,

purified, and crystallized than wild type hCA IX.[304] CA II and CA IX were expressed in BL21(DE3) *E. coli* cells induced by IPTG. The cells were then harvested and lysed for purification via affinity chromatography with p-(aminomethyl)benzenesulfonamide resin. Protein purity was confirmed vis SDS-PAGE and both CA II and CA IX were diluted to a final concentration of 10 mg/mL for crystallization. Crystals were subsequently grown using the hanging drop vaporization method with a precipitant solution of 1.6 M NaCitrate, 50 mM Tris, pH 7.8. Crystals were soaked in mM concentrations of the inhibitors before transferring to a cryoprotectant of 20% glycerol and freezing in liquid nitrogen.

Diffraction data was collected on the F1 beamline at Cornell High Energy Synchrotron Source (CHESS) using a Pilatus 6M detector. Data sets were collected with a crystal-to-detector distance of 250 mm, 1° oscillation angle, and exposure time of 2-3 sec for a total of 180 images. *XDS*[305] was used to index and integrate the data followed by *Aimless*[306] to scale the data to the $P2_1$ space group. The phases were then determined by molecular replacement with a search model of CA II (PDB: 3KS3[307]) and refinements performed in *Phenix*[301]. *Coot* was used to analyze inhibitor interactions and *PyMol*[302] to generate figures.

5.5.5 Anticancer Activity

5.5.5.1 Antiproliferative activity

The three tested cancer cell lines (A549, PC-3 and HCT116) were obtained from American Type Culture Collection (ATCC). The cells were propagated in DMEM supplemented with 10% heat-inactivated fetal bovine serum, 1% L-glutamine (2.5 mM), HEPES buffer (10 mM) and gentamycin (50 μg/mL). The hypoxia inducer $CoCl_2$ (100 μM) was added for the hypoxic conditions. All cells were maintained at 37 °C in a humidified atmosphere with CO_2 (5%). Cytotoxicity was then evaluated following the MTT assay[230], as described earlier.[308]

5.5.5.2 ELISA Immunoassay

The expression levels of the pro-apoptotic markers (Bax, caspase-3, caspase-9 and p53), in addition to the anti-apoptotic marker (Bcl-2) were evaluated using ELISA colorimetric kits per the manufacturer's instructions, as reported previously.[308,309]

5.6 Kinetic Characterization of Carbonic Anhydrases from the pathogenic protozoan *Entamoeba histolytica* and from the coral *Stylophora pistillata*

5.6.1 EhiCA production and purification

5.6.1.1 Vector construction

We produced the EhiCA as a recombinant protein in *E. coli*. The DNA sequence was retrieved from UniProt and modified for recombinant protein production. We provided the sequence of the insert, and the actual construction of the plasmid vector was performed by GeneArt (Invitrogen, Regensburg, Germany). The structure of the insert was specifically modified for production in *E. coli.* The insert was ligated into a modified plasmid vector, pBVboost.

5.6.1.2 Production of the protein

The freeze-dried plasmid was prepared, according to manufacturer's manual. Deep-frozen BL21 Star™ (DE3) cells (Invitrogen, Carlsbad, CA, USA) were slowly melted on ice. Once melted, 25 µL of the cell suspension and 1 µL of the plasmid solution were combined. The suspension was kept on ice for 30 min. Heat shock was performed by submerging the suspension-containing tube into 42 °C water for 30 s, and was then incubated on ice for 2 min. To the tube 125 µL of S.O.C Medium (Invitrogen, Carlsbad, CA, USA) was added, and the tube was incubated for 1 h with constant shaking (200 rpm) at 37 °C. Growth plates (gentamycin-LB medium, ratio 1:1000) were prewarmed at 37 °C for 40 min. Then, 20 µL and 50 µL of suspension was spread on two plates which were incubated overnight at 37 °C. A volume of 5 mL preculture was prepared by inoculating single colonies from growth plates onto an LB medium with gentamycin (ratio 1:1000). It was then incubated overnight at 37 °C with constant shaking (200 rpm). The production was executed according to pO-stat fed batch protocol, which is essentially as described in Määttä et al.[310] There were some alterations to the previously described protocol: The fermentation medium did not contain glycerol, as the cell line used did not require it. The induction of the culture was performed with 1 mM IPTG, 12 h after starting the fermentation. Temperature was decreased to 25 °C at the time of the

induction. Culturing was stopped after 12 h of the induction with the OD 34 (A_{600}). The cells were collected by centrifugation, and the wet weight of the cell pellet was 303 g. The fermentation was performed by the Tampere facility of Protein Services (PS). The cell pellet (approximately 35 g) was suspended in 150 mL of binding buffer containing 50 mM Na_2HPO_4, 0.5 M NaCl, 50 mM imidazole, and 10% glycerol (pH 8.0), and the suspension was homogenized with an EmulsiFlex-C3 (AVESTIN, Ottawa, Canada) homogenizer. The lysate was centrifuged at 13,000 x g for 15 min at 4 °C, and the clear supernatant was mixed with HisPur™ Ni-NTA Resin (Thermo Fisher Scientific, Waltham, MA, USA) and bound to the resin for 2 h at room temperature on the magnetic stirrer. Then resin was washed with the binding buffer and collected onto an empty column with an EMD Millipore™ vacuum filtering flask (Merck, Kenilworth, NJ, USA) and filter paper. The protein was eluted from the resin with 50 mM Na_2HPO_4, 0.5 M NaCl, 350 mM imidazole, and 10% glycerol (pH 7.0). The protein was re-purified with TALON® Superflow™ cobalt resin (GE Healthcare, Chicago, IL, USA). The eluted protein fractions were diluted with binding buffer (50 mM Na2HPO4, 0.5 M NaCl, and 10% glycerol pH 8.0), so that the imidazole concentration was under 10 mM. The protein binding and elution was performed as described above. The purity of the protein was determined with gel electrophoresis (SDS-PAGE), and visualized with PageBlue Protein staining solution (Thermo Fisher Scientific,Waltham, MA, USA). Protein fractions were pooled and concentrated with 10 kDa Vivaspin® Turbo 15 centrifugal concentrators (Sartorius™, Göttingen, Germany) at 4000 x g at 4 °C. Buffer exchange in 50 mM TRIS (pH 7.5) was done using the same centrifugal concentrators. His-tag was cleaved from the purified protein by Thrombin CleanCleave Kit (Sigma-Aldrich, Saint Louis, MO, USA), according to manufacturer's manual.

5.6.2 *Entamoeba histolytica* activity and inhibition measurements

The CA inhibitory profiles of anions and sulfonamides were obtained according to the general procedures described at the beginning of the experimental section.

5.6.2.1 *Entamoeba histolytica* activation measurements

An Sx.18Mv-R Applied Photophysics (Oxford, UK) stopped-flow instrument has been used to assay the catalytic activity of various CA isozymes for CO_2 hydration reaction.[169] Phenol red (at a concentration of 0.2 mM) was used as indicator, working at the absorbance maximum of 557 nm, with 10mMHepes (pH 7.5, for α-CAs) or TRIS (pH 8.3, for β-CAs) as buffers, 0.1M $NaClO_4$ (for maintaining constant ionic strength), following the CA-catalyzed CO_2 hydration reaction for a period of 10 s at 25 °C. The CO_2 concentrations ranged from 1.7 to 17 mM for the determination of the kinetic parameters and inhibition constants. For each activator at least six traces of the initial 5–10% of the reaction have been used for determining the initial velocity. The uncatalyzed rates were determined in the same manner and subtracted from the total observed rates. Stock solutions of activators (at 0.1 mM) were prepared in distilled-deionized water and dilutions up to 1 nM were made thereafter with the assay buffer. Enzyme and activator solutions were pre-incubated together for 30 min prior to assay, in order to allow for the formation of the enzyme–activator complexes. The activation constant (K_A), defined similarly with the inhibition constant K_I, can be obtained by considering the classical Michaelis–Menten equation (Equation 11), which has been fitted by nonlinear least squares by using PRISM 3:

$$v = v_{max} / \{1 + (K_M / [S]) (1 + [A]_f / K_A)\} \quad \text{(Eq. 11)}$$

where $[A]_f$ is the free concentration of activator.

Working at substrate concentrations considerably lower than K_M ($[S] << K_M$), and considering that $[A]_f$ can be represented in the form of the total concentration of the enzyme ($[E]_t$) and activator ($[A_]t$), the obtained competitive steady-state equation for determining the activation constant is given by Equation 12:

$$v = v_0 \cdot K_A/\{K_A + ([A]_t - 0.5\{([A]_t + [E]_t + K_A) - ([A]_t + [E]_t + K_A)^2 - 4[A]_t \cdot [E]_t)^{1/2}\}\} \quad \text{(Eq. 12)}$$

where v_0 represents the initial velocity of the enzyme-catalyzed reaction in the absence of activator.[135,257,258]

5.6.3 *Stylophora pistillata* production and purification

The gene of *S. pistillata* encoding for the α-CA SpiCA3 (NCBI Reference Sequence: XP_022794253.1) was identified running the "BLAST" program and using the nucleotide sequences of the coral α-CAs as query sequence, previously identified by our groups. The GeneArt Company (Invitrogen,Waltham, MA, USA), specializing in gene synthesis, designed the synthetic gene (SpiCA3-DNA) encoding for a protein of 259 amino acid residues and containing four base-pair sequences (CACC) necessary for directional cloning at the 5' end of the SpiCA3-DNA gene. The recovered SpiCA3-DNA gene and the linearized expression vector (pET-100/D-TOPO) were ligated by T4 DNA ligase to form the expression vector pET-100/SpiCA3. BL21 DE3 competent cells (Agilent) were transformed with pET-100/SpiCA3, grown at 37 °C and induced with 0.1 mM IPTG. After 30 min, $ZnSO_4$ (0.5 mM) was added to the culture medium and cells were grown for an additional 4 h. Subsequently, cells were harvested and resuspended in the following buffer: 50 mM Tris/HCl, pH 8.0, 0.5 mM PMSF, and 1 mM benzamidine. Cells were then disrupted by sonication at 4 °C. After centrifugation at 12,000x g for 45 min, the supernatant was loaded onto a His-select HF Nickel affinity column (GE Healthcare, dimension: 1.0 x 10.0 cm). The column was equilibrated with 0.02 M phosphate buffer (pH 8.0) containing 0.01 M imidazole and 0.5 M KCl at a flow rate of 1.0 mL/min. The recombinant SpiCA3 was eluted from the column with 0.02 M phosphate buffer (pH 8.0) containing 0.5 M KCl and 0.3 M imidazole at a flow rate of 1.0 mL/min. Active fractions (0.5 mL) were collected and combined to a total volume of 2.5 mL. Collected fractions were dialyzed against 50 mM Tris/HCl, pH 8.3. At this stage of purification, the protein was at least 95% pure and the obtained recovery was of about 20 mg of the recombinant protein**.**

5.6.3 *Stylophora pistillata* activity and inhibition measurements

The CA inhibitory profiles of anions and sulfonamides were obtained according to the general procedures described at the beginning of the experimental section.

Chapter 6. Conclusions

The involvement of the CAs in a multitude of diseases, mainly in an isoform-specific manner, have paved the way for decades to combination therapies such as in the case of eye drops for the treatment of glaucoma. Even the sulfonamide **SLC-0111**, which successfully completed Phase I clinical trials for the treatment of advanced, metastatic hypoxic tumors over-expressing CA IX, is now in Phase Ib/II clinical trials in combination with gemcitabine in subjects affected by metastatic pancreatic ductal adenocarcinoma because of an intense synergic anticancer efficacy.

In this Ph.D. cycle, we scheduled to exploit the validated efficacy of CA inhibition in the treatment of many disorders for designing several multi-target strategies including CAIs against cancer, inflammation, glaucoma and infections. In fact, in recent years the choice of multi-potent agents is spreading worldwide and overcoming the co-administration of multiple drugs because of improved pharmacokinetics, better patient compliance, reduced drug-drug interactions as well as a synergistic effect in the treatment of the pathology.

As first and second projects of the Ph.D. period, two series of multi-target NSAID - CAI derivatives for the management of rheumatoid arthritis were reported, which differ for the type of linker, amide or ester, connecting the active portions. A coumarin scaffold was chosen as CAI to induce a selective inhibition of CA IX and XII, that are overexpressed in inflamed tissues. In spite of a different plasma stability, and thus predicted pharmacokinetics, a subset of multi-potent derivatives from both series showed major antihyperalgesic action than clinically used NSAIDs in a rat model of rheumatoid arthritis. Of note, the derivatives were shown *in vitro* and *in silico* to produce cyclooxygenase 1/2 inhibition even as integral hybrids.

In contrast, for pharmacologically hitting glaucoma, CAIs of the sulfonamide type were assembled with portions able to block the $\beta_{1/2}$-adrenergic receptors that, as hCA II, IV and XII, are involved in the pathogenesis of the ocular disorder. Multi-potent derivatives identified within the series were evaluated in a rabbit model of glaucoma and showed to possess more effective internal ocular pressure lowering properties as eye drops than the leads, clinically used dorzolamide and timolol, and even the combination of them which is a globally marketed antiglaucoma medication.

Both sulfonamide and coumarin scaffolds were incorporated as CA IX and XII inhibitors in nitric oxide (NO)-donor derivatives based on a benzofuroxan scaffold, that was shown to induce a potent cytotoxic action against several types of cancer cells as well as an antimetastatic activity. Further, benzofuroxans were recently shown to possess activity against *Trypanosoma cruzi*, *Mycobacterium Tuberculosis* and *Leishmania*, which was assumed to be enhanced by inhibiting the α- and β-CAs encoded in these pathogens. To date, the outcomes of this study are limited to design, synthesis and *in vitro* kinetic assessment.

As it was recently found that two of the world's most marketed sweeteners, **SAC** and **ACE**, selectively inhibit the tumor-associated CAs IX and XII over ubiquitous CAs, we planned a drug design strategy that took **SAC** and **ACE** as leads and produced a new CAI chemotype, namely the 2H-benzo[e][1,2,4]thiadiazin-3(4H)-one 1,1-dioxide (**BTD**). Many synthesized derivatives showed enhanced potency and in some cases selectivity, when compared to the leads against the target CA IX and XII over off-target isoforms. A subset of compounds displayed effective cytotoxic action against A549, PC-3 and HCT-116 cell lines and anticancer effects on apoptotic markers. The expression levels of the pro-apoptotic proteins Bax, caspase-3, caspase-9, and p53 were found to significantly increase, while Bcl-2, an anti-apoptotic protein, was down-regulated. These outcomes indicate that combining characteristics from **SAC** and **ACE**, widely used as sweeteners, could be used for designing promising leads for the development of new anticancer drugs.

During my Ph.D. period, I performed a multitude of kinetic studies with inhibitors and activators of several isoforms of CA belonging to the classes α, β, γ, δ, ζ, η and θ. These studies allowed to draw up the inhibition or activation profiles of hundreds of derivatives from collaborators of us. Additionally, the CA isoforms identified in the protozoan human parasite *Entamoeba histolytica* and in the coral *Stylophora pistillata* were characterized for their kinetic activity, inhibition with anions and sulfonamides and activation with a panel of amines and amino acid derivatives.

Chapter 7. Ph.D. Internships at Institute of Biosciences and BioResources (CNR) in Naples and Istituto Superiore di Sanità in Rome

During my second Ph.D. year, I attended a stage guest of Dr. Clemente Capasso in the Institute of Biosciences and BioResources (CNR) in Naples. There, I extended my knowledge on the topic Carbonic Anhydrase by the molecular biology standpoint. In detail, I worked on the expression and purification of CA isoforms from the bacterium *Vibrio cholerae*, for scale-up reasons as these are isozyme that intensively used in kinetic evaluations in our Florence laboratory.

During my third Ph.D. year, I had the opportunity to be guest of Dr. Stefano Fais at the Istituto Superiore di Sanità in Rome. Supervised by Dr. Mariantonia Logozzi, I studied *in vitro* the anticancer effect of a series of compounds synthesized in our laboratories against aggressive tumor cell lines, such as the melanoma 501MEL. I was involved in all stages of the study from the sample's inoculation in the cell cultures, to the electron microscope observation, and flow cytometry to detect and measure the physico-chemical characteristics of the cell population using the FACS.

References

[1] Supuran, C. T. Carbonic anhydrases: novel therapeutic applications for inhibitors and activators. *Nat. Rev. Drug Discovery* **2008**, *7*, 168-181.

[2] Alterio, V.; Di Fiore, A.; D'Ambrosio, K.; Supuran, C.T.; De Simone, G. Multiple binding modes of inhibitors to carbonic anhydrases: how to design specific drugs targeting 15 different isoforms? *Chem. Rev*. **2012**, *112*, 4421-4468.

[3] Nocentini, A.; Supuran, C.T. Advances in the structural annotation of human carbonic anhydrases and impact on future drug discovery. *Expert Opin. Drug Discov.* **2019**, *14*, 1175-1197.

[4] Xu, Y.; Feng, L.; Jeffrey, P. D.; Shi, Y.; Morel, F. M. Structure and metal exchange in the cadmium carbonic anhydrase of marine diatoms. *Nature* **2008**, *452*, 56-61.

[5] Jensen, E.L.; Clement, R.; Kosta, A.; Maberly, S.C.; Gontero, B. A new widespread subclass of carbonic anhydrase in marine phytoplankton. *ISME J.* **2019**, *13*, 2094-2106.

[6] Maren, T. H. Carbonic anhydrase: chemistry, physiology, and inhibition. *Physiol. Rev.* **1967**, *47*, 595-781.

[7] Del Prete, S.; Vullo, D.; Fisher, G.M.; Andrews, K.T.; Poulsen, S.A.; Capasso, C.; Supuran, C. T. Discovery of a new family of carbonic anhydrases in the malaria pathogen Plasmodium falciparum-the η-carbonic anhydrases. *Bioorg. Med. Chem. Lett.* **2014**, *24*, 4389-4396.

[8] Tripp, B. C.; Smith, K.; Ferry, J. G. Carbonic anhydrase: new insights for an ancient enzyme. *J. Biol. Chem.* **2001**, *276*, 48615-48618.

[9] Ferry, J. F. The gamma class of carbonic anhydrases. *Biochim. Biophys. Acta* **2010**, 1804, 374-381.

[10] Smith, K.S.; Jakubzick, C.; Whittam, T. S.; Ferry, J.G. Carbonic anhydrase is an ancient enzyme widespread in prokaryotes. *Proc. Natl. Acad. Sci. U.S.A.* **1999**, *96*, 15184–15189.

[11] Kikutani, S.; Nakajima, K.; Nagasato, C.; Tsuji, Y.; Miyatake, A.; Matsuda, Y. Thylakoid luminal θ-carbonic anhydrase critical for growth and photosynthesis in the marine diatom Phaeodactylum tricornutum. *Proc. Natl. Acad. Sci. U.S.A.* **2016**, *113*, 9828–9833.

[12] Capasso, C.; Supuran, C. T. An overview of the alpha-, beta- and gamma-carbonic anhydrases from Bacteria: can bacterial carbonic anhydrases shed new light on evolution of bacteria? *J. Enzyme Inhib. Med. Chem.* **2015**, *30*, 325–332.

[13] Nocentini, A.; Supuran, C.T. Carbonic Anhydrases. Amsterdam: Elsevier; **2019**.

[14] Supuran, C. T. Structure and function of carbonic anhydrases. *Biochem. J*. **2016**, *473*, 2023-2032.

[15] Supuran, C. T.; Scozzafava, A.; Casini, A. Carbonic anhydrase inhibitors. *Med. Res. Rev.* **2003**, *23*, 146-189.

[16] Supuran, C. T.; Scozzafava, A. Carbonic anhydrases as targets for medicinal chemistry. *Bioorg. Med. Chem.* **2007**, *15*, 4336-4350.

[17] Temperini, C.; Scozzafava, A.; Supuran, C. T. In Drug Design of Zinc-Enzyme Inhibitors: Functional, Structural, and Disease Applications; Supuran, C. T., Winum, J.-Y., Eds.; Wiley: Hoboken, NJ, **2009**; p 473.

[18] Gao, B. B.; Clermont, A.; Rook, S.; Fonda, S. J.; Srinivasan, V. J.; Wojtkowski, M.; Fujimoto, J. G.; Avery, R. L.; Arrigg, P. G.; Bursell, S. E.; Aiello, L. P.; Feener, E. P. Extracellular carbonic anhydrase mediates hemorrhagic retinal and cerebral vascular permeability through prekallikrein activation. *Nat. Med.* **2007**, *13*, 181-188.

[19] Mincione, F.; Scozzafava, A.; Supuran, C. T. The development of topically acting carbonic anhydrase inhibitors as antiglaucoma agents. *Curr. Pharm. Des.* **2008**, *14*, 649-654.

[20] Supuran, C. T. Diuretics: from classical carbonic anhydrase inhibitors to novel applications of the sulfonamides. *Curr. Pharm. Des.* **2008**, *14*, 641-648.

[21] De Simone, G.; Scozzafava, A.; Supuran, C. T. Which carbonic anhydrases are targeted by the antiepileptic sulfonamides and sulfamates? *Chem. Biol. Drug Des.* **2009**, *74*, 317-321.

[22] Basnyat, B.; Gertsch, J. H.; Johnson, E. W.; Castro-Marin, F.; Inoue, Y.; Yeh, C. Efficacy of low-dose acetazolamide (125 mg BID) for the prophylaxis of acute mountain sickness: a prospective, double-blind, randomized, placebo-controlled trial. *High Alt. Med. Biol.* **2003**, *4*, 45-52.

[23] Nocentini, A.; Supuran, C.T. Carbonic anhydrase inhibitors as antitumor/antimetastatic agents: a patent review (2008-2018). *Expert Opin. Ther. Pat.* **2018,** *28*, 729-740

[24] Barreiro, E.; Hussain, S. N. A. Protein carbonylation in skeletal muscles: impact on function. *Antioxid. Redox Signal.* **2010**, *12*, 417-429.

[25] Nishimori, I.; Minakuchi, T.; Kohsaki, T.; Onishi, S.; Takeuchi, H.; Vullo, D.; Scozzafava, A.; Supuran, C. T. Carbonic anhydrase inhibitors: the beta-carbonic anhydrase from Helicobacter pylori is a new target for sulfonamide and sulfamate inhibitors. *Bioorg. Med. Chem. Lett.* **2007**, *17*, 3585-3594.

[26] Capasso, C.; Supuran, C. T. Bacterial, fungal and protozoan carbonic anhydrases as drug targets. *Expert Opin. Ther. Targets.* **2015**, *19*, 1689-1704.

[27] Iverson, T.M.; Alber, B.E.; Kisker, C.; Ferry, J.G.; Rees, D.C. A closer look at the active site of gamma-class carbonic anhydrases: high-resolution crystallographic studies of the carbonic anhydrase from *Methanosarcina thermophila*. *Biochemistry* **2000**, *39*, 9222–9231.

[28] Supuran, C.T.; De Simone, G. In Carbonic Anhydrases as Biocatalysts; Supuran C.T., De Simone G., Eds.; *Elsevier: Walthman*, MA, **2015**, p. 3.

[29] De Simone, G.; Supuran, C. T. Carbonic anhydrase IX: Biochemical and crystallographic characterization of a novel antitumor target. *Biochim. Biophys. Acta* **2010**, *1804*, 404-409.

[30] Whittington, D. A.; Waheed, A.; Ulmasov, B.; Shah, G. N.; Grubb, J. H.; Sly, W. S.; Christianson, D. W. Crystal structure of the dimeric extracellular domain of human carbonic anhydrase XII, a bitopic membrane protein overexpressed in certain cancer tumor cells. *Proc. Natl. Acad. Sci. U.S.A.* **2001**, *98*, 9545-9550.

[31] Schlicker, C.; Hall, R. A.; Vullo, D.; Middelhaufe, S.; Gertz, M.; Supuran, C. T.; Muehlschlegel, F. A.; Steegborn, C. Structure and Inhibition of the CO2-Sensing Carbonic Anhydrase Can2 from the Pathogenic Fungus Cryptococcus neoformans. *J. Mol. Biol.* **2009**, *385*, 1207-1220.

[32] Alber, B.E.; Ferry, J.G. A carbonic anhydrase from the archaeon Methanosarcina thermophila. *Proc Natl Acad Sci U S A.* **1994**, *91*, 6909-6913.

[33] Supuran C.T. Carbonic anhydrase activators. *Future Med Chem.* **2018**, *10*, 561-573.

[34] Masini, E.; Carta, F.; Scozzafava, A.; Supuran, C.T. Antiglaucoma carbonic anhydrase inhibitors: a patent review. *Expert Opin Ther Pat* **2013**, *23*, 705–716.

[35] Matsui, H.; Murakami, M.; Wynns, G. C.; Conroy, C. W.; Mead, A.; Maren, T. H.; Sears, M. L. Membrane carbonic anhydrase (IV) and ciliary epithelium. Carbonic anhydrase activity is present in the basolateral membranes of the non-pigmented ciliary epithelium of rabbit eyes. *Exp. Eye Res.* **1996**, *62*, 409-417.

[36] Tang, Y.; Xu, H.; Du, X.; Lit, L.; Walker, W.; Lu, A.; Ran, R.; Gregg, J. P.; Reilly, M.; Pancioli, A.; Khoury, J. C.; Sauerbeck, L. R.; Carrozzella, J. A.; Spilker, J.; Clark, J.; Wagner, K. R.; Jauch, E. C.; Chang, D. J.; Verro, P.; Broderick, J. P.; Sharp, F. R. Gene expression in blood changes rapidly in neutrophils and monocytes after ischemic stroke in humans: a microarray study. *J. Cereb. Blood Flow Metab.* **2006**, *26*, 1089-1102.

[37] De Simone, G.; Supuran, C. T. In Drug Design of Zinc-Enzyme Inhibitors: Functional, Structural, and Disease Applications; Supuran, C. T., Winum, J.-Y., Eds.; Wiley: Hoboken, NJ, **2009**; p 241.

[38] Liu, C.; Wei, Y.; Wang, J.; Pi, L.; Huang, J.; Wang, P.; Carbonic anhydrases III and IV autoantibodies in rheumatoid arthritis, systemic lupus erythematosus, diabetes, hypertensive renal disease, and heart failure. *Clin. Dev. Immunol.* **2012**, 354594.

[39] Margheri, F.; Ceruso, M.; Carta, F.; Laurenzana, A.; Maggi, L.; Lazzeri, S.; Simonini, G.; Annunziato F.; Del Rosso M.; Supuran C. T.; Cimaz, R. Overexpression of the transmembrane carbonic anhydrase isoforms IX and XII in the inflamed synovium. *J. Enzyme Inhib. Med. Chem.* **2016**, *31*, 60-63.

[40] De Simone, G.; Di Fiore, A.; Supuran, C. T. Are carbonic anhydrase inhibitors suitable for obtaining antiobesity drugs? *Curr. Pharm. Des.* **2008**, *14*, 655-660.

[41] De Simone, G.; Supuran, C. T. Antiobesity carbonic anhydrase inhibitors. *Curr. Top. Med. Chem.* **2007**, *7*, 879-884.

[42] Supuran, C. T.; Di Fiore, A.; De Simone, G. Carbonic anhydrase inhibitors as emerging drugs for the treatment of obesity. *Expert Opin. Emerg. Drugs.* **2008**, *13*, 383-392.

[43] Nishimori, I.; Minakuchi, T.; Onishi, S.; Vullo, D.; Scozzafava, A.; Supuran, C. T. Carbonic anhydrase inhibitors. DNA cloning, characterization, and inhibition studies of the human secretory isoform VI, a new target for sulfonamide and sulfamate inhibitors. *J. Med. Chem.* **2007**, *50*, 381-388.

[44] Kivelä, J.; Parkkila, S.; Parkkila, A. K.; Rajaniemi, H. A low concentration of carbonic anhydrase isoenzyme VI in whole saliva is associated with caries prevalence. *Caries Res.* **1999**, *33*, 178-184.

[45] Ruusuvuori, E.; Li, H.; Huttu, K.; Palva, J. M.; Smirnov, S.; Rivera, C.; Kaila, K.; Voipio, J. Carbonic anhydrase isoform VII acts as a molecular switch in the development of synchronous gamma-frequency firing of hippocampal CA1 pyramidal cells. *J. Neurosci.* **2004**, *24*, 2699-2707.

[46] Aspatwar, A.; Tolvanen, M. E.; Ortutay, C.; Parkkila, S. Carbonic anhydrase related protein VIII and its role in neurodegeneration and cancer. *Curr. Pharm. Des.* **2010**, *16*, 3264-3276.

[47] Nishimori, I. In Carbonic Anhydrase: Its Inhibitors and Activators; Supuran, C. T., Scozzafava, A., Conway, J., Eds.; *CRC Press: Boca Raton*, FL, **2004**; p 25.

[48] Neri, D.; Supuran, C.T. Interfering with pH regulation in tumours as a therapeutic strategy. *Nat. Rev. Drug Discov.* **2011**, *10*, 767-777.

[49] Pastorekova, S.; Parkkila, S.; Zavada, J. Tumor-associated carbonic anhydrases and their clinical significance. *Adv. Clin. Chem.* **2006**, *42*, 167-216.

[50] Dai, H.T.; Hong, C.C.; Liang, S.C; Yan, M.D.; Lai, G.M., Cheng, A.L.; Chuang S.E. Carbonic anhydrase III promotes transformation and invasion capability in hepatoma cells through FAK signaling pathway. *Mol Carcinog* **2008**, *47*, 956–963.

[51] Battke, C.; Kremmer, E.; Mysliwietz, J.; Gondi, G.; Dumitru, C.; Brandau, S.; Lang, S.; Vullo, D.; Supuran, C. T.; Zeidler, R. Generation and characterization of the first inhibitory antibody targeting tumour-associated carbonic anhydrase XII. *Cancer Immunol. Immunother.* **2011**, *60*, 649-658.

[52] Liao, S. Y.; Ivanov, S.; Ivanova, A.; Ghosh, S.; Cote, M. A.; Keefe, K.; Coca-Prados, M.; Stanbridge, E. J.; Lerman, M. I. Expression of cell surface transmembrane carbonic anhydrase genes CA9 and CA12 in the human eye: overexpression of CA12 (CAXII) in glaucoma. *J. Med. Genet.* **2003**, *40*, 257-261.

[53] Pastorek, J.; Pastorekova, S. Hypoxia-induced carbonic anhydrase IX as a target for cancer therapy: From biology to clinical use. *Semin. Cancer Biol.* **2015**, *31*, 52−64.

[54] Monti, S. M.; Supuran, C. T.; De Simone, G. Anticancer carbonic anhydrase inhibitors: a patent review (2008 -2013). *Expert Opin. Ther. Pat.* **2013**, *23*, 737−749.

[55] Lehtonen, J.; Shen, B.; Vihinen, M.; Casini, A.; Scozzafava, A.; Supuran, C. T.; Parkkila, A. K.; Saarnio, J.; Kivelä, A. J.; Waheed, A.; Sly, W. S.; Parkkila, S. Characterization of CA XIII, a novel member of the carbonic anhydrase isozyme family. *J. Biol. Chem.* **2004**, *279*, 2719-2727.

[56] Shah, G. N.; Ulmasov, B.; Waheed, A.; Becker, T.; Makani, S.; Svichar, N.; Chesler, M.; Sly, W. S. Carbonic anhydrase IV and XIV knockout mice: roles of the respective carbonic anhydrases in buffering the extracellular space in brain. *Proc. Natl. Acad. Sci .U.S.A.* **2005**, *102*, 16771-16776.

[57] Ogilvie, J. M.; Ohlemiller, K. K.; Shah, G. N.; Ulmasov, B.; Becker, T. A.; Waheed, A.; Hennig, A. K.; Lukasiewicz, P. D.; Sly, W. S. Carbonic anhydrase XIV deficiency produces a functional defect in the retinal light response. *Proc. Natl. Acad. Sci. U.S.A.* **2007**, *104*, 8514-8519.

[58] Alterio, V.; Di Fiore, A.; D'Ambrosio, K.; Supuran, C. T.; De Simone, G. In Drug Design of Zinc-Enzyme Inhibitors: Functional, Structural, and Disease Applications; Supuran, C. T., Winum, J.-Y., Eds.; Wiley: Hoboken, NJ, **2009**; p 73.

[59] Eriksson, A. E.; Kylsten, P. M.; Jones, T. A.; Liljas, A. Crystallographic studies of inhibitor binding sites in human carbonic anhydrase II: a pentacoordinated binding of the SCN- ion to the zinc at high pH. *Proteins* **1988**, *4*, 283-293.

[60] Boriack-Sjodin, P. A.; Heck, R. W.; Laipis, P. J.; Silverman, D. N.; Christianson, D. W. Structure determination of murine mitochondrial carbonic anhydrase V at 2.45-A resolution: implications for catalytic proton transfer and inhibitor design. *Proc. Natl. Acad. Sci. U.S.A.* **1995**, *92*, 10949-10953.

[61] Eriksson, A. E.; Liljas, A. Refined structure of bovine carbonic anhydrase III at 2.0 A resolution. *Proteins* **1993**, *16*, 29-42.

[62] Stams, T.; Nair, S. K.; Okuyama, T.; Waheed, A.; Sly, W. S.; Christianson, D. W. Crystal structure of the secretory form of membrane-associated human carbonic anhydrase IV at 2.8-A resolution. *Proc. Natl. Acad. Sci. U.S.A.* **1996**, *93*, 13589-13594.

[63] Angeli, A.; Vaiano, F.; Mari, F.; Bertol E.; Supuran, C.T. Psychoactive substances belonging to the amphetamine class potently activate brain carbonic anhydrase isoforms VA, VB, VII, and XII. *J Enzyme Inhib Med Chem.* **2017**, *32*, 1253-1259.

[64] Whittington, D. A.; Grubb, J. H.; Waheed, A.; Shah, G. N.; Sly, W. S.; Christianson, D. W. Expression, assay, and structure of the extracellular domain of murine carbonic anhydrase XIV: implications for selective inhibition of membrane-associated isozymes. *J. Biol. Chem.* **2004**, *279*, 7223-7228.

[65] Duda, D. M.; Tu, C.; Fisher, S. Z.; An, H.; Yoshioka, C.; Govindasamy, L.; Laipis, P. J.; Agbandje-McKenna, M.; Silverman, D. N.; McKenna, R. Human carbonic anhydrase III: structural and kinetic study of catalysis and proton transfer. *Biochemistry* **2005**, *44*, 10046-10053.

[66] Di Fiore, A.; Monti, S. M.; Hilvo, M.; Parkkila, S.; Romano, V.; Scaloni, A.; Pedone, C.; Scozzafava, A.; Supuran, C. T.; De Simone, G. Crystal structure of human carbonic anhydrase XIII and its complex with the inhibitor acetazolamide. *Proteins* **2008**, *74*, 164-175.

[67] Alterio, V.; Hilvo, M.; Di Fiore, A.; Supuran, C.T.; Pan, P.; Parkkila, S.; Scaloni, A.; Pastorek, J.; Pastorekova, S.; Pedone, C.; Scozzafava, A.; Monti, S.M.; De Simone, G. Crystal structure of the catalytic domain of the tumor-associated human carbonic anhydrase IX *Proc. Natl. Acad. Sci. U.S.A.* **2009**, *106*, 16233-16238.

[68] Di Fiore, A.; Truppo, E.; Supuran, C. T.; Alterio, V.; Dathan, N.; Bootorabi, F.; Parkkila, S.; Monti, S. M.; De Simone, G. Crystal structure of the C183S/C217S mutant of human CA VII in complex with acetazolamide. *Bioorg. Med. Chem. Lett.* **2010**, *20*, 5023-5026.

[69] Capasso, C.; Supuran C.T. Anti-infective carbonic anhydrase inhibitors: a patent and literature review. *Expert Opin. Ther. Pat.* **2013**, *23*, 693-704.

[70] Chirica, L.C.; Petersson, C.; Hurtig, M.; Jonsson, B.H.; Borén, T.; Lindskog, S. Expression and localization of alpha- and beta-carbonic anhydrase in Helicobacter pylori. *Biochim. Biophys. Acta.* **2002**, *1601*, 192-199.

[71] Nishimori, I.; Minakuchi, T.; Morimoto, K.; Sano, S.; Onishi, S.; Takeuchi, H.; Vullo, D.; Scozzafava, A.; Supuran, C. T. Carbonic anhydrase inhibitors: DNA cloning and inhibition studies of the alpha-carbonic anhydrase from Helicobacter pylori, a new target for developing sulfonamide and sulfamate gastric drugs. *J. Med. Chem*. **2006**, *49*, 2117-2126.

[72] Shahidzadeh, R.; Opekun, A.; Shiotani, A; Graham D. Y. Effect of the carbonic anhydrase inhibitor, acetazolamide, on Helicobacter pylori infection in vivo: a pilot study. *Helicobacter* **2005**, *10*, 136-138.

[73] Del Prete, S.; Isik, S.; Vullo, D.; De Luca, V.; Carginale, V.; Scozzafava, A.; Supuran C.T.; Capasso, C. DNA cloning, characterization, and inhibition studies of an alpha-carbonic anhydrase from the pathogenic bacterium Vibrio cholerae. *J. Med. Chem.* **2012**, *55*, 10742-10748.

[74] Vullo, D.; Isik, S.; Del Prete, S.; De Luca, V.; Carginale, V.; Scozzafava, A.; Supuran, C.T.; Capasso, C. Anion inhibition studies of the alpha-carbonic anhydrase from the pathogenic bacterium Vibrio cholerae. *Bioorg. Med. Chem. Lett.* **2013**, *23*, 1636-1638.

[75] Innocenti, A.; Hall, R. A.; Schlicker, C.; Scozzafava, A.; Steegborn, C.; Mühlschlegel, F. A.; Supuran, C.T. Carbonic anhydrase inhibitors. Inhibition and homology modeling studies of the fungal beta-carbonic anhydrase from Candida albicans with sulfonamides. *Bioorg. Med. Chem*. **2009**, *17*, 4503-4509.

[76] Monti, S.M.; Maresca, A.; Viparelli, F.; Carta, F.; De Simone, G.; Mühlschlegel, F.A.; Scozzafava, A.; Supuran, C. T. Dithiocarbamates are strong inhibitors of the beta-class fungal carbonic anhydrases from Cryptococcus neoformans, Candida albicans and Candida glabrata. *Bioorg. Med. Chem. Lett.* **2012**, *22*, 859-862.

[77] Cottier, F.; Leewattanapasuk, W.; Kemp, L.R.; Murphy, M.; Supuran, C. T.; Kurzai, O.; Mühlschlegel, F. A. Carbonic anhydrase regulation and CO(2) sensing in the fungal pathogen Candida glabrata involves a novel Rca1p ortholog. *Bioorg. Med. Chem.* **2013**, *21*, 1549-1554.

[78] Davis. R. A.; Hofmann, A.; Osman, A.; Hall, R. A.; Mühlschlegel, F.A.; Vullo, D.; Innocenti, A.; Supuran, C. T.; Poulsen, S.A. Natural product-based phenols as novel probes for mycobacterial and fungal carbonic anhydrases. *J. Med. Chem.* **2011**, *54*, 1682-1692.

[79] Isik, S.; Kockar, F.; Arslan, O.; Guler, O. O.; Innocenti, A.; Supuran, C. T. Carbonic anhydrase inhibitors. Inhibition of the beta-class enzyme from the yeast Saccharomyces cerevisiae with anions. *Bioorg. Med. Chem. Lett*. **2008**, *18*, 6327-6331.

[80] Hewitson, K. S.; Vullo, D.; Scozzafava. A.; Mastrolorenzo, A.; Supuran, C. T. Molecular cloning, characterization, and inhibition studies of a beta-carbonic anhydrase from Malassezia globosa, a potential antidandruff target. *J. Med. Chem.* **2012**, *55*, 3513-3520.

[81] Krungkrai, J.; Scozzafava, A.; Reungprapavut, S.; Krungkrai, S. R.; Rattanajak, R.; Kamchonwongpaisan, S.; Supuran C. T. Carbonic anhydrase inhibitors. Inhibition of Plasmodium falciparum carbonic anhydrase with aromatic sulfonamides: towards antimalarials with a novel mechanism of action? *Bioorg. Med. Chem.* **2005**, *13*, 483-489.

[82] Krungkrai, S. R; Suraveratum, N.; Rochanakij, S.; Krungkrai, J. Characterisation of carbonic anhydrase in Plasmodium falciparum. *Int. J. Parasitol* **2001**, *31*, 661-668.

[83] Supuran C.T.; Capasso C. The eta-class carbonic anhydrases as drug targets for antimalarial agents. *Expert Opin. Ther. Targets* **2015**, *19*, 551-563.

[84] Pan, P.; Vermelho, A. B.; Capaci Rodrigues, G.; Scozzafava, A.; Tolvanen, M. E.; Parkkila, S.; Capasso, C.; Supuran, C. T. Cloning, characterization, and sulfonamide and thiol inhibition studies of an alphacarbonic anhydrase from Trypanosoma cruzi, the causative agent of Chagas disease. *J. Med. Chem.* **2013**, *56*, 1761-1771.

[85] Guzel-Akdemir, O.; Akdemir, A.; Pan, P.; Vermelho, A. B.; Parkkila, S.; Scozzafava, A.; Capasso, C.; Supuran, C. T. A class of sulfonamides with strong inhibitory action against the alpha-carbonic anhydrase from Trypanosoma cruzi. *J. Med. Chem.* **2013**, *56*, 5773-5781.

[86] Syrjanen, L.; Vermelho, A. B.; Rodrigues Ide, A.; Corte-Real, S.; Salonen, T.; Pan, P.; Vullo, D.; Parkkila, S.; Capasso, C.; Supuran, C. T. Cloning, characterization, and inhibition studies of a beta-carbonic anhydrase from *Leishmania donovani chagasi*, the protozoan parasite responsible for leishmaniasis. *J. Med. Chem* **2013**, *56*, 7372-7381.

[87] Supuran, C. T. Structure-based drug discovery of carbonic anhydrase inhibitors. *J. Enzyme Inhib. Med. Chem.* **2012**, *27*, 759–772.

[88] Supuran, C. T. Carbonic anhydrase inhibitors. *Bioorg. Med. Chem. Lett*. **2010**, *20*, 3467–3474.

[89] Carta, F.; Supuran, C.T.; Scozzafava, A. Sulfonamides and their isosters as carbonic anhydrase inhibitors. *Future Med. Chem.* **2014**, *6*, 1149-1165.

[90] Winum, J.Y.; Supuran, C.T. Recent advances in the discovery of zinc-binding motifs for the development of carbonic anhydrase inhibitors. *J. Enzyme Inhib. Med. Chem*. **2015**, *30*, 321-324.

[91] Supuran, C.T. How many carbonic anhydrase inhibition mechanisms exist? *J. Enzyme Inhib. Med. Chem*. **2016**, *31*, 345-360.

[92] Keilin, D.; Mann, T. Carbonic anhydrase. Purification and nature of the enzyme. *Biochem. J.* **1940**, *34*, 1163-1176.

[93] Winum, J.-Y.; Monter, J,-L.; Scozzafava, A.; Supuran, C. T. In Drug Design of Zinc-Enzyme Inhibitors: Functional, Structural, and Disease Applications; Supuran, C. T., Winum, J.-Y., Eds.; *Wiley: Hoboken*, NJ, **2009**; p 39.

[94] Supuran, C. T.; De Simone, G. Carbonic Anhydrases as Biocatalysts: From Theory to Medical and Industrial Applications; Supuran, C. T., De Simone, G. Eds.; *Elsevier.* **2015**.

[95] Bozdag, M.; Ferraroni, M.; Nuti, E.; Vullo, D.; Rossello, A.; Carta, F.; Scozzafava, A.; Supuran, C. T. Combining the tail and the ring approaches for obtaining potent and isoform-selective carbonic anhydrase inhibitors: solution and X-ray crystallographic studies. *Bioorg. Med. Chem.* **2014**, *22*, 334−340.

[96] Scozzafava, A.; Menabuoni, L.; Mincione, F.; Briganti, F.; Mincione, G.; Supuran, C. T. Carbonic anhydrase inhibitors. Synthesis of water-soluble, topically effective, intraocular pressure-lowering aromatic/heterocyclic sulfonamides containing cationic or anionic moieties: Is the tail more important than the ring? *J. Med. Chem.* **1999**, *42*, 2641−2650.

[97] Menchise, V.; De Simone, G.; Alterio, V.; Di Fiore, A.; Pedone, C.; Scozzafava, A.; Supuran, C. T. Carbonic anhydrase inhibitors: stacking with Phe131 determines active site binding region of inhibitors as exemplified by the X-ray crystal structure of a membrane-impermeant antitumor sulfonamide complexed with isozyme II. *J. Med. Chem*. **2005**, *48*, 5721-5727.

[98] Scozzafava, A.; Briganti, F.; Ilies, M. A.; Supuran, C. T. Carbonic anhydrase inhibitors: synthesis of membrane-impermeant low molecular weight sulfonamides possessing in vivo selectivity for the membrane-bound versus cytosolic isozymes. *J. Med. Chem.* **2000**, *43*, 292-300.

[99] Pacchiano, F.; Carta, F.; McDonald, P. C.; Lou, Y.; Vullo, D.; Scozzafava, A.; Dedhar, S.; Supuran, C. T. Ureido-substituted benzenesulfonamides potently inhibit carbonic anhydrase IX and show antimetastatic activity in a model of breast cancer metastasis. *J. Med. Chem.* **2011**, *54*, 1896−1902.

[100] ClinicalTrials.gov, https://clinicaltrials.gov/ct2/results?term=slc-0111&Search=Search (Accessed on October 10th 2019); https://clinicaltrials.gov/ct2/show/NCT03450018 (last updated on March 1, 2018); last accessed on October 10th, 2019.

[101] Carta, F.; Aggarwal, M.; Maresca, A.; Scozzafava, A.; McKenna, R.; Supuran, C. T. Dithiocarbamates: a new class of carbonic anhydrase inhibitors. Crystallographic and kinetic investigations. *Chem. Commun. (Camb).* **2012**, *48*, 1868-1870.

[102] Carta, F.; Aggarwal, M.; Maresca, A; Scozzafava, A.; McKenna, R.; Masini, E.; Supuran, C. T. Dithiocarbamates strongly inhibit carbonic anhydrases and show antiglaucoma action in vivo. *J. Med. Chem.* **2012**, *55*,1721-1730.

[103] Carta, F.; Akdemir, A.; Scozzafava, A.; Masini, E; Supuran, C. T. Xanthates and trithiocarbonates strongly inhibit carbonic anhydrases and show antiglaucoma effects in vivo. *J. Med. Chem.* **2013**, *56*, 4691-4700.

[104] Vullo, D.; Durante, M.; Di Leva, F. S.; Cosconati, S.; Masini, E.; Scozzafava, A.; Novellino, E.; Supuran, C. T.; Carta, F. Monothiocarbamates Strongly Inhibit Carbonic Anhydrases in Vitro and Possess Intraocular Pressure Lowering Activity in an Animal Model of Glaucoma. *J. Med. Chem.* **2016**, *59*, 5857-5867.

[105] Mori, M.; Cau, Y.; Vignaroli, G.; Laurenzana, I.; Caivano, A.; Vullo, D.; Supuran, C. T.; Botta, M. Hit recycling: discovery of a potent carbonic anhydrase inhibitor by in silico target fishing. *ACS Chem. Biol.* **2015**, *10*, 1964–1969.

[106] Innocenti, A.; Vullo, D.; Scozzafava, A.; Casey, J. R.; Supuran, C. T. Carbonic anhydrase inhibitors. Interaction of isozymes I, II, IV, V and IX with carboxylates. *Bioorg. Med. Chem. Lett.* **2005**, *15*, 573–578.

[107] Scozzafava, A.; Supuran, C. T. Hydroxyurea is a carbonic anhydrase inhibitor. *Bioorg. Med. Chem.* **2003**, *11*, 2241–2246.

[108] Di Fiore, A.; Maresca, A.; Supuran, C. T.; De Simone, G. Hydroxamate represents a versatile zinc binding group for the development of new carbonic anhydrase inhibitors. *Chem. Commun. (Camb.)* **2012**, *48*, 8838–8840.

[109] Nocentini, A.; Gratteri, P.; Supuran, C.T. Phosphorus versus Sulfur: Discovery of Benzenephosphonamidates as Versatile Sulfonamide-Mimic Chemotypes Acting as Carbonic Anhydrase Inhibitors. *Chemistry.* **2019**, *5*, 1188-1192.

[110] Alterio, V.; Cadoni, R.; Esposito, D., Vullo, D.; Fiore, A.D.; Monti, S.M.; Caporale, A.; Ruvo, M.; Sechi, M.; Dumy, P.; Supuran, C.T.; De Simone, G.; Winum J.Y. Benzoxaborole as a new chemotype for carbonic anhydrase inhibition. *Chem Commun (Camb).* **2016**, *52*, 11983-11986.

[111] Angeli, A.; Tanini, D.; Nocentini, A., Capperucci, A.; Ferraroni, M.; Gratteri, P.; Supuran, C.T. Selenols: a new class of carbonic anhydrase inhibitors. *Chem Commun (Camb).* **2019**, *55*, 648-651.

[112] Nair, S. K.; Ludwig, P. A.; Christianson, D. W. Two-site binding of phenol in the active site of human carbonic anhydrase II: structural implications for substrate association. *J. Am. Chem. Soc.* **1994**, *116*, 3659–3660.

[113] Innocenti, A.; Vullo, D.; Scozzafava, A.; Supuran, C. T. Carbonic anhydrase inhibitors. Interactions of phenols with the 12 catalytically active mammalian isoforms (CA I–XIV). *Bioorg. Med. Chem. Lett*. **2008**, *18*, 1583–1587.

[114] Carta, F.; Temperini, C.; Innocenti, A.; Scozzafava, A.; Kaila, K.; Supuran, C. T. Polyamines inhibit carbonic anhydrases by anchoring to the zinc-coordinated water molecule. *J. Med. Chem.* **2010,** *53*, 5511–5522.

[115] Innocenti, A.; Ozturk Sarkaya, S. B.; Gulcin, I.; Supuran, C. T. Carbonic anhydrase inhibitors. Inhibition of mammalian isoforms I-XIV with a seriess of natural product polyphenols and phenolic acids. *Bioorg. Med. Chem.* **2010**, *18*, 2159–2164.

[116] Davis, R. A.; Hofmann, A.; Osman, A.; Hall, R. A.; Mühlschlegel, F. A.; Vullo, D.; Innocenti, A.; Supuran, C. T.; Poulsen, S. A. Natural product-based phenols as novel probes for mycobacterial and fungal carbonic anhydrases. *J. Med. Chem.* **2011**, *54*, 1682–1692.

[117] Martin, D.P.; Cohen, S. M. Nucleophile recognition as an alternative inhibition mode for benzoic acid based carbonic anhydrase inhibitors. *Chem. Commun. (Camb.)* **2012**, *48*, 5259–5261.

[118] Tars, K.; Vullo, D.; Kazaks, A.; Leitans, J.; Lends, A.; Grandane, A.; Zalubovskis, R.; Scozzafava, A.; Supuran, C. T. Sulfocoumarins (1,2- benzoxathiine-2,2-dioxides): a class of potent and isoform-selective inhibitors of tumor-associated carbonic anhydrases. *J. Med. Chem.* **2013**, *56*, 293–300.

[119] Buchieri, M.V.; Riafrecha, L.E.; Rodrıguez, O. M.; Vullo, D.; Morbidoni, H. R.; Supuran, C. T.; Colinas, P. A. Inhibition of the b-carbonic anhydrases from Mycobacterium tuberculosis with C-cinnamoyl glycosides: identification of the first inhibitor with anti-mycobacterial activity. *Bioorg. Med. Chem. Lett.* **2013**, *23*, 740–743.

[120] Maresca, A.; Temperini, C.; Vu, H.; Pham, N. B.; Poulsen, S. A.; Scozzafava, A.; Quinn, R. J. Supuran, C. T. Non-zinc mediated inhibition of carbonic anhydrases: coumarins are a new class of suicide inhibitors. *J. Am. Chem. Soc.* **2009**, *131*, 3057–3062.

[121] Maresca, A.; Temperini, C.; Pochet, L.; Masereel, B.; Scozzafava, A.; Supuran, C. T. Deciphering the mechanism of carbonic anhydrase inhibition with coumarins and thiocoumarins. *J. Med. Chem.* **2010**, *53*, 335–344.

[122] Temperini, C.; Innocenti, A.; Scozzafava, A.; Parkkila, S.; Supuran, C. T. The coumarin binding site in carbonic anhydrase accommodates structurallydiverse inhibitors: the antiepileptic lacosamide as an example and lead molecule for novel classes of carbonic anhydrase inhibitors. *J. Med. Chem*. **2010**, *53*, 850–854.

[123] Touisni, N.; Maresca, A.; McDonald, P. C.; Lou, Y.; Scozzafava, A.; Dedhar, S.; Winum, J. Y.; Supuran, C. T. Glycosyl coumarin carbonic anhydrase IX and XII inhibitors strongly attenuate the growth of primary breast tumors. *J. Med. Chem.* **2011**, *54*, 8271–8277.

[124] Bonneau, A; Maresca, A.; Winum, J. Y.; Supuran, C. T. Metronidazolecoumarin conjugates and 3-cyano-7-hydroxy-coumarin act as isoform-selective carbonic anhydrase inhibitors. *J. Enzyme Inhib. Med. Chem.* **2013**, *28*, 397–401.

[125] Sharma, A.; Tiwari, M.; Supuran, C. T. Novel coumarins and benzocoumarins acting as isoform-selective inhibitors against the tumor-associated carbonic anhydrase IX. *J. Enzyme Inhib. Med. Chem.* **2014**, *29*, 292–296.

[126] Maresca, A.; Supuran, C. T. Coumarins incorporating hydroxy- and chloro- moieties selectively inhibit the transmembrane, tumor-associated carbonic anhydrase isoforms IX and XII over the cytosolic ones I and II. *Bioorg. Med. Chem. Lett.* **2010**, *20*, 4511–4514.

[127] Maresca, A.; Scozzafava, A.; Supuran, C. T. 7,8-Disubstituted- but not 6,7-disubstituted coumarins selectively inhibit the transmembrane, tumor-associated carbonic anhydrase isoforms IX and XII over the

cytosolic ones I and II in the low nanomolar/subnanomolar range. *Bioorg. Med. Chem. Lett.* **2010**, *20*, 7255–7258.

[128] D'Ambrosio, K.; Carradori, S.; Monti, S.M.; Buonanno, M.; Secci, D.; Vullo, D.; Supuran, C.T.; De Simone, G. Out of the active site binding pocket for carbonic anhydrase inhibitors. *Chem Commun* **2015**, *51*, 302–305.

[129] D'Ascenzio, M.; Carradori, S.; De Monte, C.; Secci, D.; Ceruso, M.; Supuran, C.T. Design, synthesis and evaluation of N-substituted saccharin derivatives as selective inhibitors of tumor-associated carbonic anhydrase XII. *Bioorg Med Chem* **2014**, *22*, 1821–1831.

[130] De Monte, C.; Carradori, S.; Secci, D.; D'Ascenzio, M.; Vullo, D.; Ceruso, M.; Supuran, C.T. Cyclic tertiary sulfamates: selective inhibition of the tumor-associated carbonic anhydrases IX and XII by N- and O-substituted acesulfame derivatives. *Eur J Med Chem* **2014**, *84*, 240–246.

[131] Parkkila, S.; Innocenti, A.; Kallio, H.; Hilvo, M.; Scozzafava, A.; Supuran, C.T. The protein tyrosine kinase inhibitors imatinib and nilotinib strongly inhibit several mammalian a-carbonic anhydrase isoforms. *Bioorg Med Chem Lett* **2009**, *19*, 4102–4106.

[132] Briganti, F.; Mangani, S.; Orioli, P.; Scozzafava, A.; Vernaglione, G.; Supuran, C.T. Carbonic anhydrase activators: x-ray crystallographic and spectroscopic investigations for the interaction of isozymes I and II with histamine. *Biochemistry* **1997**, *36*, 10384–10392.

[133] Supuran, C.T. Carbonic anhydrases: from biomedical applications of the inhibitors and activators to biotechnologic use for CO2 capture. *J. Enzyme Inhib Med Chem* **2013**, *28*, 229–230.

[134] Temperini, C.; Scozzafava, A.; Supuran, C.T. Carbonic anhydrase activation and the drug design. *Curr Pharm Des*. **2008**, *14*, 708-715.

[135] Temperini, C.; Scozzafava, A.; Vullo, D.; Supuran, C.T. Carbonic anhydrase activators. Activation of isozymes I, II, IV, VA, VII, and XIV with l- and d-histidine and crystallographic analysis of their adducts with isoform II: engineering proton-transfer processes within the active site of an enzyme. *Chemistry.* **2006**, *12*, 7057-7066.

[136] Temperini, C.; Scozzafava, A.; Puccetti, L.; Supuran, C.T. Carbonic anhydrase activators: X-ray crystal structure of the adduct of human isozyme II with L-histidine as a platform for the design of stronger activators. *Bioorg Med Chem Lett.* **2005**, *15*, 5136-5141.

[137] Temperini, C.; Scozzafava, A.; Supuran, C.T. Carbonic anhydrase activators: the first X-ray crystallographic study of an adduct of isoform I. *Bioorg Med Chem Lett.* **2006**, *16*, 5152-5156.

[138] Csermely, P.; Agoston, V.; Pongor, S. The efficiency of multitarget drugs: the network approach might help drug design. *Trends Pharmacol. Sci.* **2005**, *26*, 178−182.

[139] Espinoza-Fonseca, L. M. The benefits of the multi-target approach in drug design and discovery. *Bioorg. Med. Chem*. **2006**, *14*, 896−897.

[140] Zimmermann, G. R.; Lehár, J.; Keith, C. T. Multi-target therapeutics: when the whole is greater than the sum of the parts. *Drug Discovery Today* **2007**, *12*, 34−42.

[141] Sikazwe, D. M. N. The multi-target drug design era is here, consider it. *Drug Des.: Open Access* **2012**, *1*, 1000−1101.

[142] Myasoedova, E.; Crowson, C. S.; Kremers, H. M.; Therneau, T. M.; Gabriel, S. E. Is the incidence of rheumatoid arthritis rising?: results from Olmsted County, Minnesota, 1955-2007. *Arthritis Rheum*. **2010**, *62*, 1576-1582.

[143] Yelin, E.; Lubeck, D.; Holman, H.; Epstein, W. The impact of rheumatoid arthritis and osteoarthritis: the activities of patients with rheumatoid arthritis and osteoarthritis compared to controls. *J.Rheumatol.* **1987**, *14*, 710-717.

[144] Yelin, E.; Henke, C.; Epstein, W. The work dynamics of the person with rheumatoid arthritis. *Arthritis Rheum.* **1987**, *30*, 507-512.

[145] Singh, J. A.; Saag, K. G.; Bridges, S. L. Jr.; Akl, E. A.; Bannuru, R. R.; Sullivan, M. C.; Vaysbrot, E.; McNaughton, C.; Osani, M.; Shmerling, R. H.; Curtis, J. R.; Furst, D. E.; Parks, D.; Kavanaugh, A.; O'Dell, J.; King, C.; Leong, A.; Matteson, E. L.; Schousboe, J. T.; Drevlow, B.; Ginsberg, S.; Grober, J.; St Clair, E. W.; Tindall, E.; Miller, A. S.; McAlindon, T. 2015 American College of Rheumatology Guideline for the Treatment of Rheumatoid Arthritis. *Arthritis Rheumatol*. **2016**, *68*, 1-26.

[146] Chang, X.; Han, J.; Zhao, Y.; Yan, X.; Sun, S.; Cui, Y. Increased expression of carbonic anhydrase I in the synovium of patients with ankylosing spondylitis. *BMC Musculoskelet Disord* **2010**, *11*, 279–290.

[147] Zheng, Y.; Wang, L.; Zhang, W.; Xu, H.; Chang, X. Transgenic mice over-expressing carbonic anhydrase I showed aggravated joint inflammation and tissue destruction. *BMC Musculoskelet Disord* **2012**, *13*, 256–265.

[148] Deutsch, O.; Krief, G.; Konttinen, Y. T.; Zaks, B.; Wong, D. T.; Aframian, D. J.; Palmon, A. Identification of Sjo¨gren's syndrome oral fluid biomarker candidates following high-abundance protein depletion. *Rheumatology*. **2015**, *54*, 884–890.

[149] Krishnamurthy, V. M.; Kaufman, G. K.; Urbach, A. R.; Gitlin, I.; Gudiksen, K. L.; Weibel, D. B.; Whitesides, G. M. Carbonic anhydrase as a model for biophysical and physical-organic studies of proteins and protein-ligand binding. *Chem. Rev*. **2008**, *108*, 946-1051.

[150] Tanc, M.; Carta, F.; Scozzafava, A.; Supuran, C. T. α-Carbonic Anhydrases Possess Thioesterase Activity. *ACS Med. Chem. Lett*. **2015**, *6*, 292-295.

[151] Agca, R.; Heslinga, S. C.; Rollefstad, S.; Heslinga, M.; McInnes, I. B.; Peters, M. J.; Kvien, T. K.; Dougados, M.; Radner, H.; Atzeni, F.; Primdahl, J.; Södergren, A.; Wallberg Jonsson, S.; van Rompay, J.; Zabalan, C.; Pedersen, T. R.; Jacobsson, L.; de Vlam, K.; Gonzalez-Gay, M. A.; Semb, A. G.; Kitas, G. D.; Smulders, Y. M.; Szekanecz, Z.; Sattar, N.; Symmons, D. P.; Nurmohamed, M. T. LAR recommendations for cardiovascular disease risk management in patients with rheumatoid arthritis and other forms of inflammatory joint disorders: 2015/2016 update. *Ann Rheum Dis*. **2016**, *0*, 1–12.

[152] Agarwal, S. K. Core management principles in rheumatoid arthritis to help guide managed care professionals. *J Manag Care Pharm.* **2011**, *17*, S03-8.

[153] Kharlamova, N.; Jiang, X.; Sherina, N.; Potempa, B.; Israelsson, L.; Quirke, A. M.; Eriksson, K.; Yucel-Lindberg, T.; Venables, P. J.; Potempa, J.; Alfredsson, L.; Lundberg, K. Antibodies to Porphyromonas gingivalis Indicate Interaction Between Oral Infection, Smoking, and Risk Genes in Rheumatoid Arthritis Etiology. *Arthritis Rheumatol*. **2016**, *68*, 604-613.

[154] Lundberg, K.; Wegner, N.; Yucel-Lindberg, T.; Venables, P. J. Periodontitis in RA-the citrullinated enolase connection. *Nat Rev Rheumatol*. **2010**, *6*, 727-730.

[155] Koziel, J.; Mydel, P.; Potempa, J. The link between periodontal disease and rheumatoid arthritis: an updated review. *Curr Rheumatol Rep*. **2014**, *16*, 408.

[156] Trabocchi, A.; Pala, N.; Krimmelbein, I.; Menchi, G.; Guarna, A.; Sechi, M.; Dreker, T.; Scozzafava, A.; Supuran, C. T.; Carta F. Peptidomimetics as protein arginine deiminase 4 (PAD4) inhibitors. *J Enzyme Inhib Med Chem.* **2015**, *30*, 466-471.

[157] Witalison, E. E.; Thompson, P. R.; Hofseth, L. J. Protein Arginine Deiminases and Associated Citrullination: Physiological Functions and Diseases Associated with Dysregulation. *Curr Drug Targets*. **2015**, *16*, 700-710.

[158] Maddur, M. S.; Miossec, P.; Kaveri, S. V.; Bayry, J. Th17 cells: biology, pathogenesis of autoimmune and inflammatory diseases, and therapeutic strategies. *Am. J. Pathol.* **2012**, 181, 8−18.

[159] Skapenko, A.; Leipe, J.; Lipsky, P. E.; Schulze-Koops, H. The role of the T cell in autoimmune inflammation. *Arthritis Res. Ther.* **2005**, *7*, S4−S14.

[160] Kanda, H.; Yokota, K.; Kohno, C.; Sawada, T.; Sato, K.; Yamaguchi, M.; Komagata, Y.; Shimada, K.; Yamamoto, K.; Mimura, T. Effects of low-dosage simvastatin on rheumatoid arthritis through reduction of Th1/Th2 and CD4/CD8 ratios. *Mod. Rheumatol.* **2007**, *17*, 364−368.

[161] Leipe, J.; Grunke, M.; Dechant, C.; Reindl, C.; Kerzendorf, U.; Schulze-Koops, H.; Skapenko, A. Role of Th17 cells in human autoimmune arthritis. *Arthritis Rheum.* **2010**, *62*, 2876−2885.

[162] Souza-Moreira, L.; Campos-Salinas, J.; Caro, M.; Gonzalez-Rey, E. Neuropeptides as pleiotropic modulators of the immune response. *Neuroendocrinology* **2011**, *94*, 89−100.

[163] Delgado, M.; Ganea, D. Anti-inflammatory neuropeptides: a new class of endogenous immunoregulatory agents. *Brain Behav. Immun.* **2008**, *22*, 1146−1151.

[164] Ferraroni, M.; Carta, F.; Scozzafava, A.; Supuran, C. T. Thioxocoumarins show an alternative carbonic anhydrase inhibition mechanism compared to coumarins. *J. Med. Chem.* **2016**, *59*, 462-473.

[165] Touisni, N.; Maresca, A.; McDonald, P. C.; Lou, Y.; Scozzafava, A.; Dedhar, S.; Winum, J.-Y.; Supuran, C. T. Glycosylcumarin carbonic anhydrase IX and XII inhibitors strongly attenuate the growth of primary breast tumors. *J. Med. Chem.* **2011**, *54*, 8271−8277.

[166] Bonneau, A.; Maresca, A.; Winum, J. Y.; Supuran, C. T. Metronidazole-coumarin conjugates and 3-cyano-7-hydroxy-coumarin act as isoform-selective carbonic anhydrase inhibitors. *J. Enzyme Inhib. Med. Chem.* **2013**, *28*, 397−401.

[167] Bozdag, M.; Alafeefy, A. M.; Altamimi, A. M.; Vullo, D.; Carta, F.; Supuran, C. T. Coumarins and other fused bicyclic heterocycles with selective tumor-associated carbonic anhydrase isoforms inhibitory activity. *Bioorg Med Chem.* **2017**, *25*, 677-683.

[168] Supuran, C.T.; Casini, A.; Mastrolorenzo, A.; Scozzafava, A. COX-2 selective inhibitors, carbonic anhydrase inhibition and anticancer properties of sulfonamides belonging to this class of pharmacological agents. *Mini-Rev. Med. Chem.* **2004**, *4*, 625-632.

[169] Khalifah, R. G. The carbon dioxide hydration activity of carbonic anhydrase. I. Stop-flow kinetic studies on the native human isoenzymes B and C. *J. Biol. Chem*. **1971**, *246*, 2561−2573.

[170] Di Cesare Mannelli, L.; Bani, D.; Bencini, A.; Brandi, M. L.; Calosi, L.; Cantore, M.; Carossino, A. M.; Ghelardini, C.; Valtancoli, B.; Failli, P. Therapeutic effects of the superoxide dismutase mimetic compound MnIIMe2DO2A on experimental articular pain in rats. *Mediators Inflamm*. **2013**, 905360.

[171] Mishra, G.; Hazari, P. P.; Kumar, N.; Mishra, A.K. In vitro and in vivo evaluation of 99mTc-DO3A-EA-Folate for receptor-mediated targeting of folate positive tumors. *J. Drug Target*., **2011**, *19*, 761-769.

[172] Micheli, L.; Bozdag, M.; Akgul, O.; Carta, F.; Guccione, C.; Bergonzi, M.C.; Bilia, A.R.; Cinci, L.; Lucarini, E.; Parisio, C.; Supuran, C.T.; Ghelardini, C.; Di Cesare Mannelli, L. Pain Relieving Effect of-NSAIDs-CAIs Hybrid Molecules: Systemic and Intra-Articular Treatments against Rheumatoid Arthritis. *Int J Mol Sci*. **2019**, *20*, pii: E1923.

[173] Bua, S.; Di Cesare Mannelli, L.; Vullo, D.; Ghelardini, C.; Bartolucci, G.; Scozzafava, A.; Supuran, C. T.; Carta, F. Design and Synthesis of Novel Nonsteroidal Anti-Inflammatory Drugs and Carbonic Anhydrase Inhibitors Hybrids (NSAIDs-CAIs) for the Treatment of Rheumatoid Arthritis. *J. Med. Chem.* **2017**, *60*, 1159–1170.

[174] Akgul, O.; Di Cesare Mannelli, L.; Vullo, D.; Angeli, A.; Ghelardini, C.; Bartolucci, G.; Alfawaz Altamimi, A. S.; Scozzafava, A.; Supuran, C. T.; Carta, F. Discovery of Novel Nonsteroidal Anti-Inflammatory Drugs and Carbonic Anhydrase Inhibitors Hybrids (NSAIDs-CAIs) for the Management of Rheumatoid Arthritis. *J. Med. Chem.* **2018**, *61*, 4961–4977.

[175] Menicatti, M.; Pallecchi, M.; Bua, S.; Vullo, D.; Di Cesare Mannelli, L.; Ghelardini, C.; Carta, F.; Supuran, C. T.; Bartolucci, G. Resolution of co-eluting isomers of anti-inflammatory drugs conjugated to carbonic anhydrase inhibitors from plasma in liquid chromatography by energy-resolved tandem mass spectrometry. *J. Enzyme Inhib. Med. Chem*. **2018**, *33*, 671–679.

[176] Park, J. Y.; Pillinger, M. H.; Abramson, S. B. Prostaglandin E_2 synthesis and secretion: the role of PGE2 synthases. *Clin. Immunol.* **2006**, *119*, 229–240.

[177] Leslie, C. C. Regulation of arachidonic acid availability for eicosanoid production. *Bioche Cell Biol*. **2004**, *82*, 1–17.

[178] Cryer, B.; Feldman, M. Cyclooxygenase-1 and cyclooxygenase-2 selectivity of widely used nonsteroidal anti-inflammatory drugs. *Am. J. Med.* **1998**, *104*, 413–421.

[179] Orlando, B. J.; Malkowski, M. G. Crystal structure of rofecoxib bound to human cyclooxygenase-2. *Acta Crystallogr. F. Struct. Biol. Commun.* **2016**, *72*, 772–776.

[180] Selinsky, B. S.; Gupta, K.; Sharkey, C. T.; Loll, P. J. Structural analysis of NSAID binding by prostaglandin H2 synthase: time-dependent and time-independent inhibitors elicit identical enzyme conformations. *Biochemistry* **2001**, *40*, 5172–5180.

[181] Quigley, H. A. Glaucoma. *Lancet* **2011**, 377, 1367-1377.

[182] Zhang, K.; Zhang, L.; Weinreb, R. N. Ophthalmic drug discovery: novel targets and mechanisms for retinal disease and glaucoma. *Nat. Rev. Drug. Discov.* **2012**, *11*, 541-559.

[183] Quigley, H. A. Broman AT. The number of people with glaucoma worldwide in 2010 and 2020. *Br. J. Ophthalmol.* **2006**, *90*, 151-156.

[184] Tham, Y. C.; Li, X.; Wong, T. Y.; Quigley, H. A.; Aung, T.; Cheng, C. Y. Global prevalence of glaucoma and projections of glaucoma burden through 2040: a systematic review and meta-analysis. *Ophthalmology.* **2014**, *121*, 2081–2090.

[185] Carta, F.; Supuran, C.T.; Scozzafava, A. Novel therapies for glaucoma: a patent review 2007-2011. *Expert Opin. Ther. Patents* **2012**, *22*, 79-88.

[186] Sommer, A.; Tielsch, J. M.; Katz J, Quigley, H. A.; Gottsch, J. D.; Javitt, J.; Singh, K. Relationship between intraocular pressure and primary open angle glaucoma among white and black Americans. *The Baltimore Eye Survey. Arch. Ophthalmol.* **1991**, *109*, 1090-1095.

[187] Schehlein, E. M.; Novack, G.; Robin, A. L. New pharmacotherapy for the treatment of glaucoma. *Expert Opin. Pharmacother*. **2017**, *18*, 1939-1946.

[188] Conlon, R.; Saheb, H.; Ahmed, II. Glaucoma treatment trends: a review. *Can. J. Ophtalmol.* **2017**, *52*, 114-124.

[189] Realini, T. A history of glaucoma pharmacology. *Optom. Vis. Sci.* **2011**, *88*, 36-38.

[190] Kass, M. A.; Heuer, D. K.; Higginbotham, E. J.; Johnson, C. A.; Keltner, J. L.; Miller, J. P.; Parrish, R. K.; Wilson, M. R.; Gordon, M. O. The ocular hypertension treatment study: a randomized trial determines that topical ocular hypotensive medication delays or prevents the onset of primary open-angle glaucoma. *Arch. Ophthalmol.* **2002**, *120*, 701-713.

[191] Nocentini, A.; Ceruso, M.; Bua, S.; Lomelino, C.L.; Andring, J.T.; McKenna, R.; Lanzi, C.; Sgambellone, S.; Pecori, R.; Matucci, R.; Filippi, L.; Gratteri, P.; Carta, F.; Masini, E.; Selleri, S.; Supuran, C.T. Discovery of β-Adrenergic Receptors Blocker-Carbonic Anhydrase Inhibitor Hybrids for Multitargeted Antiglaucoma Therapy. *J Med Chem.* **2018**, *61*, 5380-5394.

[192] Hollo, G.; Topouzis, F.; Fechtner, R. D. Fixed combination intraocular pressure-lowering therapy for glaucoma and ocular hypertension: advantages in clinical practice. *Expert Opin. Pharmacother.* **2014**, *15*, 1737-1747.

[193] Brooks, A.M.; Gillies, W.E. Ocular beta-blockers in glaucoma management. *Clinical pharmacological aspects. Drugs Aging* **1992**, *2*, 208-221.

[194] Mincione, F.; Menabuoni, L.; Supuran, C. T. Clinical Applications of the Carbonic Anhydrase Inhibitors in Ophthalmology. In: Supuran CT, Scozzafava A, Conway J, editors. Carbonic Anhydrase - Its Inhibitors and Activators. *CRC Press; Boca Raton (FL)* **2004**. p. 243-254.

[195] Mincione, F.; Scozzafava, A.; Supuran, C. T. Antiglaucoma Carbonic Anhydrase Inhibitors as Ophthalomologic Drugs. In: Supuran CT, Winum JY, editors. Drug Design of Zinc-Enzyme Inhibitors: Functional, Structural, and Disease Applications. *Wiley; Hoboken* **2009**. p. 139-154.

[196] Musch, D. C.; Lichter, P. R.; Guire, K. E.; Standardi, C. L. The collaborative initial glaucoma treatment study: study design, methods, and baseline characteristics of enrolled patients. *Ophthalmology.* **1999**, *106*, 653–662.

[197] Schwartz, G. F.; Quigley, H. A. Adherence and persistence with glaucoma therapy. *Surv. Ophthalmol.* **2008**, *53*, S57–68.

[198] Hennessy, A. L.; Katz, J.; Covert, D.; Protzko, C.; Robin, A. L. Videotaped evaluation of eyedrop instillation in glaucoma patients with visual impairment or moderate to severe visual field loss. *Ophthalmology* **2010**, *117*, 2345–2352.

[199] Csermely, P.; Agoston, V.; Pongor, S. The efficiency of multi-target drugs: the network approach might help drug design. *Trends Pharmacol. Sci.* **2005**, *26*, 178-182.

[200] Steele, R. M.; Batugo, M. R.; Benedini, F.; Borghi, V.; Carzaniga, L.; Impagnatiello, F.; Miglietta, D.; Chong, W. K.; Rajapakse, R.; Cecchi, A.; Temperini, C.; Supuran, C. T. Nitric oxide-donating carbonic anhydrase inhibitors for the treatment of open-angle glaucoma. *Bioorg. Med. Chem. Lett.* **2009**, *19*, 6565-6570.

[201] Mincione, F.; Benedini, F.; Biondi; S.; Cecchi, A.; Temperini, C.; Formicola, G.; Pacileo, I.; Scozzafava, A.; Masini, E.; Supuran, C. T. Synthesis and crystallographic analysis of new sulfonamides incorporating NO-donating moieties with potent antiglaucoma action. *Bioorg. Med. Chem. Lett.* **2011**, *21*, 3216-3221.

[202] Fabrizi, F.; Mincione, F.; Somma, T.; Scozzafava, G.; Galassi, F.; Masini, E.; Impagnatiello, F.; Supuran, C. T. A new approach to antiglaucoma drugs: carbonic anhydrase inhibitors with or without NO donating moieties. Mechanism of action and preliminary pharmacology. *J. Enzyme Inhib. Med. Chem.* **2012**, *27*, 138-147.

[203] Supuran, C.T. Carbonic anhydrase inhibitors and activators for novel therapeutic applications. *Future Med. Chem.* **2011**, *3*, 1165-1180.

[204] Nocentini, A.; Ferraroni, M.; Carta, F.; Ceruso, M.; Gratteri, P.; Lanzi, C.; Masini, E.; Supuran, C. T. Benzenesulfonamides incorporating flexible triazole moieties are highly effective carbonic anhydrase inhibitors: synthesis and kinetic, crystallographic, computational, and intraocular pressure lowering investigations. *J. Med. Chem.* **2016**, *59*, 10692-10704.

[205] Nocentini, A.; Bua, S.; Lomelino, C. L.; McKenna, R.; Menicatti, M.; Bartolucci, G.; Tenci, B.; Di Cesare Mannelli, L.; Ghelardini, C.; Gratteri, P.; Supuran, C. T. Discovery of new sulfonamide carbonic anhydrase IX inhibitors incorporating nitrogenous bases. *ACS Med. Chem. Lett.* **2017**, *8*, 1314-1319.

[206] Smith, C.; Teitler, M. Beta-blocker selectivity at cloned human beta1- and beta2-adrenergic receptors. *Cardiovasc. Drugs Ther.* **1999**, *13*, 123–126.

[207] Baker, G. J. The selectivity of β-adrenoceptor antagonists at the human β1, β2 and β3 adrenoceptors. *Br. J. Pharmacol.* **2005**, *144*, 317-322.

[208] Krauss, A. H. P.; Impagnatiello, F.; Toris, C. B.; Gale, D. C.; Prasanna, G.; Borghi, V.; Chiroli, V.; Chong, W. K. M.; Carreiro, S. T.; Ongini, E. Ocular hypotensive activity of BOL-303259-X, a nitric oxide donating prostaglandin F2α agonist, in preclinical models. *Exp. Eye Res.* **2011**, *93*, 250−255.

[209] Scozzafava, A.; Menabuoni, L.; Mincione, F.; Supuran, C.T. Carbonic anhydrase inhibitors. A general approach for the preparation of water soluble sulfonamides incorporating polyamino-polycarboxylate tails and of their metal complexes possessing long lasting, topical intraocular pressure lowering properties. *J. Med. Chem*. **2002**, *45*, 1466-1476.

[210] Zhang, H.; Wang X, Mao J.; Huang, Y.; Xu, W.; Duan, Y.; Zhang, J. Synthesis and biological evaluation of novel benzofuroxan-based pyrrolidine hydroxamates as matrix metalloproteinase inhibitors with nitric oxide releasing activity. *Bioorg Med Chem.* **2018**, *26*, 4363-4374.

[211] Bao, N.; Ou, J.; Xu, M.; Guan, F.; Shi, W.; Sun, J.; Chen, L. Novel NO-releasing plumbagin derivatives: Design, synthesis and evaluation of antiproliferative activity. *Eur J Med Chem*. **2017**, *137*, 88-95.

[212] Huang, Z.; Fu, J.; Zhang, Y. Nitric Oxide Donor-Based Cancer Therapy: Advances and Prospects. *J Med Chem.* **2017**, *60*, 7617-7635.

[213] Chugunova, E.A.; Burilov, A.R. Novel Structural Hybrids on the Base of Benzofuroxans and Furoxans. *Mini-Review. Curr Top Med Chem.* **2017**, *17*, 986-1005.

[214] Rosselli, M.; Keller, P.J.; Dubey, R.K. Role of nitric oxide in the biology, physiology and pathophysiology of reproduction. *Hum Reprod Update.* **1998**, *4*, 3-24.

[215] Jorge, S.D.; Palace-Berl, F.; Mesquita Pasqualoto, K.F.; Ishii, M.; Ferreira, A.K.; Berra, C.M.; Bosch, R.V.; Maria, D.A.; Tavares, L.C. Ligand-based design, synthesis, and experimental evaluation of novel benzofuroxan derivatives as anti-Trypanosoma cruzi agents. *Eur J Med Chem.* **2013**, *64*, 200-214.

[216] Dos Santos Fernandes, G.F.; de Souza, P.C.; Moreno-Viguri, E.; Santivañez-Veliz, M.; Paucar, R.; Pérez-Silanes, S.; Chegaev, K.; Guglielmo, S.; Lazzarato, L.; Fruttero, R.; Man Chin, C.; da Silva, P.B.; Chorilli, M.; Solcia, M.C.; Ribeiro, C.M.; Silva, C.S.P.; Marino, L.B.; Bosquesi, P.L.; Hunt, D.M.; de Carvalho, L.P.S.; de Souza Costa, C.A.; Cho, S.H.; Wang, Y.; Franzblau, S.G.; Pavan, F.R.; Dos Santos, J.L. Design, Synthesis, and Characterization of N-Oxide-Containing Heterocycles with in Vivo Sterilizing Antitubercular Activity. *J Med Chem.* **2017**, *60*, 8647-8660.

[217] Antônio Dutra, L.; de Almeida, L.; Passalacqua, T.G.; Santana Reis, J.; Torres, F.A.E.; Martinez, I.; Peccinini, R.G.; Chin, C.M.; Chegaev, K.; Guglielmo, S.; Fruttero, R.; Graminha, M.A.S.; dos Santos. J.L. Leishmanicidal Activities of Novel Synthetic Furoxan and Benzofuroxan Derivatives. *Antimicrob Agents Chemother.* **2014**, *58*, 4837-4847.

[218] Lomelino, C.L.; Andring, J.T.; McKenna, R. Crystallography and Its Impact on Carbonic Anhydrase Research. *Int J Med Chem*. **2018**, 9419521.

[219] Köhler, K.; Hillebrecht, A.; Schulze Wischeler, J.; Innocenti, A.; Heine, A.; Supuran, C.T.; Klebe, G. Saccharin inhibits carbonic anhydrases: possible explanation for its unpleasant metallic aftertaste. *Angew Chem Int Ed Engl.* **2007**, *46*, 7697-7699.

[220] Mahon, B.P.; Hendon, A.M.; Driscoll, J.M.; Rankin, G.M.; Poulsen, S.A.; Supuran, C.T.; McKenna, R. Saccharin: a lead compound for structure-based drug design of carbonic anhydrase IX inhibitors. *Bioorg Med Chem.* **2015**, *23*, 849-854.

[221] Koruza, K.; Mahon, B.P.; Blakeley, M.P.; Ostermann, A.; Schrader, T.E.; McKenna, R.; Knecht, W.; Fisher, S.Z. Using neutron crystallography to elucidate the basis of selective inhibition of carbonic anhydrase by saccharin and a derivative. *J Struct Biol.* **2019**, *205*, 147-154.

[222] Murray, A.B.; Lomelino, C.L.; Supuran, C.T.; McKenna, R. "Seriously Sweet": Acesulfame K Exhibits Selective Inhibition Using Alternative Binding Modes in Carbonic Anhydrase Isoforms. *J Med Chem.* **2018**, *61*, 1176-1181.

[223] Carradori, S.; Secci, D.; De Monte, C.; Mollica, A.; Ceruso, M.; Akdemir, A.; Sobolev, A.P.; Codispoti, R.; De Cosmi, F.; Guglielmi, P.; Supuran, C.T. A novel library of saccharin and acesulfame derivatives as potent and selective inhibitors of carbonic anhydrase IX and XII isoforms. *Bioorg Med Chem.* **2016**, *24*, 1095-1105.

[224] Nocentini, A.; D. Vullo, G. Bartolucci, C.T. Supuran, N-Nitrosulfonamides: A new chemotype for carbonic anhydrase inhibition, *Bioorg. Med. Chem.* **2016**, *24*, 3612-3617;

[225] Kornahrens, A.F.; Cognetta, A.B.; Brody, D.M.; Matthews, M.L.; Cravatt, B.F.; Boger, D.L. Design of Benzoxathiazin-3-one 1,1-Dioxides as a New Class of Irreversible Serine Hydrolase Inhibitors: Discovery of a Uniquely Selective PNPLA4 Inhibitor. *J Am Chem Soc.* **2017**, 139, 7052-7061.

[226] Zhang, S.; Chen, X.; Parveen, S.; Hussain, S.; Yang, Y.; Jing, C.; Zhu, C. Effect of C7 modifications on benzothiadiazine-1,1-dioxide derivatives on their inhibitory activity and selectivity toward aldose reductase. *ChemMedChem*. 2013, *8*, 603-613.

[227] Nocentini, A.; Donald, W.A.; Supuran C.T. Human carbonic anhydrases: tissue distribution, physiologic role, and druggability. In Carbonic Anhydrases; Nocentini, A.; Supuran CT. *Amsterdam: Elsevier*. **2019**. p. 149-185.

[228] Ambrosio, M.R.; Di Serio, C.; Danza, G.; Rocca, B.J., Ginori, A.; Prudovsky, I.; Marchionni, N.; Del Vecchio, M.T.; Tarantini, F. Carbonic anhydrase IX is a marker of hypoxia and correlates with higher Gleason scores and ISUP grading in prostate cancer. *Diagn. Pathol.* **2016**, *11*, p. 45.

[229] Korkeila, E.; Talvinen, K.; Jaakkola, P.M.; Minn, H.; Syrjänen, K.; Sundström, J.; Pyrhönen, S. Expression of carbonic anhydrase IX suggests poor outcome in rectal cancer, *Br. J. Cancer.* **2009**, *100*, 874–880.

[230] Mosmann, T. Rapid colorimetric assay for cellular growth and survival: Application to proliferation and cytotoxicity assays. *J. Immunol. Methods* **1983**, *65*, 55–63.

[231] Coviello, V.; Marchi, B.; Sartini, S.; Quattrini, L.; Marini, A.M.; Simorini, F.; Taliani, S.; Salerno, S.; Orlandi, P.; Fioravanti, A.; Desidero, T.D. 1, 2-Benzisothiazole derivatives bearing 4-, 5-, or 6-alkyl/arylcarboxamide moieties inhibit carbonic anhydrase isoform IX (CAIX) and cell proliferation under hypoxic conditions. *J. Med. Chem.* **2016**, *59*, 6547–6552.

[232] Hashmey, N.; Genta, N.; White, N., Jr. Parasites and Diarrhea. I: Protozoans and Diarrhea. *J. Travel Med.* **1997**, *4*, 17–31.

[233] Meier, A.; Erler, H.; Beitz, E. Targeting Channels and Transporters in Protozoan Parasite Infections. *Front. Chem.* **2018**, *6*, 88.

[234] Quach, J.; St-Pierre, J.; Chadee, K. The future for vaccine development against Entamoeba histolytica. *Hum. Vaccin. Immunother.* **2014**, *10*, 1514–1521.

[235] Loftus, B.; Anderson, I.; Davies, R.; Alsmark, U.C.M.; Samuelson, J.; Amedeo, P.; Roncaglia, P.; Berriman, M.; Hirt, R.P.; Mann, B.J.; et al. The genome of the protist parasite Entamoeba histolytica. *Nature* **2005**, *433*, 865–868.

[236] Bootorabi, F.; Jänis, J.; Smith, E.; Waheed, A.; Kukkurainen, S.; Hytönen, V.; Valjakka, J.; Supuran, C.T.; Vullo, D.; Sly, W.S. Analysis of a shortened form of human carbonic anhydrase VII expressed in vitro compared to the full-length enzyme. *Biochimie* **2010**, *92*, 1072–1080.

[237] Covarrubias, A.S.; Bergfors, T.; Jones, T.A.; Högbom, M. Structural mechanics of the pH-dependent activity of beta-carbonic anhydrase from Mycobacterium tuberculosis. *J. Biol. Chem.* **2006**, *281*, 4993–4999.

[238] Rowlett, R.S. Structure and catalytic mechanism of the β-carbonic anhydrases. *Biochim. Biophys. Acta Proteins Proteomics* **2010**, *1804*, 362–373.

[239] Zolfaghari Emameh, R.; Barker, H.; Hytönen, V.P.; Tolvanen, M.E.E.; Parkkila, S. Beta carbonic anhydrases: Novel targets for pesticides and anti-parasitic agents in agriculture and livestock husbandry. *Parasites Vect.* **2014**, *7*, 403.

[240] Nishimori, I.; Onishi, S.; Takeuchi, H.; Supuran, C.T. The α and β classes carbonic anhydrases from helicobacter pylori as novel drug targets. *Curr. Pharm. Des.* **2008**, *14*, 622–630.

[241] Syrjänen, L.; Parkkila, S.; Scozzafava, A.; Supuran, C.T. Sulfonamide inhibition studies of the β Carbonic anhydrase from Drosophila melanogaster. *Bioorg. Med. Chem. Lett.* **2014**, *24*, 2797–2801.

[242] Supuran, C.T.; Capasso, C. An overview of the bacterial carbonic anhydrases. *Metabolites* **2017**, *7*, 56.

[243] Nishimori, I.; Minakuchi, T.; Vullo, D.; Scozzafava, A.; Innocenti, A.; Supuran, C.T. Carbonic anhydrase inhibitors. Cloning, characterization, and inhibition studies of a new beta-carbonic anhydrase from Mycobacterium tuberculosis. *J. Med. Chem.* **2009**, *52*, 3116–3120.

[244] Ferraroni, M.; Del Prete, S.; Vullo, D.; Capasso, C.; Supuran, C.T. Crystal structure and kinetic studies of a tetrameric type II β-carbonic anhydrase from the pathogenic bacterium Vibrio cholerae. Acta *Crystallogr. D Biol. Crystallogr.* **2015**, *71*, 2449–2456.

[245] McGurn, L.D.; Moazami-Goudarzi, M.; White, S.A.; Suwal, T.; Brar, B.; Tang, J.Q.; Espie, G.S.; Kimber, M.S. The structure, kinetics and interactions of the β-carboxysomal β-carbonic anhydrase, CcaA. *Biochem. J.* **2016**, *473*, 4559–4572.

[246] De Simone, G.; Supuran, C.T. (In)organic anions as carbonic anhydrase inhibitors. *J. Inorg. Biochem*. **2012**, *111*, 117–129.

[247] Abbate, F.; Supuran, C.T.; Scozzafava, A.; Orioli, P.; Stubbs, M.T.; Klebe, G. Nonaromatic sulfonamide group as an ideal anchor for potent human carbonic anhydrase inhibitors: Role of hydrogen-bonding networks in ligand binding and drug design. *J. Med. Chem.* **2004**, *47*, 550–557.

[248] Murray, A.B.; Aggarwal, M.; Pinard, M.; Vullo, D.; Patrauchan, M.; Supuran, C.T.; McKenna, R. Structural Mapping of Anion Inhibitors to β-Carbonic Anhydrase psCA3 from Pseudomonas aeruginosa. *ChemMedChem* **2018**, *13*, 2024–2029.

[249] Supuran, C.T. Carbonic anhydrase inhibitors and their potential in a range of therapeutic areas. *Expert Opin. Ther. Pat.* **2018**, *28*, 709–712.

[250] Supuran, C.T. Applications of carbonic anhydrases inhibitors in renal and central nervous system diseases. *Expert Opin Ther Pat.* **2018**, *28*, 713–721.

[251] Nocentini, A.; Supuran, C.T. Carbonic anhydrase inhibitors as antitumor/antimetastatic agents: A patent review (2008–2018). *Expert Opin Ther Pat.* **2018**, *28*, 729–740.

[252] Muñoz,W.; Lamm, A.; Poppers, D.; Lamm, S. Acetazolamide promotes decreased consumption of carbonated drinks and weight loss. *Oxf. Med. Case Rep.* **2018**, *11*, omy081.

[253] Meldrum, N. U.; Roughton, F. J. Carbonic anhydrase. Its preparation and properties. *J. Physiol.* **1933,** *80*, 113-142.

[254] Supuran, C.T.; Capasso, C. Biomedical applications of prokaryotic carbonic anhydrases. *Expert Opin. Ther. Pat.* **2018**, *28*, 745–754.

[255] Borras, J.; Scozzafava, A.; Menabuoni, L.; Mincione, F.; Briganti, F.; Mincione, G.; Supuran, C.T. Carbonic anhydrase inhibitors: Synthesis of water-soluble, topically effective intraocular pressure lowering aromatic/heterocyclic sulfonamides containing 8-quinoline-sulfonyl moieties: Is the tail more important than the ring? *Bioorg. Med. Chem.* **1999**, *7*, 2397–2406.

[256] Vullo, D.; Del Prete, S.; Di Fonzo, P.; Carginale, V.; Donald, W.A.; Supuran, C.T.; Capasso, C. Comparison of the Sulfonamide Inhibition Profiles of the β- and γ-Carbonic Anhydrases from the Pathogenic Bacterium Burkholderia Pseudomallei. *Molecules* **2017**, *22*, 421.

[257] Supuran, C.T. Carbonic anhydrase activators. *Future Med. Chem.* **2018**, *10*, 561–573.

[258] Angeli, A.; Kuuslahti, M.; Parkkila, S.; Supuran, C.T. Activation studies with amines and amino acids of the α-carbonic anhydrase from the pathogenic protozoan Trypanosoma cruzi. *Bioorg. Med. Chem*. **2018**, *26*, 4187–4190.

[259] Bua, S.; Haapanen, S.; Kuuslahti, M.; Parkkila, S.; Supuran, C.T. Sulfonamide Inhibition Studies of a New β-Carbonic Anhydrase from the Pathogenic Protozoan Entamoeba histolytica. *Int. J. Mol. Sci.* **2018**, *19*, E3946.

[260] Haapanen, S.; Bua, S.; Kuuslahti, M.; Parkkila, S.; Supuran, C.T. Cloning, Characterization and Anion Inhibition Studies of a β-Carbonic Anhydrase from the Pathogenic Protozoan Entamoeba histolytica. *Molecules* **2018**, *23*, E3112.

[261] Bertucci, A.; Moya, A.; Tambutte, S.; Allemand, D.; Supuran, C.T.; Zoccola, D. Carbonic anhydrases in anthozoan corals—A review. *Bioorg. Med. Chem.* **2013**, *21*, 1437–1450.

[262] Al-Horani, F.A.; Al-Moghrabi, S.M.; de Beer, D. The mechanism of calcification and its relation to photosynthesis and respiration in the scleractinian coral Galaxea fascicularis. *Mar. Biol.* **2003**, *142*, 419–426.

[263] Al-Moghrabi, S.; Goiran, C.; Allemand, D.; Speziale, N.; Jaubert, J. Inorganic carbon uptake for photosynthesis by the symbiotic coral/dinoflagellate association. II. Mechanisms for bicarbonate uptake. *J. Exp. Mar. Biol. Ecol.* **1996**, *29*, 309–322.

[264] Tambutté, É.; Allemand, D.; Mueller, E.; Jaubert, J. A compartmental approach to the mechanism of calcification in hermatypic corals. *J. Exp. Biol.* **1996**, *199*, 1029–1041.

[265] Weis, V.M.; Smith, G.J.; Muscatine, L. A CO_2 supply'mechanism in zooxanthellate cnidarians: Role of carbonic anhydrase. *Mar. Biol.* **1989**, *100*, 195–202.

[266] Marshall, A.T.; Clode, P.L. Effect of increased calcium concentration in sea water on calcification and photosynthesis in the scleractinian coral Galaxea fascicularis. *J. Exp. Biol.* **2002**, *205*, 2107–2113.

[267] De Boer, M.L.; Krupp, D.A.; Weis, V.M. Two atypical carbonic anhydrase homologs from the planula larva of the scleractinian coral Fungia scutaria. *Biol. Bull.* **2006**, *211*, 18–30.

[268] Moya, A.; Tambutte, S.; Bertucci, A.; Tambutte, E.; Lotto, S.; Vullo, D.; Supuran, C.T.; Allemand, D.; Zoccola, D. Carbonic anhydrase in the scleractinian coral Stylophora pistillata: Characterization, localization, and role in biomineralization. *J. Biol. Chem.* **2008**, *283*, 25475–25484.

[269] Bertucci, A.; Tambutte, S.; Supuran, C.T.; Allemand, D.; Zoccola, D. A new coral carbonic anhydrase in stylophora pistillata. *Mar. Biotechnol.* **2011**, *13*, 992–1002.

[270] Grasso, L.C.; Maindonald, J.; Rudd, S.; Hayward, D.C.; Saint, R.; Miller, D.J.; Ball, E.E. Microarray analysis identifies candidate genes for key roles in coral development. *BMC Genom.* **2008**, *9*, 540.

[271] Bertucci, A.; Innocenti, A.; Zoccola, D.; Scozzafava, A.; Allemand, D.; Tambutte, S.; Supuran, C.T. Carbonic anhydrase inhibitors: Inhibition studies of a coral secretory isoform with inorganic anions. *Bioorg. Med. Chem. Lett.* 2009, *19*, 650–653.

[272] Bertucci, A.; Innocenti, A.; Scozzafava, A.; Tambutte, S.; Zoccola, D.; Supuran, C.T. Carbonic anhydrase inhibitors. Inhibition studies with anions and sulfonamides of a new cytosolic enzyme from the scleractinian coral Stylophora pistillata. *Bioorg. Med. Chem. Lett.* **2011**, *21*, 710–714.

[273] Karako-Lampert, S.; Zoccola, D.; Salmon-Divon, M.; Katzenellenbogen, M.; Tambutte, S.; Bertucci, A.; Hoegh-Guldberg, O.; Deleury, E.; Allemand, D.; Levy, O. Transcriptome analysis of the scleractinian coral Stylophora pistillata. *PLoS ONE* **2014**, *9*, e88615.

[274] Bhattacharya, D.; Agrawal, S.; Aranda, M.; Baumgarten, S.; Belcaid, M.; Drake, J.L.; Erwin, D.; Foret, S.; Gates, R.D.; Gruber, D.F.; et al. Comparative genomics explains the evolutionary success of reef-forming corals. *Elife* **2016**, *5*, e13288.

[275] Voolstra, C.R.; Li, Y.; Liew, Y.J.; Baumgarten, S.; Zoccola, D.; Flot, J.-F.; Tambutte, S.; Allemand, D.; Aranda, M. Comparative analysis of the genomes of stylophora pistillata and acropora digitifera provides evidence for extensive differences between species of corals. *Sci. Rep.* **2017**, *7*, 17583.

[276] Bertucci, A.; Moya, A.; Tambutte, S.; Allemand, D.; Supuran, C.T.; Zoccola, D. Carbonic anhydrases in anthozoan corals-A review. *Bioorg. Med. Chem*. **2013**, *21*, 1437–1450.

[277] Supuran, C. T. Carbonic anhydrase inhibitors. *Bioorg. Med. Chem. Lett*. **2010**, *20*, 3467–3474.

[278] Supuran, C.T. Carbonic anhydrases-an overview. *Curr. Pharm. Des.* **2008**, *14*, 603–614.

[279] Supuran, C.T. Carbonic anhydrase inhibitors: An editorial. *Expert Opin. Ther. Pat.* **2013**, *23*, 677–679.

[280] Huang, S.; Hainzl, T.; Grundstrom, C.; Forsman, C.; Samuelsson, G.; Sauer-Eriksson, A.E. Structural studies of beta-carbonic anhydrase from the green alga Coccomyxa: Inhibitor complexes with anions and acetazolamide. *PLoS ONE* **2011**, *6*, e28458.

[281] Le Goff, C.; Ganot, P.; Zoccola, D.; Caminiti-Segonds, N.; Allemand, D.; Tambutte, S. Carbonic anhydrases in cnidarians: Novel perspectives from the octocorallian Corallium rubrum. *PLoS ONE* **2016**, *11*, e0160368.

[282] Kingsley, R.J.;Watabe, N. Role of carbonic anhydrase in calcification in the gorgonian Leptogorgia virgulata. *J. Exp. Zool*. **1987**, *241*, 171–180.

[283] Kilkenny, C.; Browne, W. J.; Cuthill, I. C.; Emerson, M.; Altman, D. G. Improving bioscience research reporting: the ARRIVE guidelines for reporting animal research. *J. Pharmacol. Pharmacother*. **2010**, *1*, 94−99.

[284] Butler, S. H.; Godefroy, F.; Besson, J. M.; Weil-Fugazza, J. A limited arthritic model for chronic pain studies in the rat. *Pain* **1992**, *48*, 73−81.

[285] Di Cesare Mannelli, L.; Micheli, L.; Cinci, L.; Maresca, M.; Vergelli, C.; Pacini, A.; Quinn, M. T.; Giovannoni, M. P.; Ghelardini, C. Effects of the neutrophil elastase inhibitor EL-17 in rat adjuvant-induced arthritis. *Rheumatology* **2016**, *55*, 1285−1294.

[286] Leighton, G. E.; Rodriguez, R. E.; Hill, R. G.; Hughes, J. κ-Opioid agonist produce antinociception after i.v. and i.c.v. but not intrathecal administration in the rat. *Br. J. Pharmacol*. **1988**, *93*, 553−560.

[287] Bove, S. E.; Calcaterra, S. L.; Brooker, R. M.; Huber, C. M.; Guzman, R. E.; Juneau, P. L.; Schrier, D. J.; Kilgore, K. S. Weight bearing as a measure of disease progression and efficacy of anti- inflammatory compounds in a model of monosodium iodoacetate- induced osteoarthritis. *Osteoarthr. Cartil*. **2003**, *11*, 821−830.

[288] Bigagli, E.; Cinci, L.; Paccosi, S.; Parenti, A.; D'Ambrosio, M.; Luceri, C. Nutritionally relevant concentrations of resveratrol and hydroxytyrosol mitigate oxidative burst of human granulocytes and monocytes and the production of pro-inflammatory mediators in LPS-stimulated RAW 264.7 macrophages. *Int. Immunopharmacol*. **2017**, *43*, 147–155.

[289] Bani, D.; Nistri, S.; Cinci, L.; Giannini, L.; Princivalle, M.; Elliott, L.; Bigazzi, M.; Masini, E. A novel, simple bioactivity assay for relaxin based on inhibition of platelet aggregation. *Regul. Pept.* **2007**, *144*, 10–16.

[290] Schrödinger Suite Release 2019-1, Schrödinger, LLC, New York, NY, 2019: (a) Prime, v.5.5; Maestro v.11.9; (b) Epik, v.4.7; (c) Impact, v.8.2; (d) Macromodel v.12.3. (e) Glide, v.8.2.

[291] Schrödinger Release 2019-2: Desmond Molecular Dynamics System, D. E. Shaw Research, New York, NY, 2019, v.5.7.

[292] Liu, P.; Wu, T.; Ye, G.; Xu, J. Novel polyarylates containing aryl ether units: synthesis, characterization and properties *Polim. Int.* **2013**, *62*, 751-758.

[293] Bormans, G.; Verbruggen, A. Blood Imaging. WO **2009**/140743, 2009.

[294] Blum, S.; Katz, B.; Wilgong, C.; Levy, B. Topical Formulations Comprising Ion Channel Modulators. WO **2010**/091362, 2010.

[295] Stephenson, K. A.; Wilson, A.A.; Meyer, J. H.; Houle, S.; Vasdev, N. Facile radiosynthesis of fluorine-18 labeled beta-blockers. Synthesis, radiolabeling, and ex vivo biodistribution of [18F]-(2S and 2R)-1-(1-fluoropropan-2-ylamino)-3-(m-tolyloxy)propan-2-ol. *J. Med. Chem.* **2008**, *51*, 5093-5100.

[296] Apparu, M.; Tiba, Y. B.; Léo, P.; Hamman, S.; Coulombeau, C. Determination of the enantiomeric purity and the configuration of β-aminoalcohols using (R)-2-fluorophenylacetic acid (AFPA) and fluorine-19 NMR: application to β-blockers *Tetrahedron* **2000**, *11*, 2885-2898.

[297] Carta, F.; Mannelli, L.; Pinard, M.; Ghelardini, C.; Scozzafava, A.; McKenna, R.; Supuran, C.T. A class of sulfonamide carbonic anhydrase inhibitors with neuropathic pain modulating effects. *Bioorg. Med. Chem.* **2015**, *23*, 1828–1840.

[298] Arakawa, H.; Hauschild, J.; Buerstedde, J.M. Requirement of the activation-induced deaminase (AID) gene for immunoglobulin gene conversion. *Science* **2002**, *295*, 1301–1306.

[299] Pinard, M. A.; Mahon, B.; McKenna, R. Probing the surface of human carbonic anhydrase for clues towards the design of isoform specific inhibitors. *BioMed Res. Int*. **2015**, Vol. 2015, e453543.

[300] Otwinowski, Z.; Minor, W. Processing of X-ray Diffraction Data Collected in Oscillation Mode. *Meth. Enzymol*. **1997**, *276*, 307–326.

[301] Adams, P.D.; Afonine, P.V.; Bunkóczi, G.; Chen, V.B.; Davis, I.W.; Echols, N.; Headd, J.J.; Hung, L.W.; Kapral, G.J.; Grosse-Kunstleve, R.W.; McCoy, A.J.; Moriarty, N.W.; Oeffner, R.; Read, R.J.; Richardson, D.C.; Richardson, J.S.; Terwilliger, T.C.; Zwart, P.H. PHENIX : a comprehensive Python-based system for macromolecular structure solution. *Acta Crystallogr. D Biol. Crystallogr.* **2010**, *66*, 213–221.

[302] The PyMOL Molecular Graphics System, Version 1.5.0.4 Schrödinger, LLC.

[303] Marshall, A. G.; Hendrickson, C. L. High-resolution mass spectrometers. *Annu. Rev. Anal. Chem.* **2008**, *1*, 579–599.

[304] Pinard, M.P.; Boone, C.D.; Rife, B.D.; Supuran C.T.; McKenna, R. Structural study of interaction between brinzolamide and dorzolamide inhibition of human carbonic anhydrases. *Bioorg Med Chem.* **2013**, *21*, 7210-7215.

[305] Kabsch, W. XDS. *Acta Cryst.* D66, 125-132, **2010**.

[306] Winn, M.D.; Ballard, C.C.; Cowtan, K.D.; Dodson, E.J.; Emsley, P.; Evans, P.R.; Keegan, R.M.; Krissinel, E.B.; Leslie, A.G.W.; McCoy, A.; McNicholas, S.J.; Murshudov, G.N.; Pannu, N.S.; Potterton, E.A.; Powell, H.R.; Read, R.J.; Vagin, A.; Wilson, K.S. Overview of the CCP4 suite and current developments. *Acta Crystallogr D Biol Crystallogr.* **2011**, *67*, 235–242.

[307] Avvaru, B.S.; Kim, C.U.; Sippel, K.H.; Gruner, S.M.; Agbandje-McKenna, M.; David N. Silverman, D.N.; McKenna, R. A Short, Strong Hydrogen Bond in the Active Site of Human Carbonic Anhydrase II. A short, strong hydrogen bond in the active site of human carbonic anhydrase II. *Biochemistry.* **2010**, *49*, 249-251.

[308] Almahli, H.; Hadchity, E.; Jaballah, M.Y.; Daher, R.; Ghabbour, H.A.; Kabil, M.M.; Al-Shakliah, N.S.; Eldehna, W.M. Development of novel synthesized phthalazinone-based PARP-1 inhibitors with apoptosis inducing mechanism in lung cancer. *Bioorg. Chem.* **2018**, *77*, 443–456.

[309] Eldehna, W.M.; Almahli, H.; Al-Ansary, G.H.; Ghabbour, H.A.; Aly, M.H.; Ismael, O.E.; Al-Dhfyan, A.; Abdel-Aziz, H.A. Synthesis and in vitro anti-proliferative activity of some novel isatins conjugated with quinazoline/phthalazine hydrazines against triple-negative breast cancer MDA-MB-231 cells as apoptosis-inducing agents. *J. Enzym. Inhib. Med. Chem.* **2017**, *32*, 600–613.

[310] Määttä, J.A.E.; Eisenberg-Domovich, Y.; Nordlund, H.R.; Hayouka, R.; Kulomaa, M.S.; Livnah, O. Chimeric avidin shows stability against harsh chemical conditions—Biochemical analysis and 3D structure. *Biotechnol. Bioengin.* **2011**, *108*, 481–490.